

AN EVALUATION OF THE DISTRIBUTION OF ABSORBED  
DOSE IN CHILD PHANTOMS EXPOSED TO  
DIAGNOSTIC MEDICAL X RAYS

A THESIS

Presented to

The Faculty of the Division of Graduate  
Studies and Research

By

Wei-Li Chen

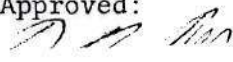
In Partial Fulfillment  
of the Requirements for the Degree  
Doctor of Philosophy  
in the  
School of Nuclear Engineering


Georgia Institute of Technology

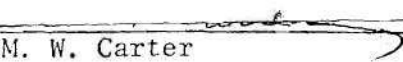
June, 1977

AN EVALUATION OF THE DISTRIBUTION OF ABSORBED  
DOSE IN CHILD PHANTOMS EXPOSED TO DIAGNOSTIC  
MEDICAL X-RAYS

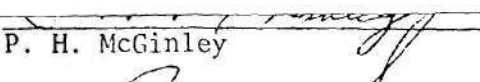
Approved:


  
K. Z. Morgan, Chairman

  
G. G. Eichholz

  
M. W. Carter

  
J. D. Clement

  
P. H. McGinley

  
J. W. Poston

Date Approved by Chairman May 21, 1977

## ACKNOWLEDGMENTS

The author would like to express his appreciation to his employer, the Institute of Nuclear Energy Research, Chinese Atomic Energy Council, for the opportunity they provided him to pursue graduate study. Deepest gratitude is expressed to J. W. Poston, who, as Laboratory research advisor, provided the opportunity to work on this project and inspiration, support, understanding, and criticism needed to complete this study. Appreciation is expressed to K. Z. Morgan, thesis advisor, and G. G. Eichholz, thesis committee member, for their interest and helpful advice. Thanks also to C. J. Roberts who made the initial arrangements for my work at Oak Ridge and initially served as my academic and thesis advisor. The author is grateful to J. A. Auxier, Director of the Health Physics Division at the Oak Ridge National Laboratory, for the opportunity to use the facilities of this organization.

The author especially wishes to acknowledge the assistance of G. G. Warner and T. D. Jones in performing some of the computer-coded calculations needed in this study. In addition, thanks go to T. D. Jones for his assistance in seeing this manuscript through its final phases and to G. D. Kerr for his careful reading of the manuscript and the many helpful suggestions he made to improve the quality of the text. Thanks are expressed also to B. G. Foutz, H. S. Roach, and R. S. Jones who provided valuable assistance in the fabrication of the phantoms.

The author especially thanks P. S. Stansbury and H. M. L. Hwang for their kind help during the course of the work.

The author is grateful to K. E. Cowser for his kind assistance preparing drafts and other paper work. Thanks are expressed to K. M. Branam and B. S. Varnadore for their patience and technical assistance in preparing this manuscript.

Finally, the author thanks his wife and other members of his family for their loving patience, understanding, and encouragement.

This research was performed at the Oak Ridge National Laboratory which is operated by Union Carbide Corporation under contract with the Energy Research and Development Administration.



## TABLE OF CONTENTS

	Page
ACKNOWLEDGMENTS . . . . .	ii
LIST OF TABLES . . . . .	vi
LIST OF FIGURES . . . . .	ix
SUMMARY . . . . .	xiii
Chapter	
I. INTRODUCTION . . . . .	1
II. THEORY . . . . .	27
X-Ray Generation	
Photon Interactions with Matter	
Theory of the Monte Carlo Method	
Introduction	
Random Number	
Probability Distribution Function and Cumulative	
Distribution Function	
Translation between the Different Probability	
Distribution Functions and Different	
Cumulative Distribution Functions	
The Monte Carlo Technique Applied to Dose Calculations	
III. EXPERIMENTAL APPARATUS AND PROCEDURES . . . . .	49
Phantom Design and Fabrication	
Phantom Material Evaluation	
X-Ray Machine Calibration	
Dosimetry	
Victoreen 550 System	
Thermoluminescent Dosimetry Theory	
TLD X-Ray Exposure Calibration	
TLD Tandem Technique	
Measurements of Absorbed Dose in Pediatric Phantoms	
Experimental Procedure	

Chapter	Page
Collection and Reduction of Data	
Tissue Dose Estimation	
Monte Carlo Calculation	
Bone Marrow Dose Estimation	
Calculated Active Bone Marrow Dose	
Measured Active Bone Marrow Dose	
IV. RESULTS . . . . .	141
Comparison of Calculated and Measured Absorbed Doses	
Trends of Absorbed Dose in Organs as Function of Age	
Risk Factor Estimation	
Error Evaluation	
V. CONCLUSION . . . . .	157
Discussion	
Recommendations	
APPENDICES . . . . .	163
A. Cross Sectional Plots of the One-Year- and Five-Year-Old Phantoms	
B. Summary of Some Phantom Materials	
C. Tissue-Air Ratio Comparison	
BIBLIOGRAPHY . . . . .	197
VITA . . . . .	211

## LIST OF TABLES

Table	Page
1. Annual Genetically Significant Dose (GSD) per Capita from Diagnostic X-Ray Examinations . . . . .	9
2. Comparison of Absorbed Fractions for the Pediatric and Similitude Phantom—One-Year-Old . . . . .	14
3. Comparison of Absorbed Fractions for the Pediatric and Similitude Phantom—Five-Year-Old . . . . .	15
4. Amount of Radiation per Exposure Received during Routine Roentgenographic Procedures in Children . . . . .	19
5. Measured Maximum Skin Doses in X-Ray Examinations (rads) . .	21
6. Calculated Mean Whole-Body Doses in X-Ray Examinations (rads) . . . . .	22
7. Summary of Literature on Pediatric Dosimetry . . . . .	23
8. Comparison of Subregion Volumes of the Physical and Mathematical Phantom—One-Year-Old . . . . .	65
9. Comparison of Subregion Volumes of the Physical and Mathematical Phantom—Five-Year-Old . . . . .	66
10. Description of Snyder-Fisher Phantom Subregions and the Pediatric Phantom Equivalents . . . . .	70
11. Calculated Partial Mass Attenuation Coefficients for Snyder-Fisher Composition and Comparison of Equivalent Material Used in the Pediatric Phantom—Soft Tissue . . . .	72
12. Calculated Partial Mass Attenuation Coefficients for Snyder-Fisher Composition and Comparison of Equivalent Material Used in the Pediatric Phantom—Skeleton . . . . .	73
13. Calculated Partial Mass Attenuation Coefficients for Snyder-Fisher Composition and Comparison of Equivalent Material Used in the Pediatric Phantom—Lung . . . . .	74
14. Victoreen Model 550-0.1 Ionization Probe Calibration Data . . . . .	87

Table	Page
15. Parameters Used in the Energy Response Determinations . . .	106
16. Technical Factors for Pediatric Phantom Exposures to Some Typical Diagnostic X-Ray Procedures . . . . .	113
17. The Distribution of Active Bone Marrow in Children . . . . .	128
18. Masses of Red and Yellow Marrow and Bone in the One-Year-Old Child Phantom . . . . .	129
19. Masses of Red and Yellow Marrow and Bone in the Five-Year-Old Child Phantom . . . . .	130
20. The Absorbed Dose and Risk Factors for Representative Radiological Exposures—One-Year-Old Phantom . . . . .	151
21. The Absorbed Dose and Risk Factors for Representative Radiological Exposures—Five-Year-Old Phantom . . . . .	152
B-1. Composition of Soft Tissue Equivalent Material (Weight Percentage) . . . . .	175
B-2. Composition of Some Dosimetry Materials and Their Important Dosimetric Constants . . . . .	179
B-3. Composition of Bone Equivalent Material . . . . .	180
C-1. Tissue-Air Ratio Comparison, One-Year-Old Phantom Head Examination (Posterior/Anterior View, 75 kVcp, 287 mAs, FSD = 101.6 cm) . . . . .	181
C-2. Tissue-Air Ratio Comparison, One-Year-Old Phantom Head Examination (Left Lateral View, 60 kVcp 685 mAs, FSD = 101.6 cm) . . . . .	182
C-3. Tissue-Air Ratio Comparison, One-Year-Old Phantom Chest Examination (Anterior/Posterior View, 60 kVcp, 990 mAs, FSD = 121.9 cm) . . . . .	183
C-4. Tissue-Air Ratio Comparison, One-Year-Old Phantom Chest Examination (Posterior/Anterior View, 60 kVcp 990 mAs, FSD = 121.9 cm) . . . . .	184
C-5. Tissue-Air Ratio Comparison, One-Year-Old Phantom Chest Examination (Left Lateral View, 75 kVcp, 417 mAs, FSD = 121.9 cm) . . . . .	185



Table	Page
C-6. Tissue-Air Ratio Comparison, One-Year-Old Phantom Abdomen Examination (Anterior/Posterior View, 75 kVcp, 287 mAs, FSD = 101.6 cm) . . . . .	186
C-7. Tissue-Air Ratio Comparison, One-Year-Old Phantom Abdomen Examination (Posterior/Anterior View, 75 kVcp, 287 mAs, FSD = 101.6 cm) . . . . .	187
C-8. Tissue-Air Ratio Comparison, One-Year-Old Phantom Abdomen Examination (Left Lateral View, 90 kVcp, 191 mAs, FSD = 101.6 cm) . . . . .	188
C-9. Tissue-Air Ratio Comparison, Five-Year-Old Phantom Head Examination (Posterior/Anterior View, 80 kVcp, 240 mAs, FSD = 101.6 cm) . . . . .	189
C-10. Tissue-Air Ratio Comparison, Five-Year-Old Phantom Head Examination (Left Lateral View, 70 kVcp, 439 mAs, FSD = 101.6 cm) . . . . .	190
C-11. Tissue-Air Ratio Comparison, Five-Year-Old Phantom Chest Examination (Anterior/Posterior View, 80 kVcp, 827 mAs, FSD = 182.9 cm) . . . . .	191
C-12. Tissue-Air Ratio Comparison, Five-Year-Old Phantom Chest Examination (Posterior/Anterior View, 80 kVcp, 827 mAs, FSD = 182.9 cm) . . . . .	192
C-13. Tissue-Air Ratio Comparison, Five-Year-Old Phantom Chest Examination (Left Lateral View, 100 kVcp, 521 mAs, FSD = 182.9 cm) . . . . .	193
C-14. Tissue-Air Ratio Comparison, Five-Year-Old Phantom Abdomen Examination (Anterior/Posterior View, 80 kVcp, 240 mAs, FSD = 101.6 cm) . . . . .	194
C-15. Tissue-Air Ratio Comparison, Five-Year-Old Phantom Abdomen Examination (Posterior/Anterior View, 80 kVcp, 240 mAs, FSD = 101.6 cm) . . . . .	195
C-16. Tissue-Air Ratio Comparison, Five-Year-Old Phantom Abdomen Examination (Left Lateral View, 100 kVcp, 152 mAs, FSD = 101.6 cm) . . . . .	196

## LIST OF FIGURES

Figure	Page
1. Illustration of the Theory of Continuous X-Ray Generation . . . . .	28
2. X-Ray Beam Absorption in a Biological System . . . . .	36
3. Dimensions and Coordinate System of the One-Year-Old Phantom . . . . .	50
4. Dimensions and Coordinate System of the Five-Year-Old Phantom . . . . .	51
5. Anterior View of the Principal Organs in the Head and Trunk of the Child Phantoms Used for the One-Year-, and Five-Year-Old . . . . .	53
6. The One-Year-, and Five-Year-Old Phantoms . . . . .	55
7. The Head Regions of the One-Year-, and Five-Year-Old Phantoms . . . . .	56
8. The Trunk of the One-Year-Old Phantom . . . . .	57
9. The Legs and Genitalia Region of the One-Year-Old Phantom . . . . .	58
10. The Skeleton of the One-Year-Old Phantom . . . . .	59
11. The Skeleton of the Five-Year-Old Phantom . . . . .	60
12. The Pelvis of the One-Year-, and Five-Year-Old Phantoms . .	61
13. The Spines of the One-Year-, and Five-Year-Old Phantoms, Detector Probes, and TLD Holder . . . . .	62
14. The Lungs of the One-Year-, and Five-Year-Old Phantoms . .	63
15. The Principal Devices of an X-Ray Generating Apparatus . .	75
16. The Coolidge-Type X-Ray Tube and the Variation in Intensity of the X-Ray Beam along the Longitudinal Axis of the Tube . . . . .	76

Figure	Page
17. X-Ray Machine Output Spectrum Measured with a Ge(Li) Detector—60 kVcp . . . . .	79
18. X-Ray Machine Output Spectrum Measured with a Ge(Li) Detector—80 kVcp . . . . .	80
19. X-Ray Machine Output Spectrum Measured with a Ge(Li) Detector—100 kVcp . . . . .	81
20. Normalized Exposure Rate as a Function of Tube Current (Error Bars Correspond to $\pm 2\%$ Plus the Least Significant Digit Uncertainty) . . . . .	84
21. Exposure Rate at a Target to Detector Distance of 100 cm as a Function of Generating Potential . . . . .	85
22. The Correction Factors of the Victoreen Model 550-0.1 Ionization Probe as a Function of the Effective Energy . . . . .	88
23. Schematic Representation of Thermoluminescence Processes in TLD Crystal . . . . .	90
24. LiF:Mn Fading Rate Test . . . . .	97
25. CaF <sub>2</sub> :Mn Fading Rate Test . . . . .	99
26. TLD Angular Dependence Tests . . . . .	100
27. LiF:Mn Response as a Function of Exposure . . . . .	102
28. CaF <sub>2</sub> :Mn Response as a Function of Exposure . . . . .	103
29. The Transmission of the X Rays through Aluminum . . . . .	105
30. Relative Response of LiF:Mn as Function of Effective Photon Energy . . . . .	108
31. Relative Response of CaF <sub>2</sub> :Mn as Function of Effective Photon Energy . . . . .	109
32. CaF <sub>2</sub> :Mn and LiF:Mn Dosimeter Response Ratio versus Effective Photon Energy . . . . .	112
33. The Positions of the Fields and Measuring Sites for One-Year-Old Phantoms . . . . .	115
34. The Positions of the Fields and Measuring Sites for Five-Year-Old Phantoms . . . . .	116



Figure	Page
35. Simulation of the Experimental Arrangement Showing the X-Ray Machine, Ion Chamber, and Five-Year-Old Phantom . . . . .	118
36. Mass Energy Absorption Coefficient Ratios, Active Marrow to Skeleton, as a Function of Photon Energy . . . . .	133
37. The Absorbed Dose Distribution in the Spine of the One-Year-Old Phantom—Chest Examinations . . . . .	137
38. The Absorbed Dose Distribution in the Spine of the One-Year-Old Phantom—Abdominal Examinations . . . . .	138
39. The Absorbed Dose Distribution in the Spine for the Five-Year-Old Phantom—Chest Examinations . . . . .	139
40. The Absorbed Dose Distribution in the Spine of the Five-Year-Old Phantom—Abdominal Examinations . . . . .	140
41. The Mean Active Bone Marrow Dose as Function of Age for Selected Radiological Exposures . . . . .	143
42. The Absorbed Dose of the Thyroid as Function of Age for Selected Radiological Exposures . . . . .	144
43. The Absorbed Dose of the Ovaries as Function of Age for Selected Radiological Exposures . . . . .	145
44. The Absorbed Dose of the Testes as Function of Age for Selected Radiological Exposures . . . . .	146
A-1. X-Z Sectional Plots of the One-Year-Old Phantom . . . . .	163
A-2. X-Y Sectional Plots of the One-Year-Old Phantom Showing the Upper Leg and Hip Regions . . . . .	164
A-3. X-Y Sectional Plots of the One-Year-Old Phantom Showing the Lower Abdomen . . . . .	165
A-4. X-Y Sectional Plots of the One-Year-Old Phantom Showing the Upper Abdomen . . . . .	166
A-5. X-Y Sectional Plots of the One-Year-Old Phantom Showing the Chest Region . . . . .	167
A-6. X-Y Sectional Plots of the One-Year-Old Phantom Showing the Shoulder and Head Regions . . . . .	168

Figure	Page
A-7. X-Z Sectional Plots of the Five-Year-Old Phantom . . . . .	169
A-8. X-Y Sectional Plots of the Five-Year-Old Phantom Showing the Upper Leg and Hip Regions . . . . .	170
A-9. X-Y Sectional Plots of the Five-Year-Old Phantom Showing the Lower Abdomen . . . . .	171
A-10. X-Y Sectional Plots of the Five-Year-Old Phantom Showing the Upper Abdomen . . . . .	172
A-11. X-Y Sectional Plots of the Five-Year-Old Phantom Showing the Chest Region . . . . .	173
A-12. X-Y Sectional Plots of the Five-Year-Old Phantom Showing the Shoulder and Head Regions . . . . .	174

## SUMMARY

The purpose of this study was to determine, by theoretical calculation and experimental measurement, the absorbed dose distributions in two heterogeneous phantoms representing one-year- and five-year-old children from typical radiographic examinations for those ages.

Theoretical work included the modification of an existing internal dose code which uses Monte Carlo methods to determine doses within the Snyder-Fisher mathematical phantom. A Ge(Li) detector and a pinhole collimator were used to measure x-ray spectra which served as input (i.e., the source routine) to the modified Monte Carlo codes which were used to calculate organ doses in children.

Experimental work included the fabrication of child phantoms to match the existing mathematical models. These phantoms were constructed of molded lucite shells filled with differing materials to simulate lung, skeletal, and soft-tissue regions. The skeleton regions of phantoms offered the opportunity to perform meaningful measurements of absorbed dose to bone marrow and bone. A Victoreen Model 550 Radocon III Integrating Rate Electrometer system and ion chamber were used as the primary dosimetry reference instrument for radiation measurement and thermoluminescent dosimeter (TLD) calibration. Thermoluminescent dosimetry techniques were used extensively in this study. The TLD calibration studies were focused on use in the diagnostic x-ray region. These studies included: grading, fading tests, angular

dependence tests, sensitivity and linearity tests, energy response tests, and a TLD LiF:Mn and  $\text{Ca}_2\text{F}_2\text{:Mn}$  "in tandem technique" which was used to determine the effective energy at selected sites inside the phantoms. Thirteen to fourteen sites in various bones of the skeleton were chosen for placement of TLDs. These sites represented important regions in which active bone marrow is located.

Sixteen typical radiographic examinations were performed representing common pediatric diagnostic procedures. A multiple exposure method was used to provide good TLD readings both for in-beam and out-beam locations during the exposure processes. The maximum exposure used per field was 6000 milliamp-sec regardless of tube voltage. Uncertainty associated with the measured doses was estimated to be  $\pm 7\%$ .

The calculated and measured tissue-air values were compared for a number of organs. For most organs, the results of the calculated absorbed doses agreed with the measured absorbed doses within twice the coefficient of variation of the calculated value. The absorbed dose to specific organs for several selected radiological examinations are given for one-year-old, five-year-old, and adult phantoms. For selected radiological exposures, the risk factors of leukemia, thyroid cancer, and genetic death are estimated for one-year- and five-year-old children.



## CHAPTER I

### INTRODUCTION

Ever since Wilhelm Conrad Roentgen detected and identified the x ray, physicians have learned to use x rays as a powerful tool in diagnosis. X rays have been used as a means of photographing the bones and setting fractures. X rays are used also for detecting and locating foreign objects inside the body. This use of x rays became an important part of radiography.

During the early period, many experimenters suffered severe x-ray burns (Morgan and Turner, 1967) that were found to be incurable in many cases. Often fingers, hands, and arms were lost. Eventually physicians learned to use x rays to kill tumors and other diseased regions. It was found also that x rays in some cases had a more pronounced effect (killing) on those diseased tissues than on normal healthy ones. Thus, gradually the technique of x-ray therapy was developed.

Laue et al. (1913) discovered that x rays could be diffracted by crystals and, soon, this discovery provided a new method for investigating the nature of solids. The method has been used broadly in science and industry. Human beings have been exposed throughout the ages to radiation from natural sources. During the last eighty years, however, many apparatuses have been designed for generating ionizing radiation artificially, and in some cases radioactive materials are

produced and extracted from them contributing potentially to personnel exposure. Some historic milestones in early radiation protection and dosimetry can be found in the summaries of Taylor (1971) and Glasser et al. (1961).

In the late 1940's and early 1950's, as a result of the tests of nuclear weapons, public concern arose about the potential effects of ionizing radiation on the human population. This concern led to a series of reports by the National Academy of Sciences (NAS), issued from 1956 to 1961. These reports are usually referred to as the "BEAR" (Biological Effects of Atomic Radiation) reports. The BEAR reports led to a basis for improved understanding of expected effects due to radiation resulting from the testing of nuclear devices that had occurred to that date. In addition, the reports introduced the important concept of regulation of the average population dose on the basis of genetic risk to future generations. The reports also emphasized medical and dental x rays as the greatest source of man-made radiation exposure of the population.

Beginning in the 1950's and extending to the present time, the International Commission on Radiological Protection (ICRP) and National Council on Radiation Protection and Measurement (NCRP) have published many reports dealing with the effects of ionizing radiation on man and have made many recommendations for radiation control. Now, ionizing radiations are used in many types of peaceful activity in everyday life. Hence, the hazard of excessive exposure has become a matter of interest not only for a relatively small number of occupationally exposed persons,

but for the population as a whole. In the late 1960's, concern arose that developing peacetime applications of nuclear energy, particularly the growth of a nuclear power industry for production of electricity, could cause growing exposure of the human population to radiation. In 1970, the Federal Radiation Council (now part of the Environmental Protection Agency) requested that the NAS-National Research Council Advisory Committee review and reevaluate the existing scientific knowledge concerning radiation exposure of human populations. The NAS-NRC Advisory Committee Report (Biological Effects of Ionizing Radiations, BEIR) was published in 1972. In that report, again, it was emphasized that the major contributors to radiation exposure for human beings were natural background and medical applications. The main contributor to the total dose from medical exposure was diagnostic x rays. Medical diagnostic radiology accounts for at least 90% of the total man-made radiation dose to which the U.S. population is exposed. This exposure is at least 35% of the total radiation dose from all sources including natural radioactivity.

Generally, the radiation effects on man can be considered as either genetic or somatic effects. The BEAR Genetics Committee recommended that man-made radiation be kept at such a level that the average individual exposure be less than 10 roentgens (R) before the mean age of reproduction, a period of time taken to be 30 years. This upper dose limit included medical radiation which was estimated to amount to 5 R at that time. In contrast, the Federal Radiation Council (FRC) (FRC, 1960; ICRP, 1958) did not include medical radiation in



their deliberations, and therefore, took 5 R as the 30-year limit for the average population exposure in their Radiation Protection Guides. This limit results in an average dose rate of 170 mR/year; the value now in effect. The 1956 Genetics report relied mainly on data from *Drosophila* and mice as there were almost no relevant human data. The genetic effects of radiation are gene mutations (recessive and dominant) and chromosome aberrations. These effects may lead to different genetic and teratogenic diseases such as sickle cell anemia, physical abnormalities, mental deficiency, as well as more numerous nonvisible mutations (Miller, 1953, 1956).

A recent report by the United National Scientific Committee on the Effects of Atomic Radiation (UNSCEAR, 1972) suggests that genetic effects should not be considered the only primary hazard of radiation exposure. An increased emphasis is being placed on the somatic effects of radiation (cancer and leukemia) and models for estimating the effects on other organs, such as active bone marrow, are being developed.

The somatic effects are usually concerned with two types of exposure:

1. A single high-level exposure to radiation during a short period of time, which is commonly called "acute" exposure. Common acute radiation syndrome will include:
  - a. nausea and vomiting;
  - b. malaise and fatigue;
  - c. increased body temperature;
  - d. blood changes (e.g., lymphocyte drop);
  - e. epilation.

2. A long-term, low-level over-exposure is commonly called "chronic" exposure. Latent or delayed effects may result from either a single large over-exposure or continuing low-level over-exposure.

These latent effects include:

- a. retardation of growth and development;
- b. induction of many types of neoplasms and leukemia;
- c. shortening of life span.

In addition there are many long-term genetic effects such as dominant diseases, chromosomal and recessive diseases, congenital anomalies and anomalies expressed later and constitutional and degenerative diseases.

There is no doubt that ionizing radiation can induce cancer in man (Miller, 1972). The first definite demonstration of the role of ionizing radiation in the aetiology of brain tumors in man was reported by Baruch et al. (1974). About 11,000 children irradiated for tinea capitis, a fungal scalp infection, and two matched control groups were retrospectively followed for twelve to twenty-three years (Modal et al., 1974; Silverman and Hoffman, 1974). The irradiated group had a significantly higher risk of both malignant and benign head and neck tumors, especially in the brain, the parotid gland, and thyroid.

Detailed studies of the neoplasms in children treated with x rays for thymic enlargement have been reported by Pifer and his colleagues (Pifer et al., 1963; Toyooka et al., 1963a, 1963b; Hempelmann et al., 1974, 1975). These reports revealed a high incidence of tumors, particularly leukemia, thyroid adenomas, and osteochondromas (tumor of the bone and cartilage). Several cases of salivary gland tumor and

neurilemmomas (tumor of the nerve sheath), which are very rare neoplasms in children and young adults, were observed. The most recent followup study was reported by Hempelmann et al. (1974). Frequencies of asthma and altered immunologic features in the irradiated children were reported to be two and three times those in the nonirradiated sibling (Hempelmann et al., 1975).

Wilms' tumor, neuroblastoma and medulloblastoma are three common childhood neoplasms. In the treatment of these neoplasms the vertebral column is exposed to irradiation in radiotherapy. The postirradiation effects of scoliosis (abnormal curvature of the spine) were studied by Neuhauser et al. (1952) and Rubin et al. (1962). It appears that disturbances of the growing spine (disturbances produced by irradiation of the human vertebrae) are directly related to dose and inversely related to age. Usually, for a radiation dose less than 1000 R, no detectable deformity of the vertebrae was found in a growing child. As the dose level increased, a different vertebral aberration was noted. Although irradiation of normal tissue in infants and children carries the hazard of producing growing disorders, this risk is considered clinically acceptable in curative treatment of malignant disease.

A 25-year followup study of a 26-year-old woman who had received postbiopsy irradiation of the entire pelvis for a botryoid sarcoma of the vagina at age 13 months was reported by Anas et al. (1974). Changes were apparent in the skin, muscles, primary sex organ, bone, and bone marrow. Although the sequelae of irradiation in this patient cannot be disregarded, the treatment has provided the patient with a useful and almost normal existence.



Reliable estimates of chronic radiation effects can be expected only when we have exact medical and physical observations on a large population or when we have a full understanding of biological mechanisms by which the effects are produced. Since we have neither, our present estimates are based on the results of the following studies, for example:

- a. Japanese A-bomb survivors in Hiroshima and Nagasaki (Ishimaru et al., 1971; Beebe et al., 1971; Jabon and Belsky, 1970);
- b. British patients treated with intensive spinal irradiation for ankylosing spondylitis (Court-Brown and Doll, 1957, 1965);
- c. Studies on practicing radiologists (Seltser and Sartwell, 1965; Warren, 1966; Reissland et al., 1976);
- d. Human populations exposed to alpha emitters, such as underground miners (Goldman, 1965), thorotrast or radium-treated patients (Norris et al., 1955) and radium dial painters (Clark, 1958);
- e. Children irradiated for tinea capitis (Beach and Dolphin, 1962; Albert and Omran, 1968; Baruch et al., 1974; Harley et al., 1976);
- f. Children irradiated for thymic enlargement (Pifer et al., 1963; Toyooka et al., 1963a, 1963b; Modal, 1974; Hempelmann et al., 1967, 1968, 1974, 1975; Silverman and Hoffman, 1974);
- g. Retrospective interview surveys for pregnant women who received obstetric x-ray examinations (Debakan, 1968; Dawson, 1962; Stewart and Kneal, 1970; Bross, 1972).

From the above studies, both the BEIR or UNSCEAR (1972) reports have concluded that "Cancer is the major long-term somatic effect of radiation on human beings and cancer induction is considered to be the only source of somatic risk that needs to be taken into account in setting radiation protection standards for the general population." The BEIR reports also mention that "the risk estimates of radiation damage effects lack precision but do indicate that the mean dose both to the population and to each individual must be kept as low as practicable."

Since 1950 many authors and/or national bodies have been concerned with the genetically significant dose\* to populations, e.g., Martin (Australia, 1955, 1958), Adrian Committee (United Kingdom, 1956, 1960, 1966), Larsson (Sweden, 1958), Hammer-Jacobsen (Denmark, 1963), Hashizume et al. (Japan, 1972a), United Nations Scientific Committee (1962, 1972). Their estimates of genetically significant dose are summarized in Table 1. One of the early assessments of effects resulted in the 1956 report of the Medical Research Council by the Adrian Committee (Adrian, 1956), which contained a detailed summary of population exposures in England and Wales from various radiation sources. In that report doses to the skin and gonads of patients due to the diagnostic x rays were taken from an investigation conducted by Stanford and Vance (1955). Ionization chambers were used to measure the gonad and ovary dose in the

---

\*The genetically significant dose is the dose which, if received by every member of the population, would be expected to produce the same total genetic injury to the population as do the actual doses received by the various individuals (UNSCEAR, 1972).

Table 1. Annual Genetically Significant Dose (GSD) per Capita  
from Diagnostic X-Ray Examinations

Region	Period of Study	GSD	Reference
Australia	1955-1957	160 mrem	Martin, 1958
Sweden	1955	38 mrem	Larsson, 1958
United Kingdom	1957-1958	14 mrem	Adrian, 1960
Denmark	1956-1960	22 mrem	Hammer-Jacobsen, 1963
Japan	1969	26.5 mrad	Hashizume et al., 1972a
USA, City of Richland	1953-1956	46 mrem	Norwood et al., 1959
USA	1955-1956	140 $\pm$ 100 mrem	Laughlin and Pullman, 1957
USA	1956-1957	40-50 mrem	Brown et al., 1960
USA, New York	1962	50 mrad	Pasternack and Heller, 1968
USA	1964	54.6 <sup>a</sup> mrad	USPHS, 1969
USA	1970	35.5 <sup>a</sup> mrad	USPHS, 1973

<sup>a</sup>FDA, Bureau of Radiological Health, Bulletin 9 (No. 3), pp. 1-3 (February 18, 1975) recently announced errors in their estimates of GSD for 1964 (54.6 mrad) and 1970 (35.5 mrad). The current estimate for 1964 is 16 mrad and for 1970 20 mrad.

different types of examinations. For phantom dose measurements, Mix D or water phantoms and cadavers were used in the experiment to estimate the absorbed doses in patients. In 1960 and 1966, the Adrian Committee published the second and final report entitled "Radiation Hazard to Patients" in London (Adrian, 1960, 1966). In these reports, the absorbed doses received by the patients were classified according to sex, age, and type of x-ray diagnosis. The effective genetic dose and bone marrow dose to the population from diagnostic x-ray procedures were estimated.

In the United States of America there were also many systematic studies of population exposure to medical x rays, e.g., Norwood et al. (City of Richland, 1959), Laughlin and Pullman (USA, 1957), Brown et al. (USA, 1960), Pasternack and Heller (New York, 1968). Recently, two studies of general population exposure to x rays were conducted by agencies of the U.S. Government in 1964 and 1970, respectively (USPHS, 1969, 1973). One of the main objectives of these studies was to guide the development of programs that would assist professional groups, health agencies, and equipment manufacturers in more efficient and safe use of x rays in medical applications. The following summary covers the principal aspects of these two studies.

1. Medical diagnostic x rays have continued to lead as the major man-made source of population exposure to ionizing radiation.
2. It is estimated that 130 million persons (or 65% of the U.S. population) had one or more x-ray examinations in 1970.



3. There were 212 million diagnostic x-ray examinations (about 661 million films exposed). Of these examinations, 76 million were medical, including more than 10 million persons having fluoroscopic examinations, and 59 million dental x-ray examinations in 1970.
4. The annual number of medical x-ray exposures increased from 48 visits per 100 people in the population to 55.9 visits per 100 population between 1964 and 1970. The annual dental x-ray exposure rate increased from 26.8 visits per 100 people in the population in 1964 to 33.8 per 100 population in 1970.
5. In 1970, it is estimated that approximately 70% of the medical x-ray procedures were performed under the supervision of a radiologist compared to 61% estimated in 1964.
6. The mean ratio of beam area to film area for radiographic films declined approximately 30% between 1964 and 1970.
7. The percentage of dental films that were within the 3-inch maximum beam size recommended by the National Committee on Radiation Protection and Measurements was 80% in 1964 compared with 87% in 1970.
8. The estimated mean exposure per film for posterior-anterior and anterior-posterior views of the abdomen increased from an estimated 480 mR in 1964 to 620 mR in 1970.
9. The estimated mean exposure per film for chest examination remained about the same, approximately 28 mR/film in 1964 and 27 mR/film in 1970.

Recently, Nader reviewed the current problems in medical x-ray diagnostic exposure in the United States (Nader, 1975). Since unnecessary and avoidable exposure persists as the rate of use of medical x rays increases, solutions to this problem are necessary. These solutions may be available through policies to ensure improved equipment, qualified operators, medical and dental professionals who are knowledgeable about radiation protection principles, and mandatory performance standards and enforcement mechanisms. Based on information presently available (Gitlin, 1972; USPHS, 1969), it appears that the mean per capita radiation dose from diagnostic medical radiology may remain stable in future years if technical improvements keep pace with increased usage rates. In order to accomplish this, better means of predicting local and whole body doses during diagnostic or therapeutic exposure are needed.

There are many excellent papers on the assessment of risk or hazard from medical x rays (Stanford and Vance, 1955; Martin, 1955; Billings et al., 1957; Epp et al., 1961, 1963; Laughlin, 1963; and Koblinger and Zarand, 1972). Most of them were related to the adult or "Reference Man." The information may be applied generally to the average adult patient. However, it does not apply to the field of pediatric x-ray diagnosis (Robinow and Silverman, 1957; Kereiakes et al., 1965; Dolphin, 1968; Conrad et al., 1971; Hwang, 1976).

Fisher and Snyder (1966) have attempted to solve this lack of data by introducing their "similitude" phantoms. These phantoms represent children of ages newborn, 1-year, 5-years, 10-years, and 15-years. The

phantoms were obtained by "shrinking," through a set of mathematical transformations, the outer dimensions of the three regions (head, trunk, and legs) of the adult phantom. The pediatric phantoms described in this study were designed from anatomical data to be representative of children 1-year and 5-years of age.

Tables 2 and 3 are comparisons of the absorbed fractions of some organs between the similitude phantom and pediatric phantom. The absorbed fraction is defined as the fraction of photon energy emitted from the x-ray machine that is deposited in the target organ. The target organs selected were the brain, thyroid, thymus, ovaries, testes, and active red marrow. The differences in absorbed fraction calculated for the similitude phantom and the pediatric phantom are generally high.

In the similitude phantoms all organs and structures in the body are reduced in size according to factor selected to force the outer dimensions of the adult phantom to correspond to those of another age. No consideration is given to exact organ location, organ shape or organ size.

As an example, consider the distribution of the red bone marrow. In the adult the red bone marrow comprises only one-half of the total marrow in the skeleton and there are regions in which no red marrow exists. In the pediatric phantom for the one-year old all the bone marrow is red and is distributed uniformly in the skeleton. Therefore, when the adult phantom is "shrunk" by use of the similitudes, the distribution of red (and yellow) bone marrow is carried to the younger age phantom. This results in an error in the estimate of the dose

Table 2. Comparison of Absorbed Fractions for the Pediatric and Similitude Phantom—One-Year-Old

Chest Examination (Posterior/Anterior View)					
Organ	Absorbed Fraction		Coefficient of Variation Difference <sup>a</sup>		
	Pediatric	Similitude	(%)		(%)
Brain	$1.27 \times 10^{-3}$	$0.31 \times 10^{-3}$	8.00	14.20	75.14
Thyroid	$8.28 \times 10^{-5}$	$12.82 \times 10^{-5}$	1.40	17.83	-54.83
Thymus	$1.08 \times 10^{-3}$	$0.14 \times 10^{-3}$	7.21	18.57	87.06
Ovaries	----	----	----	----	----
Testes	----	----	----	----	----
Red Marrow	$3.20 \times 10^{-2}$	$4.71 \times 10^{-2}$	0.70	0.67	-47.09

Abdomen Examination (Posterior/Anterior View)					
Organ	Absorbed Fraction		Coefficient of Variation Difference <sup>a</sup>		
	Pediatric	Similitude	(%)		(%)
Brain	$4.15 \times 10^{-5}$	$2.80 \times 10^{-5}$	44.49	92.47	32.61
Thyroid	----	----	----	----	----
Thymus	$6.30 \times 10^{-5}$	$0.40 \times 10^{-5}$	22.75	56.78	93.70
Ovaries	$6.64 \times 10^{-5}$	$8.18 \times 10^{-5}$	24.02	26.21	-23.16
Testes	$5.12 \times 10^{-5}$	$8.45 \times 10^{-5}$	28.95	24.79	-64.98
Red Marrow	$3.61 \times 10^{-2}$	$5.09 \times 10^{-2}$	1.03	1.06	-40.79

$$^a \text{Difference} = \frac{(\text{Absorbed Fraction})_{\text{ped.}} - (\text{Absorbed Fraction})_{\text{sim.}}}{(\text{Absorbed Fraction})_{\text{ped.}}}$$



Table 3. Comparison of Absorbed Fractions for the Pediatric and Similitude Phantom--Five-Year-Old

Chest Examination (Posterior/Anterior View)					
Organ	Absorbed Fraction		Coefficient of Variation Difference <sup>a</sup>		
	Pediatric	Similitude	(%)		(%)
Brain	$2.40 \times 10^{-3}$	$0.78 \times 10^{-3}$	5.92	10.98	67.36
Thyroid	$0.97 \times 10^{-4}$	$1.60 \times 10^{-4}$	19.75	18.90	-64.99
Thymus	$8.07 \times 10^{-4}$	$1.91 \times 10^{-4}$	7.96	14.98	76.28
Ovaries	----	----	----	----	----
Testes	----	----	----	----	----
Red Marrow	$3.83 \times 10^{-2}$	$4.18 \times 10^{-2}$	0.72	0.72	-9.14

Abdomen Examination (Posterior/Anterior View)					
Organ	Absorbed Fraction		Coefficient of Variation Difference <sup>a</sup>		
	Pediatric	Similitude	(%)		(%)
Brain	----	----	----	----	----
Thyroid	----	----	----	----	----
Thymus	$3.19 \times 10^{-5}$	$1.47 \times 10^{-5}$	30.55	78.24	53.99
Ovaries	$1.15 \times 10^{-4}$	$0.93 \times 10^{-4}$	19.05	20.39	18.94
Testes	$8.01 \times 10^{-5}$	$12.61 \times 10^{-5}$	33.19	20.90	-57.39
Red Marrow	$5.12 \times 10^{-2}$	$5.53 \times 10^{-2}$	1.00	1.00	-8.02

$$^a \text{Difference} = \frac{(\text{Absorbed Fraction})_{\text{ped.}} - (\text{Absorbed Fraction})_{\text{sim.}}}{(\text{Absorbed Fraction})_{\text{ped.}}} \times 100.$$

to the red bone marrow. These errors are reflected in the comparisons shown in Tables 2 and 3.

Similar arguments can be made for other organs such as the thyroid and thymus. The size and depth below the surface of the neck is an important parameter in estimating the absorbed fraction in the thyroid from a diagnostic x-ray exposure. This factor was not considered in the similitude phantom. In the adult, the thymus has a very small size and this gland is significantly smaller than the gland found in children. In early life, the gland is very active and is large. It actually shrinks in size in adulthood. Obviously, reducing the size of the thymus in the adult by a set of factors chosen to be representative in the child will produce a much smaller organ which is not representative. Further, the absorbed fraction in this "reduced" gland will be significantly less than that obtained from calculations using a more realistic shape and mass for the organ. Children also have proportionately smaller genitalia than adults. Therefore, the absorbed fraction of the ovaries and testes of the pediatric phantoms are less than those of the similitude phantoms.

In 1960, the Federal Radiation Council in its first report (FRC, 1960) emphasized the need for defining a series of "standard children" because:

1. It is a generally accepted view that children, both prenatally and postnatally, are more radiosensitive than adults. Children are also more susceptible than adults to the deleterious late effects of ionizing radiation (Miller, 1953, 1956; Blair, 1954; Hursh and Casarette, 1955;

Graham and Hamilton, 1957; Morgan, 1961; MacMahon, 1963; Saengerte, 1964; Jablon and Belsky, 1970; Jablon et al., 1971; Rugh, 1973; Silverman, 1974).

2. The obvious physical and physiological differences between children and adults (Tanner et al., 1966).

3. The body proportions and relative organ sizes of infants and children are obviously different from the adult (FRC, 1961).

4. Half the population is less than 25 years old and children form an important part of this genetically significant population.

5. People in clinics need better information on the dosimetry for exposure of children.

6. A relatively small amount of information is available on mean bone marrow dose to children (James, 1974; Hashizume et al., 1972b; Shleien, 1973).

For diagnostic x-ray examinations the gonadal dose and average bone marrow dose are usually considered the principal indicators (critical organs) of relative hazard (UNSCEAR, 1962; ICRP, 1970a). The critical organ is defined as that part of the body that is most susceptible to radiation damage under the specific conditions considered. It is well known that in a diagnostic x-ray examination the organ of maximum dose is inevitably the skin which is not usually considered as a critical organ. However, the skin dose is an indicator of the dose to critical organs such as the thyroid, kidney, brain, and liver, which are fairly close to the surface of the body; substantial fractions of these organs may receive 30% to 80% of the skin dose (James, 1974). A



relatively large amount of information has been published on skin and gonad doses in diagnostic x-ray examinations in children (Billings et al., 1957; Webster and Merrill, 1957; Larsson, 1958; Adrian, 1960; Hammer-Jacobsen, 1963; ISBHUMC, 1969; Hashizume et al., 1969a; James, 1974). However, little information is available on mean bone marrow dose to children (James, 1974), although much data are available for adults (Epp et al., 1961, 1963; Adrian, 1966; Hashizume et al., 1969b; Antoku et al., 1972; Takeshita et al., 1972). Using unit-density Masonite blocks of different sizes, Billings et al. measured the gonad dose to child phantoms in examinations of the skull, chest, abdomen, lumbar spine, and pelvis with Victoreen thimble chambers. Differences in height of children resulted in a variation in the gonad dose. The results, for three different age groups, are shown in Table 4. To calculate the average gonad dose per examination for children in clinical practice the distribution of x-ray examinations in a children's clinic and the gonad dose given in Table 2, page 14, (Billings et al., 1957) were used. An average gonad dose per examination of 0.49 R in boys and 0.29 R in girls was computed (Billings et al., 1957).

Direct measurements in children during examinations were made by Larsson (1958) and Hammer-Jacobsen (1963). Larsson used ionization chambers to measure the mean gonad doses in different types of pediatric x-ray examinations. The results were presented for different sexes and ages of children. Similarly, Hammer-Jacobsen used a "kondimeter" with condenser chambers to measure the gonad doses for different types of x-ray examinations. A "Mix D" phantom was constructed with pelvis,

Table 4. Amount of Radiation per Exposure Received during Routine Roentgenographic Procedures in Children<sup>a</sup>

	Skull Basal View	Chest AP	Abdomen AP-KUB	Lumbar Spine AP	Lateral	Pelvis AP
infants 0-2 yrs.	65 kV., 25 mA-s.	45 kV., 10 mA-s.	60 kV., 20 mA-s.		60 kV., 20 mA-s.	60 kV., 20 mA-s.
S	0.18 r	0.023 r	0.16 r		0.8 r	0.16 r
F	0.001 r	0			0.3 r	0.09 r
M	0.001 r	0.002 r	0.15 r		0.8 r	0.16 r
children 2-7 yrs.			50 kV., 50 mA-s.	60 kV., 50 mA-s.	70 kV., 120 mA-s.	46 kV., 50 mA-s.
S			0.31 r	0.42 r	1.3 r	0.28 r
F	0	0	0.13 r	0.49 r	0.5 r	0.14 r
M	0	0	0.31 r	0.42 r	1.2 r	0.28 r
children 7-11 yrs.			58 kV., 75 mA-s.		74 kV., 160 mA-s.	76 kV., 50 mA-s.
S			0.6 r		1.8 r	0.73 r
F	0	0	0.24 r		0.73 r	0.3 r
M	0	0	0.25 r		0.3 r	0.7 r
Average gonad dose per examination: males, 0.49 R; females 0.29 R						

<sup>a</sup>The letters S, F, and M refer respectively to measurements on the skin, female gonad region, and male gonad region. Measurements in roentgens were taken with a Victoreen thimble chamber (Billings et al., 1957).

lumbar vertebrae, and femora from an adult female. The ovary dose and skin dose on the abdomen of the phantom was measured. By means of phantom measurements, conversion factors were then found that could be used to estimate ovary dose from the measurement of the patient's skin dose on her abdomen. However, the method is useful only in the estimation of dose to the ovaries of an adult female. In boys, the gonad dose was measured on the anterior surface of the scrotum.

Webster et al. (James, 1974) assumed a trunk thickness and weight for different aged children and constructed a Mix D phantom of variable thicknesses and weight, 10 cm trunk thickness and 12 kg for one-year-old phantom and 12 cm trunk thickness and 20 kg for five-year-old phantom. Using these phantoms they studied different x-ray examination procedures. Skin doses were measured and mean whole-body doses were calculated from the estimated skin exposures, typical field size, and the operating peak kilovoltage. The results are shown in Tables 5 and 6.

Table 7 is a summary of some pediatric phantom dosimetry studies. Different phantom material and detector systems were used in these studies. In early times, ionization chambers were the favorite detector system. Recently thermoluminescent detectors have been widely used because of their small size and ease of use. The results of these studies are difficult to compare, because of variation among the studies of several factors (such as target-skin distance, peak kilovoltage, milliamperere second, inherent and added filtration, and field size, etc.). Generally, these results reveal that for any given examination there may be a wide variation of gonad dose, depending on

Table 5. Measured Maximum Skin Doses in X-Ray Examinations<sup>a</sup> (rads)

X-Ray Examination	Age in Years			
	1	5	10	15
1. <u>Cerebral Studies</u>				
Radiography, skull series, 5 films	0.3	0.7	0.9	1.1
Biplane cerebral angiography, 48 films	8.4	11.4	12.0	13.2
Fluoroscopy, 6 minutes	3	4.8	7.2	9.6
2. <u>Angiocardiography</u>				
Biplane serial radiography, 40 films	1.8	3.3	5.7	7.2
Cineradiography 35 mm 60 fps., 60 sec.	2.8	4.2	6.6	10.6
Fluoroscopy, 30 minutes	24	36	51	66
3. <u>Kidney, Ureters, Bladder</u>				
Intravenous pyelography, 4 films	0.2	0.3	0.5	0.75
Renal angiography, 20 films AP	1.4	3.0	4.8	7.5
Fluoroscopy, 4 minutes	3.2	4.8	6.8	8.8
Cinecystourethrography, 16 mm., 7 1/2 fps, 1.6 mins	0.8	1.3	2.1	2.7
Fluoroscopy, 2 minutes	2.2	3.0	4.3	5.2
4. <u>Chest</u>				
Radiography, PA and lateral	0.05	0.03	0.05	0.07
Pulmonary arteriography, 30 films AP	3.0	6.4	10.2	15.9
Fluoroscopy, 1.5 minutes	1.2	1.8	2.6	3.3
5. <u>Liver</u>				
Radiography, abdomen AP film	0.05	0.08	0.18	0.25
Abdominal angiography, 30 films <sup>b</sup>	2.1	4.5	15	23
Fluoroscopy, 5 minutes	4	6	8.5	11
6. <u>Bone</u>				
Cervical spine, AP and lateral	0.05	0.4	0.1	0.15
Dorsal or lumbar spine, AP and lateral	0.2	0.4	0.9	1.6
Pelvis, AP and lateral	0.1	0.15	0.3	0.45
7. <u>Obstetrics</u>				
Obstetric abdomen	Fetal dose 1.0			
Pelvimetry	Fetal dose 4.0			

<sup>a</sup>James, 1974.<sup>b</sup>Magnification technique for 1 and 5 years.



Table 6. Calculated Mean Whole-Body Doses in X-Ray Examinations<sup>a</sup> (rads)

X-ray Examination	Age in Years			
	1	5	10	15
1. <u>Cerebral Studies</u>				
Radiography, skull series, 5 films	0.02	0.04	0.04	0.04
Biplane cerebral angiography, 48 films	0.6	0.65	0.5	0.4
Fluoroscopy, 6 minutes	0.025	0.05	0.07	0.08
2. <u>Angiocardiography</u>				
Biplane serial radiography, 40 films	0.13	0.22	0.27	0.25
Cineradiography, 35 mm, 60 fps., 60 sec.	0.08	0.08	0.08	0.08
Fluoroscopy, 30 minutes	0.25	0.5	0.6	0.6
3. <u>Kidney, Ureters, Bladder</u>				
Intravenous pyelography, 4 films	0.03	0.04	0.06	0.07
Renal angiography, 20 films AP	0.03	0.06	0.06	0.06
Fluoroscopy, 4 minutes	0.15	0.2	0.2	0.2
Cinecystourethrography, 16 mm., 7 1/2 fps., 1.6 minutes	0.04	0.06	0.06	0.06
Fluoroscopy, 2 minutes	0.11	0.15	0.15	0.15
4. <u>Chest</u>				
Radiography, PA and lateral	0.005	0.005	0.008	0.007
Pulmonary arteriography, 30 films, AP	0.3	0.6	0.8	0.9
Fluoroscopy, 1.5 minutes	0.05	0.07	0.08	0.08
5. <u>Liver</u>				
Radiography, abdomen, AP film	0.005	0.015	0.03	0.03
Abdominal angiography, 30 films <sup>b</sup>	0.2	0.4	1.2	1.3
Fluoroscopy, 5 minutes	0.2	0.25	0.3	0.3
6. <u>Bone</u>				
Cervical spine, AP and lateral	0.005	0.015	0.015	0.015
Dorsal or lumbar spine, AP and lateral	0.02	0.07	0.15	0.15
Pelvis, AP and lateral	0.01	0.03	0.05	0.05
7. <u>Obstetrics</u>				
Obstetric abdomen	Fetal dose 1.0			
Pelvimetry	Fetal dose 2.0			

<sup>a</sup>James, 1974.<sup>b</sup>Magnification technique for 1 and 5 years.

Table 7. Summary of Literature on Pediatric Dosimetry

Time, Author	Dosimetry	Result
Billings et al. (1957)	Unit density Masonite blocks. $10.6 \times 2.5 \times 2.5$ cm.  Victoreen thimble chambers 0.1Y, 1.0Y, 2.5Y.	0-2, 2-7, 7-11 year-old child phantom and clinical measurement.  Average gonad dose per examination for males, 0.49R, females 0.29 R.
Webster et al. (1957)	Unit-density Pressdwood phantom, $30 \times 30$ cm square and variable thickness Victoreen 25R thimble chamber. Baldwin-Farmer ionization chambers, type BD-2, Victoreen minometer.	3-year and 10-year child phantom. Skin and gonadal dose for different radiographic techniques was reported.
Adrian Committee (1960)	Phantom-polyethylene skin filled with soft tissue--equivalent materials and human skeleton. Baldwin-Farmer ionization chamber and small ionization chambers.	For the male, the gonad dose was obtained by direct measurement.  For the female, the ovary dose was estimated by measuring skin dose and multiplying by a conversion factor. The depth of the ovaries for a 0-2 years-old child was assumed to be half the depth of an adult.
Hammer-Jacobson (1963)	2 "Mix D" phantoms with built in pelvis, lumbar vertebrae and femora from an adult female. (One phantom for foetal dose.) Kondimeter with condenser chamber.	By means of phantom measurements, conversion ratios were then found which could be used in calculations of ovary dose.
Hashizume et al. (1972)	Three M3 phantoms consisting of paraffin 76.9%, MgO 22.4%, $\text{CaCO}_3$ 0.7% by weight with cork ( $0.3 \text{ g/cm}^3$ ) for lung tissue. These phantoms represented children 0-2, 2-7, 8-14 years old	Phantom irradiation was made according to the technical data obtained by different type diagnostic medical x-ray examinations.

Table 7 (continued)

---

	<p>Detector: Thermoluminescent dosimeters made of magnesium silicate powder <math>[\text{Mg}_2\text{SiO}_4(\text{Tb})]</math> encapsulated in a glass rod 2 mm in diameter and 10 mm in length. Calibration by Baldwin-Farmer secondary standard chamber at energies of 23, 29, and 34 keV.</p>	<p>The dose measured in the phantoms was used to estimate the genetically significant dose and leukemia significant dose from diagnostic medical x-ray examinations in Japan.</p>
James (1974)	<p>Mix D phantom of variable thicknesses and weight (Table 3). Thermoluminescent dosimeters and Victoreen ionization chamber.</p>	<p>The maximum skin dose and whole-body dose in different type x-ray examinations were given (Tables 4,5).</p>

---

the particular technique used. Second, there is very little information available on mean bone marrow dose from these examinations in children. However, many data are available for adults (James, 1974).

The present project was intended to supplement existing data by performing dosimetric measurements on improved phantoms more closely simulating dimensions and organ sizes of children aged one and five years.

To estimate and predict accurately the effect of radiation equivalent dosages and to indicate methods which would minimize unnecessary radiation exposure, phantoms were designed and fabricated to represent one-year-, and five-year-old children. These phantoms were used to assess the medical x-ray absorbed dose to different critical organs and tissue during exposure situations typical of pediatric radiology.

The purpose of this study, therefore, has been to perform an indepth dosimetric analysis of the field of diagnostic pediatric radiology. In this study the following tasks were undertaken:

1. Perform a careful literature review of pediatric diagnostic radiology to identify typical diagnostic procedures to be studied, expected absorbed doses to critical organs, and any followup studies that may link subsequent ill-health to the effects of the radiation exposure.

2. Installation and calibration of an x-ray machine for use in this study. The machine was designed previously (Stansbury, 1977). The author has taken part in the installation of the machine and shared the responsibility of calibrating it before use.



3. Construction of phantoms representing children of one- and five-years.
4. Design of experiments for in-bone dosimetry measurements.
5. Measurement of x-ray spectra from the x-ray machine for typical diagnostic procedures.
6. Calibration of dosimetric devices for use in the experimental phases of the research.
7. Measurement of the absorbed doses to selected tissues and organs in the one- and five-year-old phantom during simulated diagnostic procedures.
8. Calculation of the absorbed doses to selected tissues and organs in the phantoms for situations representing, as closely as possible, the experimental arrangement.
9. Comparison of theoretical and experimental results.
10. Reevaluation of dose estimates currently available in the literature for certain critical organs of the body and the relation of these estimates to the published cancer risk factors for exposure to ionizing radiation.

## CHAPTER II

### THEORY

#### X-Ray Generation

When a target substance is bombarded by high speed electrons, x rays are produced. The spectrum of these x rays can be resolved by means of a crystal spectrometer. Usually the heterogeneous beam of x rays from the target is found to consist of two distinct spectra: a continuous spectrum and a sharp line spectrum superimposed on the continuous spectrum. The two distinctively different spectra from the same target have different origins. The sharp line spectrum is produced by the energy changes which take place as a result of rearrangement of the electrons in various electronic energy levels of the atoms of the x-ray target following the transfer of energy to the atom by the bombarding electrons. The continuous spectrum, on the other hand, results from the radiation emitted by the electrons as they are accelerated and decelerated in the Coulomb force field of the nuclei of the target atoms. The continuous x-ray spectrum also is called bremsstrahlung radiation.

According to electrical theories of classical physics, an electron will generate an electromagnetic wave when subjected to such an acceleration or deceleration. In Figure 1, an electron is assumed to travel along the line OX with velocity  $\vec{v}$  until it strikes the atoms of

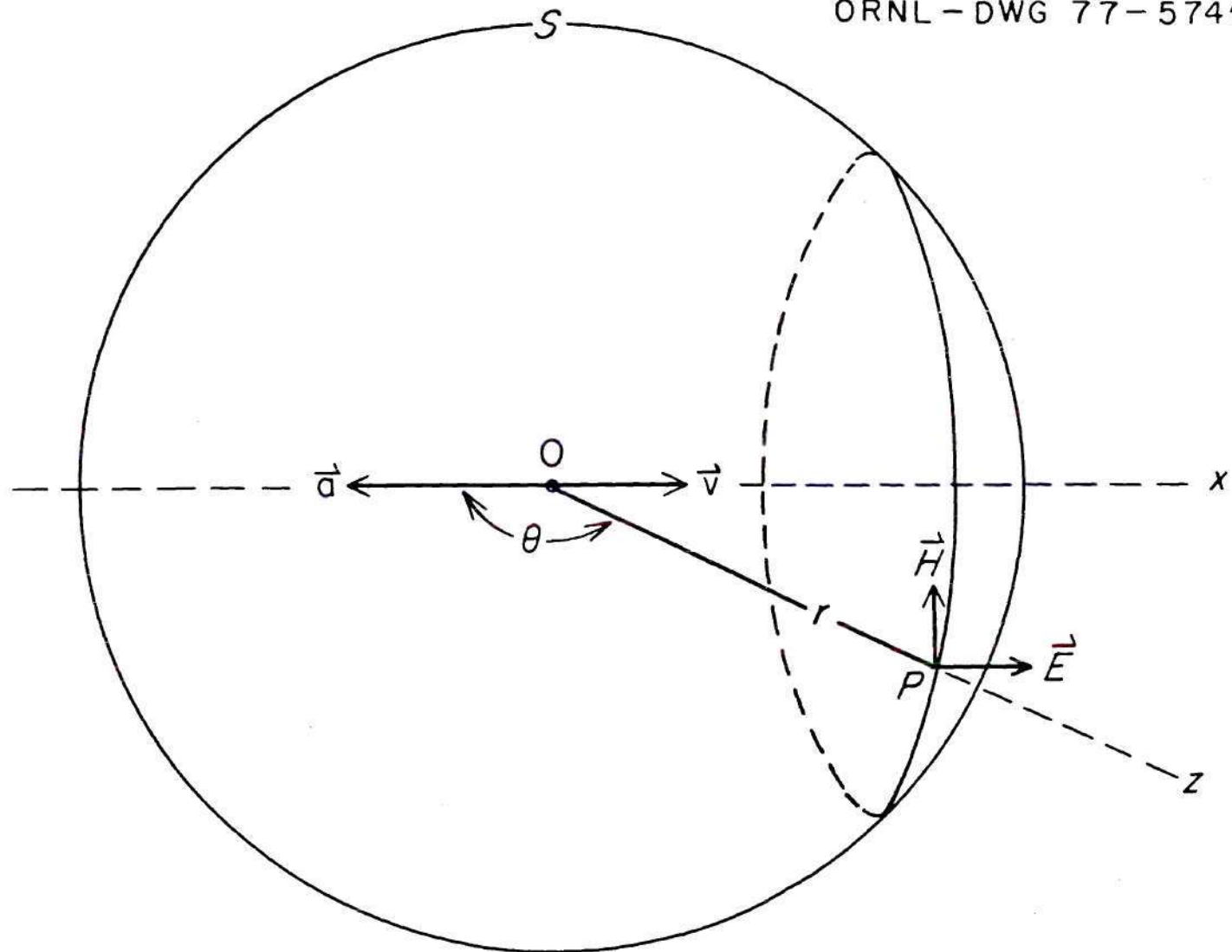


Figure 1. Illustration of the Theory of Continuous X-Ray Generation.

the target. The electron experiences a deceleration  $\vec{a}$  in the opposite direction. Based on classical theory, the electromagnetic wave (both  $\vec{E}$  and  $\vec{H}$  vectors) will be emitted in all directions with the velocity of light,  $c$  (in vacuum). The intensity of the emitted electromagnetic wave is function of angle  $\theta$ . It has a maximum value at right angles to vector  $\vec{a}$  ( $\theta = \pm 90^\circ$ ) and a minimum value in the parallel direction with vector  $\vec{a}$  ( $\theta = 0^\circ$  or  $180^\circ$ ). After  $r/c$  sec, the position of wave front will be represented by the sphere  $S$  of radius  $r$  with center at  $O$ . If an arbitrary direction  $\vec{OP}$  is selected which makes an angle  $\theta$  with the direction of vector  $\vec{a}$ , the electric field intensity at  $P$ , where  $OPZ$  pierces the sphere  $S$ , is represented by the vector  $\vec{E}$ .  $\vec{E}$  is perpendicular to  $OZ$  and lies in the plane  $XOZ$ . The associated magnetic field is represented by the vector  $\vec{H}$ .  $\vec{H}$  is perpendicular to the plane  $XOZ$ . Calculations based on classical electrodynamics lead to the result

$$\vec{E} = \vec{H} = \frac{\vec{a}e}{rc^2} \sin \theta \quad (2-1)$$

where

$\vec{E}$  = electric field intensity, in e.s.u.

$\vec{H}$  = magnetic field, in gauss.

$\vec{a}$  = the acceleration of electron, in  $\text{cm/sec}^2$ .

$e$  = the charge of electron, in e.s.u.

$r$  = the distance  $OP$ , in cm.

$c$  = the velocity of light, in  $\text{cm/sec}$ .

$\theta$  = the angle between  $OP$  and the velocity of electron  $\vec{v}$ .



These vectors  $\vec{E}$  and  $\vec{H}$  move along the line of travel OZ with velocity  $c$ , their magnitude decreasing inversely in proportion to their distance  $r$  from 0.

It is well known that the energy per unit volume space,  $w$ , through which the electromagnetic wave passes is

$$w \text{ (energy/cm}^3\text{)} = \frac{\vec{E}^2}{8\pi} + \frac{\vec{H}^2}{8\pi} \quad (2-2)$$

$$= \frac{\vec{E}^2}{4\pi} \text{ (in free space).}$$

This quantity multiplied by  $c$  gives the energy passing per second through  $1 \text{ cm}^2$  of an imaginary plane perpendicular to the direction of motion of radiation, which, of course, is the intensity  $I$  of the x rays.

$$I = \frac{a^2 e^2}{4\pi r^2 c^3} \sin^2 \theta \text{ (erg/cm}^2 \text{ - sec).} \quad (2-3)$$

It has been found that the x-ray intensity from a thin target varies with voltage and direction in a manner which is represented approximately by (2-3). Application of the special theory of relativity and quantum theory gives a more accurate expression for the intensity of the continuous x-ray spectrum (Scherzer, 1932).

Using an ionization chamber, Ulrey measured the intensity for the spectral distribution of x rays in 1918. A set of curves for x rays from a Coolidge tube with a tungsten target was obtained at different generating voltages. From those curves Ulrey found that the area under those curves, i.e., intensity of x rays, increased proportionally to the square of the x-ray tube voltage. This means that, over the ordinary voltage range used in x-ray work, the total intensity of the continuous x-ray radiation generated in the tube, considering all wavelengths, increases with the square of the voltage when other things, such as the tube current, remain constant. That is

$$I = KV^2, \quad (2-4)$$

where

$I$  is the intensity of the x-ray beam,

$K$  is  $kZ$ ,  $k$  being a proportionality constant and  $Z$  being the atomic number of the target, and

$V$  is the generating potential.

Since, in diagnostic medical radiology, characteristic x rays are not of interest, the detailed theory of characteristic x rays will not be given here.

#### Photon Interactions with Matter

Generally, electromagnetic radiation, including x rays, interacts with matter through several different processes. In these processes,

the energy of electromagnetic radiation (or photons) can be removed from the incident beam by a single or a series of events. The events may involve absorption, in which the photon completely disappears, or scattering, in which the direction of the photon and perhaps its energy is changed. The absorption and scattering of a narrow or collimated beam of electromagnetic radiation leads to an exponential decrease in intensity with path length.

There are three major interaction processes, the photoelectric effect, the Compton effect, and pair production, that contribute significantly to the absorption of photon energy. A fourth process, coherent scattering, also occurs in which the scattered photon has the same wavelength as the incident photon but different direction. The relative probabilities for the various processes depend on the properties of the material with which the photon interacts and the energy of the photon regardless of its source.

For the four most abundant elements in human tissue, hydrogen, oxygen, carbon, and nitrogen, the coherent scattering process is negligible in comparison to the other photon interaction processes unless the photon energy is lower than 30 keV (Neufeld et al., 1967). Except for low energy photons or interaction with high Z material, the scattering angles are small.

In the low energy photon region (below 20 keV) the photoelectric effect is dominant in soft tissue. In this case, an incident photon interacts with the atomic system and loses its entire energy to one of the more tightly bound electrons. The electron (usually from the K or

L shell) is ejected from the atom with a kinetic energy  $T$  given by the Einstein relation:

$$T = h\nu - E_b \quad , \quad (2-5)$$

where

$T$  is the kinetic energy of ejected electron, in erg,

$h$  is Planck's constant equal to  $6.63 \times 10^{-27}$  erg-sec,

$\nu$  is the frequency of incident photon, in  $\text{sec}^{-1}$ , and

$E_b$  is the binding energy of ejected electron, in erg.

The angular distribution of the ejected electrons is given by

$$dn = \frac{\sin^2 \theta}{(1 - \beta^2 \cos^2 \theta)^4} d\Omega \quad , \quad (2-6)$$

where

$dn$  is the number of photoelectrons ejected into a small solid angle  $d\Omega$ ,

$\theta$  is the angle between the incident photon and ejected electron,

$\beta$  is  $v/c$ , the velocity ratio of the ejected electron to light.

In the intermediate photon energy region (20 keV to 1 MeV) the dominant photon interaction in soft tissue is the Compton effect which is incoherent scattering by unbound electrons. If the energy of the incident photon is expressed as  $h\nu$ , the scattered photon is emitted at some angle  $\theta$  with an energy of  $h\nu'$  and the electron recoils with kinetic



energy  $T$ . This reaction may be expressed by the relations:

$$\frac{1}{h\nu'} - \frac{1}{h\nu_0} = \frac{1}{m_0 c^2} (1 - \cos \theta) \quad (2-7)$$

and

$$T = h\nu_0 - h\nu' , \quad (2-8)$$

where  $m_0$  is the rest mass of the electron and  $c$  is the velocity of the light.

The angular distribution of the scattered photons is given by the Klein-Nishina formula:

$$d\sigma = \frac{\gamma_0^2}{2} \left( \frac{\nu'}{\nu_0} \right)^2 \left[ \frac{\nu_0}{\nu'} + \frac{\nu'}{\nu_0} - \sin^2 \theta \right] d\Omega , \quad (2-9)$$

where  $d\sigma$  is the collision differential cross section, which refers to the number of photons that are scattered in a small solid angle  $d\Omega$  having an angle  $\theta$  with incident photon, and

$$\gamma_0 = \frac{e^2}{m_0 c^2} , \quad (2-10)$$

where  $e$  is the charge of the electron.

When the energy of the incident photon is much greater than 1.02 MeV, the important process by which electromagnetic radiation is absorbed by matter becomes pair production. A photon, interacting with the electric field surrounding a charged particle, is completely absorbed and in its place appears an electron-positron pair whose total energy is just equal to the incident photon energy  $h\nu$ . This incident energy is beyond the range of interest here.

In this study, the energy range of photons considered is 10 keV to 130 keV. This range was chosen because it includes most of the photons generated in diagnostic x-ray practice (USPHS, 1973). For those elements which are most abundant in tissue, hydrogen, oxygen, carbon and nitrogen, the photoelectric effect is dominant below 20 keV. In the energy region between 20 keV to 130 keV, the dominant interaction is the Compton effect.

When an x-ray beam passes into an absorbing medium such as body tissues the energy of the beam is converted into chemical potential energy that can result in biological changes. The sequence of events is illustrated in Figure 2 (Johns and Cunningham, 1974). The initial step in the process is the collision between one photon and an electron in the body. This interaction may be a photoelectric or a Compton interaction, each of which sets in motion a high speed electron. In traveling through the tissue, the high speed electron produces a track along which ionizations occur, excitation of atoms and molecules takes place, and molecular bonds are broken. All of these processes can result in biological damage. Most of the energy, however, is converted into

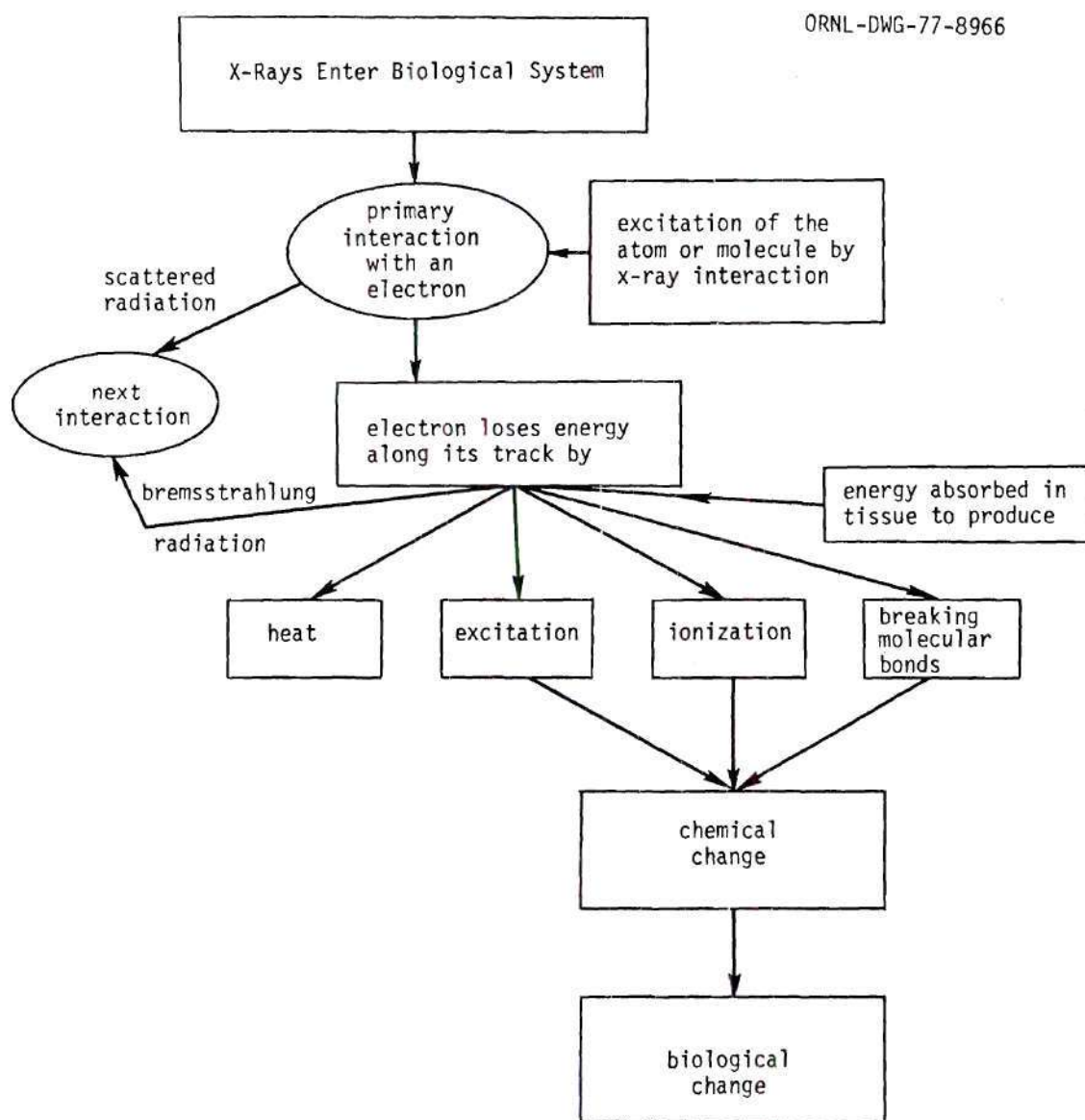


Figure 2. X-Ray Beam Absorption in a Biological System.

Source: Johns and Cunningham, 1974.

heat, producing little biological damage. Typically, some 30 interactions are required before all the energy of the photon is converted into electronic motion (Johns and Cunningham, 1974).

Radiation damage depends on the absorption of energy from radiation and is considered to be proportional to the absorbed energy in tissue. The concentration of absorbed energy in tissue depends on the mass energy absorption coefficient. Bone, which consists of higher-atomic-number-elements, such as calcium and phosphorous (which have higher mass energy absorption coefficients than soft tissue), absorbs more energy from an x-ray beam, per unit mass of absorber than does tissue. Usually, the intensity of x-ray field is expressed by the quantity "exposure" and its special unit, the Roentgen (R), which specifies the amount of energy transferred from the x-ray field to a unit mass of air. However, in most cases, the primary interest is the energy absorbed in tissue. When electronic equilibrium exists the measurement of exposure can be converted to absorbed dose in tissue by:

$$D = 0.869 \frac{(\mu(E)/\rho)_t}{(\mu(E)/\rho)_{\text{air}}} \times \quad (2-11)$$

where

$D$  is the absorbed dose, in rad,  
 $(\mu(E)/\rho)_t$  is the mass energy absorption coefficient of tissue  
 which depends on the energy of the interacting x ray,  
 in  $\text{cm}^2 - \text{gm}^{-1}$ ,



$(\mu(E)/\rho)_{\text{air}}$  is the mass energy absorption coefficient of air  
 which depends on the energy of the interacting x ray,  
 in  $\text{cm}^2 - \text{gm}^{-1}$ , and

X is the exposure, in R.

If the x-ray energy spectrum at the position of interest is known,  
 the absorbed dose can be obtained by multiplying the exposure by the  
 suitable conversion factor  $\frac{(\mu(E)/\rho)_t}{(\mu(E)/\rho)_{\text{air}}}$ .

### Theory of the Monte Carlo Method

#### Introduction

The Monte Carlo method is a statistical approach to the prediction of interaction rates and energy distributions in a large system such as the human body or a phantom. One may estimate the dose to various organs of the body from a source of photons incident on the body by following a large number of them, in a statistically valid fashion, until they are absorbed in the system or scattered out of the system. Using known physical laws and probabilities, it is possible to obtain an estimate of a physical function, such as absorbed dose, or of the fraction of absorbed energy. Thus, basically the Monte Carlo method involves an interesting combination of random sampling theory, physical law (simulated photon histories), and numerical analysis. The real problems are: Given a function, is there a stochastic process which yields a distribution such that it, or some set of its parameters, includes the physical quantities which we desire to know? If so, what is an

efficient method of obtaining these statistical results and a meaningful way of interpreting them?

### Random Number

When a Monte Carlo calculation is performed many "random numbers" are always involved. A random number is a particular value of a sequence of numbers which appear to be drawn at random from particular probability distributions. The random number generator is an indispensable part in all Monte Carlo calculations. Many different methods have been introduced and used to produce random numbers (Hall, 1962; Jansson, 1966). Generally, these methods can be placed into one of three categories: (1) monitoring the output of some dice-like or other physical devices; (2) drawing samples from specially constructed tables (Kendall, 1939; Rand, 1965); or (3) calculation using a specified mathematical algorithm. The first category is rarely used, because the sequence of generated numbers cannot be reproduced, thus making the retracing of the exact steps of the calculation impossible. The second category is seldom used in present day Monte Carlo calculations because the storage of tables in a computer memory system and the calling of entries one at a time is a very inefficient way to utilize a computer. The third category actually does not produce random numbers at all. This category does, however, produce numbers which, in many respects, behave like random numbers. Since these numbers have a completely predictable sequence of numbers or digits, the term "pseudo-random numbers" is often used to describe numbers produced by such deterministic methods. In fact, the

third category is the most important method used to obtain random numbers at the present. For example, Lehmer (1951) introduced the "multiplicative congruential" method to generate pseudo-random number sequences by the formula:

$$T_i \equiv kT_{i-1} \pmod{m} \quad (2-12)$$

where

$i = 1, 2, 3 \dots$ ,

$T_i$  = the  $i^{\text{th}}$  random number,

$k$  = an arbitrary constant, and

$T_{i-1}$  = the  $(i - 1)^{\text{th}}$  random number.

The relation  $a \equiv b \pmod{c}$  simply means that the ratio  $a/c$  and  $b/c$  have the same remainder. For a given seed number  $T_0$  and some constant  $k$ , the first random number  $T_1$  is obtained by multiplying the seed number  $T_0$  by the constant  $k$ . To obtain the second random number  $T_2$ , multiply the constant  $k$  by the seed number  $T_1$ , repeat the process using the number just generated in place of the seed number, and so on.

One characteristic of the pseudo-random number generated by mathematical algorithm methods is that after a certain number of distinct elements have been produced, the sequence begins to repeat itself, the number of distinct digits produced being called the period. The period of a given pseudo-random number generator must have an acceptable length for its intended purpose. Also the pseudo-numbers have to pass reasonable randomness tests such as moments test, the

frequency test, serial test, poker test, and gap test (Kendall, 1939).

### Probability Distribution Function and Cumulative Distribution Function

The probability is defined as the likelihood of occurrence of any particular form of an event, estimated as the ratio of the number of ways in which that form might occur to the total number of ways in which the event might occur in any form. The distribution of the ratio is called a probability distribution function. Generally, the probability distribution functions are of two types, continuous and discrete. Since both types can be dealt with in a similar way, only the continuous type will be described here.

Let  $x$  be a stochastic variable and  $f(x)$  be a continuous probability distribution function for  $a \leq x \leq b$ , then  $f(x)dx$  is the probability of  $x$  lying between  $x$  and  $x + dx$ . We may also define the cumulative distribution function  $F(x)$  as:

$$F(x_0) = \int_a^{x_0} f(x)dx \quad x \leq x_0 \quad . \quad (2-13)$$

$F(x)$  is always a nondecreasing function and it is assumed that  $F(a) = 0$  and  $F(b) = 1$ .

### Translation between the Different Probability Distribution Functions and Different Cumulative Distribution Functions

Let  $x$  be a stochastic variable and  $y = \phi(x)$ , a function of  $x$  which determines  $y$  uniquely. The variable  $y$  is then a stochastic



variable and the distribution of  $y$  can be derived from the distribution of  $x$ . Let the cumulative distribution function of  $y$  be  $G(y)$ . If  $y = \phi(x)$  is an increasing function the inequalities  $x \leq x_0$  and  $y = \phi(x) \leq \phi(x_0) = y_0$  will always be satisfied simultaneously so that (Hald, 1952):

$$G(y_0) = F(x_0) . \quad (2-14)$$

If  $y = \phi(x)$  is a decreasing function, we get

$$G(y_0) = 1 - F(x_0) \quad (2-15)$$

i.e., the two cumulative distribution functions take on the same values for corresponding values of the variable.

Usually we have a method of generating the uniform probability distribution function of a random number and its cumulative distribution function. Also we can equate the cumulative distribution of a random number with other cumulative distribution functions associated with the physical phenomenon in which we are interested. From this equality we find the stochastic variable  $x$  as a function of the random number. For example, suppose that the probability distribution function which determines the first collision distance for photon interactions with matter is (Cashwell and Everett, 1959)

$$f(x) = \Sigma e^{-\Sigma x} \quad 0 \leq x < \infty \quad (2-16)$$

Here  $\Sigma$  is the total cross section of collision and  $x$  is the first collision distance. The probability for the first collision to occur between 0 and  $x_0$  is

$$\begin{aligned} F(x_0) &= \int_0^{x_0} f(x) dx \\ &= \int_0^{x_0} \Sigma e^{-\Sigma x} dx \\ &= 1 - e^{-\Sigma x_0} \end{aligned} \tag{2-17}$$

Suppose the random number has the uniform probability distribution  $g(r) = 1$  for  $0 \leq r < 1$ , then the cumulative distribution function of the random number  $r$  is

$$\begin{aligned} G(r) &= \int_0^{r_0} 1 dr \\ &= r_0 \end{aligned} \tag{2-18}$$

Equalizing the two cumulative distribution functions, equations (2-17) and (2-18), we get:

$$1 - e^{-\Sigma x_0} = r_0 \tag{2-19}$$

and

$$x_0 = \frac{-1}{\Sigma} \ln(1 - r_0) \tag{2-20}$$

Because  $r_0$  is uniform on  $0 \leq r_0 < 1$ , then  $1 - r_0$  is equidistributed and we simply use

$$x_0 = \frac{-1}{\Sigma} \ln r_0 . \quad (2-21)$$

The Monte Carlo calculation uses the distance  $x_0$  from point of departure to the collision site as one bit of data determining a photon history. A random walk process can be defined for individual photons. Hence a large number of photon histories must be generated by a random walk and this is essentially the Monte Carlo process. In the present study a sample size of 50,000 photons histories was used as a compromise between adequate precision and a reasonable limitation on computer time.

#### The Monte Carlo Technique Applied to Dose Calculations

The average photon energy delivered to a given target region or to a point region can be determined using Monte Carlo techniques. Random sampling techniques are used to simulate the entire sequence of scattering and absorption events that follow the emission of each source photon. Such a sequence is known as a history of the photon and each history consists of a number of successive photon interactions. Thus, Monte Carlo calculations provide a direct means of determining the typical x-ray energy deposition in phantoms from photon emitters, either internal or external to the body.

Usually photon histories are determined using the mass-attenuation coefficients,  $\mu_{pe}(E)$ ,  $\mu_c(E)$  and  $\mu_{pp}(E)$ , for the

photoelectric, Compton and pair-production interaction, respectively. These coefficients are calculated from atomic attenuation coefficients and composition. For the first step of the procedure, an initial attenuation coefficient,  $\mu_0(E)$ , is selected which is greater than or equal to those of any of the regions, i.e., skeletal, lung, and the remainder of the phantom (Warner, 1968). A potential site for an interaction is chosen by the procedure of first taking a distance traversed,  $x_0$ , defined as

$$x_0 = \frac{1}{\mu_0(E)} \ln r_0 , \quad (2-22)$$

where  $r_0$  is a random number uniformly distributed between 0 and 1. The coordinates of a point at this distance (from the departure point) are tested to determine its location in the phantom; this region is designated as  $i$ . One then plays a game of chance with probability  $\mu_i(E)/\mu_0(E)$  of acceptance of this as an interaction site where  $\mu_i$  is the total mass attenuation coefficient for the region  $i$ . If the outcome of the game is favorable, this site is accepted, then the second random number  $r$  is generated to determine the scattering angle and energy; if it is unfavorable, the photon is allowed to continue with the same direction and energy, but beginning at point  $i$ . In addition to scattering, the photon has a finite probability of absorption which predominates at low energies. Thus, very few photons will penetrate to large distances, and therefore, the statistics of the estimates will



be poor (Warner, 1968). To compensate partially for this, each photon is given a statistical weight that initially is set at unity. With each Compton scattering interaction, this weight is reduced to allow for the probability of survival, and the photon is allowed to continue. The reduction of weight is expressed by

$$W_n = W_{n-1} \frac{\mu_c(E_{n-1})}{\mu(E_{n-1})} \quad (2-23)$$

in which  $W_n$  is the weight carried by the photon after the  $n^{\text{th}}$  collision and  $\mu_c(E_{n-1})$  and  $\mu(E_{n-1})$  are the coefficients for Compton scattering and the total coefficient before the  $n^{\text{th}}$  collision, respectively.

This reduction of the weight carried by the photon is equal to the expectation of Compton scattering which the photon would have in the actual physical processes. The total flight history of a photon is terminated: (1) if it escapes from the phantom; (2) if its energy falls below 4 keV; or (3) if its weight falls below  $10^{-5}$ ; in the latter two cases, the energy is considered to be absorbed locally.

The energy deposition for the  $n^{\text{th}}$  interaction is

$$E_n^* = W_{n-1} \left[ \frac{\mu_{pe}(E_{n-1})}{\mu(E_{n-1})} E_{n-1} + \frac{\mu_c(E_{n-1})}{\mu(E_{n-1})} (E_{n-1} - E_n) + \frac{\mu_{pp}(E_{n-1})}{\mu(E_{n-1})} (E_{n-1} - 2m_0c^2) \right] \quad (2-24)$$

in which  $\mu_{pe}(E_{n-1})$ ,  $\mu_c(E_{n-1})$  and  $\mu_{pp}(E_{n-1})$  are the mass-attenuation coefficients for the photoelectric, Compton, and pair production processes before the collision at the site considered, respectively, and  $m_0c^2$  is the rest mass energy of an electron. It should be noted that the total energy of the photon is absorbed locally when a photoelectric interaction occurs, and this is also the case for the kinetic energy of the electron and positron produced by pair production. The positron will be annihilated, and two photons of energy  $m_0c^2$  ( $\approx 0.511$  MeV) will be emitted. The computer code is designed to take account of these photons since a new photon of energy 0.511 MeV with weight

$$2 W_{n-1} \frac{\mu_{pp}(E_{n-1})}{\mu(E_{n-1})} \quad (2-25)$$

and random orientation is started at the site of the pair production and followed independently afterward. Since the energy of the diagnostic medical x ray is much lower than the threshold energy (1.022 MeV) of pair production, this process will not be considered here. Also no procedure has been used to account for the finite range of the electrons produced. Generally, these ranges are small compared with the diameter of most organs and the absorbed dose will not change abruptly with distance except at an interface where the composition and density change, or at the boundary of the source organ. At such an interface, the number of photon interactions per unit volume

may change abruptly, but changes in absorbed dose will be somewhat less abrupt due to the finite range of the secondary particles. No attempt has been made here to estimate boundary effects.

Bremsstrahlung may be considered as a further example of a secondary form of radiation which may have an extended range, and may be followed using Monte Carlo methods. But this has not been done, because the probability of producing a photon with an energy approaching the kinetic energy of the electron is rather small—although greater than zero—and, the total energy accounted for by bremsstrahlung is very small in tissue of the human body (Snyder et al., 1969; Ellett et al., 1968).

### CHAPTER III

#### EXPERIMENTAL APPARATUS AND PROCEDURES

##### Phantom Design and Fabrication

Mathematical descriptions (phantoms) representing one-year-old and five-year-old children have been designed (Hwang et al., 1976) in a manner similar to the adult phantom of Fisher and Snyder (1967). These representations were assumed to be in a Cartesian coordinate system. Physical representations of these mathematical child phantoms were constructed for use in this research. The body of each was represented as erect with the positive z axis directed upward toward the head, the positive x axis is directed to the phantom's left, and the positive y axis is directed toward the posterior side of the phantom. The origin of the coordinate system is taken at the center of the base of the "trunk" section of the phantom. Outer dimensions of the one-year-old and five-year-old phantoms are shown in Figures 3 and 4, respectively.

Volumes for the whole bodies of children represented by these phantoms were calculated from the available data of specific gravity and weight (Snyder et al., 1975) as a function of age. The specific gravity for the one-year-old child was found to be 1.017 and that for the five-year-old child was 1.019. Specific gravities for children tended to be lower than those for adults. The mathematical representation of a one-year-old child had a weight of 10.4 kg and was 76 cm in



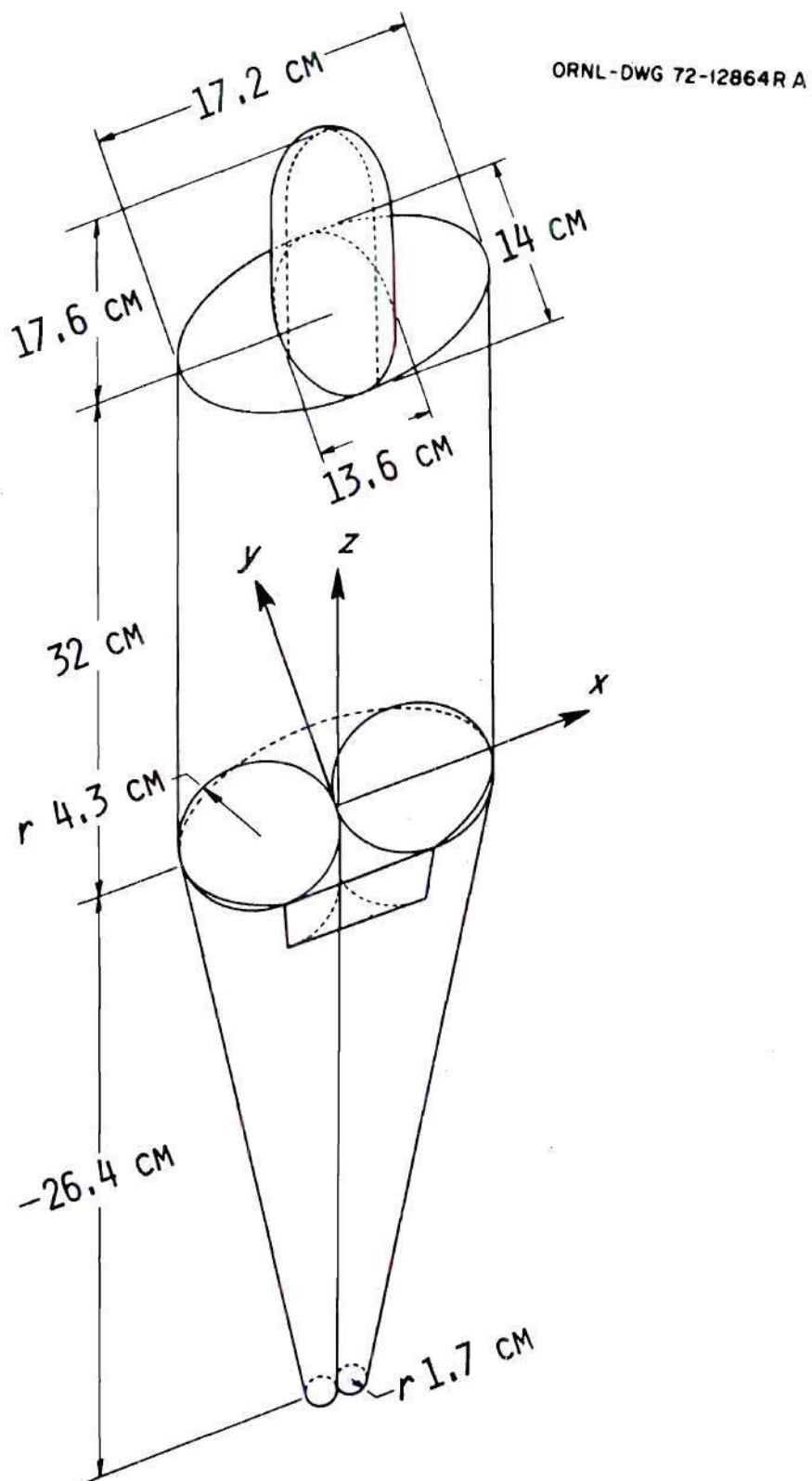


Figure 3. Dimensions and Coordinate System of the One-Year-Old Phantom.

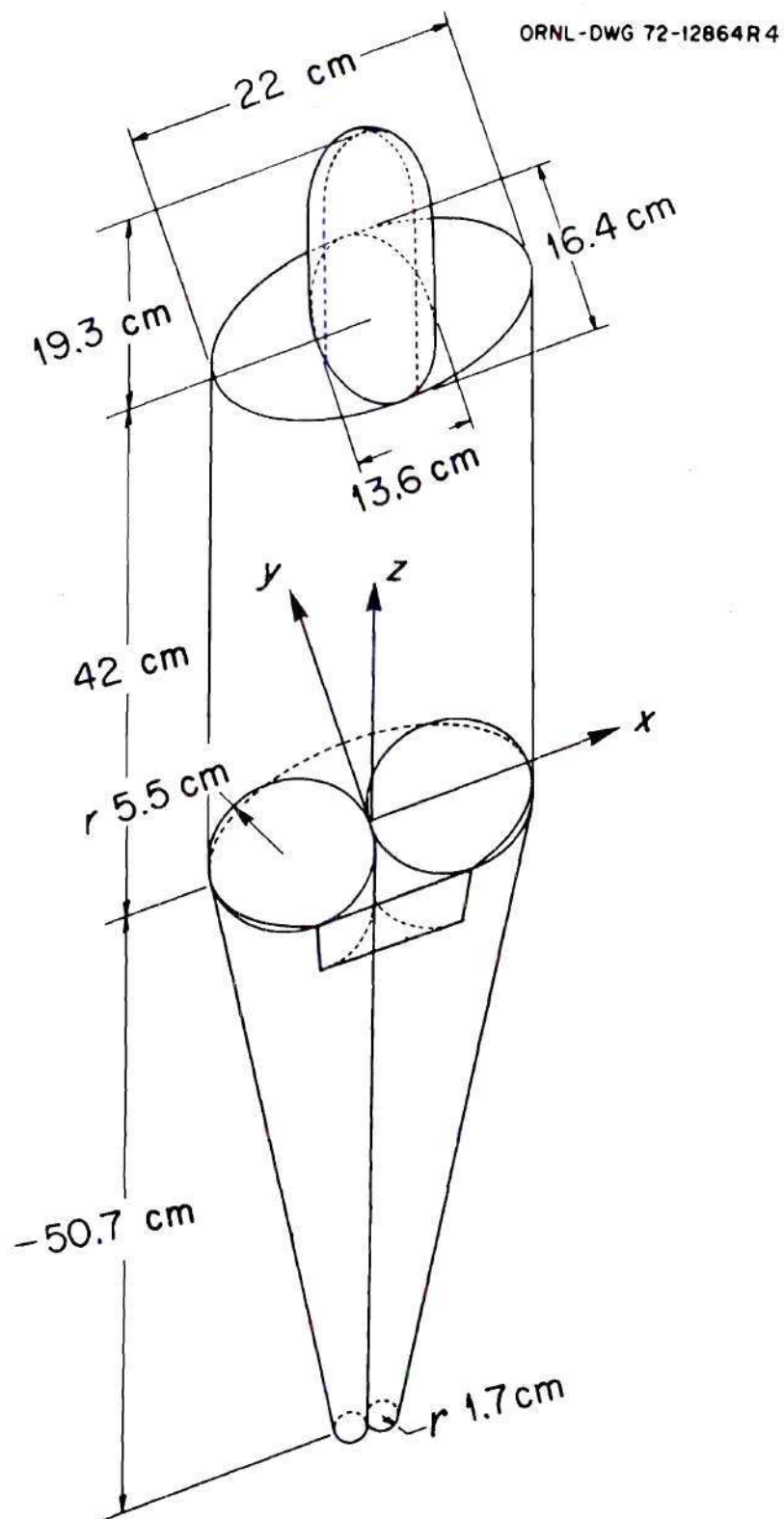


Figure 4. Dimensions and Coordinate System of the Five-Year-Old Phantom.

height, while the five-year-old child had a weight of 20 kg and was 112 cm in height. Once the total size of the body was established, the volume of each part—head, trunk, arms, and legs—was partitioned. The volume percentages of the different parts of the total volume were different for each of the different ages. The head section was 25.5% and 16.2% of the total volume for a one-year-old and a five-year-old child, respectively. The trunk section was 50% and 52.3% of the total volume for a one-year-old and five-year-old, respectively. The leg section was 15.5% and 23% of the total volume for a one-year-old and five-year-old child, respectively. The remaining volume was assigned to the arms, 9% for a one-year-old and 8.5% for a five-year-old. In designing the phantoms, the volumes for the trunk and arms were composited and referred to as the volume of the trunk section. For all these sections the circumference of each section was found in the anatomical references (Snyder et al., 1975); all of the remaining dimensions were then determined to fit within the assigned volumes.

Figure 5 shows an anterior view of some of the larger organs and their position in the phantoms. The representations of the organs by mathematical equations are only approximate, since the goal in constructing these organs mathematically was to obtain the approximate size and shape of an average organ through the use of a few simple mathematical equations. If the size and shape approximated those of the real organ, the dose estimate should be correspondingly accurate. However, to minimize computer running time and thus the cost, the formulas used were as simple as possible. The detailed description of

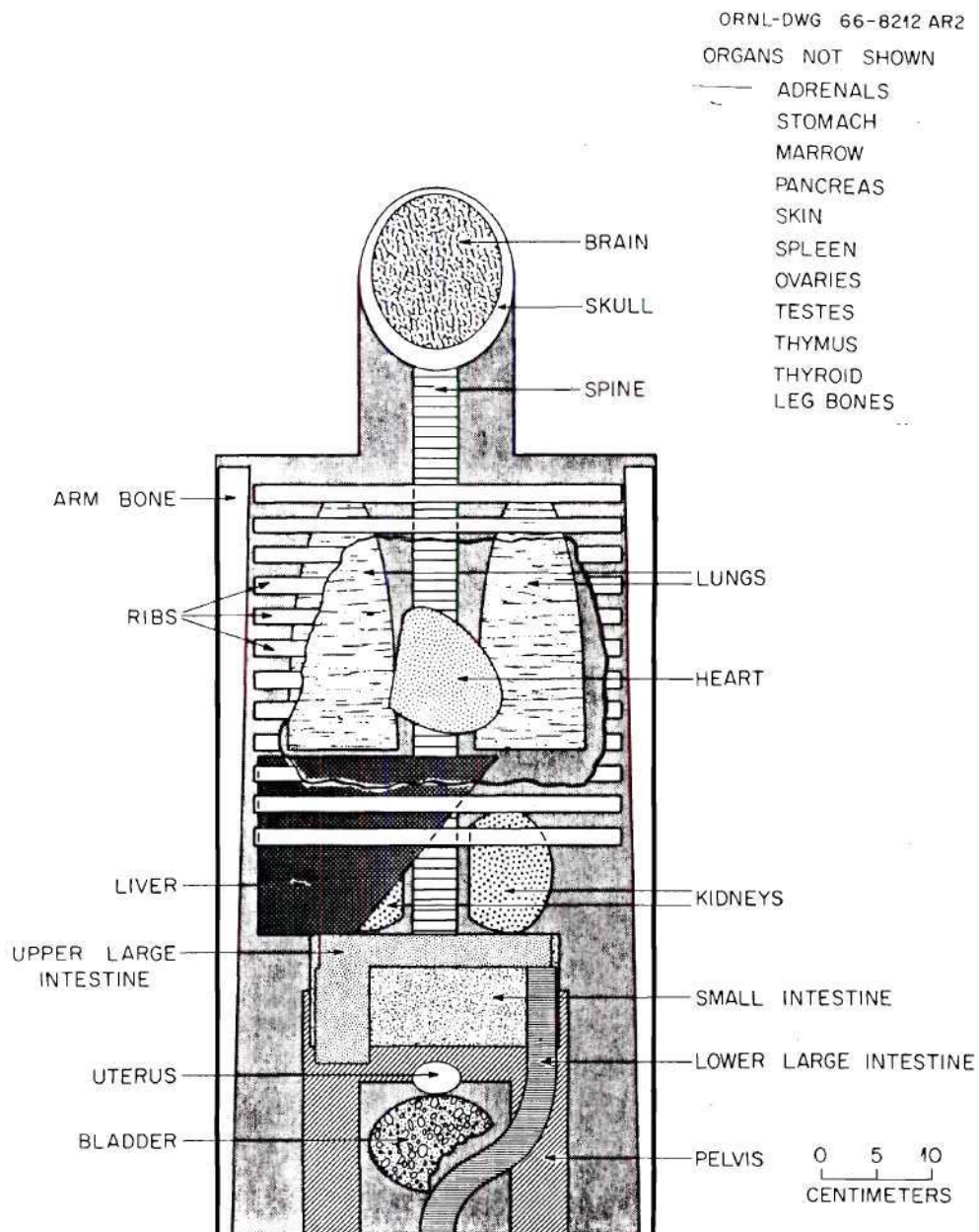


Figure 5. Anterior View of the Principal Organs in the Head and Trunk of the Child Phantoms Used for the One-Year-, and Five-Year-Old.



the mathematical equations describing the child phantoms are given by Hwang et al. (1976).

In order to check the proper position of the organs and organ shape and that no two organs overlap, the mathematical descriptions for these phantoms were coded and checked with a computer plotting program. The plot routine simply scans diagonally back and forth in a specified plane of the phantom using the mathematically encoded geometries of the organ. Some of the plots are shown in Appendix A, Figures A-1 through A-12. Both X-Z and X-Y cross section plots are shown and give a pictorial image of the mathematical construct. Cross-section plots such as these also were extremely valuable in that they provided drawings which facilitated the construction of the physical phantoms.

Physical representations of the mathematical phantom described above are shown in Figures 6-14. Exterior shells of the phantoms were fabricated from Lucite in three principal, separable regions: (1) an elliptical cylinder topped by half an ellipsoid containing the head and neck (see Figure 7); (2) an elliptical cylinder containing the arms, torso, and hips (see Figure 8); and (3) two truncated circular cones containing both legs and the feet and attached to this is a small region with a plane front surface to contain an approximation to the testicles (see Figure 9). The physical representations of the skeleton of the mathematical phantom were fabricated from Lucite and polystyrene (see Figures 10 and 11). To make in-bone dosimetry possible, each major skeletal region was designed to have detector probes which were used to

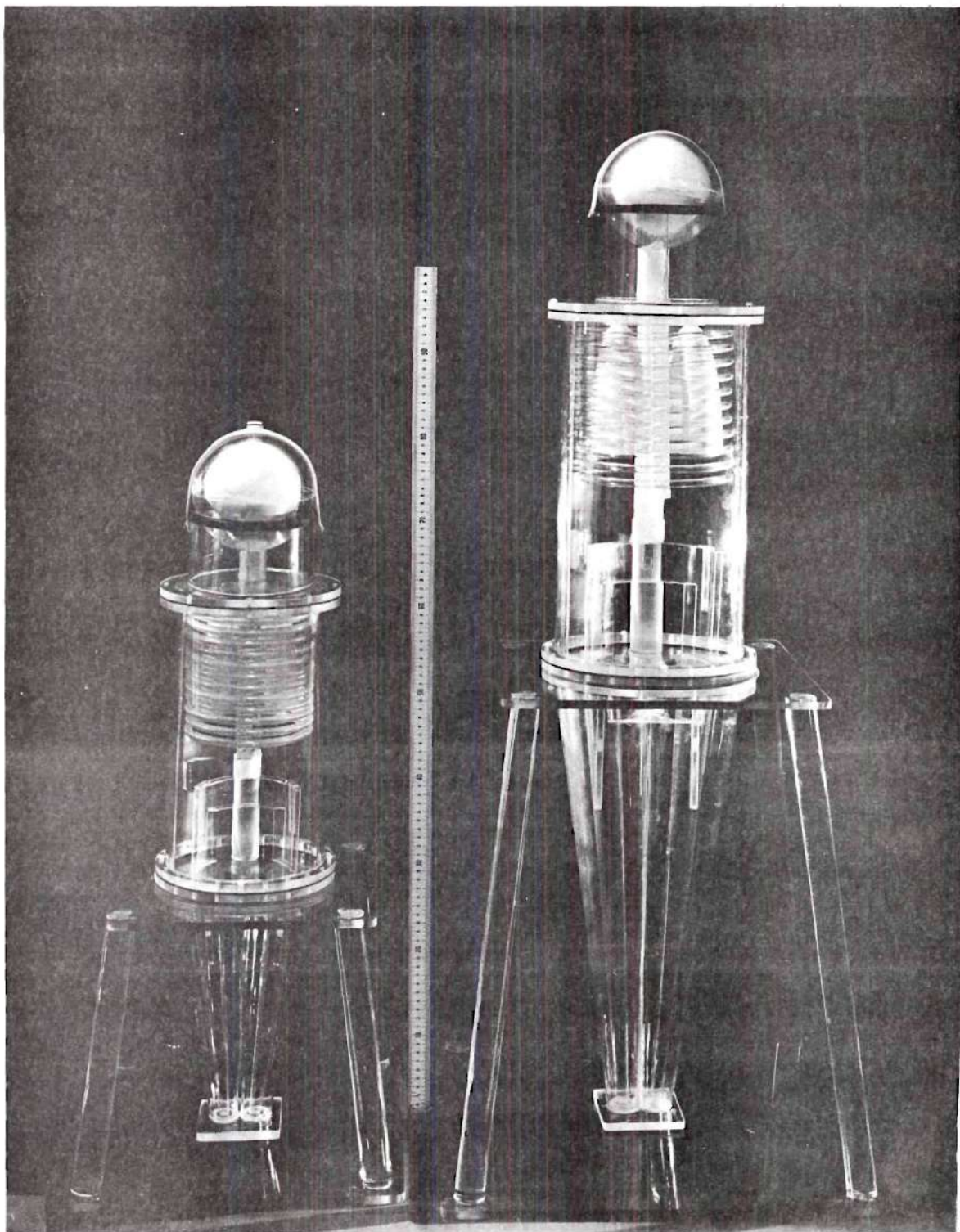


Figure 6. The One-Year-, and Five-Year-Old Phantoms.





Figure 7. The Head Regions of the One-Year-, and Five-Year-Old Phantoms.

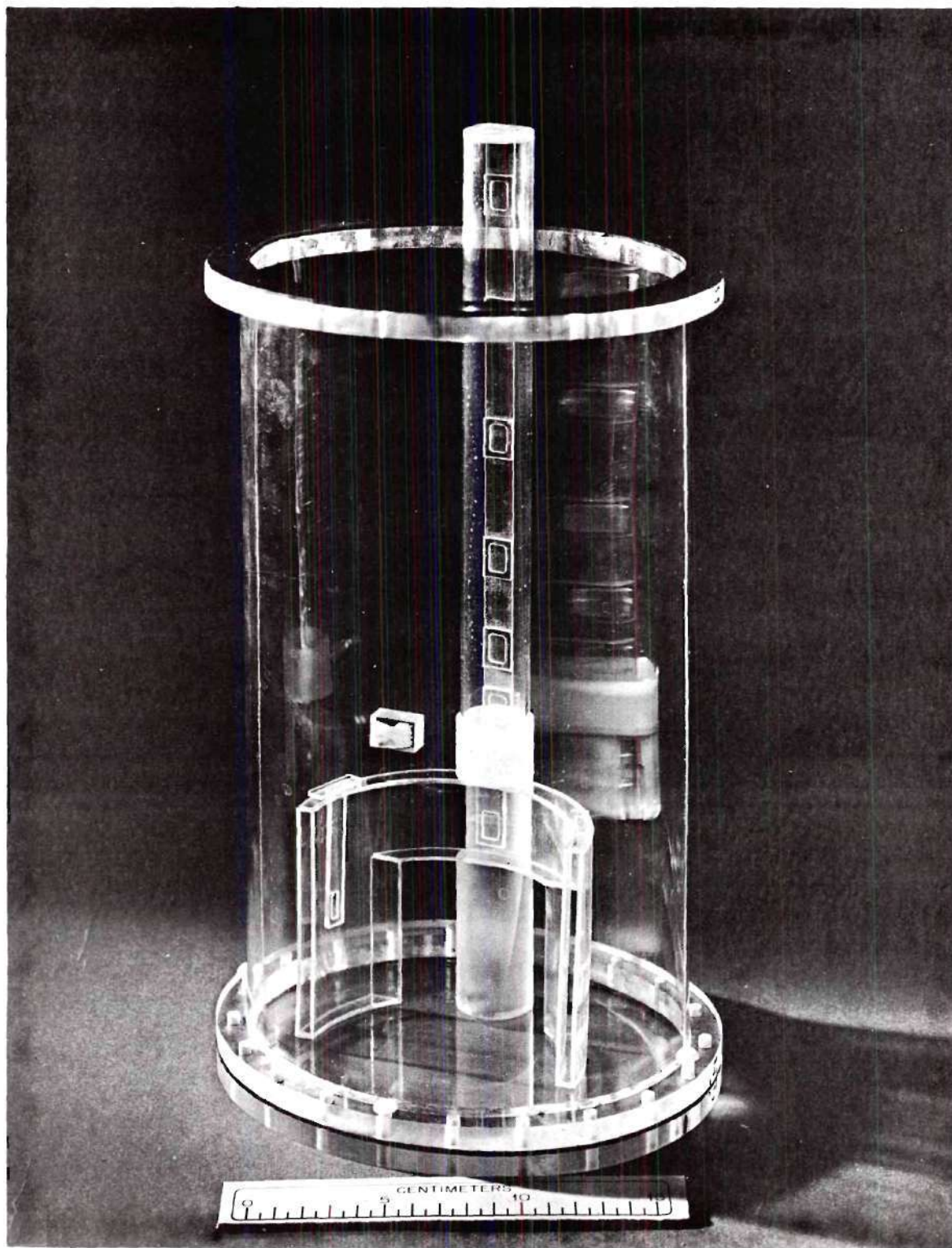


Figure 8. The Trunk of the One-Year-Old Phantom.



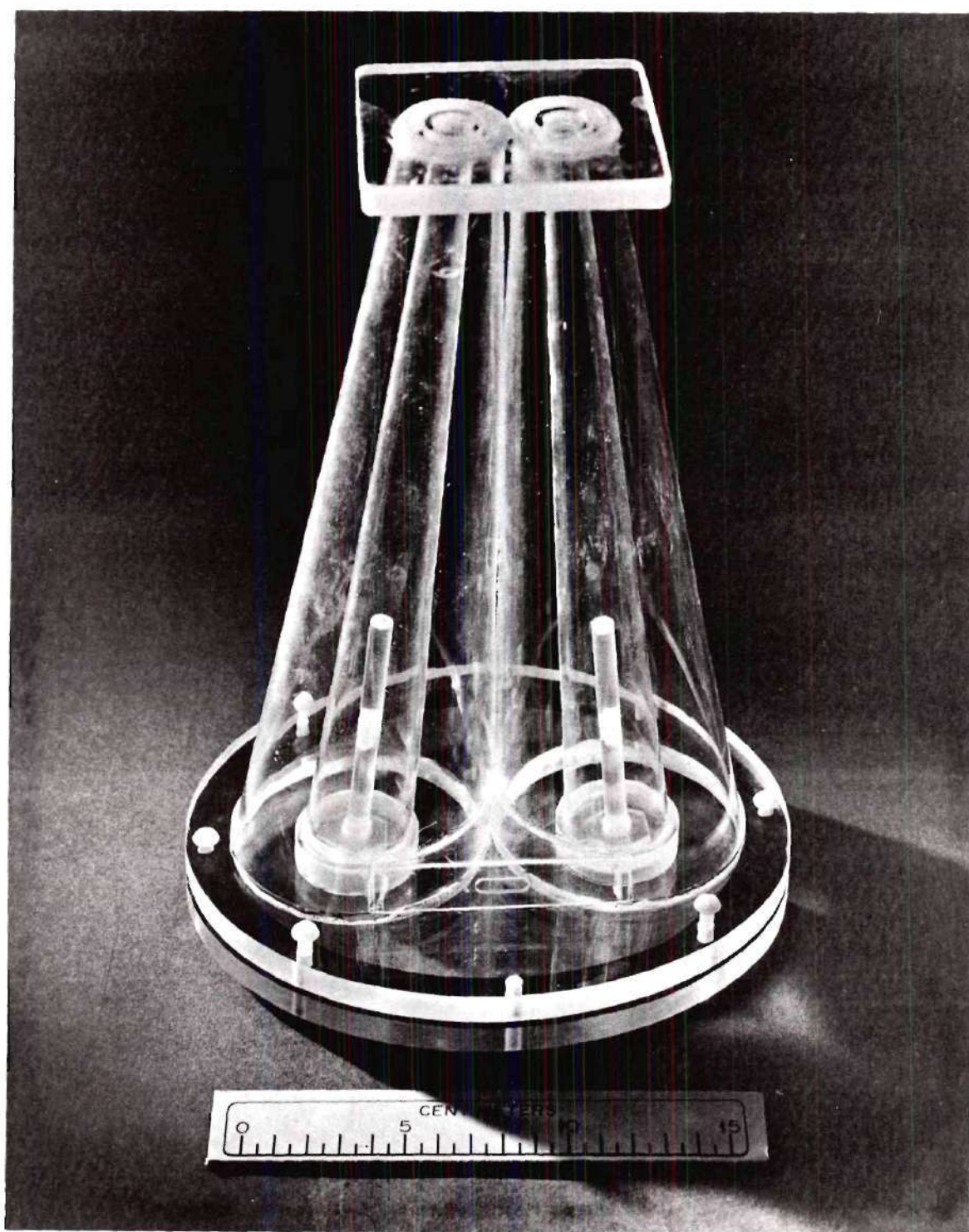


Figure 9. The Legs and Genitalia Region of the One-Year-Old Phantom.

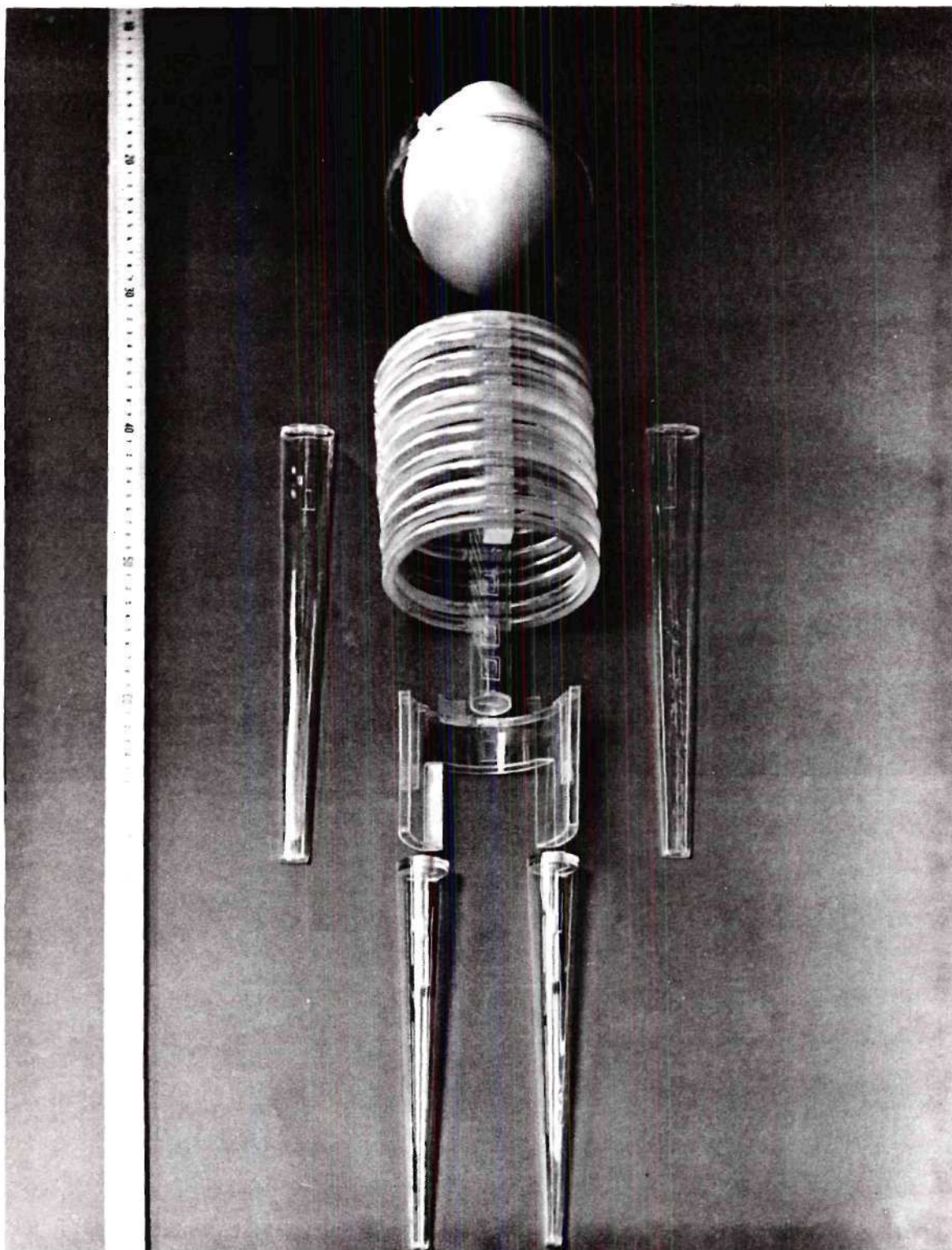


Figure 10. The Skeleton of the One-Year-Old Phantom.



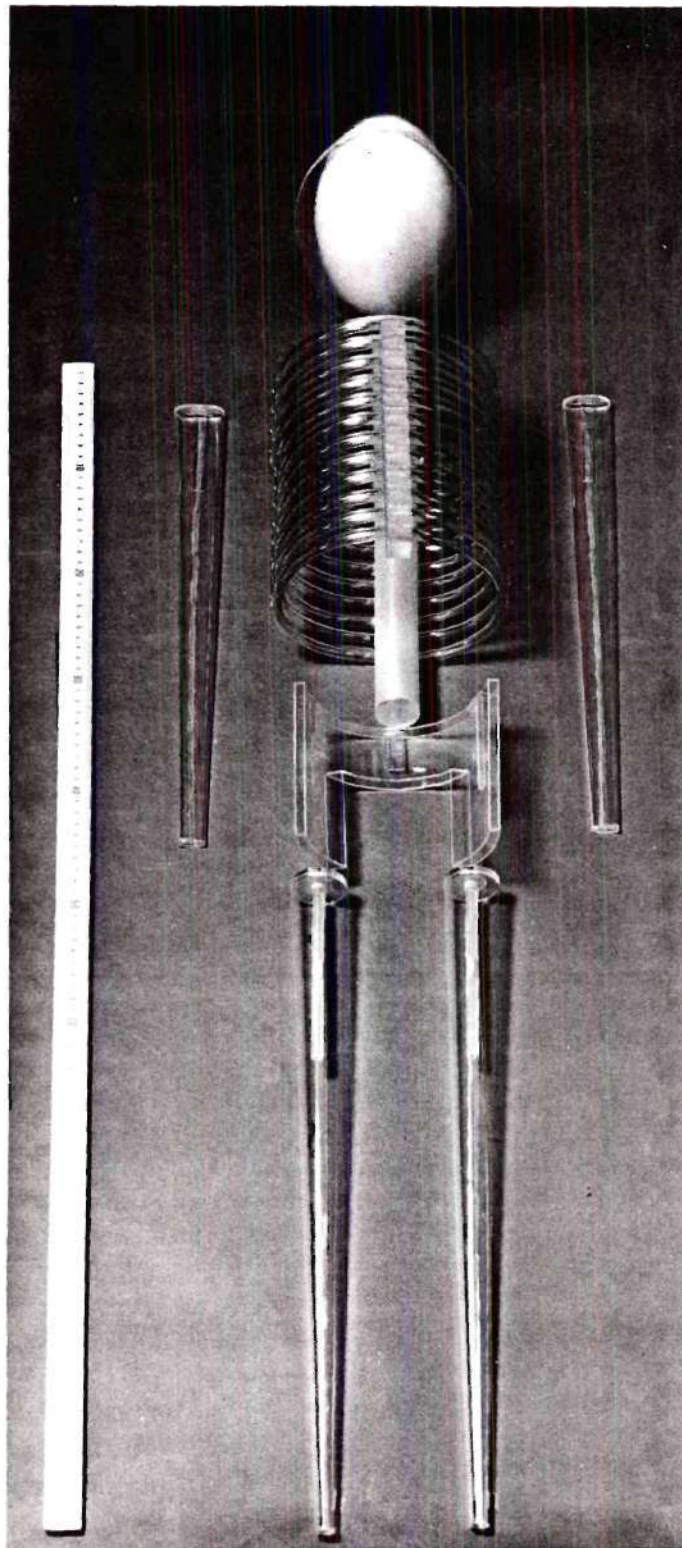


Figure 11. The Skeleton of the Five-Year-Old Phantom.

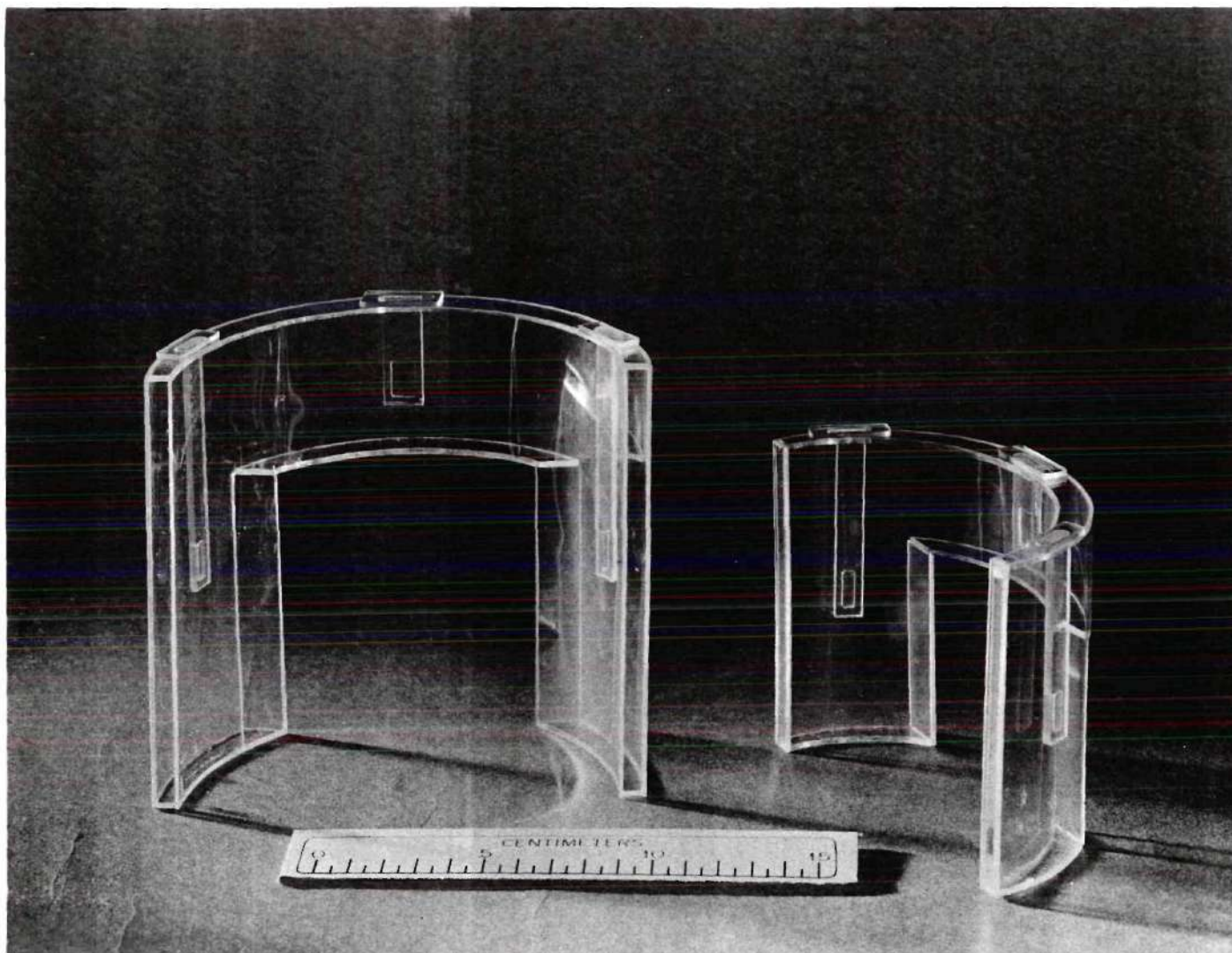


Figure 12. The Pelvis of the One-Year-, and Five-Year-Old Phantoms.



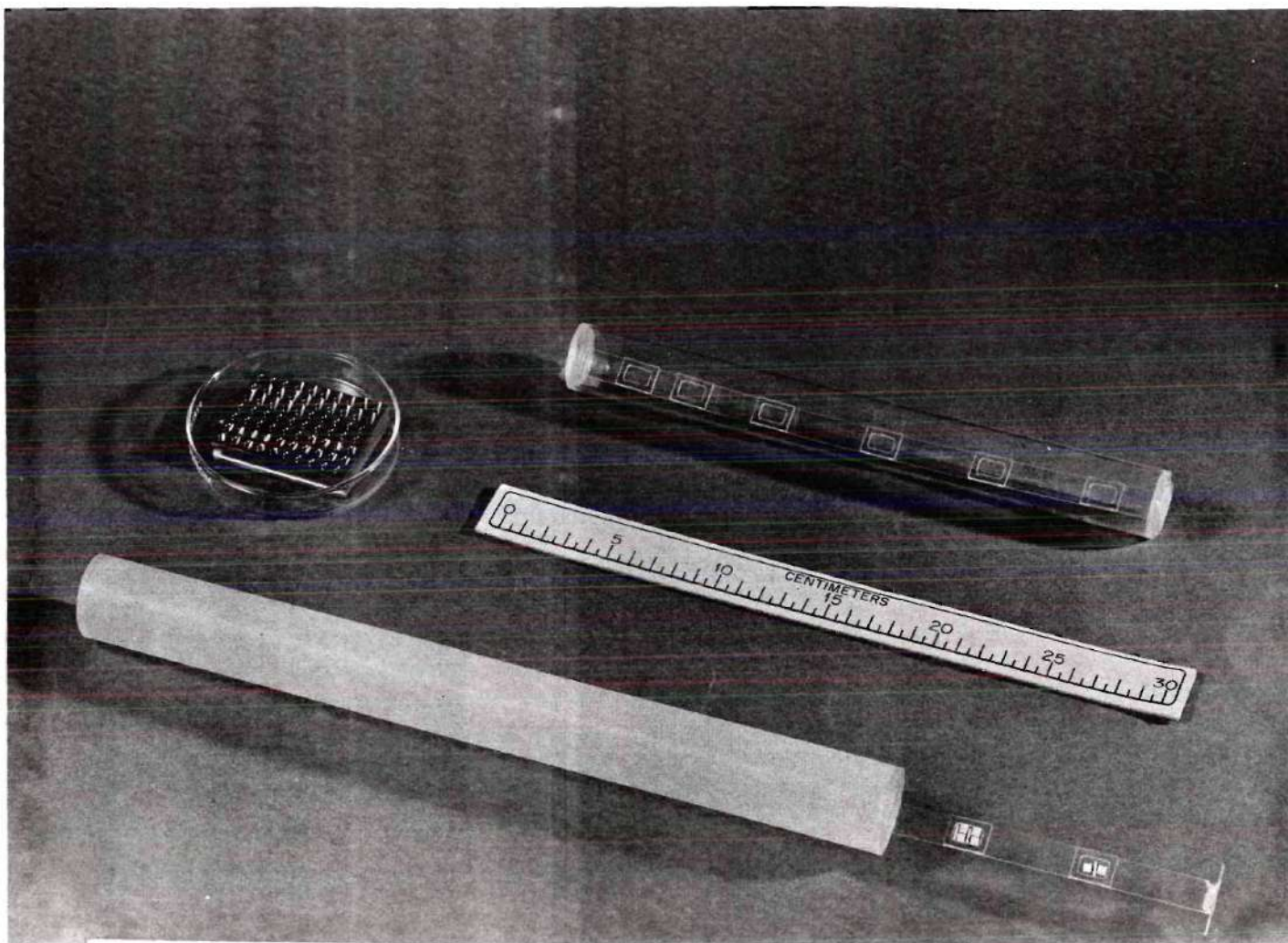


Figure 13. The Spines of the One-Year-, and Five-Year-Old Phantoms, Detector Probes, and TLD Holder.

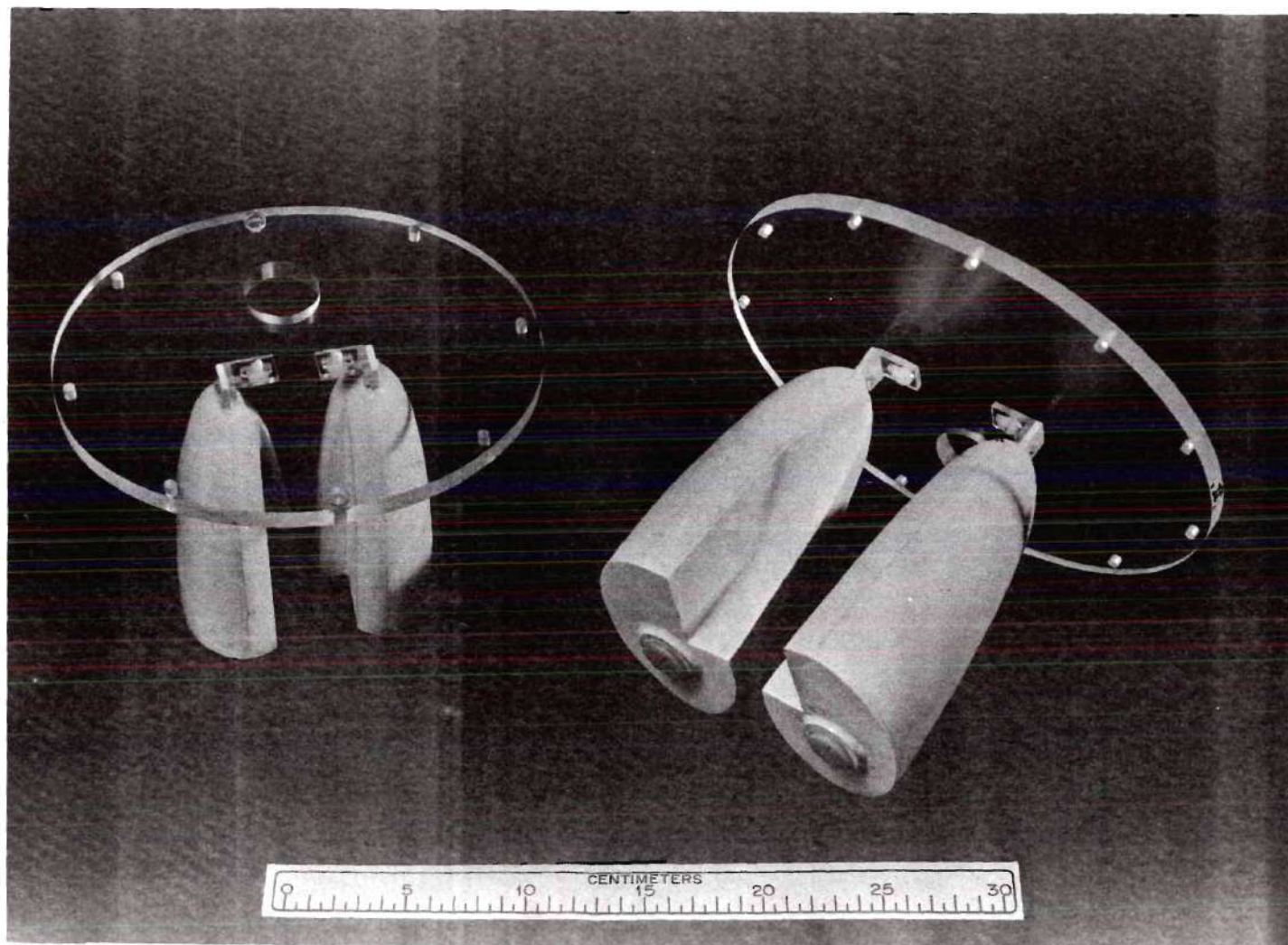


Figure 14. The Lungs of the One-Year-, and Five-Year-Old Phantoms.



hold thermoluminescent detectors inside the bone (see Figures 8, 12, and 13). Exterior shells of the lungs were fabricated from polystyrene (see Figure 14). The lung regions were attached rigidly beneath the top cover of the trunk region.

After the phantoms were fabricated, the subregion volumes of the physical phantoms were compared to the subregion volumes of the mathematical phantoms. The results are shown in Tables 8 and 9. For most subregion volumes the percentage differences were within  $\pm 5\%$  for the five-year-old phantom. However, for the one-year-old phantom, the subregion volume differences generally were large ( $\pm 10\%$ ). This is probably due to the difficulty in fabricating the small volumes representing these regions in the one-year-old child.

#### Phantom Material Evaluation

The chemical composition for most phantom materials is not actually the same as that for human tissue. In fact, most human tissues differ significantly in chemical composition from each other. However, assuming the interaction of photons are nearly independent of small changes in the chemical composition of tissue materials, one may represent human tissue by reproducing the elemental composition (% weight by element) (Snyder et al., 1975). The mean atomic composition of various biological molecules is readily available in the scientific literature (Spector, 1956; Long, 1961) and the mean atomic composition of human tissues can be calculated from these data. Frequently, for dosimetric experiments related to biological systems, the biological materials are replaced by a substitute because of ease of handling,

Table 8. Comparison of Subregion Volumes of the Physical and Mathematical Phantom—One-Year-Old

Region	Mathematical Phantom Volume (cm <sup>3</sup> )	Physical Phantom Volume (cm <sup>3</sup> )	Percent Difference <sup>a</sup> (%)
Head	2609.00	2535.00	-2.84
Brain	977.00	863.00	-11.67
Trunk	6052.00	7112.30	17.52
Legs	1586.00	1710.49	7.85
Genitalia	12.00	13.50	12.50
Skull	489.00	520.00	6.34
Spine	130.00	135.60	4.31
Ribs	97.70	99.00	1.33
Pelvis	89.76	85.10	-5.19
Arm bones	104.00	109.20	5.00
Leg bones	219.00	213.40	-2.56
Lungs	429.40	421.50	-1.84
Total Soft Tissue	8700.14	9777.49	12.38
Total Skeleton	1129.46	1162.30	3.79
Total Volume	10259.00	11361.29	10.75

$$^a \text{Percent Difference} = \frac{V_{\text{phys.}} - V_{\text{math.}}}{V_{\text{math}}} \times 100\%.$$



Table 9. Comparison of Subregion Volumes of the Physical and Mathematical Phantom—Five-Year-Old

Region	Mathematical Phantom Volume (cm <sup>3</sup> )	Physical Phantom Volume (cm <sup>3</sup> )	Percent Difference <sup>a</sup> (%)
Head	3170.80	3020.00	-4.76
Brain	1146.00	990.63	-3.56
Trunk	11901.60	12545.00	5.41
Legs	4511.80	4651.47	3.10
Genitalia	37.86	36.00	-4.91
Skull	542.00	554.00	2.21
Spine	258.00	273.60	6.05
Ribs	212.80	198.20	-6.86
Pelvis	174.43	180.30	3.37
Arm bones	181.20	180.00	-0.66
Leg bones	588.00	506.30	3.11
Lungs	850.00	844.50	-0.65
Total Soft Tissue	16815.63	17415.60	3.57
Total Skeleton	1956.43	1992.40	1.84
Total Volume	19622.06	20252.50	3.21

$$^a \text{Percent Difference} = \frac{V_{\text{phys.}} - V_{\text{math.}}}{V_{\text{math.}}} \times 100\%.$$

availability, mechanical properties, or physical state (such as solid, liquid, or gaseous). Ideally, the substituted material should have the same number of photon absorption events and scattering events as the natural material it replaces. The energy absorption in a given material can be calculated by means of well-established formulas, if certain constants are known. These necessary constants are the effective atomic number and the electron density of the material. Theoretical considerations of energy absorption, based on calculated values of the effective atomic numbers of typical carbohydrates, fats, and proteins, have been published by Mayneord (1937). The effective atomic number is defined as:

$$\bar{Z} = \left[ \sum_i a_i Z_i^{2.94} \right]^{\frac{1}{2.94}}, \quad (3-1)$$

where

$\bar{Z}$  is the effective atomic number of the compound,

$i$  is the number of the individual elements in the compound,

$a_i = \frac{W_i Z_i}{A_i} / \sum_i \frac{W_i Z_i}{A_i}$  is the fractional electron content of the  $i^{\text{th}}$  element in the compound,

$W_i$  is the fraction, by weight, of the individual elements in the compound,

$Z_i$  is the atomic number of the  $i^{\text{th}}$  element in the compound, and

$A_i$  is the atomic weight of the  $i^{\text{th}}$  element in the compound.

When the effective atomic number of a compound is known, the mass absorption coefficient of the compound can be calculated as

$$\frac{\mu(E)^x}{\rho} = n_0 \left[ {}_e\sigma(E) + k\bar{Z}^{2.94} \cdot \lambda^3 \right], \quad (3-2)$$

where

$\frac{\mu}{\rho}$  is the mass absorption coefficient of the compound, in  $\text{cm}^2 - \text{gm}^{-1}$ ,

$n_0$  is the number of electrons per gm in the compound,

${}_e\sigma(E)$  is the Compton scatter-absorption coefficient per electron,

$k = 2.64 \times 10^{-26}$  is a constant (Walter, 1929) for the photoelectric absorption,

$\bar{Z}$  is the effective atomic number of the compound, and

$\lambda$  is the wavelength of interacting photons, in  $\text{\AA}(10^{-8} \text{ cm})$ .

If the mass attenuation and mass absorption coefficient of the individual elements in a mixture are known, then the total mass attenuation and mass absorption coefficient of the mixture can be calculated by using the "mixture rule." This states, that for a mixture or compound,

$$\frac{\mu}{\rho} = \sum_i w_i \left( \frac{\mu}{\rho} \right)_i, \quad (3-3)$$

where

$\frac{\mu}{\rho}$  is the total mass attenuation or absorption for the compound,  
 $i$  is the number of elements in the compound,  
 $W_i$  is the fraction by weight of the  $i^{\text{th}}$  element, and  
 $\left(\frac{\mu}{\rho}\right)_i$  is the individual mass attenuation or absorption coefficient  
of the  $i^{\text{th}}$  element.

The absorbed dose, in rad, is given by the equation

$$D(\text{rad}) = \psi \times E \times \frac{\mu}{\rho} \times 0.01 \frac{\text{rad} \cdot \text{gm}}{\text{erg}}, \quad (3-4)$$

where

$D$  is the absorbed dose,

$\psi$  is the fluence of interacting photons, in  $\text{cm}^{-2}$ ,

$E$  is the energy of interacting photons, in ergs, and

$\frac{\mu}{\rho}$  is the mass energy absorption coefficient, in  $\text{cm}^2 \cdot \text{gm}^{-1}$ .

One method of evaluating the photon equivalence of one material with another is to compare the densities of the two materials, the total mass attenuation coefficient, and total mass absorption coefficient over the range of energies of photons which are present in the material. To aid in the selection and evaluation of tissue equivalent materials a program, TECALC (Stansbury, 1974), was used. The elemental composition of the pediatric phantoms was compared with those of the Snyder-Fisher Phantom (Reference Man) in Table 10.



Table 10. Description of Snyder-Fisher Phantom Subregions and the Pediatric Phantom Equivalents<sup>a</sup>

	Soft tissue		Skeleton		Lung <sup>e</sup>	
	Snyder-Fisher <sup>b</sup>	Equivalent <sup>c</sup>	Snyder-Fisher <sup>b</sup>	Equivalent <sup>d</sup>	Snyder-Fisher <sup>b</sup>	Equivalent <sup>b</sup>
Elemental composition, %						
H	10.474	11.26	7.036	6.47	10.208	9.78
C	23.020	18.36	22.793	19.15	10.008	11.11
N	2.339		3.865	3.94	2.802	
O	63.206	69.38	48.559	52.98	75.958	77.61
Na	0.128	0.393	0.315	0.17	0.190	0.59
Mg	0.016		0.111	0.18	0.008	
P	0.236		6.937	6.80	0.081	
S	0.221		0.169	0.01	0.230	
Cl	0.141	0.607	0.139		0.270	0.91
K	0.208		0.145		0.200	
Ca			9.914	10.30	0.007	
Fe	0.006		0.008		0.037	
Zn	0.005		0.010		0.002	
Density, g/cm <sup>3</sup>	1.0	0.99 ± 0.01	1.5	1.50 ± 0.01	0.3	0.30 ± 0.01

<sup>a</sup>Stansbury, 1977.

<sup>b</sup>Composition given here is the same as given in MIRD Pamphlet No. 5 except that all elements with atomic number greater than zinc are considered zinc.

<sup>c</sup>Made from 66% H<sub>2</sub>O, 25% isopropyl alcohol, 8% sucrose, and 1% NaCl.

<sup>d</sup>Made from bone flour, water sucrose, and salts. (Ga74).

<sup>e</sup>Made from 73.5% H<sub>2</sub>O, 25.0% cellulose (sponge), and 1.5% NaCl.

Tables 11-13 give the partial mass-attenuation coefficients of the phantom substitute materials and their comparisons with the coefficients calculated for Snyder-Fisher Phantom specifications. In most cases the coefficients agree within  $\pm 1\%$ . The coefficients calculated for the Snyder-Fisher Phantom were used in the Monte Carlo computer program to simulate the photon transport process inside the phantom.

Some of the more useful phantom or dosimetry materials and their important dosimetrical parameters, such as chemical composition, density, effective atomic number, and electron density, are presented in Appendix B, Tables B-1 through B-3, which can be used as a reference to select the phantom material in the phantom dosimetry study.

#### X-Ray Machine Calibration

Generally, the principal components that permit the control and operation of an x-ray machine are an x-ray tube, an autotransformer, a high-voltage transformer, a rectifier, a low-voltage transformer for filament current to the x-ray tube, and a choke coil to adjust the current supply to the filament. The relation of these parts is shown diagrammatically in Figure 15.

A great majority of x-ray tubes used today are the Coolidge x-ray tube, as shown in Figure 16. This tube is evacuated to the best vacuum attainable. The cathode of this tube consists of a spiral tungsten wire filament, which is inside a small metal cup, which can be heated to incandescence by passing an electric current through it. The surrounding

Table 11. Calculated Partial Mass Attenuation Coefficients for Snyder-Fisher Composition and Comparison<sup>a</sup> of Equivalent Material Used in the Pediatric Phantom—Soft Tissue<sup>b</sup>

Energy (keV)	Photoelectric		Coherent		Compton	
	Coefficient (cm <sup>2</sup> /g)	Comparison (%)	Coefficient (cm <sup>2</sup> /g)	Comparison (%)	Coefficient (cm <sup>2</sup> /g)	Comparison (%)
10	4.34	1.7	0.231	1.7	0.153	-0.7
15	1.18	1.5	0.132	1.6	0.176	-0.8
20	0.465	1.4	0.0862	1.6	0.186	-0.9
30	0.124	1.1	0.0513	1.6	0.192	-0.9
40	0.0485	1.0	0.0277	1.5	0.190	-0.9
50	0.0235	0.9	0.0187	1.5	0.185	-0.8
60	0.0130	0.8	0.0135	1.5	0.180	-0.8
80	5.12E-3	0.7	7.93E-3	1.5	0.169	-0.7
100	2.50E-3	0.6	5.20E-3	1.4	0.160	-0.7
150	6.96E-4	0.4	2.37E-3	1.4	0.141	-0.6
200	2.85E-4	0.3	1.34E-3	1.5	0.128	-0.6
300	8.40E-5	0.1	5.91E-4	1.5	0.111	-0.5
400	3.62E-5	0.1	3.30E-4	1.5	0.100	-0.6
500	1.92E-5	0.3	2.09E-4	1.6	0.0926	-0.6
600	1.15E-5	0.4	1.44E-4	1.6	0.0871	-0.6
800	5.36E-6	0.7	8.05E-5	1.7	0.0798	-0.8
1000	3.01E-6	0.9	5.13E-5	1.8	0.0751	-0.9

<sup>a</sup>Percent comparison of coefficients for equivalent material calculated as

$$100 \times \frac{(\mu/\rho)_{\text{equivalent}} - (\mu/\rho)_{\text{Snyder-Fisher}}}{(\mu/\rho)_{\text{Snyder-Fisher}}}$$

<sup>b</sup>Stansbury, 1977.

Table 12. Calculated Partial Mass Attenuation Coefficients for Snyder-Fisher Composition and Comparison<sup>a</sup> of Equivalent Material Used in the Pediatric Phantom—Skeleton<sup>b</sup>

Energy (keV)	Photoelectric		Coherent		Compton	
	Coefficient (cm <sup>2</sup> /g)	Comparison (%)	Coefficient (cm <sup>2</sup> /g)	Comparison (%)	Coefficient (cm <sup>2</sup> /g)	Comparison (%)
10	15.4	-1.2	0.327	1.5	0.143	-1.2
15	4.62	-0.9	0.192	1.4	0.164	-0.9
20	1.93	-0.8	0.126	1.4	0.174	-0.8
30	0.554	-0.6	0.0671	1.4	0.181	-0.6
40	0.267	-0.5	0.0416	1.4	0.179	-0.5
50	0.113	-0.5	0.0282	1.4	0.176	-0.5
60	0.0641	-0.5	0.0204	1.3	0.172	-0.5
80	0.0261	-0.5	0.0120	1.3	0.162	-0.5
100	0.0131	-0.5	7.90E-3	1.3	0.154	-0.5
150	3.76E-3	-0.6	3.61E-3	1.3	0.138	-0.6
200	1.57E-3	-0.6	2.04E-3	1.3	0.126	-0.6
300	4.73E-4	-0.6	9.02E-4	1.3	0.109	-0.6
400	2.06E-4	-0.6	5.02E-4	1.4	0.0981	-0.6
500	1.10E-4	-0.6	3.18E-4	1.4	0.0905	-0.6
600	6.66E-5	-0.5	2.19E-4	1.4	0.0848	-0.5
800	3.08E-5	-0.5	1.22E-4	1.4	0.0768	-0.5
1000	1.73E-5	-0.4	7.80E-5	1.5	0.0715	-0.4

<sup>a</sup>Percent comparison of coefficients for equivalent material calculated as

$$100 \times \frac{(\mu/\rho)_{\text{equivalent}} - (\mu/\rho)_{\text{Snyder-Fisher}}}{(\mu/\rho)_{\text{Snyder-Fisher}}}$$

<sup>b</sup>Stansbury, 1977.



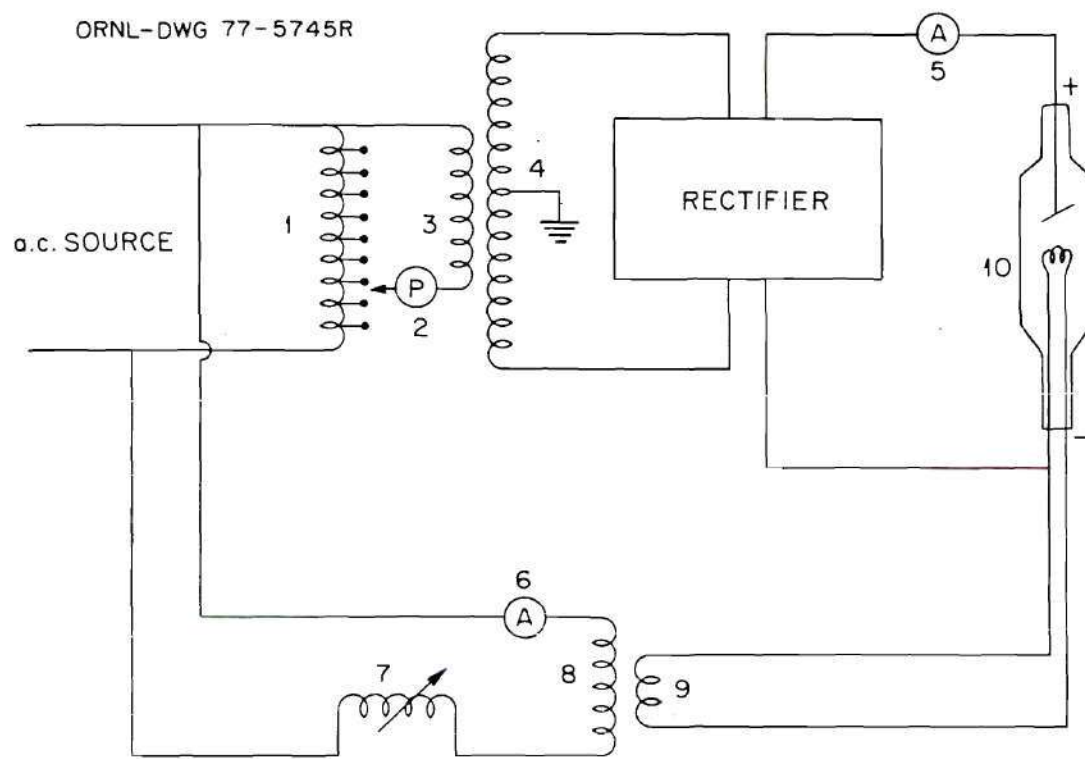
Table 13. Calculated Partial Mass Attenuation Coefficients for Snyder-Fisher Composition and Comparison<sup>a</sup> of Equivalent Material Used in the Pediatric Phantom—Lung<sup>b</sup>

Energy (keV)	Photoelectric		Coherent		Compton	
	Coefficient (cm <sup>2</sup> /g)	Comparison (%)	Coefficient (cm <sup>2</sup> /g)	Comparison (%)	Coefficient (cm <sup>2</sup> /g)	Comparison (%)
10	4.85	1.4	0.246	1.0	0.152	-0.8
15	1.33	1.3	0.141	1.0	0.176	-0.7
20	0.524	1.2	0.0918	1.0	0.186	-0.6
30	0.140	1.0	0.0480	1.0	0.192	-0.5
40	0.0549	0.8	0.0295	1.0	0.190	-0.5
50	0.0266	0.7	0.0199	1.0	0.185	-0.5
60	0.0147	0.6	0.0143	1.0	0.180	-0.5
80	5.81E-3	0.5	8.43E-3	1.0	0.169	-0.4
100	2.85E-3	0.4	5.52E-3	1.0	0.160	-0.4
150	7.91E-4	0.2	2.51E-3	1.1	0.140	-0.4
200	3.25E-4	0.1	1.42E-3	1.1	0.128	-0.4
300	9.57E-5	0.1	6.29E-4	1.1	0.111	-0.4
400	4.13E-5	0.2	3.51E-4	1.1	0.100	-0.4
500	2.19E-5	0.3	2.23E-4	1.1	0.0926	-0.4
600	1.32E-5	0.4	1.54E-4	1.1	0.0872	-0.4
800	6.10E-6	0.5	8.60E-5	1.1	0.0798	-0.4
1000	3.43E-6	0.6	5.49E-5	1.2	0.0751	-0.4

<sup>a</sup>Percent comparison of coefficients for equivalent material calculated as

$$100 \times \frac{(\mu/\rho)_{\text{equivalent}} - (\mu/\rho)_{\text{Snyder-Fisher}}}{(\mu/\rho)_{\text{Snyder-Fisher}}}$$

<sup>b</sup>Stansbury, 1977.



- |   |   |
|---|---|
| 1 AUTOTRANSFORMER                       | 6 AMMETER FOR CATHODE FILAMENT TRANSFORMER                                    |
| 2 PREREADING VOLTMETER                  | 7 VOLTAGE CONTROL FOR CATHODE FILAMENT WITH ADJUSTABLE IRON CORE (CHOKE COIL) |
| 3 PRIMARY OF HIGH-VOLTAGE TRANSFORMER   | 8 PRIMARY OF CATHODE FILAMENT TRANSFORMER                                     |
| 4 SECONDARY OF HIGH-VOLTAGE TRANSFORMER | 9 SECONDARY OF CATHODE FILAMENT TRANSFORMER                                   |
| 5 MILLIAMMETER IN HIGH-VOLTAGE CIRCUIT  | 10 X-RAY TUBE   |

Figure 15. The Principal Devices of an X-Ray Generating Apparatus.

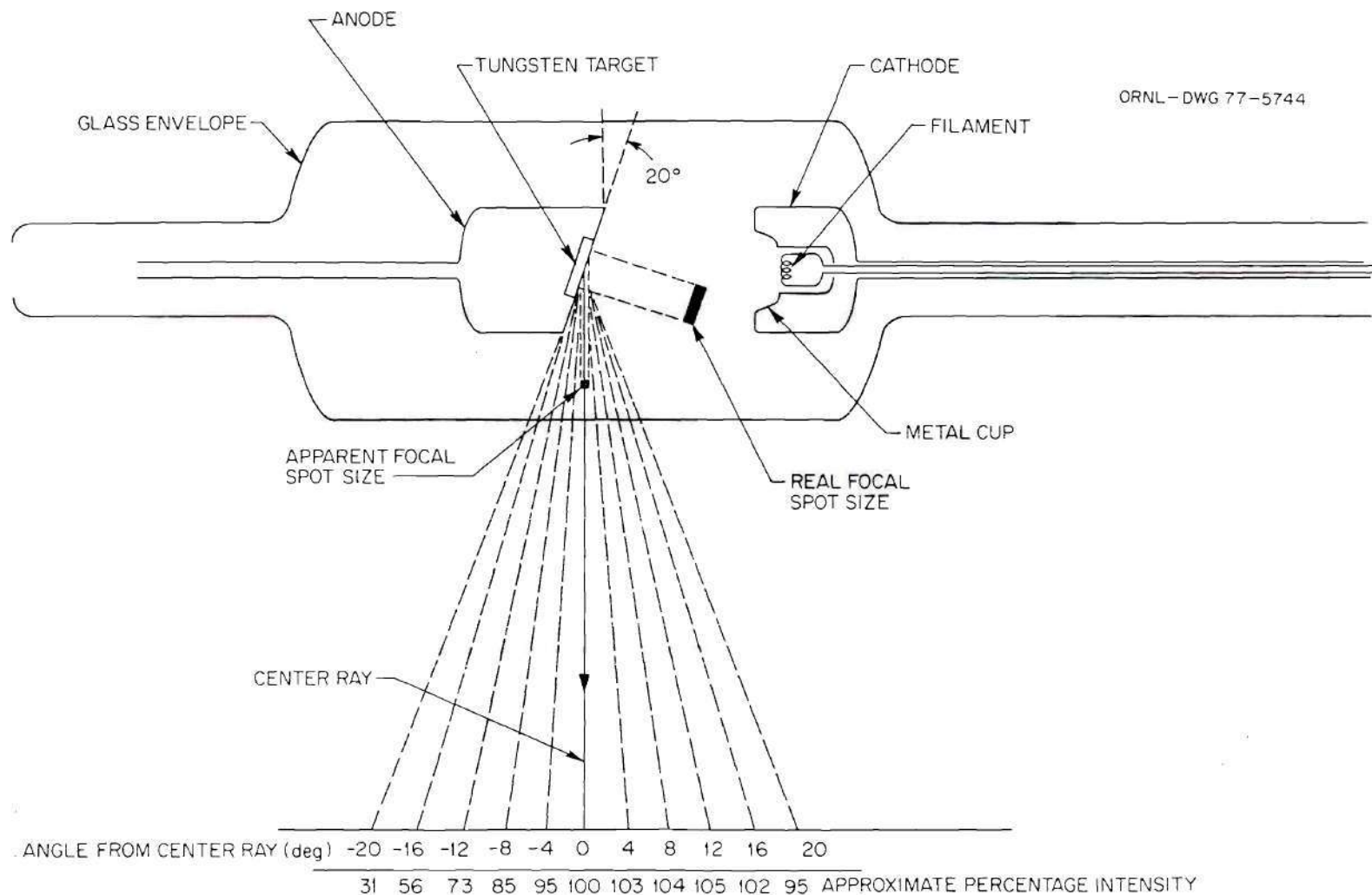


Figure 16. The Coolidge-Type X-Ray Tube and the Variation in Intensity of the X-Ray Beam along the Longitudinal Axis of the Tube.

metal cup causes the electrostatic field between the anode and cathode, set up by the high voltage applied to the tube, to distribute itself in such a way that electrons emitted from the hot filament inside the cup will be focused into a narrow beam of cathode rays, which will strike the anode with a small definite spot on its surface that is called the focal spot.

The quality and usefulness of the radiograph depends largely upon the size of the source of x rays, that is, upon the size of the focal spot on the target of the x-ray tube. It is a great advantage to have a source of x rays that approaches the ideal of a "point source." It is quite possible to achieve a small focal spot by "electron optics" techniques. However, if the spot has an area as small as  $1 \text{ cm}^2$ , the concentration of one or two kilowatts of power on such a small spot might melt the metal there, even though the anode were adequately cooled by a generous flow of cold oil or water inside it. This local melting occurs because the thermal conductivity of the target is not great enough to carry the heat away from such small spots rapidly enough to prevent the spot from rising to the melting point under such concentrated generation of heat. One common method of reducing the focal-spot size makes use of a trick in which the apparent size of the spot is reduced without reducing the actual size as shown in Figure 16. The anode face is a flat surface which has an angle  $\theta$  of perhaps  $20^\circ$  with the direction of cathode rays. This design produces the so-called "heel-effect" which is a variation in the intensity of x-ray output with the angle of x-ray emission from the focal spot as shown in Figure 16.



In order to do x-ray spectrometry inside the phantom, an x-ray machine of a special design was constructed by Stansbury (1977). This x-ray machine was able to operate over the range of 10  $\mu$ A to 20 mA. Further, the high voltage of the x-ray machine was well regulated. A conventional orthovoltage therapy machine (a Siemens Stabillipan 250 kVcp) was modified for this purpose. A therapy-type tube, with tube shield, oil cooler, and tube stand were modified to conform to a cathode-ground configuration. The anode was powered by a 5 to 125 kV, 0 to 10 mA high voltage supply with 0.1% ripple and no load-full load regulation of 0.1%. Filament power was supplied by a conventional 10 V, 10 A power supply. Maintaining the filament at near ground potential facilitated current sensing and interfacing of the filament and its power supply. The usual milliammeter and timer were replaced with a current integrator (Stansbury, 1977).

The x-ray machine calibration included the following measurements.

1. Spectral output of the x-ray machine.—A lithium-drifted germanium, Ge(Li), spectrometer and a pinhole collimator were used to measure the spectral output of the x-ray machine. The Ge(Li) detector had an active depth of 7.1 mm and a 0.25-mm beryllium window. Resolution for the Ge(Li) spectrometer was determined to be 0.9 keV full-width at half maximum (FWHM) at 60 keV photon energy ( $^{241}\text{Am}$ ). Some spectra (shown in Figures 17-19) were measured for 60, 80, and 100 kVcp generating potential with the tube currents of 25, 10, and 6  $\mu$ A, respectively.

Here the cp in kVcp denotes the constant potential nature of the generating potential. The raw data in Figures 17-19 are the pulse

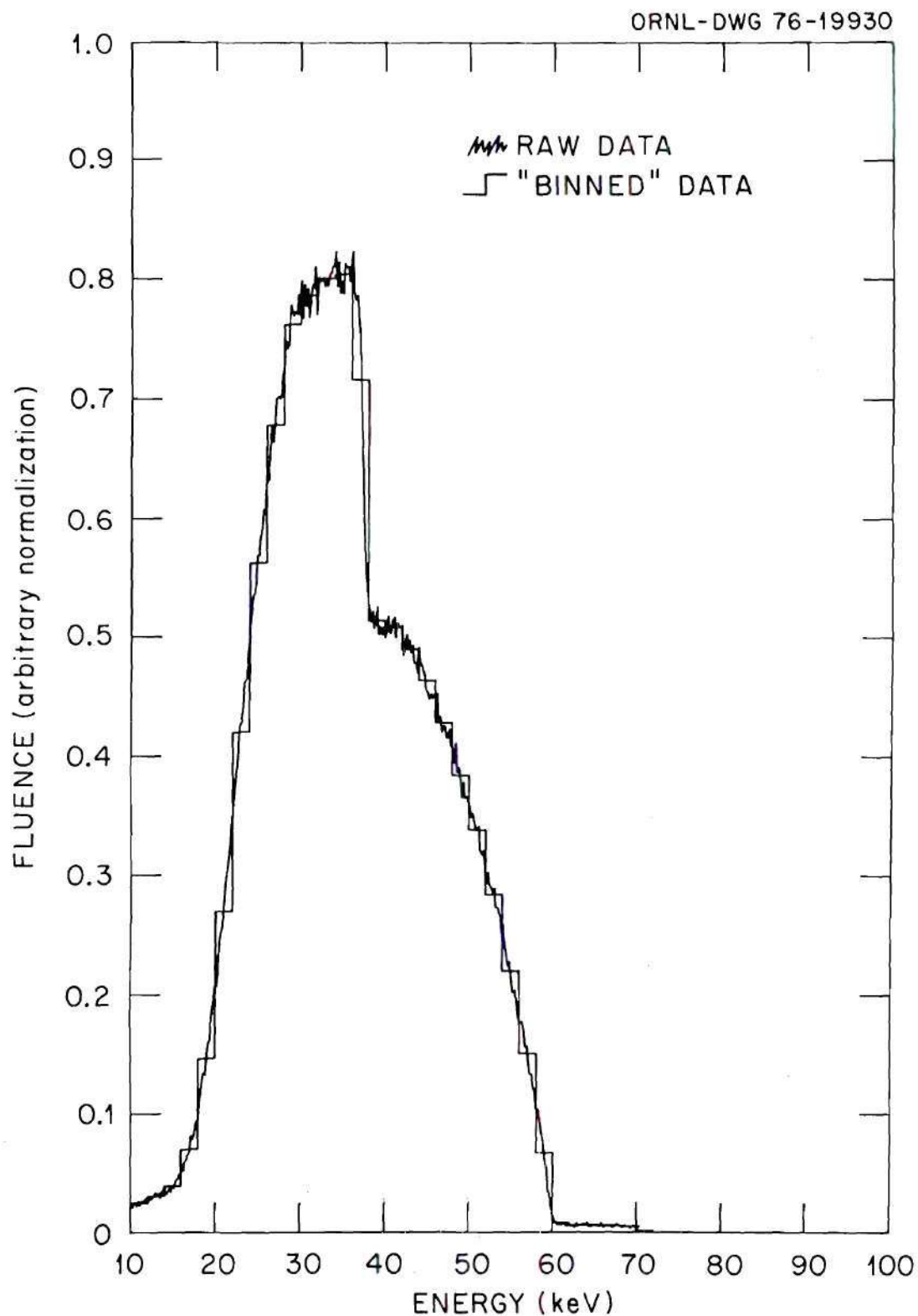


Figure 17. X-Ray Machine Output Spectrum Measured with a Ge(Li) Detector—60 kVcp.

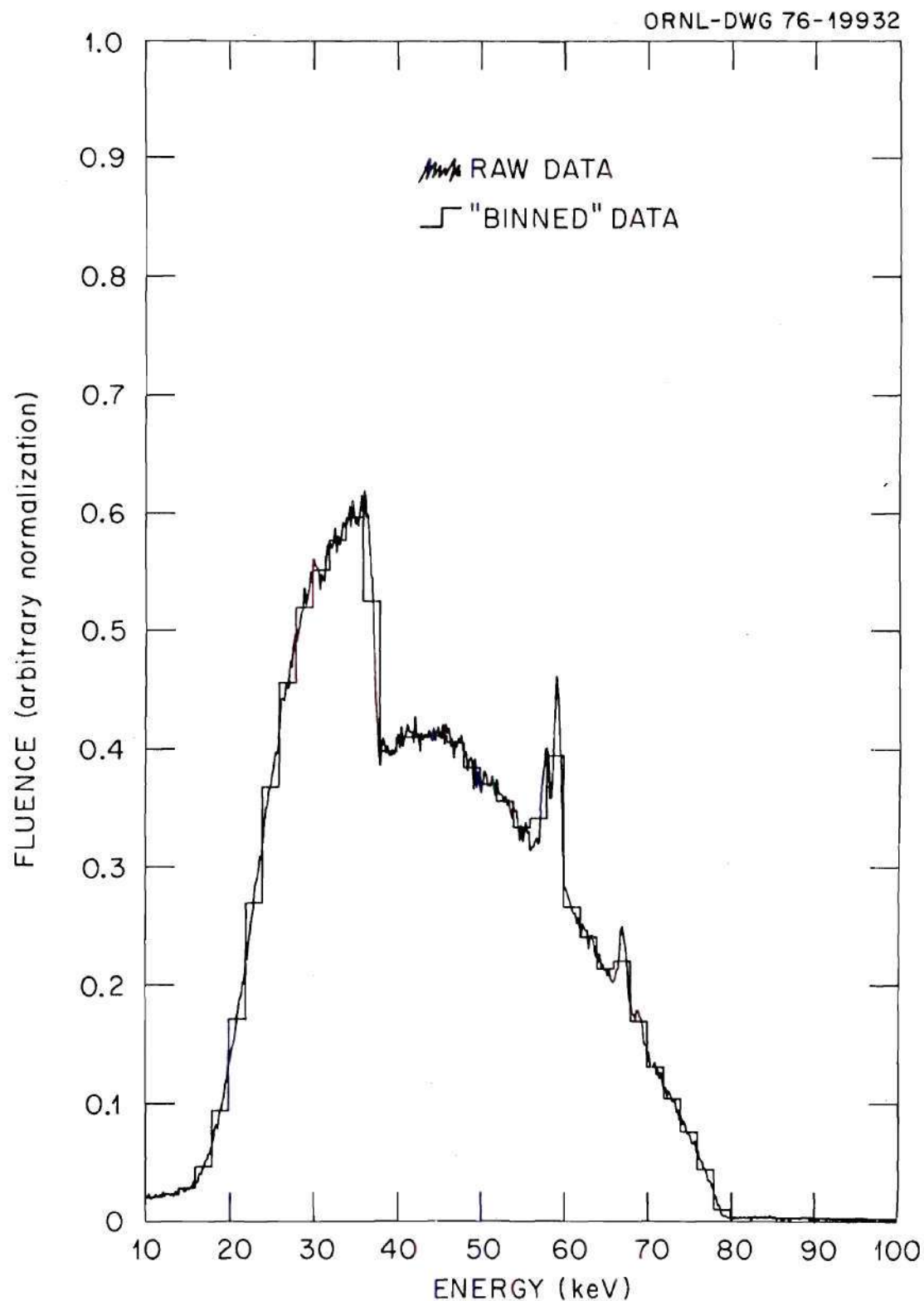


Figure 18. X-Ray Machine Output Spectrum Measured with a Ge(Li) Detector—80 kVcp.

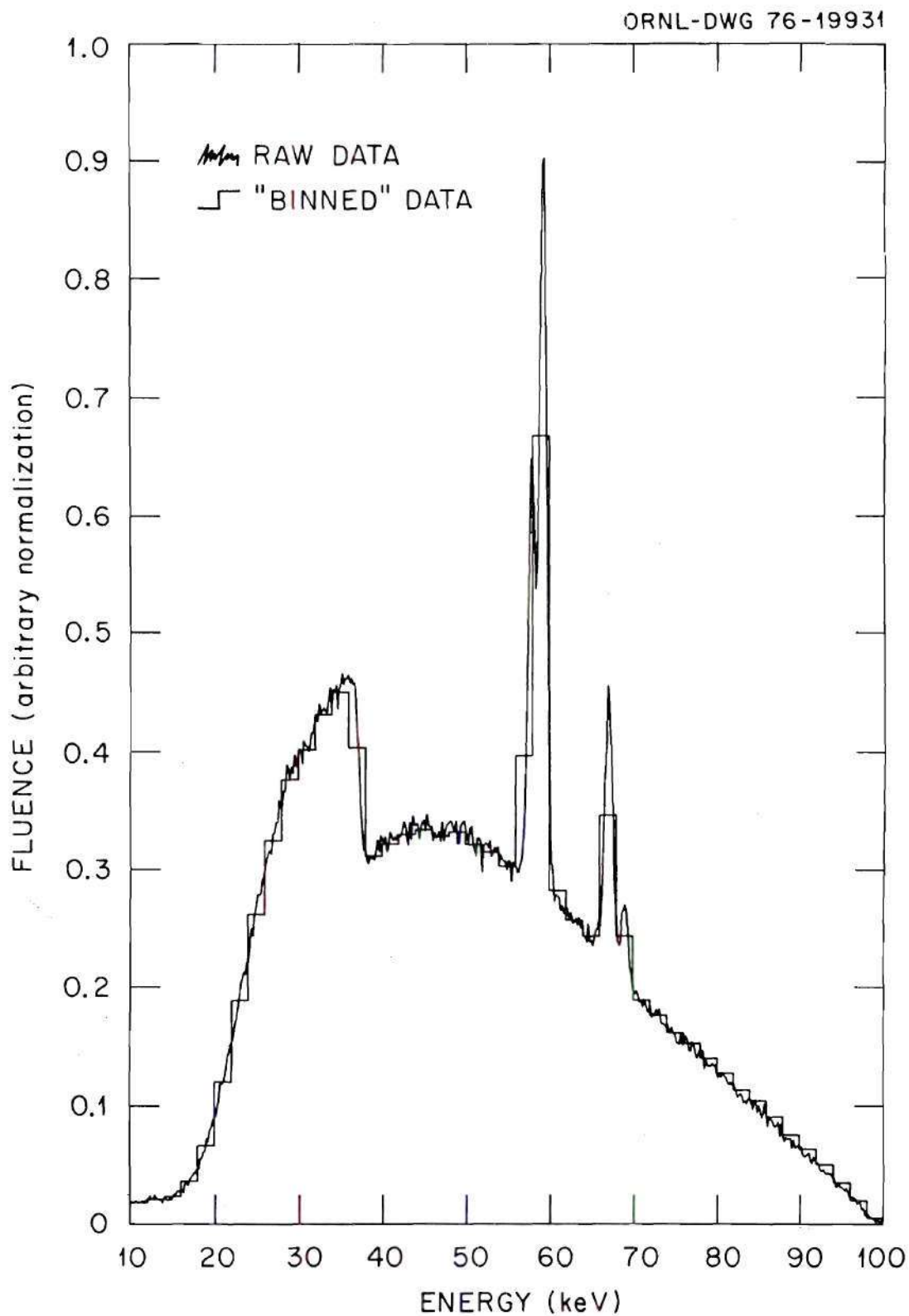


Figure 19. X-Ray Machine Output Spectrum Measured with a Ge(Li) Detector—100 kVcp.



height spectra measured with a Ge(Li) detector. "Binned" data were grouped into intervals 2 keV wide as follows. The raw data were corrected channel by channel to account for intrinsic efficiency losses due to the finite thickness (7.1 mm) of the Ge(Li) detector. Fluence in any "bin" was taken to be the average value of the corrected counts in the raw data channels whose energy lay within the boundaries of the "bin."

The absorption edge prominent in Figures 17-19 is centered at energy 37.4 keV. This edge was caused by barium contained in the glass envelope of the therapy-type tube, and a similar barium edge has been observed by other researchers studying the spectrum of a similar tube of the same brand (Gibson et al., 1975). Barium oxide is one of the materials added to glass to adjust its thermal expansion coefficient. Glass used to make x-ray tubes must have a thermal expansion coefficient similar to the metal components which penetrate the glass envelope in order that adequate glass-to-metal high vacuum seal can be made. The amount of barium added to the x-ray tube glass varies from manufacturer to manufacturer and from one batch of glass to another produced by the same manufacturer.

The measured x-ray spectra could be used to check the generating potential of the x-ray machine. Those x-ray spectra also served as input (i.e., the source routine) in an existing Monte Carlo code which was used to calculate organ doses in children.

2. Exposure rate as a function of tube current.—Exposures were measured with a Victoreen Radocon III ionization chamber and

electrometer dosimetry system. For three different generating potentials, 60 kVcp, 80 kVcp, and 100 kVcp, the exposure rate per unit tube current was measured with various tube currents, respectively. The target-to-chamber distance was 100 cm. After temperature and atmospheric pressure corrections of the Radocon III ionization chamber exposure rate reading, results were obtained as shown in Figure 20. The exposure rates per unit tube current was generally slightly higher with increasing tube current. However, the variations were less than  $\pm 2\%$  which was the error uncertainty claimed for the Radocon III. The dotted lines in Figure 20 are not "best fit" but are presented for reference only.

3. Exposure rate as a function of x-ray generating potential.—The exposure rate of the x-ray machine was measured with a Victoreen Radocon III ionization and electrometer dosimetry system. Exposure rate as a function of generating potential is shown in Figure 21. The slope of the curve is equal to 2 which follows the well-known empirical law that the x-ray output is proportional to the square of the generating potential (Equation 2-4).

4. Focal spot size and penumbra size determination.—Focal spot size was determined by using a 0.5 mm pinhole collimator and photographic film. The focal spot size was found to be 8 mm  $\times$  8 mm square. A photographic film was also used to check the accuracy of the light localizer of the collimator of the x-ray machine. A penumbra was observed around the edge of the x-ray beam defined by the collimator of the x-ray machine. At a focal-spot-to-film distance of 100 cm the penumbra was 0.75 cm wide, which was larger than for the usual

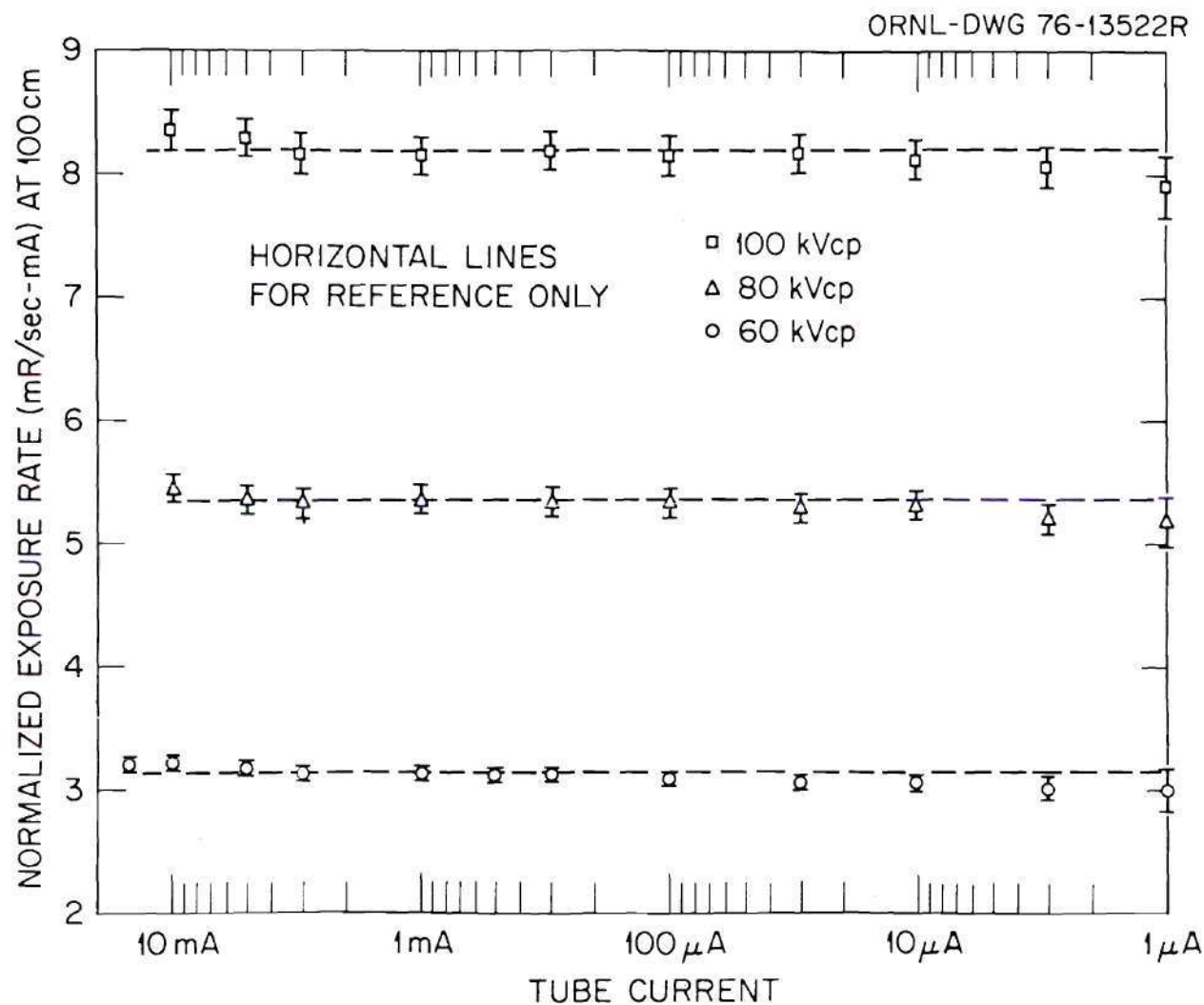


Figure 20. Normalized Exposure Rate as a Function of Tube Current (Error Bars Correspond to  $\pm 2\%$  Plus the Least Significant Digit Uncertainty).

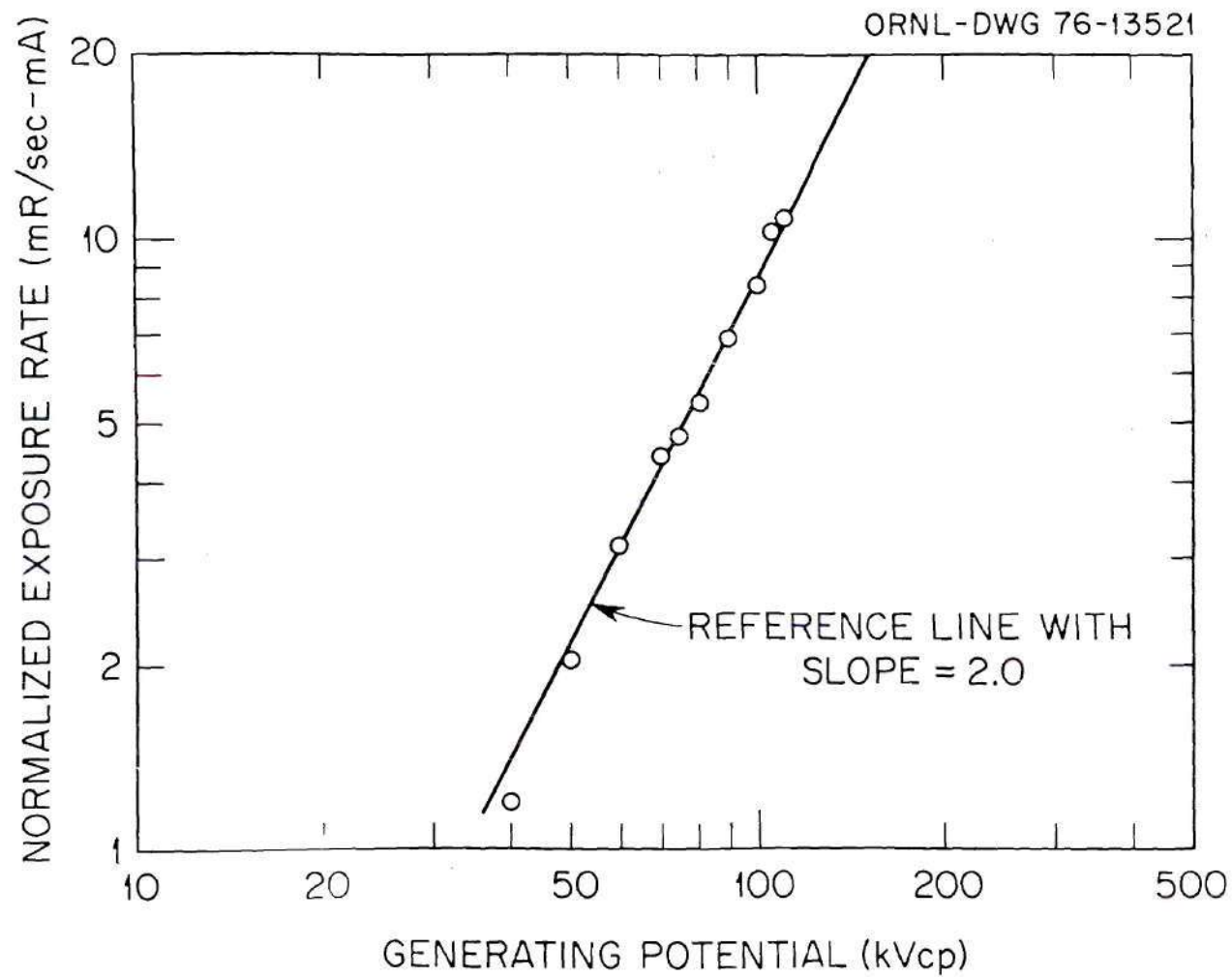


Figure 21. Exposure Rate at a Target to Detector Distance of 100 cm as a Function of Generating Potential.



diagnostic x-ray machine. This is because usual diagnostic x-ray machines have a much smaller focal spot size (1 to 2 mm square).

### Dosimetry

#### Victoreen 550 System

A Victoreen Model 550 Radocon III Integrating Rate Electrometer System was used as the primary dosimetry reference instrument for radiation measurements performed in this study. Victoreen claims that the basic electrometer inaccuracy measured at 22°C, less than 6 months after calibration, is  $\pm 0.5\%$  of reading ( $\pm 1$  digit on the digital readout). Temperature drift is  $\pm 0.03\%$  per degree centigrade difference from 22°C and input offset current is less than 2 digits on the most sensitive range, i.e.,  $\pm 0.02$  mR/sec. The zero drift is less than 5 digits per hour on the most sensitive range, i.e.,  $\pm 0.05$  mR/sec or 0.05 mR after 1 hour operation and long-term drift is  $\pm 0.5\%$  per 6 months.

The chamber used in this study was a 550-0.1 ionization probe. Victoreen claims that the chamber calibration uncertainty for the 550-0.1 probe is  $\pm 2\%$  over the energy range of 21 to 1250 keV. Calibration data are given in Table 14 and the correction factors are plotted as a function of the effective energy in Figure 22.

#### Thermoluminescent Dosimetry Theory

Thermoluminescent dosimetry (TLD) techniques were used extensively in this study. TLD offers a number of advantages for the assessment of the absorbed dose associated with diagnostic x-ray

Table 14. Victoreen Model 550-0.1 Ionization Probe Calibration Data<sup>a</sup>

Generating Potential (kVcp)	Total Filtration (mm)					Effective Energy (keV)	Half value layer			Correction Factor
	Be	+	Al	+	Cu		mmAl	or	mmCu	
30	1.0		0.5		0.00	15.0	0.33 <sup>b</sup>			1.11
50	1.0		1.0		0.00	21.0	0.90 <sup>b</sup>			1.02
60	0.0		4.0		0.00	32.0	2.80		0.09	1.05
76	0.0		4.0		0.00	34.5	3.40		0.11	1.04
100	0.0		5.0		0.00	42.0	5.1		0.20	1.04
150	0.0		5.0		0.25	64.0	10.0		0.16	1.03
200	0.0		5.0		0.50	84	13.0		1.30	0.95
250	0.0		5.0		3.2	140	18.0		3.20	0.95
<sup>137</sup> Cs						660				0.96
<sup>60</sup> Co						1250				0.94

<sup>a</sup>Data supplied by manufacturer.

<sup>b</sup>Filter to target distance is 25 cm.

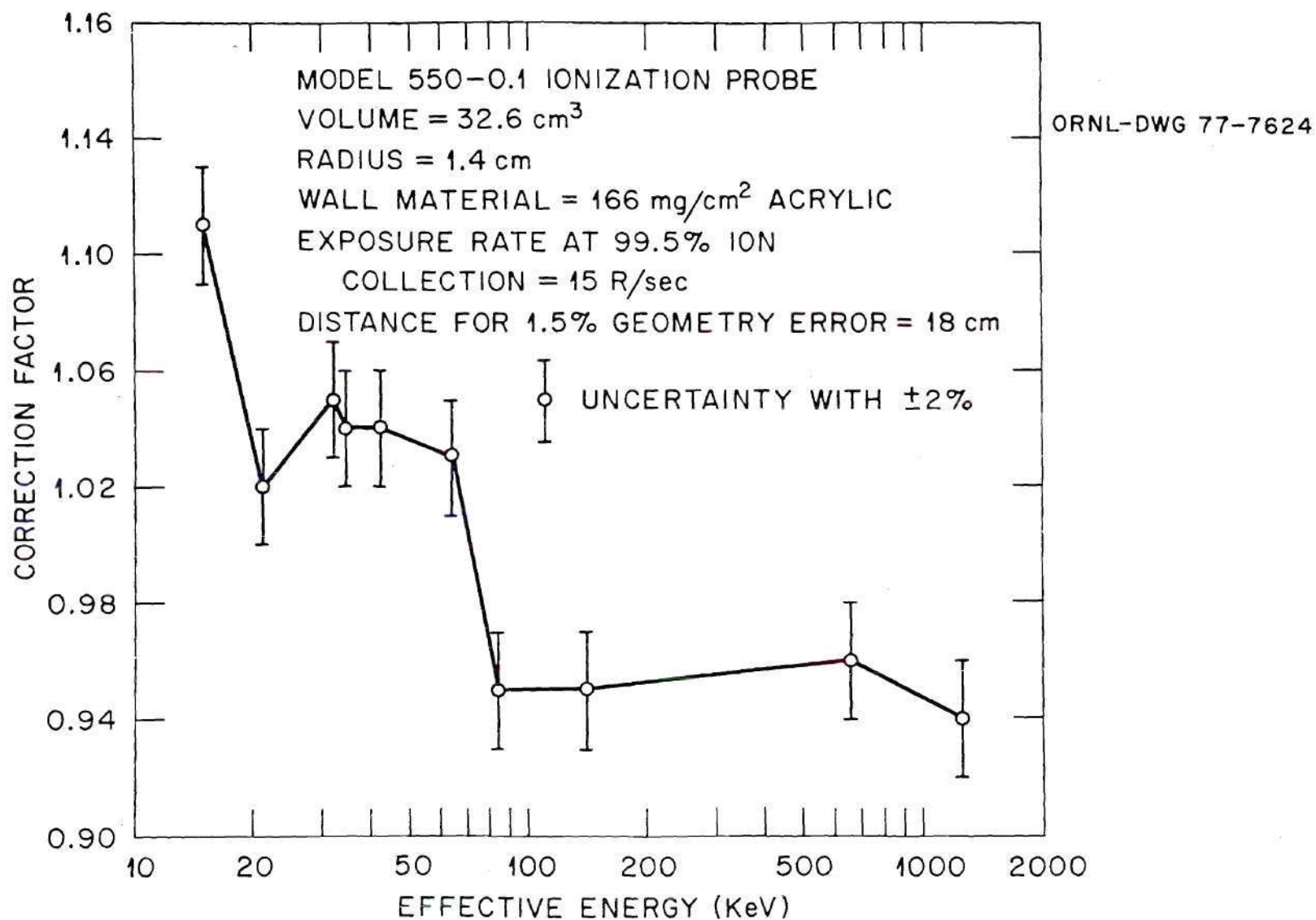


Figure 22. The Correction Factors of the Victoreen Model 550-0.1 Ionization Probe as a Function of the Effective Energy.

procedures, when compared to alternate techniques such as film or ionization methods. The size of each TLD is small,  $3.2 \times 3.2 \times 0.9$  mm for the hot-pressed chip and  $1 \times 1 \times 6$  mm for the rod, compared to ionization chambers or film that usually are much larger. Also the angular dependence of the TLD is relatively small. In addition, two phosphors of differing atomic numbers can be utilized to estimate the effective energy of an x- or gamma-ray field. All these advantages make it possible to use TLD for in-bone dosimetry.

Utilization of TLD as a radiation dosimetry technique is based on the quantification of light emitted from a heated crystalline material that was previously exposed to ionizing radiation. The basic physical principle is associated with the excitation of electrons from the valence band to the conduction band when a crystal is exposed to radiation, as shown in Figure 23, step 1. The free electron and associated hole migrate independently through the crystal lattice. In reality the crystal has imperfections and impurities, also called activators, locked in the lattice structure. Some of these defects can capture a free electron or hole. These are called electron trapping centers or hole trapping centers. Usually these trapping centers are like an ionized hydrogen atom and have various energy states,  $E_0$ ,  $E_1$ ,  $E_2$ , ..., which are shown also in Figure 23. Once a migrating electron gets trapped, it remains there, as shown in step 2, Figure 23. A trap that has caught an electron is called a filled trap. The greater the radiation dose, the more electrons are excited, and the greater the number of filled traps. Each trap can only supply so much holding



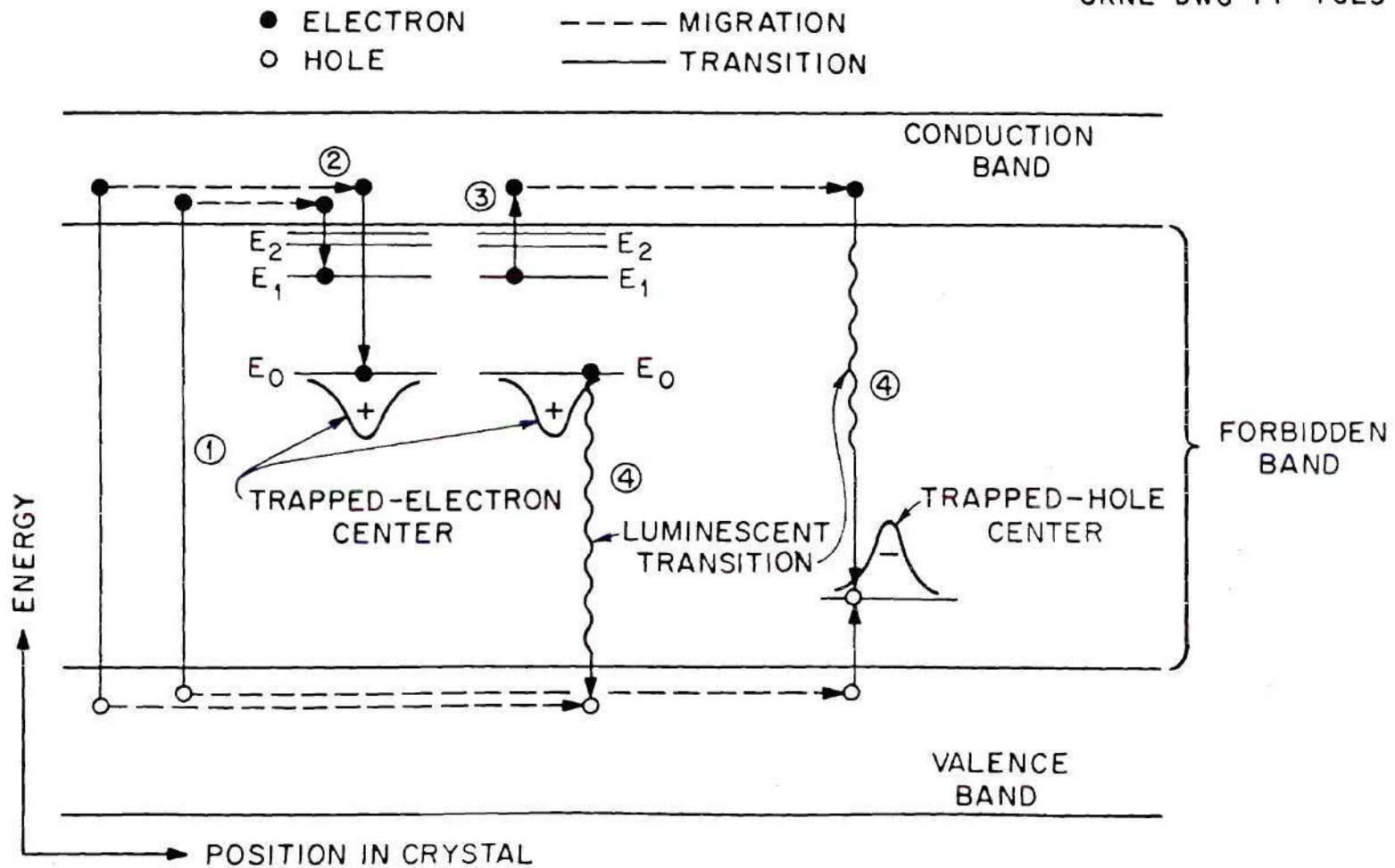


Figure 23. Schematic Representation of Thermoluminescence Processes in TLD Crystal.

energy to an electron or hole. These electrons or holes are called metastable. When an irradiated crystal is subsequently heated, see step 3 in Figure 23, the electrons or holes can receive enough additional thermal energy so that the trap releases them from the metastable trap level and they return to their ground state (valence band). During this readjustment in energy states, certain types of traps will cause the electrons or holes to release their excess energy in the form of light. This light energy is emitted when a "release temperature" is reached, as step 4, shown in Figure 23. This process is called thermoluminescence.

The traps generally fall into several groups based on the energy which must be supplied to release the electrons; traps which hold onto electrons very tenaciously represent deep energy traps while other traps which retain electrons weakly represent energy traps very near the conduction band. Each group of traps releases its electrons at a different and characteristic temperature. There are usually many more low energy traps than there are high energy traps. A slight temperature increase can empty a low energy trap, while a large temperature increase is needed to empty a high energy trap.

When an irradiated crystal is heated at a constant rate, the stored energy in the crystal is emitted in the form of light. The luminescence output during heat treatment will vary with time depending on the schedule of heating, the impurities in the dosimeter and the properties of the crystal. The curve of luminescence output versus temperature obtained when the crystal temperature is steadily increased

is called the "glow curve." The theory of glow curves (Randall et al., 1945; Townsend et al., 1967; Cameron et al., 1968) has been studied very extensively with the aim of deducing the depths, shapes, and other properties of electron or hole traps from these curves. The shape of the glow curve depends upon the material selected. Total area under the glow curve, or total light produced, is proportional to the radiation dose received by the crystal. While the heating rate will affect the height of the glow peaks, it does not affect the total amount of light produced. Generally the thermoluminescent output can be measured either as the integrated light output (the light sum) or as the glow-peak height. The former measurement has the advantage of being independent of the heating rate; therefore, heating rate need not be accurately reproducible between one reading and the next. A disadvantage is that a certain degree of arbitrariness is introduced in deciding when the integration should be cut off. This is particularly true in dealing with a small signal of light (resulting from a low dose sample) which may be masked by the incandescence signal from the heater. The peak-height method of measurement requires that the heating schedule be accurately reproducible from reading to reading because the peak height is a very sensitive function of the heating rate. For samples exposed to the same dose, the faster the heating rate, the higher the peak height. In spite of such required control measures, reproducibility of the heating schedule is not hard to achieve in practice (Cameron, 1964).

To reuse the TLD crystal and to erase all its previous radiation history, an annealing process is generally used. This annealing is accomplished by heating the TLD at a suitable temperature and for a specified time. The annealing effectiveness varies with different TLD materials. Sensitivity and stability of some TLD materials, such as LiF:Mn, are highly influenced by their prior irradiation and thermal history (Ginther and Kirk, 1956, 1957). Also, many variations in annealing procedures have been developed by different investigators (Shiragai, 1967; Harris and Jackson, 1970; Dahr et al., 1973). Cameron et al. (1964) and Zimmerman et al. (1966) have suggested a "standard annealing" procedure for LiF. This procedure includes a 400°C anneal for one hour followed by an anneal at 80°C for 24 hours before irradiation or 100°C for 10 minutes after irradiation.

In this study, a Victoreen Model 2800 TLD reader which had a "built-in" anneal cycle was used to read all the LiF:Mn dosimeters. In this built-in anneal cycle, the LiF:Mn dosimeter is first quickly preheated to 120°C for 17-18 seconds. Then the heating temperature is increased, at a heating rate of 10°/sec, to 255°C for 23-24 seconds. After this period the digital display on the reader shows the exposure received by the LiF:Mn dosimeter. Following a brief cooling period, the heating temperature is raised again quickly to approximately 340°C for 37 seconds, then the annealing process is completed. This technique is based on carefully controlling the heating and cooling rate during the reading process. The lower temperature (120°C) preheating portion of the cycle eliminates low temperature peaks from the glow curve.



The higher temperature (340°C) annealing portion of the cycle and suitable cooling time resets the sensitivity and stability of the LiF:Mn dosimeter. All new LiF:Mn dosimeters, or those that have not been read out within one week, were run through the built-in anneal cycle before exposure. Following each reading, the built-in cycle will automatically reset the dosimeter's sensitivity for a period of about one week, thus eliminating the time-consuming external annealing procedures normally required. However, an external low-temperature oven anneal (80°C  $\pm$  3°C for 16 hours within  $\pm$  1/2 hour), in addition to the built-in anneal cycle, was helpful in minimizing signal fading for exposure/readout periods greater than one week or for dosimeters exposed to higher dose levels.

Because of the trap structure of CaF<sub>2</sub>:Mn dosimeters, annealing is not very critical (Ginther and Kirk, 1956, 1957). It is only necessary to heat these dosimeters long enough to remove any residual signal before reuse. Usually heating the dosimeter to 400°C for five minutes will "dedose" a CaF<sub>2</sub>:Mn dosimeter which has been exposed to less than 500 mR.

#### TLD X-Ray Exposure Calibration

LiF:Mn and CaF<sub>2</sub>:Mn have a relatively large difference in energy response and have similar TL light output spectra. In addition, similar physical size crystals were commercially available and can be read by the same reader. These advantages made them very attractive for use in a tandem technique. Four types of TLDs were used in this study. They were the LiF:Mn chip, LiF:Mn rod, CaF<sub>2</sub>:Mn chip, and

CaF<sub>2</sub>:Mn rod. In all, 75 dosimeters of each type were available. The sensitivity, stability, and other dosimetric properties of TLDs may be slightly different even for TLDs in the same batch (Carlsson et al., 1968). Therefore, for a precise experiment, the careful calibration of each individual TLD is necessary (Burch, 1968; Gooden and Brickner, 1972; Jacobson et al., 1973; Law, 1973). The TLD is not an absolute radiation detector. Thus, grading and calibration are the keys to satisfactory use of TLDs as reliable dosimeters. The grading process consisted of the following steps:

1. Four types of TLDs, 75 dosimeters each, were annealed and arranged in a specific order such that each individual dosimeter could be identified throughout the whole process.
2. The dosimeters were given a dose of approximately 200 mR by irradiating the dosimeters with a calibrated <sup>226</sup>Ra gamma-ray source.
3. After 24 hours delay, to minimize any fading variation, the individual dosimeters were read and the readings were recorded. It was important that the identity of the dosimeters be maintained.
4. The mean of the group readings was divided by the reading of each individual dosimeter to obtain an individual correction factor for each dosimeter.
5. The entire group of dosimeters was then annealed and the procedures described in 3 and 4 were repeated nine additional times.

6. The average value of individual correction factors for the ten exposures was taken as the relative sensitivity factor for each dosimeter.
7. After ten exposures, 50 dosimeters were selected from each group of 75 which had the best reproducibility. These dosimeters were used in the rest of the experiment.
8. According to the value of their relative sensitivity factor, the 50 dosimeters were arranged, in decreasing or increasing order such that each individual dosimeter could be identified permanently. Each dosimeter had a sensitivity and reproducibility similar to that of its neighboring dosimeters.

After the dosimeters had been graded and their reproducibility and other characteristics had been determined, they were calibrated for use in the remaining experiments. The calibration of the dosimeters focused on the following characteristics:

1. Stability—After irradiation, a part of the radiation energy which is stored in TLDs will be lost even at low temperature. If a TLD shows insignificant loss of TL at room temperature it is said to have good stability or a low fading rate. The TLDs used in this study were irradiated to 200 mR using a calibrated  $^{226}\text{Ra}$  gamma-ray source. The irradiation time was 30 minutes. After irradiation, the dosimeters were divided into ten groups and read at different time periods. For  $\text{LiF:Mn}$ , the fading was negligible in the first three days after exposure (Figure 24). This result was consistent with those reported by other authors (Schulman et al., 1960; Cameron et al., 1964;

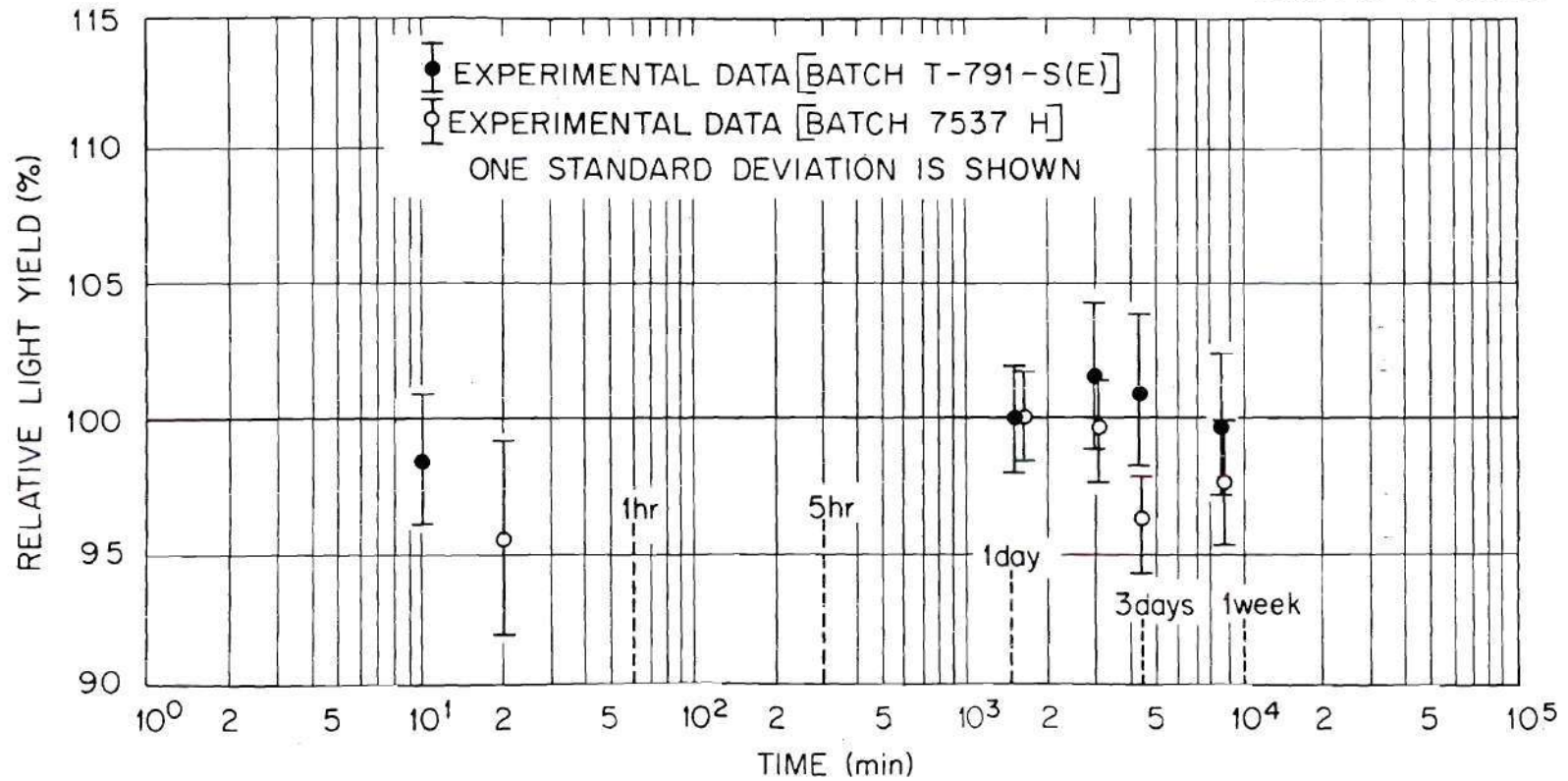
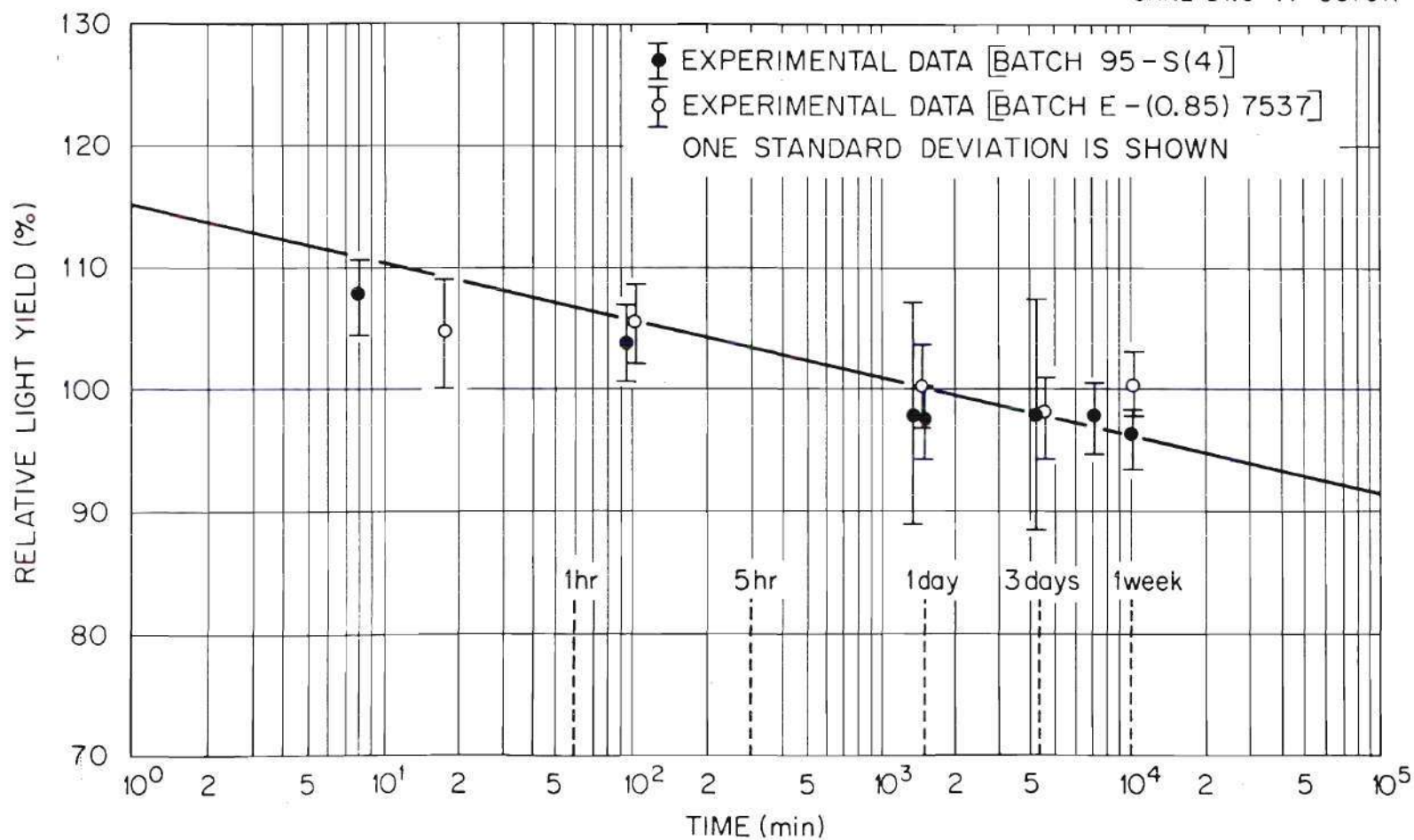


Figure 24. LiF:Mn Fading Rate Test.



Suntharalingam et al., 1968; Schayes et al., 1968). For  $\text{CaF}_2\text{:Mn}$ , the fading was very rapid during the first day after exposure (Figure 25). However, the fading rate became slow after this period. This was confirmed also by comparing these results with the work of others in the field (Schmid and Mooney, 1963; Bjarngard and Jones, 1966; Gorbics et al., 1967). All TL readings of  $\text{CaF}_2\text{:Mn}$ , obtained at different times after exposure, were normalized to the TL readings taken at 24 hours and a fading curve was obtained (see Figure 25). The solid line shows the fading data supplied by the manufacturer of the TLD system. The experimental data were slightly lower than the expected fading rate (solid line) for periods of less than one hour. This is probably due to loss of signal (rapid fading) which occurred in the dosimeters during the exposure time (30 minutes).

2. Orientation Dependence Test—To measure the absorbed dose inside a bone cavity, the in-bone detector should have a response that is relatively independent on the angle of incidence of the radiation, whether it is primary or scattered radiation. Thus, the four types of dosimeters were irradiated by a calibrated  $^{137}\text{Cs}$  gamma-ray source at various angles of incidence on the dosimeter. The results are shown in Figure 26. The response of LiF chips, LiF rods, and  $\text{CaF}_2$  chips has an uncertainty within  $\pm 5\%$  when the incident radiation varies from  $0^\circ$  to  $90^\circ$ . The response of  $\text{CaF}_2$  rods decreases with the increasing angle of the incident radiation. Whenever the angle between the incident beam and a surface normal to the crystal is less than  $50^\circ$ , the angular response varies no more than  $\pm 5\%$ . Thus, to simplify analysis

Figure 25.  $\text{CaF}_2\text{:Mn}$  Fading Rate Test.

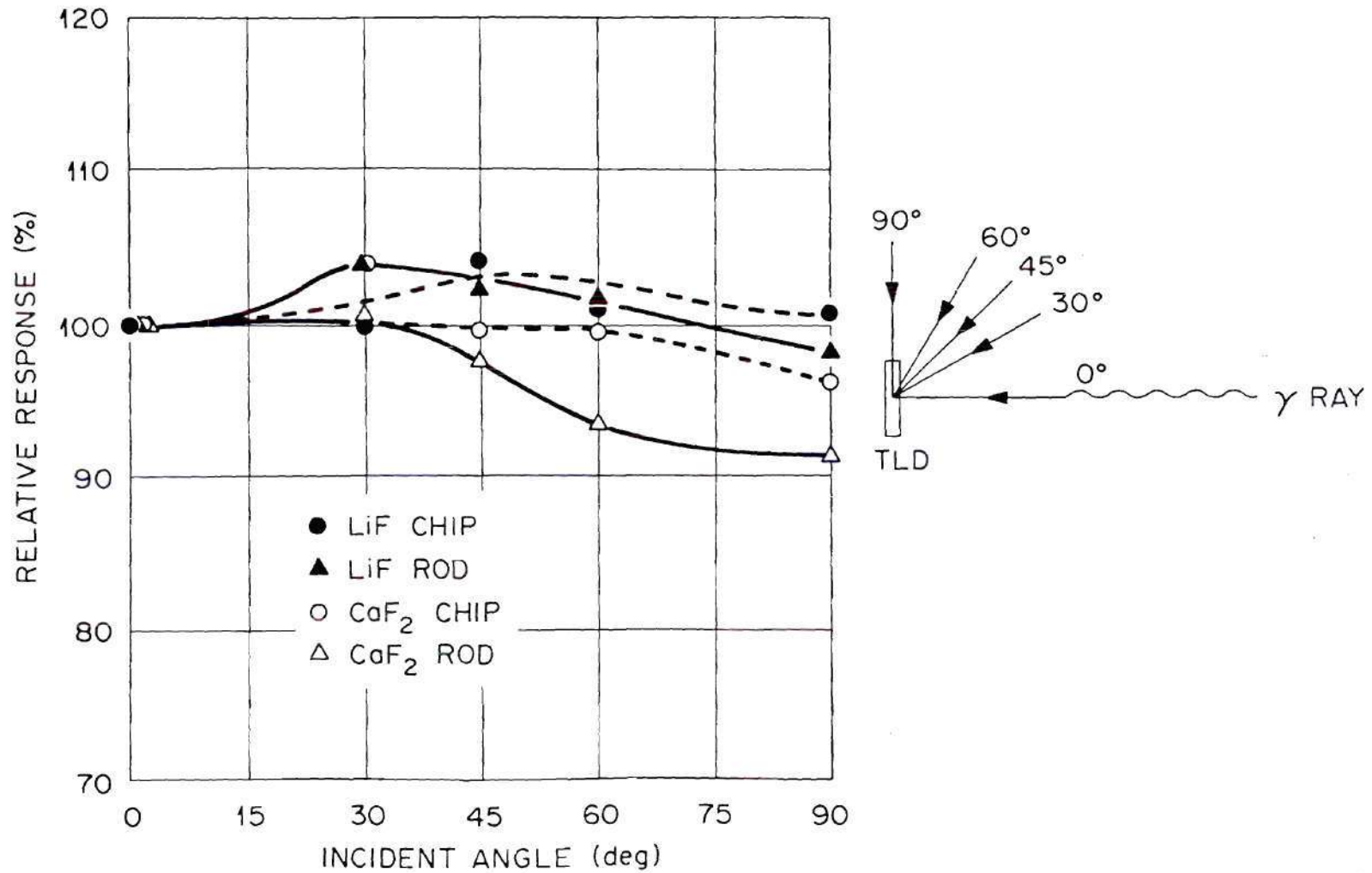


Figure 26. TLD Angular Dependence Tests.

of the experimental data, the error induced by the angular dependence was neglected.

3. Sensitivity and Linearity—Thermoluminescent sensitivity may be defined as the amount of light released by the phosphor per unit of radiation exposure. The lower limit of useful sensitivity depends on the characteristics of the TLD and the TLD reader. A calibrated  $^{137}\text{Cs}$  gamma-ray source was used to irradiate TLD dosimeters placed at different distances from the source. The results are shown in Figures 27 and 28. The lower detection limit for  $\text{LiF}$  and  $\text{CaF}_2$  was 10 mR and 1 mR, respectively. Response of both TLD materials was linear above 10 mR. The "built-in-anneal" process of the  $\text{LiF}$ -TLD reader works most effectively when reading dosimeters exposed to less than 400 mR. All the TLD exposures for the remaining experiments were controlled carefully to give an exposure between 50 mR and 250 mR. The exposure of the TLD can be controlled by variation of the exposure time and x-ray tube current.

4. Energy Response and the Tandem Technique—Energy response of a detector at a particular photon energy may be defined as the response of the detector at that photon energy relative to its response at some reference energy, such as  $^{137}\text{Cs}$  (662 keV) or  $^{60}\text{Co}$  (1.17 and 1.33 MeV) gamma rays. The dosimeter has a good energy response if the response per roentgen shows little change with photon energy; the energy response is poor if this change is large.

Based on the assumption that the integrated light output of a TLD is directly proportional to the energy absorbed in the crystal,



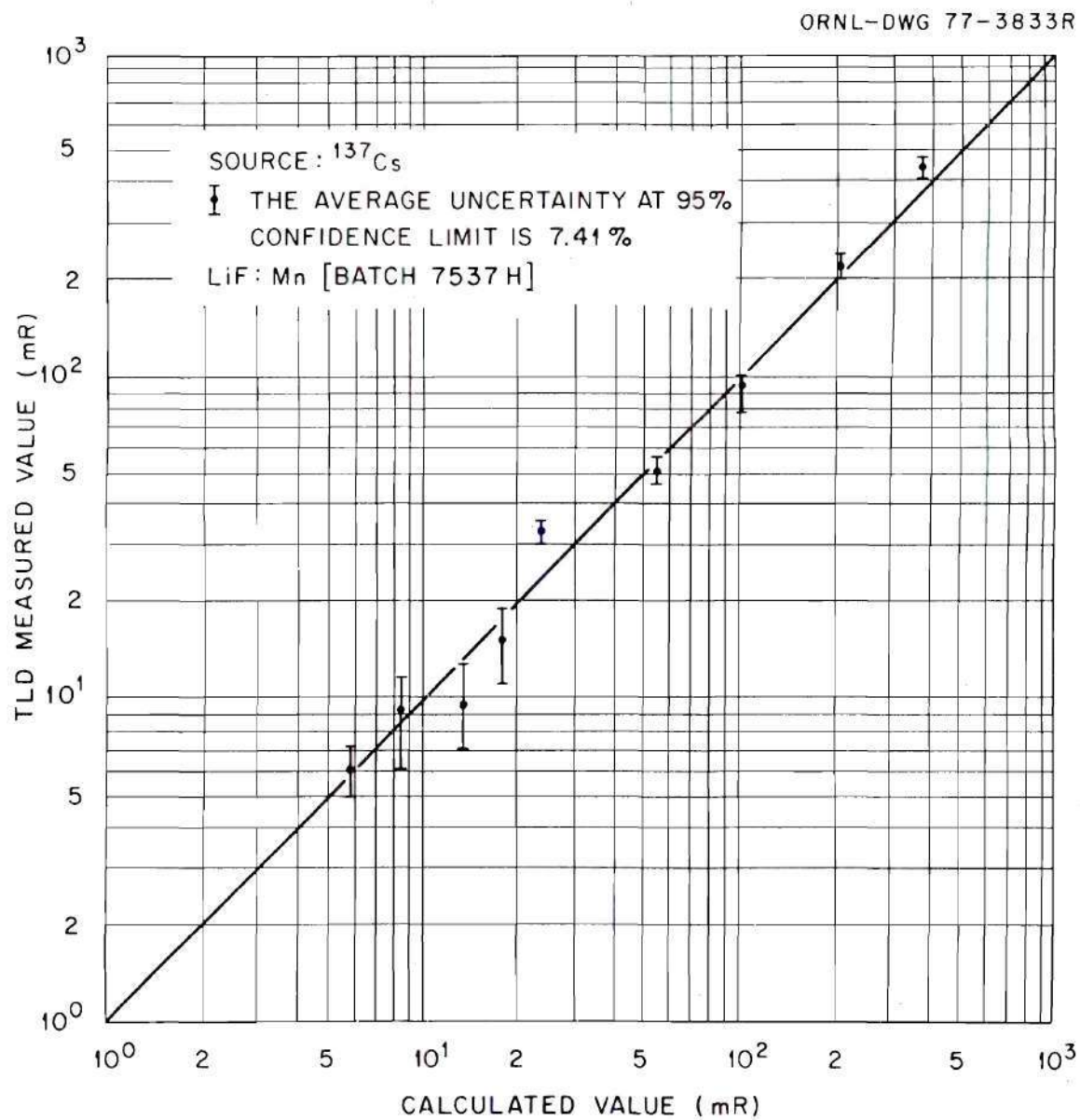


Figure 27. LiF:Mn Response as a Function of Exposure.

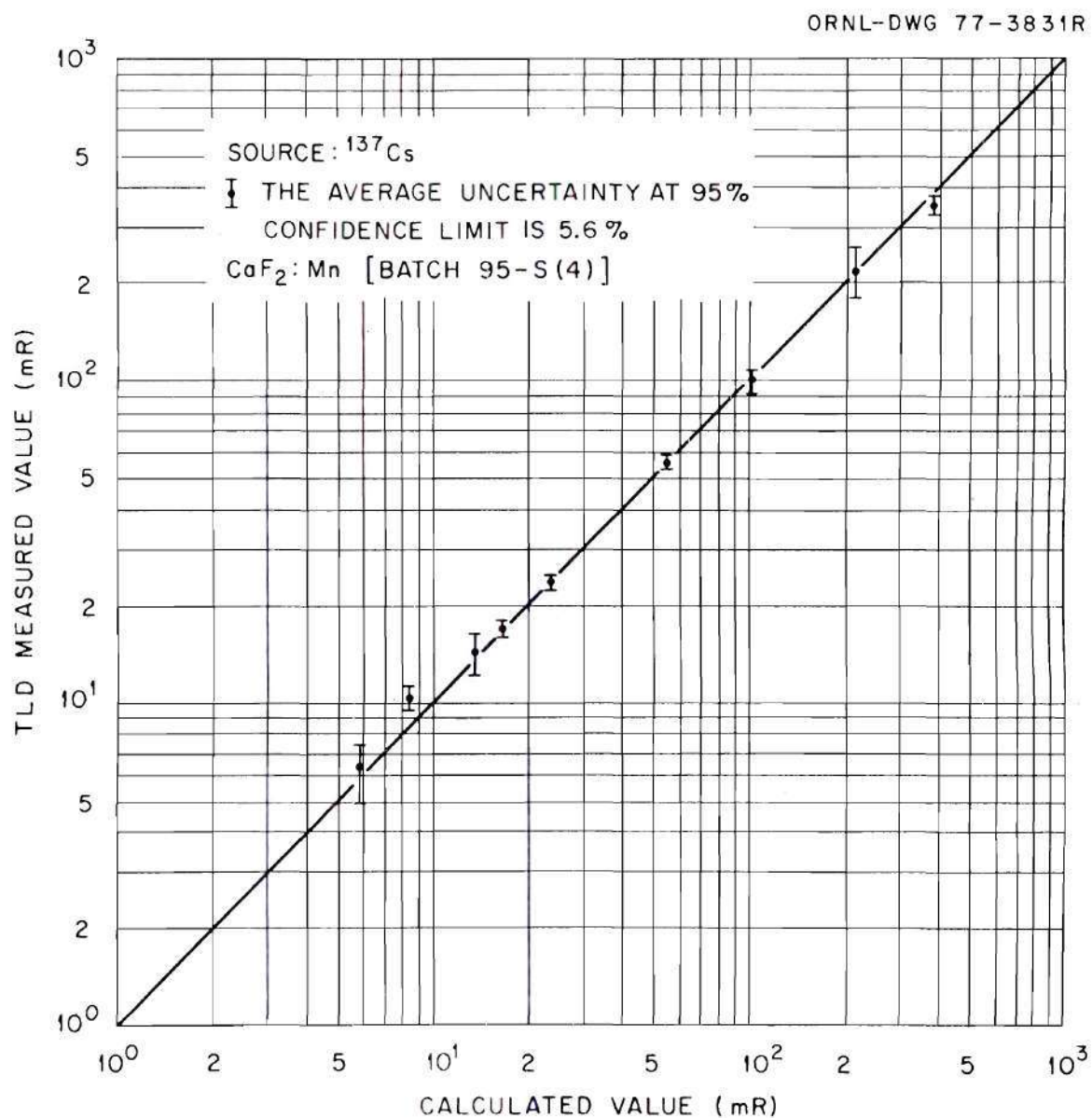


Figure 28.  $\text{CaF}_2:\text{Mn}$  Response as a Function of Exposure.

then general cavity theory can be used to determine that the radiation energy absorbed by the TLD follows the relation (Gorbics and Attix, 1968; Almond and McCray, 1970):

$$D_{\text{TLD}} = \frac{\left(\frac{\mu_{\text{en}}}{\rho}\right)_{\text{TLD}}}{\left(\frac{\mu_{\text{en}}}{\rho}\right)_{\text{med}}} D_{\text{med}} \quad , \quad (3-5)$$

where

$D_{\text{TLD}}$  is the energy absorbed in the TLD,

$\left(\frac{\mu_{\text{en}}}{\rho}\right)_{\text{TLD}}$  is the mass energy absorption coefficient of the TLD,

$\left(\frac{\mu_{\text{en}}}{\rho}\right)_{\text{med}}$  is the mass energy absorption coefficient of the medium,  
and

$D_{\text{med}}$  is the energy absorbed in the medium.

The mass energy absorption coefficient of a high-Z material increases more rapidly with decreasing photon energy than that of low-Z material. Thus LiF, with a low effective atomic number, has a smaller energy dependence than CaF, with a high effective atomic number.

The Victoreen Model 550 Radocon III ionization chamber system and a set of high-purity Al-filters were used to obtain x-ray transmission curves for a number of accelerating potentials used in this research (see Figure 29). Results of these measurements are also presented in Table 15. Here the first half-value layer (HVL) is the thickness of the absorber required to attenuate the exposure rate of the x-ray beam

ORNL-DWG 77-3679R

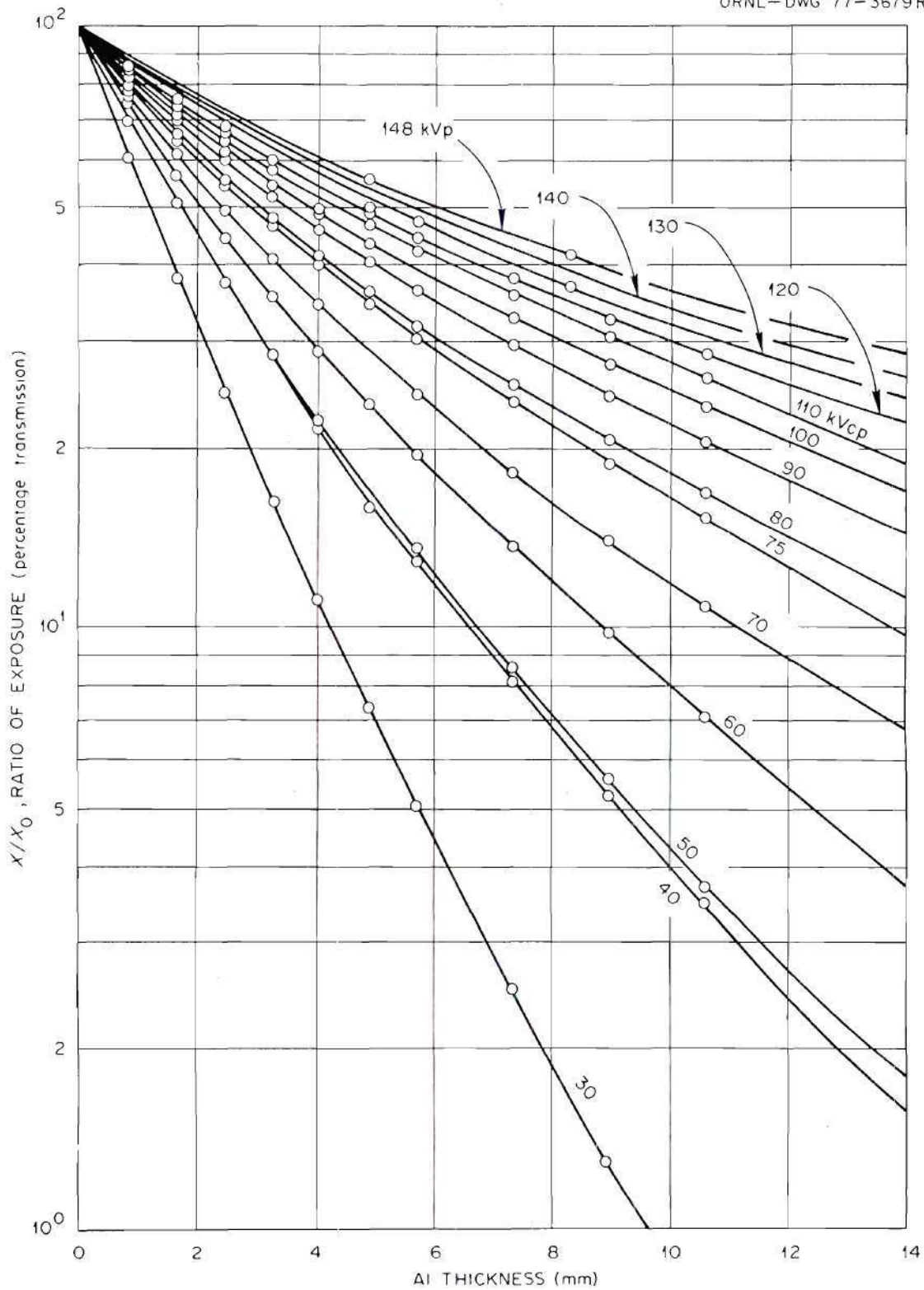


Figure 29. The Transmission of the X Rays through Aluminum.



Table 15. Parameters Used in the Energy Response Determinations<sup>a</sup>

Generating Potential	Tube Current	Additional <sup>b</sup> Filtration	First HVL	Second HVL	Homogeneity Factor	Mass Attenuation Coefficient	Effective Energy
kilovolts	mA	cm-Al	cm-Al	cm-Al	%		keV
148	100	<sup>c</sup>	0.61	1.04	59	0.421	46
140	100	<sup>c</sup>	0.56	0.94	63	0.458	44
130	100	<sup>c</sup>	0.52	0.83	61	0.494	43
120	10	0.08	0.47	0.76	62	0.55	41
110	10	0.08	0.43	0.68	63	0.60	38
100	10	0.08	0.39	0.60	65	0.68	37
90	10	0.08	0.35	0.53	66	0.73	36
80	10	0.08	0.30	0.45	67	0.82	34
75	10	0.08	0.29	0.41	71	0.89	33
70	10	0.08	0.24	0.32	75	1.03	31
60	10	0.08	0.21	0.25	84	1.22	30
50	10	0.08	0.17	0.20	85	1.51	27
40	10	0.08	0.16	0.20	80	1.51	27
30	10	0.08	0.11	0.13	85	2.14	23

<sup>a</sup>Transmission data shown in Figure 29.

<sup>b</sup>Inherent filtration approximately 0.5 cm Al equivalent plus 76.2 cm air for generating potential 148 to 130 Kilovolts and 0.2 cm Al equivalent plus 150 cm air for generating potential 120 to 30 Kilovolts.

<sup>c</sup>No additional filtration.

by 50%. The second half-value layer is the thickness of the absorber required to attenuate the exposure rate of the x-ray beam by another 50%. The homogeneity factor is defined as the ratio of the second HVL to the first HVL. The larger the homogeneity factor, the closer the x-ray beam is to approaching a monoenergetic x-ray beam. During the calibration two x-ray machines were used to obtain a reasonable rate half-value measurement. Effective energy means that monoenergetic x or gamma photons with that energy were required to have a half-value layer identical to that of the inhomogeneous x-ray beam in question. A calibrated  $^{137}\text{Cs}$  gamma-ray source was used to obtain a reference point while the x-ray machine provided 14 different effective energies from 23 to 45 keV. Energy response of LiF used in this study is shown in Figure 30. The energy dependence of the response per exposure normalized to 1.00 at 662 keV is shown. The TL emission of LiF:Mn increases slowly as the effective energies decrease. However, below an effective energy of 28 keV, the response declines. The maximum response occurred at an effective energy of about 28 keV which gave a value for the ratio of response to  $^{137}\text{Cs}$  of about 1.35. These results were in very close agreement with data of other authors (1.2 ~ 1.5) (Cameron et al., 1964; Greenhouse et al., 1967; Thomas et al., 1967; Gorbics and Attix, 1967; Jayachandran, 1970; Spurny et al., 1973; Bushong et al., 1974). Energy dependence of  $\text{CaF}_2\text{:Mn}$  used in this study is shown in Figure 31. The energy response per roentgen of  $\text{CaF}_2\text{:Mn}$  was normalized to 1.00 at 662 keV. This TLD material was highly energy-dependent as the radiation energy decreased

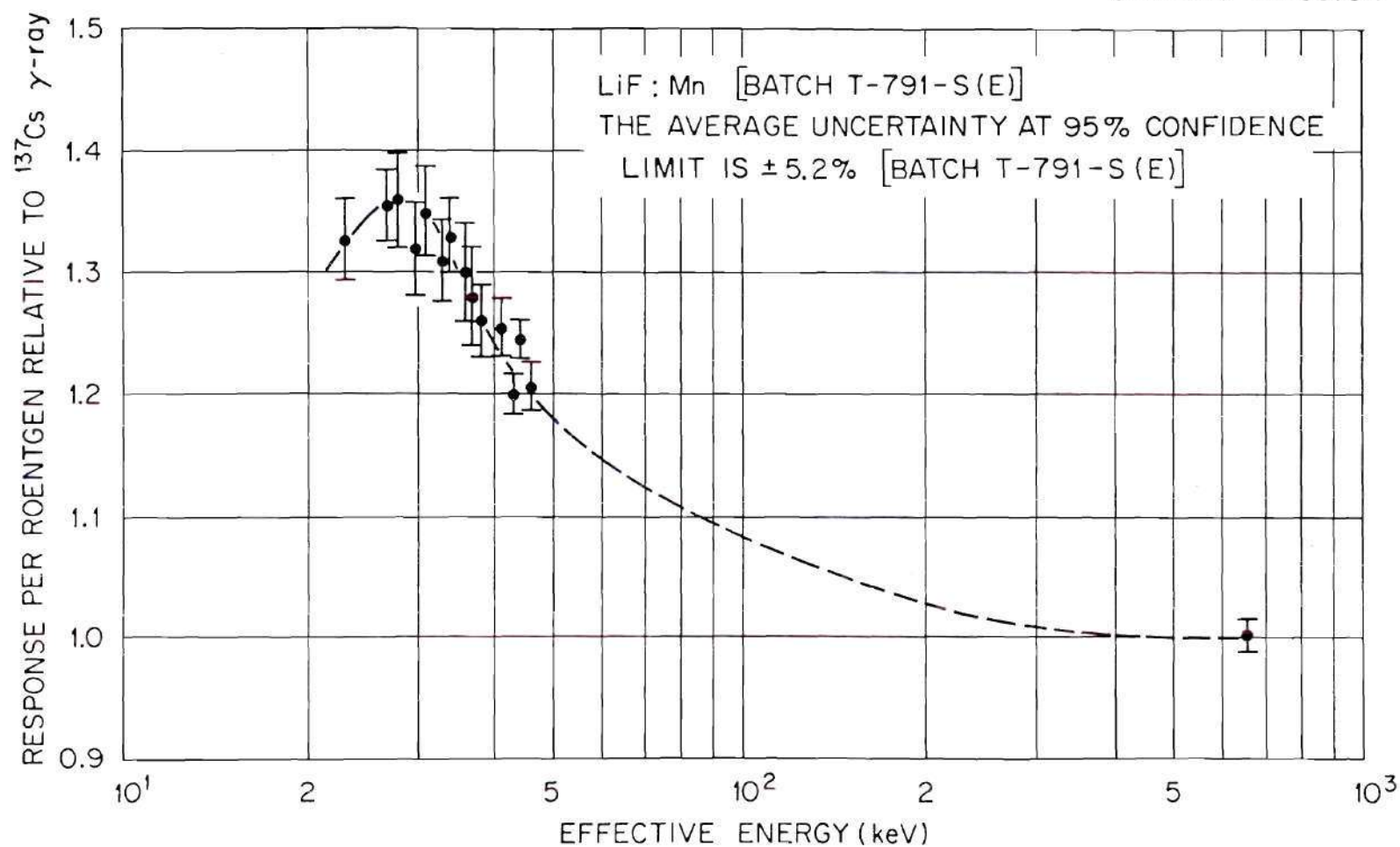


Figure 30. Relative Response of LiF:Mn as Function of Effective Photon Energy.

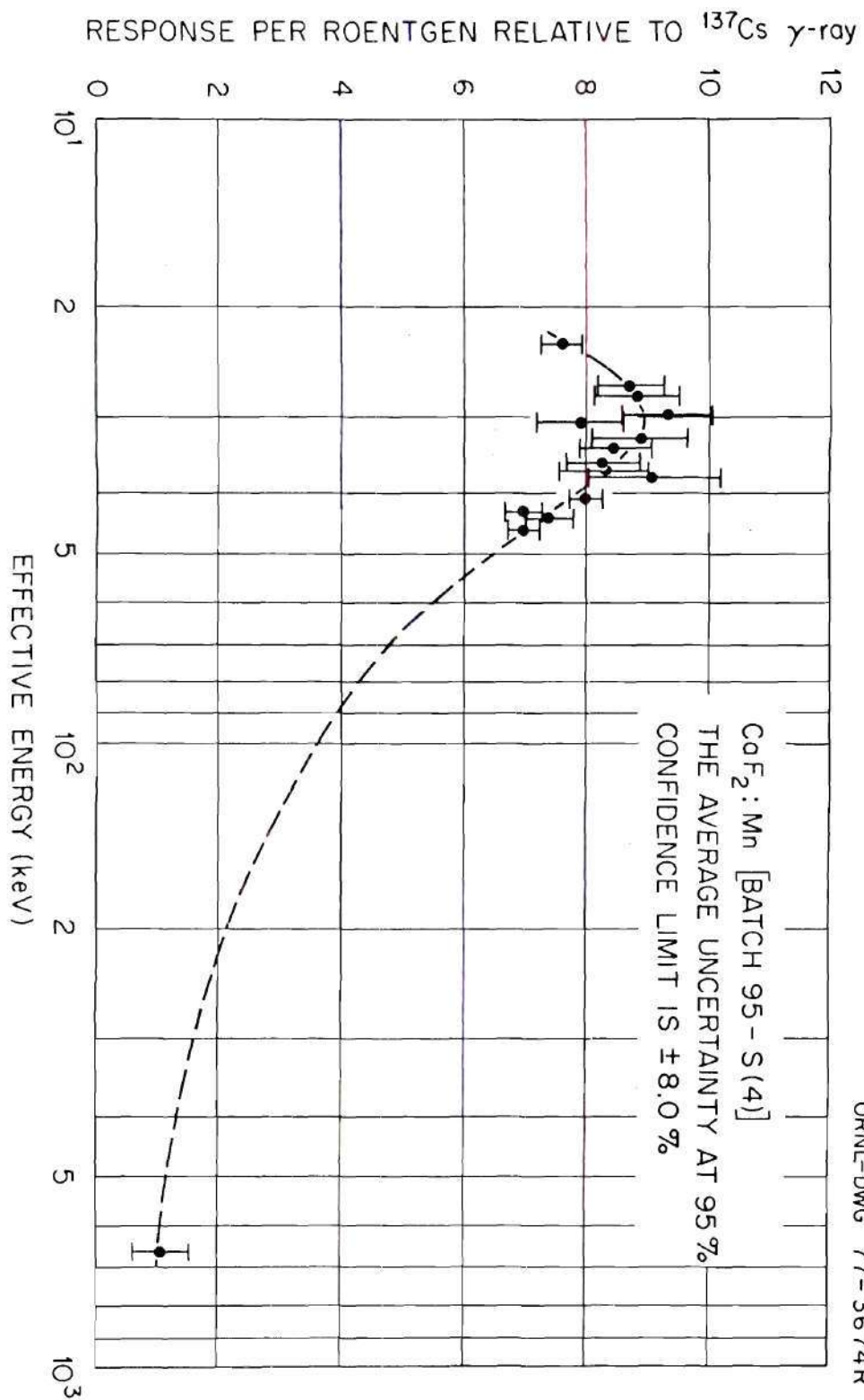


Figure 31. Relative Response of  $\text{CaF}_2:\text{Mn}$  as Function of Effective Photon Energy.



below 100 keV. The maximum response occurred at an effective energy of about 31 keV and had a value for the ratio of response to  $^{137}\text{Cs}$  of about 9. The response declined rapidly for an effective energy lower than 31 keV because of the attenuation of x rays in the phosphor blocks. The maximum value of the response ratio was in close agreement with the data of other authors (7 ~ 12) (Greenhouse et al., 1967; Thomas, 1967; Gorbics and Attix, 1967; Almond and McCray, 1970; Dixon, 1972; Spurny et al., 1973; Puite and Grebolder, 1974; Puite, 1976).

#### TLD Tandem Technique

If two kinds of TL material have two different response rates for a wide range of effective energies, then the ratio of their responses can be used to determine the effective energy of the incident radiation. This method which is used to estimate radiation quality is called the "tandem technique." Cameron and Kenny (1963) described the simultaneous use of LiF and  $\text{Al}_2\text{O}_3$  in tandem to estimate the photon energy. Facey (1968) has reported the use of  $\text{CaSO}_4$  Sm and LiF in tandem to estimate beam quality in a Mix-D phantom. Gorbics and Attix (1968) investigated the use of LiF and  $\text{CaF}_2$ :Mn in tandem as a personnel dosimeter. Rossiter (1975) discussed the possibility of the determination of beam quality of medium-energy x rays by employing TLD-700 and  $\text{CaSO}_4$ :Dy in tandem. Puite (1976) using  $\text{CaF}_2$ :Mn and TLD-700 in tandem measured the absorbed dose at various depths in water. In this study, groups of five LiF:Mn and  $\text{CaF}_2$ :Mn dosimeters were exposed simultaneously to 15 different photon beams with effective energies ranging from 23 to 662 keV. The ratio of the thermoluminescence

response of  $\text{CaF}_2:\text{Mn}$  to  $\text{LiF}:\text{Mn}$  was found to vary from approximately 7.2 to 1 at  $^{137}\text{Cs}$  energy to a maximum of 45 to 1 at about 31 keV and then decline sharply at lower energies because of the attenuation of the phosphor (see Figure 32). These results were slightly different from those reported by other authors. However, Binder and Cameron (1969) have pointed out that the relative sensitivity of these dosimeters is dependent on the type of instrumentation employed and the manner in which the dosimeters are analyzed. Generally the amount of ambiguity in effective energy determinations by these tandem techniques is inversely proportional to the absolute value of the slope of the response ratio of the tandem curve.

#### Measurements of Absorbed Dose in Pediatric Phantoms

##### Experimental Procedure

Field size and beam location simulating typical pediatric x-ray examinations in the better medical facilities of the U.S. are given in Table 16. Such examinations were simulated in this research. Several factors were considered in choosing the particular radiological examinations to be simulated. It was desired to choose a set of exposure configurations that would be representative of the most frequent medical x-ray examinations and yet not redundant. Most of the technical factors considered in these examinations are those used routinely in the Department of Radiology of the Henrietta Egleston Hospital for Children (McClure, 1976). Examinations of the extremities were not included because of the oversimplified geometry of the phantoms in these regions.

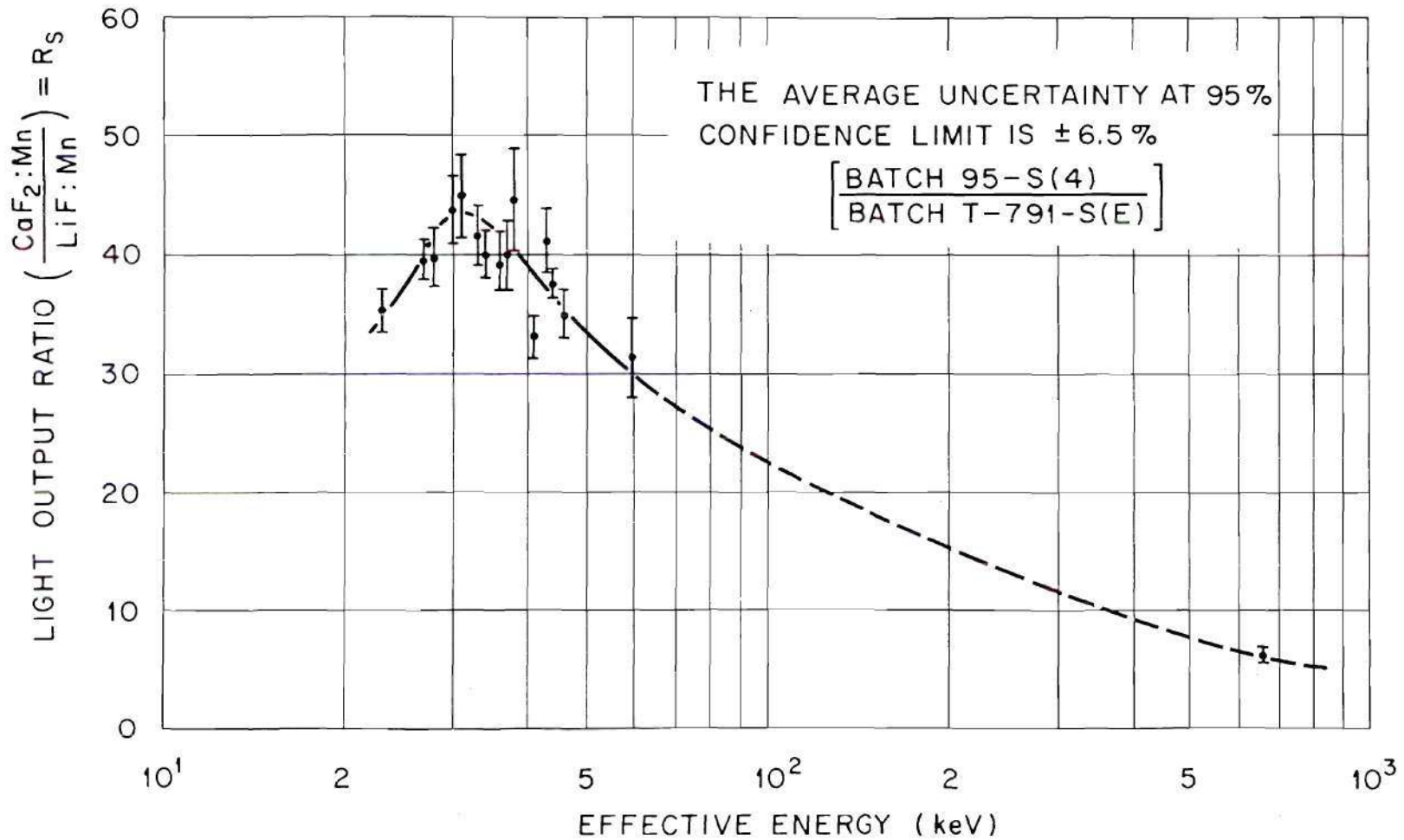


Figure 32.  $\text{CaF}_2\text{:Mn}$  and  $\text{LiF:Mn}$  Dosimeter Response Ratio versus Effective Photon Energy.

Table 16. Technical Factors for Pediatric Phantom Exposures to Some Typical Diagnostic X-Ray Procedures<sup>a</sup>

One-Year Old	Generating Potential (kV)	FSD <sup>b</sup> (cm)	Field Size (width × high cm <sup>2</sup> )	Center of the beam <sup>c</sup> (X, Y, Z)	Tube Current × Exposure Time (mA-sec)
Skull					
PA	75	101.6	13.6 × 17.6	(0, 0, 40.8)	12.0
Lat	60	101.6	16.0 × 17.6	(0, 0, 40.8)	12.0
Chest					
PA	60	121.9	15.0 × 16.0	(0, 0, 26.0)	3.3
AP	60	121.9	15.0 × 16.0	(0, 0, 26.0)	3.3
Lat	75	121.9	14.0 × 16.0	(0, 0, 26.0)	3.3
Abdomen					
PA	75	101.6	15.0 × 19.2	(0, 0, 9.6)	6.5
AP	90	101.6	14.0 × 19.2	(0, 0, 9.6)	10.0
Lat	75	101.6	15.0 × 19.2	(0, 0, 9.6)	6.5
<u>Five-Year-Old</u>					
Skull					
PA	80	101.6	13.6 × 19.3	(0, 0, 51.6)	22.0
Lat	70	101.6	18.0 × 19.3	(0, 0, 51.6)	22.0
Chest					
PA	80	182.9	18.0 × 22.0	(0, 0, 36.0)	3.3
AP	80	182.9	18.0 × 22.0	(0, 0, 36.0)	3.3
Lat	100	182.9	16.4 × 22.0	(0, 0, 36.0)	3.3
Abdomen					
PA	80	101.6	18.0 × 26.0	(0, 0, 13.0)	10.0
AP	80	101.6	18.0 × 26.0	(0, 0, 13.0)	10.0
Lat	100	101.6	16.4 × 26.0	(0, 0, 13.0)	15.0

<sup>a</sup>The total filtration of all exposures was 0.28 cm-Al.

<sup>b</sup>Focus to surface distance.

<sup>c</sup>Relative to the coordinate system of the mathematical phantom.



All examinations were simulated with the phantom standing erect. All simulated focal-spot-to-surface distances (FSD) used are described in Table 16. For each simulated examination the collimator and tube height were adjusted and the field size was positioned at the mid-plane of the phantoms. For the abdominal examinations, measurements were performed with the male genitalia region both unshielded and shielded to determine the protection provided by gonadal shielding. The shielding material was a sheet of lead of thickness 0.16 cm.

Twenty or twenty-one measuring sites were chosen at the center or at suitable positions in nine regions of interest for the one-year-old and the five-year-old children phantoms, respectively (see Figures 33 and 34). The nine regions selected were the brain, thyroid, thymus, spine, arm bones, pelvis, ovaries, testes, and the leg bones. The brain (central nervous system), thyroid, and thymus were chosen because it is commonly believed that, in children, these organs are the most sensitive to ionizing radiation (Miller, 1953; Rugh, 1973; Silverman, 1974; Hempelmann, 1974, 1975). Ovaries and testes were chosen because the dose to these organs can be directly related to the genetic dose. Thirteen and fourteen sites were used for bone marrow dose measurements; see the shaded areas in Figures 33 and 34 for the one-year-old and five-year-old child phantoms, respectively. Each measuring site had six TLDs, three  $\text{LiF}_2:\text{Mn}$  and three  $\text{CaF}_2:\text{Mn}$  as shown in Figure 13, page 62. The TLDs located outside the direct beam received only scattered radiation and many repeated or long-time exposures were necessary to obtain reliable TLD readings. In such cases, a multiexposure procedure

ORNL-DWG-77-5743R

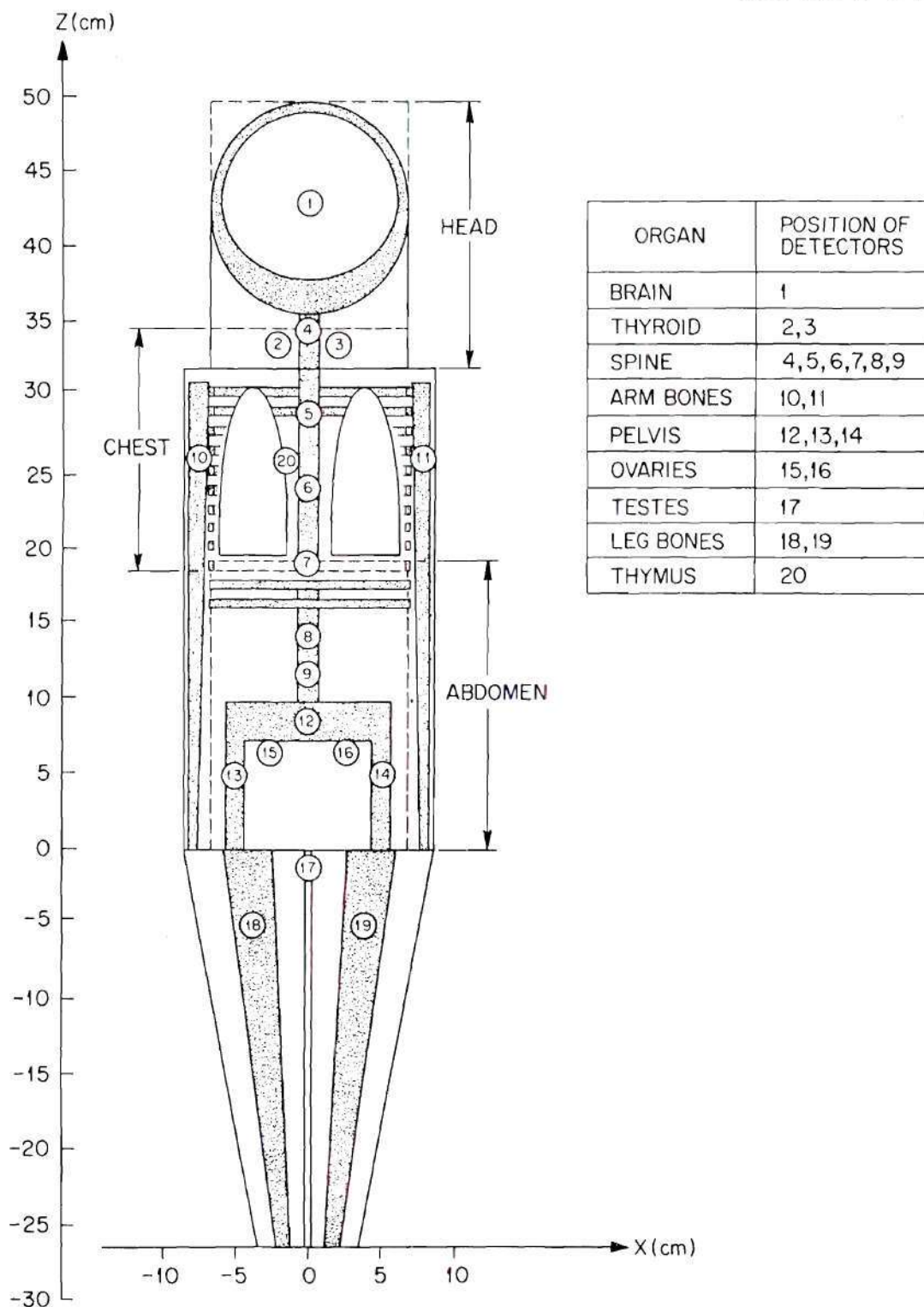


Figure 33. The Positions of the Fields and Measuring Sites for One-Year-Old Phantoms.

ORNL-DWG 77-5742R

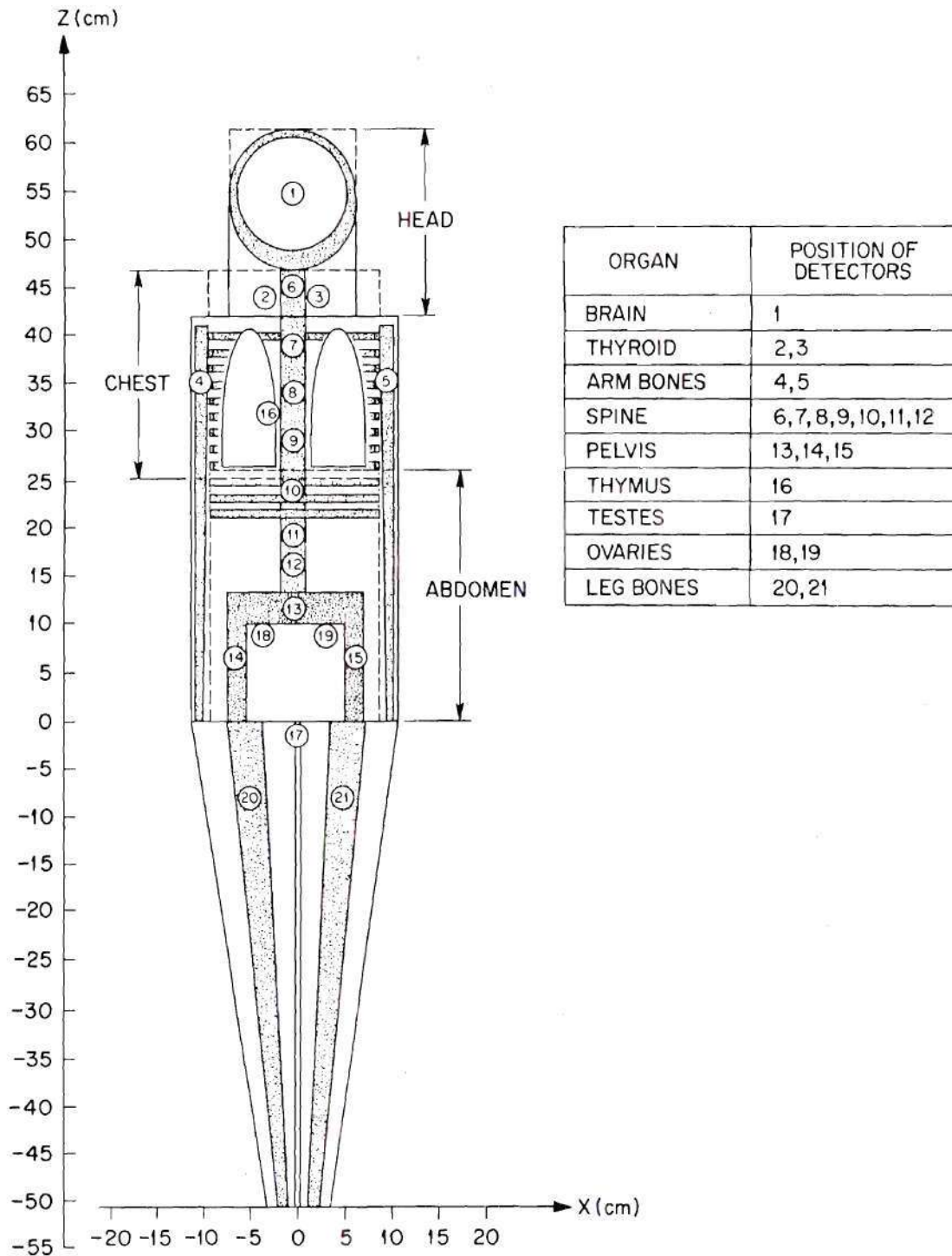


Figure 34. The Positions of the Fields and Measuring Sites for Five-Year-Old Phantoms.

was used. The TLDs, at that site, were removed when a calculation of the expected exposure indicated that the total exposure approached 200 mR. Irradiation of the phantom was continued until all TLDs had been exposed and removed. The maximum exposure used per field was 6000 mA-sec regardless of tube voltage. Experimental procedures were as follows:

1. Geometrical Arrangement (see Figure 35)
  - a. Determine and set the focus to surface distance.
  - b. Locate the center of beam on the phantom surface and adjust the field size accordingly (Table 16, page 113).
2. TLD Handling
  - a. According to the field size scheduled, select the TLDs for use at the different sites in the phantom.
  - b. Pack the TLDs into the dosimeter holders.
  - c. Using the heat-sealing device, seal the dosimeter holders into suitable size polyethylene bags. The sealed packages provide a waterproof covering so that the dosimeters can be immersed in the liquid materials of the phantom.
3. Exposure Procedures
  - a. Determine the exposure voltage setting from Table 16, page 113.
  - b. Adjust the x-ray machine to the voltage which is desired in step a. Operate the machine five minutes at 5 mA for warmup.



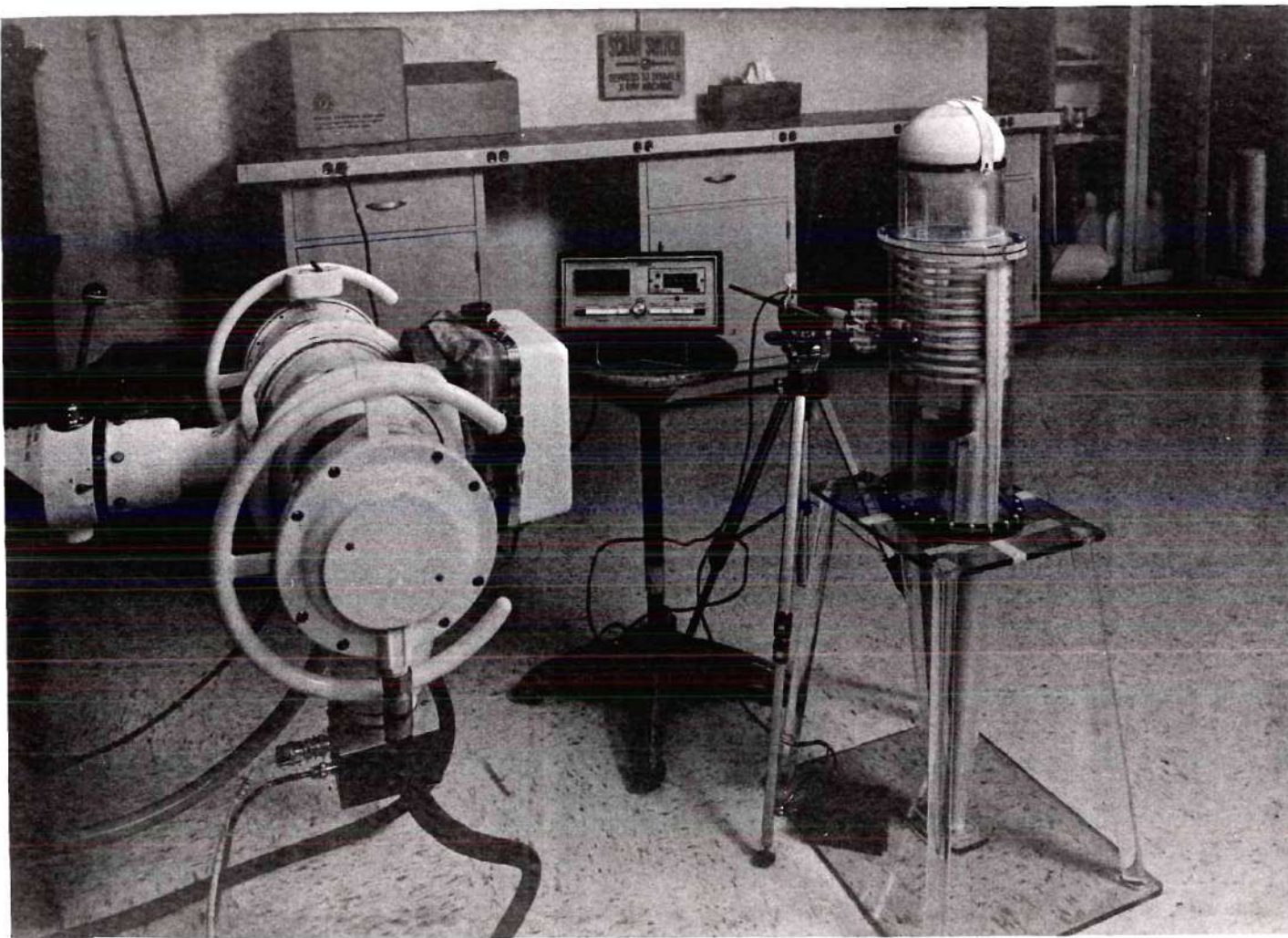


Figure 35. Simulation of the Experimental Arrangement Showing the X-Ray Machine, Ion Chamber, and Five-Year-Old Phantom.

- c. Using the Victoreen Radocon III Model 555 ion chamber dosimetry system measure the air exposure rate at the position which is the center of the incident x-ray beam and also on the surface of the phantom (air dose rate measurement).
- d. From the air exposure rate, estimate the exposure time and tube current which will give a suitable exposure (approximately 200 mR) to the TLDs on the surface of the phantom. This set of TLDs, three LiF:Mn and three  $\text{CaF}_2\text{:Mn}$ , served as reference dosimeters which would indicate any systematic change in the TLD during later procedures.
- e. Measure the surface exposure rate with ion chamber only on the surface of the phantom (surface dose measurement).
- f. From the surface exposure rate, estimate exposure time and tube current for the "in-beam" organs and the "out-of-beam" organs.
- g. Put the packed TLDs into the phantom, using the multiple exposure method. According to the schedule in step f, irradiate the phantom and remove TLDs at suitable times after the irradiation of the phantom has begun.
- h. At the end of the exposure, all the TLDs removed from the phantom are stored in a lead box. After a 24-hour delay, read the TLDs.

### Collection and Reduction of Data

All TLD readings from the exposure were processed in the following manner:

1. Correct all TLD readings by multiplying each TLD by its own relative sensitivity factor  $C^r$  which was determined from the grading process.
2. Use the TLDs exposed on the surface of the phantom as reference dosimeters to normalize the systematic variation of the TLDs and the reader. This method is discussed below.
3. Average the three  $\text{CaF}_2\text{:Mn}$  readings of the reference dosimeters and call this  $\bar{R}_{\text{Ca}}$ .
4. Average the three  $\text{LiF:Mn}$  readings of the reference dosimeters and designate  $\bar{R}_{\text{Li}}$ .
5. Take the ratio of  $\bar{R}_{\text{Ca}}$  to  $\bar{R}_{\text{Li}}$  and define this ratio as

$$R_r = \frac{\bar{R}_{\text{Ca}}}{\bar{R}_{\text{Li}}} \quad (3-6)$$

6. Since we know the operating tube voltage and other parameters such as the filtration, the corresponding effective energy may be found from Table 15 (page 106).
7. From Figure 32, page 112, and the effective energy value the so-called "standard  $\text{CaF}_2\text{:Mn}$  to  $\text{LiF:Mn}$  ratio" can be obtained. This ratio is designated as  $R_s$ .



8. Divide the  $R_s$  by  $R_r$  to get a systematic correction factor  $C^S$ .
9. Multiply all  $\text{CaF}_2\text{:Mn}$  to  $\text{LiF:Mn}$  ratios inside phantom by  $C^S$  to get the corrected  $\text{CaF}_2\text{:Mn}$  to  $\text{LiF:Mn}$  ratio,  $R_c$ .
10. Using  $R_c$  and Figure 32, page 112, determine the effective energy inside the phantom for the different organs.
11. Whenever the effective energies are determined, the exposure of  $\text{LiF:Mn}$  and  $\text{CaF}_2\text{:Mn}$  dosimeters can be calculated from their energy response curves, Figures 30 and 31, pages 108 and 109, and their thermoluminescent measurement (dosimeter reading).

#### Tissue Dose Estimation

The absorbed dose inside the phantom in which the TLD dosimeters were positioned can be determined by the expression:

$$\text{A.D.} = T_i \times C_i^r \times C^S \times R(E) \times f(E) , \quad (3-7)$$

where

A.D. = the absorbed dose inside phantom (rad),

$T_i$  = the TLD reading for  $i^{\text{th}}$  detector,

$C_i^r$  = the individual relative sensitivity factor for the  $i^{\text{th}}$  detector,

$C^S$  = the correction factor for systematic variations of the TLD and the reading system,

$R(E)$  = the TLD reading to exposure conversion factor which is a function of the effective energy, and



$f(E) = 0.869 \left( \frac{\mu_{en}}{\rho} \right)_{med} / \left( \frac{\mu_{en}}{\rho} \right)_{air}$  is the exposure (R) to absorbed dose (rad) conversion factor which is a function of the effective energy.

The effective energies determined in the soft tissue regions of the phantoms varied from 32 keV for a chest (AP or PA) examination to 40 keV for an abdomen (lateral) examination. In this range the value of  $R(E)$  varied from 1.35 to 1.30 for LiF:Mn and 9 to 8 for  $CaF_2$ :Mn. The value of  $f(E)$  varied from 0.7975 to 0.8033. The energy correction factor is equal to the product of  $R(E)$  and  $f(E)$ . Values of this factor were calculated and found to vary from 1.0764 to 1.0443 for the LiF:Mn dosimeters and from 7.1757 to 6.4264 for the  $CaF_2$ :Mn dosimeters. The absorbed dose in organs of interest was measured for different examinations. The results are listed in Tables C-1 through C-8 for the one-year-old phantom, and Tables C-9 through C-16 for the five-year-old phantom in Appendix C.

#### Monte Carlo Calculation

A photon transport code has been written to simulate random histories of photons which originate in one source organ and to estimate the fraction of the initial photon energy absorbed in each of the target organs (absorbed fraction) (Warner et al., 1968). The computer code employs the Monte Carlo technique and is named ALGAM (a Computer Program for Estimating Internal Dose from Gamma-Ray Source in a Man Phantom). The computer program can be used to calculate the average absorbed energies in target organs for a variety of gamma-rays in a

source organ. A particular radioactive source can be specified through a computer subroutine.

A magnetic tape was prepared from tables of the photoelectric and pair-production cross sections. (Note: There was no pair production at energies used in these studies.) These data were combined with computer values of Compton cross-sections to produce, on the disk, the following tables:

1. total mass attenuation coefficient for all media under study,
2. ratio of scattering to total mass attenuation coefficient for all media,
3. ratio of pair-production to total mass attenuation coefficient for all media.

An indexing procedure was required for use in locating data in the above tables for a particular energy during the calculation. A subroutine describing the source can be written to describe the specific exposure situation, i.e., internal exposure or external exposure. This routine also describes the energy spectrum of the photons and the geometrical situation for a given source. The measured x-ray spectra from the calibrated x-ray machine for some typical diagnostic procedures served as the source routines in this study.

Each photon from the source routine was given eight of the nine parameters which characterize it, and they were changed as a result of subsequent events in its history. The eight initial

parameters with which the source photon starts included:

1. three starting coordinates relative to the phantom coordinate system;
2. three starting direction cosines relative to the axes of the phantom coordinate system;
3. the initial energy of the photon;
4. the initial statistical weight.

The statistical weight is related to the probability of existence of the photon. An initial weight of 1.0 was given to each photon and was reduced following each interaction by multiplying the initial weight by the ratio of the cross section for Compton scattering to total mass attenuation coefficient (see Equation 2-23). In this way, photons were never absorbed, thus improving the statistics of the dose estimates. A ninth characteristic parameter of the photon was defined by the mean path length which was a function of the reciprocal of the total macroscopic cross section. The mean path length for a particular energy was made constant regardless of the medium.

Energy deposition at an interaction site  $n$  by a photon coming from a previous interaction site  $n-1$  is calculated by Equation 2-24. After an interaction, the photon had a new energy and new direction both of which were governed by the well-known Klein-Nishina scattering formula (see Equation 2-9). This equation gives the cross section per electron,  $d\sigma$ , for the scattering of a photon of energy  $h\nu$  into the element of solid angle  $d\Omega$  at the angle  $\theta$  (with the energy  $h\nu'$ ).

When the histories of all source photons had been compiled and the accumulated energies were recorded, standard deviations, coefficients of variation, absorbed fractions and tissue-air ratios for each subregion (organ) were computed (Warner et al., 1968). Here the tissue-air ratio is defined as the average absorbed dose to the subregion of interest (rad) per unit exposure (R) at the surface of the phantom. The dose to the organ includes contributions from both the primary and scattered photons. Calculated tissue-air values and measured tissue-air values for selected critical organs are compared in Tables C-1 through C-16, Appendix C.

#### Bone Marrow Dose Estimation

UNSCEAR (1972) indicates that genetic effects should not be considered the primary hazard of radiation exposure. Increasing emphasis is being placed on the somatic effects of radiation (cancer, including leukemia). Generally the genetic effects are mainly associated with low-level chronic exposure. For acute high-level exposure somatic damage is more significant. The correlation between radiation dose to the active bone marrow and the induction of leukemia as indicated in studies of persons treated with radiation for ankylosing spondylitis (Court-Brown and Doll, 1957, 1965), in Japanese A-bomb survivors in Hiroshima and Nagasaki (Ishimaru et al., 1971), in fetal exposures to x rays (Stewart et al., 1958, 1970; MacMahon, 1963; Graham et al., 1966; Bross, 1972), and individuals receiving diagnostic medical x-ray examinations (Gibson et al., 1972), places a high priority on the determination of radiation dose to those organs



potentially involved in leukemogenesis. If it is assumed that:

(1) the endpoint of concern is leukemia; (2) radiation induced leukemia is produced by irradiation of active bone marrow; (3) the active bone marrow is uniformly sensitive; and (4) a linear nonthreshold dose-response effect is operative; then an evaluation of radiation dose to bone marrow sites averaged over the whole of a man's active bone marrow is proportional to the probability of that person becoming a case of radiation induced leukemia.

The mean dose to active bone marrow is given by the expression

$$\bar{D} = \frac{\sum_j D_j M_j}{\sum_j M_j} = \frac{\text{total energy of radiation imparted}}{\text{total mass of active marrow}}, \quad (3-8)$$

where

$D_j$  is the mean local active bone marrow dose for  $j^{\text{th}}$  subregion,  
and

$M_j$  is the mass of active bone marrow in  $j^{\text{th}}$  subregion.

In this study, the mean active bone marrow dose was estimated by two methods: (a) calculated by the Monte Carlo method, and (b) by experimental measurement within a phantom.

Calculated Active Bone Marrow Dose. There are two classifications of bone marrow in an adult which commonly are referred to as red and yellow marrow; however, in one-year-old children there is essentially no yellow marrow and in five-year-old children only about 5 to 10% of

the bone marrow is yellow marrow (see Table 17). Red bone marrow is hematopoietically active, while yellow marrow has no hematopoietic activity, being composed mostly of fat. The active bone marrow is assumed to be the organ associated with leukemia. Active bone marrow is located mostly in cavities of trabecular bone. The principal sites of active marrow are the pelvis, spine, ribs, sternum, skull, scapulae, and the heads and necks of the femora and humeri. For the one-year-old phantom the total mass of active marrow in the skeleton is 150 g. For the five-year-old phantom 401 g were assigned as the total mass of active bone marrow in the skeleton. The active bone marrow distributions are given in Tables 18 and 19. Each of the bone regions in Table 17 is programmed into the Monte Carlo calculation separately and therefore the energy deposition is recorded in each. The tissue-air ratios in Tables C-1 to C-16, Appendix C, are based on the summation of energy depositions for all skeleton regions after appropriate weighting for the active marrow fraction in each. This procedure is consistent with the recommendations of the International Commission of Radiological Protection for partial organ irradiation when the doses are less than 100 rad (ICRP, 1970b). After the photon histories are followed and energy depositions are recorded for each of the skeletal regions described in Table 17, the deposited energy is partitioned to marrow and bone by the following weighting method:

Table 17. The Distribution of Active Bone Marrow in Children<sup>a</sup>

Site	One-Year		Five-Year	
	Distribution of Red Bone Marrow in Skeleton (%)	Red Marrow Fraction of Total Marrow (Red & Yellow) in the Bone	Distribution of Red Bone Marrow in Skeleton (%)	Red Marrow Fraction of Total Marrow (Red & Yellow) in the Bone
Arms	4.08	1	4.08	0.8
Upper	1.38	1	1.38	0.8
Lower	2.70	1	2.70	0.8
Clavicles	1.12	1	1.12	0.9
Legs	8.81	1	8.81	0.8
Upper	4.54	1	4.54	0.8
Lower	4.27	1	4.27	0.8
Pelvis	34.44	1	34.44	0.9
Ribs	13.00	1	13.00	0.85
Scapulae	3.48	1	3.48	0.9
Skull	7.00	1	7.00	0.9
Cranium	6.37	1	6.37	0.9
Mandible	0.63	1	0.63	0.9
Spine	28.04	1	28.04	0.95
Upper	3.14	1	3.14	0.95
Middle	14.00	1	14.00	0.95
Lower	10.90	1	10.90	0.95

<sup>a</sup>Shleien, 1973.

Table 18. Masses of Red and Yellow Marrow and Bone in the One-Year-Old Child Phantom<sup>a</sup>

Bone Region	Red Marrow (g)	Bone (g)	Yellow Marrow (g)
Arms <sup>b</sup>			
Upper <sup>b</sup>	2.07	50.42	0
Lower	4.06	89.13	0
Clavicles	1.68	9.35	0
Legs			
Upper <sup>c</sup>	6.81	148.81	0
Lower	6.41	144.57	0
Pelvis	51.57	73.99	0
Ribs	19.50	117.25	0
Scapulae	5.23	34.30	0
Skull			
Cranium <sup>d</sup>	9.56	423.20	0
Mandible	0.95	251.10	0
Spine			
Upper <sup>e</sup>	4.71	22.64	0
Middle	21.00	91.60	0
Lower <sup>f</sup>	16.35	25.90	0
TOTAL	150.000	1482.26	0

<sup>a</sup>Hwang et al., 1976.

<sup>b</sup>Defined as the region  $31.2 \geq Z \geq 23.5$ .

<sup>c</sup>Defined as the region  $0 \geq Z \geq -8$ .

<sup>d</sup>Defined as the region  $Z \geq -3Y + 35.6$ .

<sup>e</sup>Defined as the region  $32 \leq Z \leq 36.5$ .

<sup>f</sup>Defined as the region  $0 \leq Z \leq 16.1$ .



Table 19. Masses of Red and Yellow Marrow and Bone in the Five-Year-Old Child Phantom<sup>a</sup>

Bone Region	Red Marrow (g)	Bone	Yellow Marrow (g)
Arms			
Upper <sup>b</sup>	5.52	84.5	1.38
Lower	10.84	148.72	2.71
Clavicles	4.48	17.22	0.50
Legs			
Upper <sup>c</sup>	18.16	395.13	4.54
Lower	17.08	384.00	4.27
Pelvis	137.80	91.10	15.31
Ribs	52.00	236.74	9.17
Scapulae	13.96	61.45	1.55
Skull			
Cranium <sup>d</sup>	26.80	449.75	2.98
Mandible	2.52	276.47	0.28
Spine			
Upper <sup>e</sup>	12.56	44.35	0.66
Middle	56.00	159.83	2.95
Lower <sup>f</sup>	43.60	38.89	2.30
TOTAL	401.32	2388.15	48.60

<sup>a</sup>Hwang et al., 1976.

<sup>b</sup>Defined as the region  $41.2 \geq Z \geq 31$ .

<sup>c</sup>Defined as the region  $0 \geq Z \geq -14.5$ .

<sup>d</sup>Defined as the region  $Z \geq -3Y + 46.7$ .

<sup>e</sup>Defined as the region  $42 \leq Z \leq 47.5$ .

<sup>f</sup>Defined as the region  $0 \leq Z \leq 21.1$ .

$$E_{mi} = E_{si} W_{mi} \frac{\left( \frac{\mu_{en}(E)}{\rho} \right)_m}{\left( \frac{\mu_{en}(E)}{\rho} \right)_s}, \quad (3-9)$$

where

$E_{mi}$  = the energy deposited in the active bone marrow in a specific skeletal region  $i$ ,

$E_{si}$  = the energy deposited in the skeletal region  $i$ ,

$W_{mi} = \frac{M_i}{S_i} = \frac{\text{mass of the active marrow in region } i}{\text{mass of the skeleton (bone + marrow) in region } i}$ , and

$\frac{\left( \frac{\mu_{en}(E)}{\rho} \right)_m}{\left( \frac{\mu_{en}(E)}{\rho} \right)_s}$  = the ratio of the mass energy absorption coefficients for active bone marrow and homogeneous skeletal composition.

The absorbed dose,  $D_{mi}$ , to the active bone marrow can be calculated by:

$$D_{mi} = \frac{E_{mi}}{M_i}. \quad (3-10)$$

Substituting  $E_{mi}$  from Equation (3-9) into Equation (3-10)

$$D_{mi} = \frac{1}{M_i} \left[ E_{si} W_{mi} \frac{\left( \frac{\mu_{en}(E)}{\rho} \right)_m}{\left( \frac{\mu_{en}(E)}{\rho} \right)_s} \right] \quad (3-11)$$

$$\begin{aligned}
&= \frac{1}{M_i} \left[ E_{si} \frac{M_i}{S_i} \frac{\left( \frac{\mu_{en}(E)}{\rho} \right)_m}{\left( \frac{\mu_{en}(E)}{\rho} \right)_s} \right] \\
&= \frac{E_{si}}{S_i} \frac{\left( \frac{\mu_{en}(E)}{\rho} \right)_m}{\left( \frac{\mu_{en}(E)}{\rho} \right)_s} \\
&= D_{si} \frac{\left( \frac{\mu_{en}(E)}{\rho} \right)_m}{\left( \frac{\mu_{en}(E)}{\rho} \right)_s} \tag{3-12}
\end{aligned}$$

where

$D_{si}$  is the absorbed dose to the skeleton in region  $i$ .

The values of  $\left( \frac{\mu_{en}(E)}{\rho} \right)_m$  and  $\left( \frac{\mu_{en}(E)}{\rho} \right)_s$  were calculated using a small computer program, TECALC, (Stansbury, 1974) and the ratio

$$\left( \frac{\mu_{en}(E)}{\rho} \right)_m / \left( \frac{\mu_{en}(E)}{\rho} \right)_s$$

versus energy is shown in Figure 36.

The bone and marrow in the phantoms are mixed homogeneously in the skeleton, i.e., there is no geometrical representation of the marrow cavities. Therefore, a correction for the enhancement of the absorbed dose in the marrow cavities is necessary. The average value of 1.05 for the correction factor (Spiers, 1968) was chosen and the active bone marrow dose was expressed as

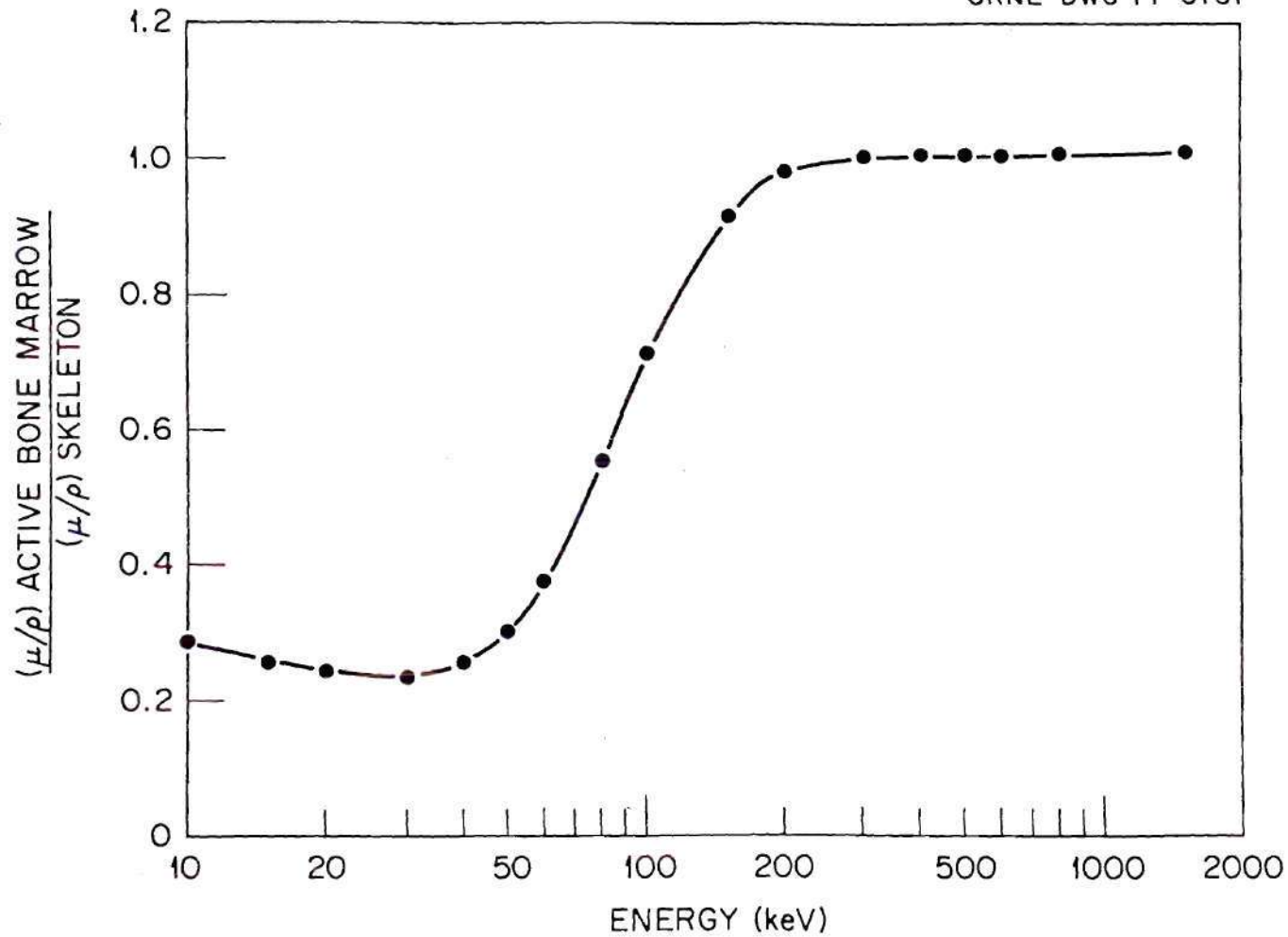


Figure 36. Mass Energy Absorption Coefficient Ratios, Active Marrow to Skeleton, as a Function of Photon Energy.



$$D_{mi} = 1.05 D_{si} \frac{\left( \frac{\mu_{en}(E)}{\rho} \right)_m}{\left( \frac{\mu_{en}(E)}{\rho} \right)_s} . \quad (3-13)$$

The active bone marrow doses were calculated by the Monte Carlo method for some typical x-ray diagnostic examinations. These results were compared with the absorbed dose measurements obtained with TLD. Most of the experimental and calculational results agreed within twice the coefficient of variation of the calculation (see Tables C-1 to C-16, Appendix C).

Measured Active Bone Marrow Dose. First, the exposure at the bone marrow sites that were selected was determined by TLD measurements. Secondly, the absorbed dose at bone marrow sites were calculated. This calculation took into account the attenuation of bone substitute material and the size of the cavity in which the specific increment of active marrow  $m_i$  was located. The small size of the TLDs allows them to be placed into selected sites without significant perturbation of the radiation field. Thirteen to fourteen sites in various bones of the skeleton were chosen for placement of TLDs to represent the important regions in which active bone marrow is located, as shown in Figures 33 and 34, pages 115 and 116. The value of 1.05 was selected to correct the small size of bone marrow cavity (Spiers, 1968). Active bone marrow doses which were measured by TLD can be expressed as

$$D_{mj} = A.D. \times C^c \times C^f \times C^a(E) , \quad (3-14)$$

where

- $D_{mj}$  is the active bone marrow dose in the  $j^{\text{th}}$  region,
- A.D. is the absorbed dose for soft tissue defined in Equation (3-7),
- $C^c = 1.05$  is the cavity size correction factor,
- $C^f$  is the yellow marrow fraction correction factor, and
- $C^a(E)$  is the attenuation correction factor for the bone substitute material.

The generating potential used in most diagnostic procedures is usually less than 120 kVp. Use of generating potentials in this range produces x-ray spectra with effective energies in the range 30 to 40 keV. Since the effective energy is in the range 30 to 40 keV, photons with these energies have a mean free path of less than 1.5 cm. The radius of the spine is 1.27 cm and 1.8 cm for the one-year-old and five-year-old phantoms, respectively. These dimensions are comparable with the mean free path of x rays inside the spine. Thus an attenuation correction is necessary in this case. When the subregion active marrow dose had been estimated for various types of diagnostic examinations, the total-body active marrow dose was calculated from Equation (3-8). All measurement results are listed in Tables C-1 to C-16, Appendix C. Generally, these results agreed with the calculated values to within twice the coefficient of variation of the calculated values.

The main contribution to the average active marrow dose in the total body was from irradiation of the pelvis and the spine. Usually the posterior-anterior (PA) view examination gave a higher

active bone marrow dose than either the lateral view of the anterior-posterior (AP) examination. The active bone marrow dose distributions in the spine were plotted for chest and abdomen examinations.

Figures 37 and 38 are the active bone marrow dose distributions of the one-year-old phantom for chest and abdominal examinations.

Figures 39 and 40 are the active bone marrow dose distributions for the five-year-old phantom for chest and abdominal examinations.

The dose distributions were reasonably uniform inside the primary field and decreased sharply when out of the primary field, as shown in these figures.

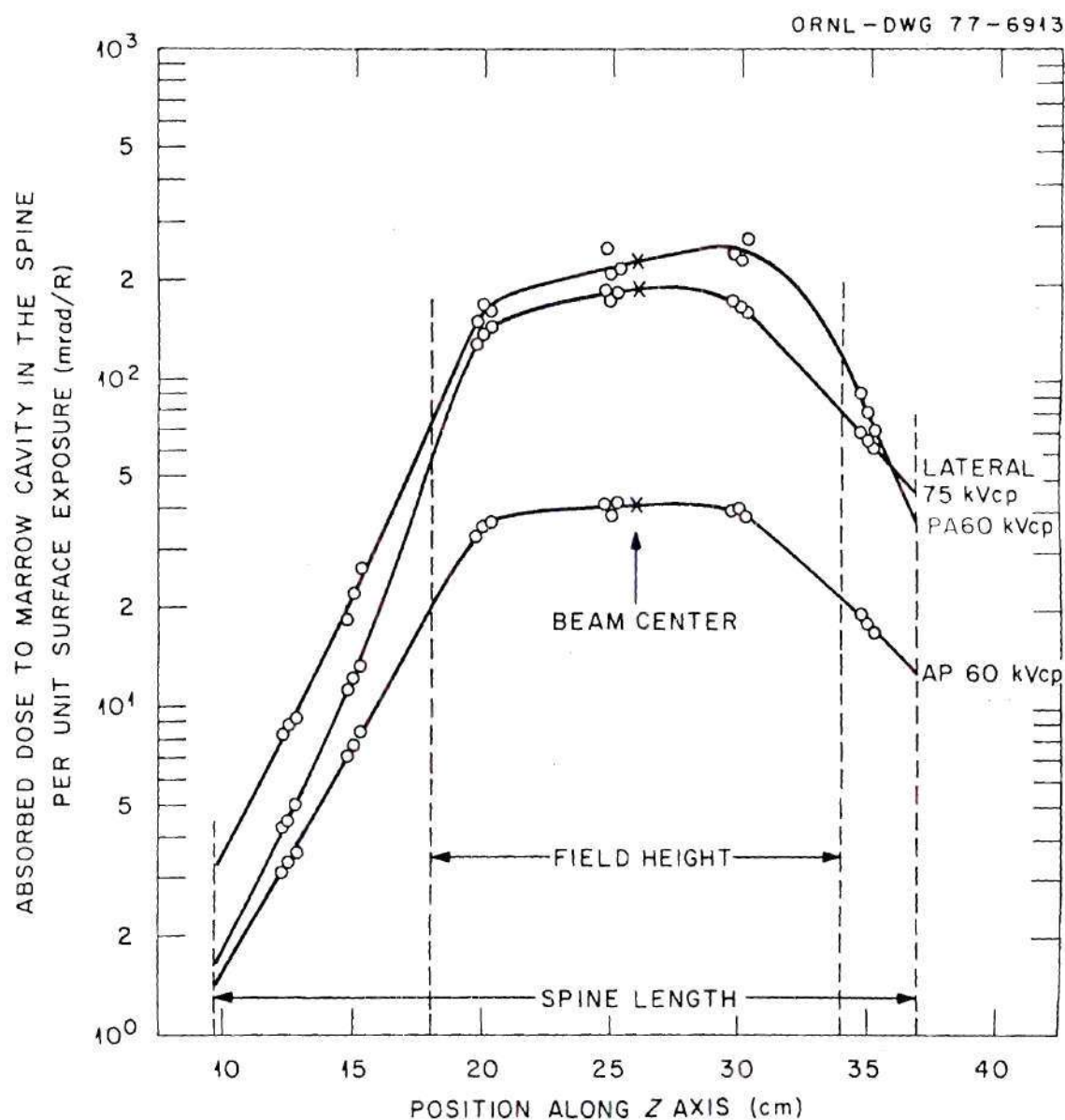


Figure 37. The Absorbed Dose Distribution in the Spine of the One-Year-Old Phantom—Chest Examinations.



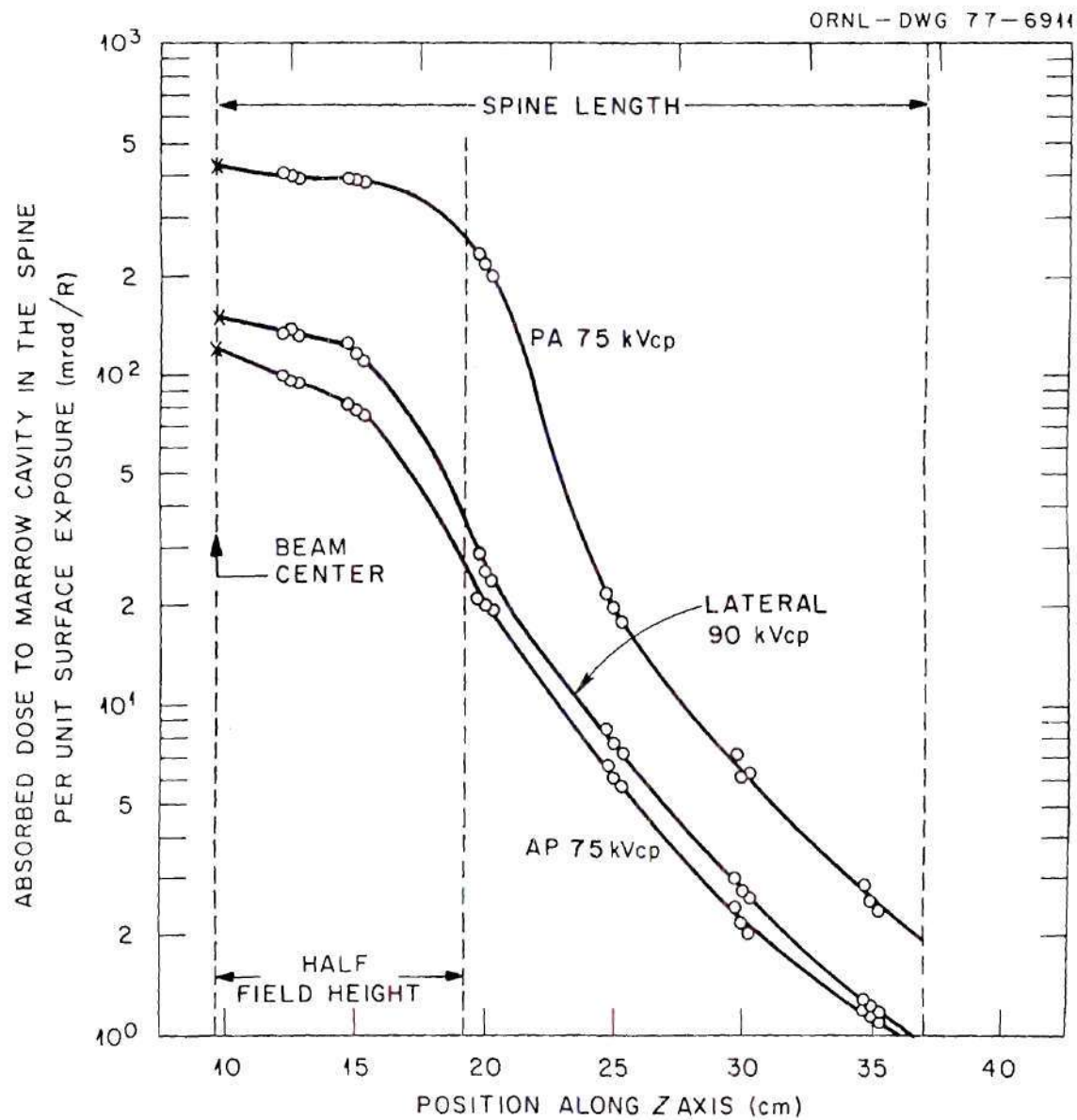


Figure 38. The Absorbed Dose Distribution in the Spine of the One-Year-Old Phantom—Abdominal Examinations.

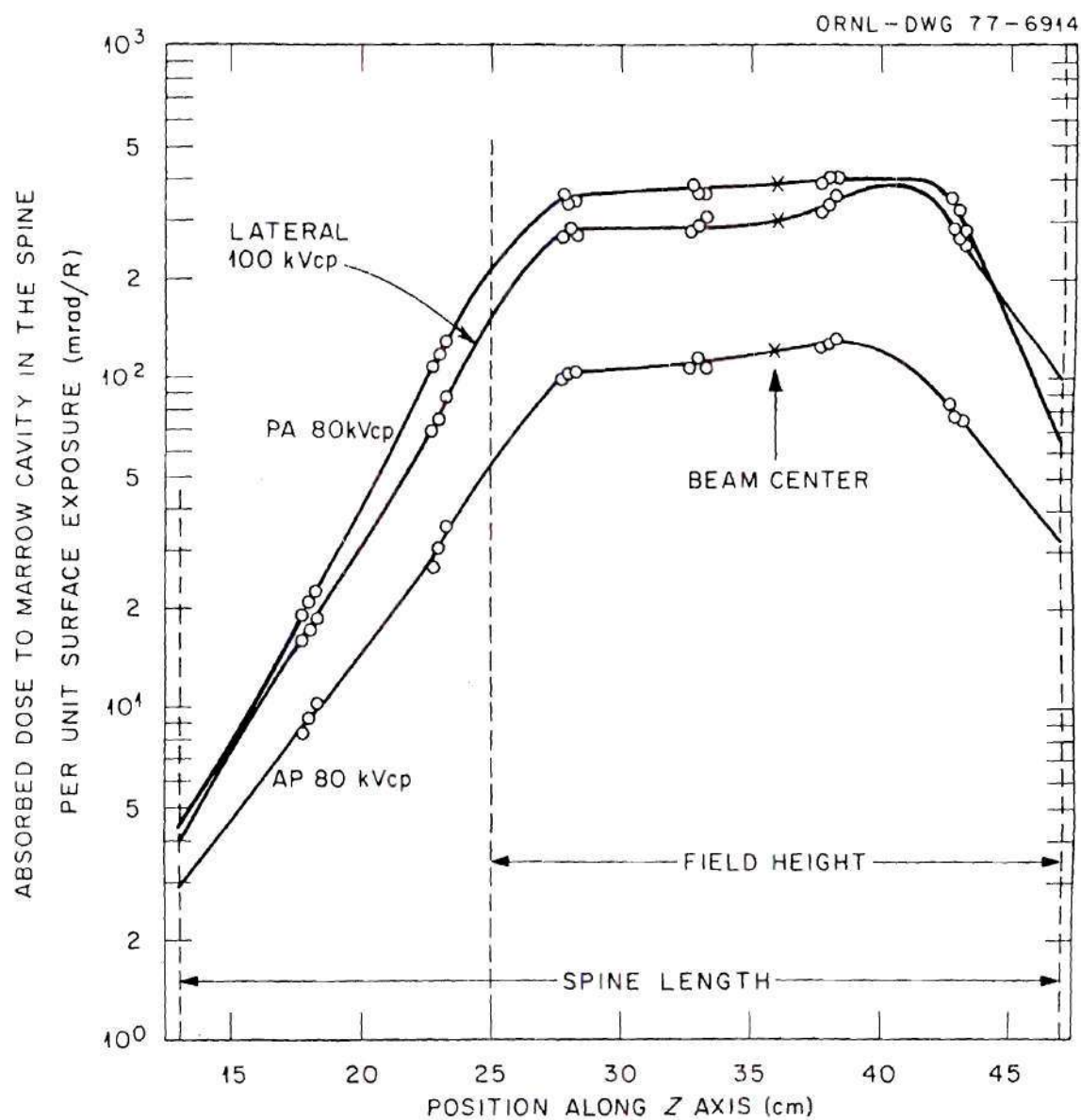


Figure 39. The Absorbed Dose Distribution in the Spine for the Five-Year-Old Phantom—Chest Examinations.

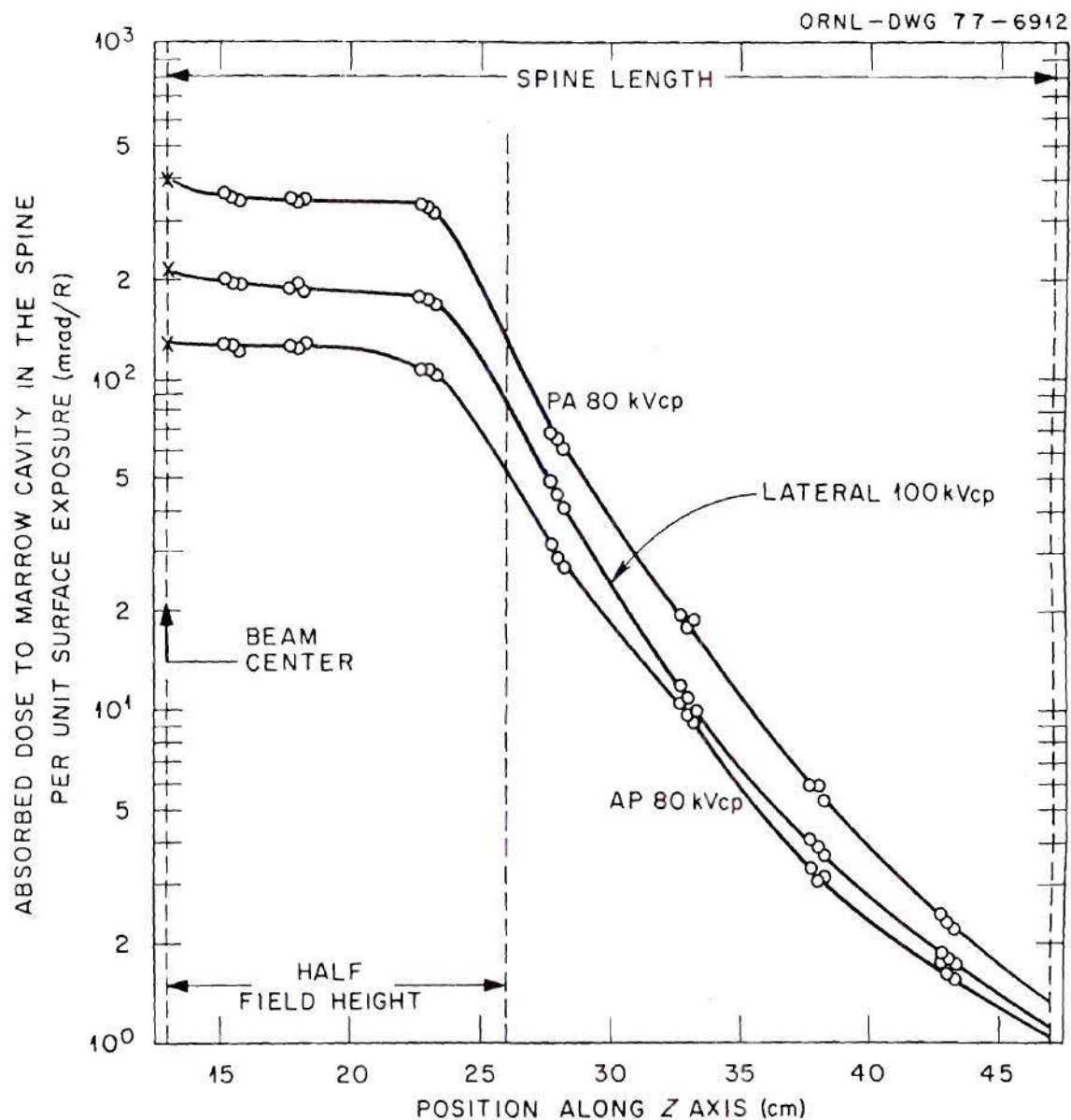


Figure 40. The Absorbed Dose Distribution in the Spine of the Five-Year-Old Phantom—Abdominal Examinations.

## CHAPTER IV

## RESULTS

Comparison of Calculated and  
Measured Absorbed Doses

For eight different examinations the tissue-air ratio (T.A.R.), the coefficient of variation (C.V.), the upper limit of acceptability of the T.A.R. (T.A.R. + 2 C.V.), and the lower limit of acceptability of the T.A.R. (T.A.R. - 2 C.V.) are given in Tables C-1 through C-16 in Appendix C. The data are for different organs or tissue subregions of interest. Both the Monte Carlo calculated values of the T.A.R. and measured values of the T.A.R. are compared in these tables. If the C.V. of the Monte Carlo estimates was greater than 50% or the measured value of T.A.R. was less than  $10^{-4}$  (rad/R) no comparison is given in the tables. For most small organs, such as the thyroid, ovaries, testes, etc., the value of the C.V. was generally high (20-30%) even for in-beam situations. The high values of the C.V. are due to the small number of photon interactions in these small organs. The values of the C.V. for the measurements were generally less than 10% for in-beam situations and higher for out-of-beam situations. This is a direct result of high exposure rates in the beam and significantly reduced exposure rates outside the direct beam. For larger organs, such as brain, spine, and pelvis, the values of the C.V. were generally lower for the Monte Carlo calculations because a large number of



interactions occurred in these larger organs. However, for the larger organs more measuring sites were needed to obtain an average absorbed dose to these organs. In the case of the brain the TLDs were located at the geometrical center of the brain. As expected the measured absorbed dose was generally lower than the calculated value which was the average absorbed dose to the organ. An attenuation correction factor was used to correct for the attenuation effect.

For most organs in this study, the Monte Carlo calculated absorbed doses agreed with the measured absorbed doses within twice the coefficient of variation of the calculated value. The absorbed dose was not measured in all the organs of the phantom, and absorbed dose estimates for some other organs may be required. In this case, if the absorbed dose determined by the Monte Carlo calculation has a low statistical error (i.e., a C.V.  $\leq 20\%$ ), the calculated absorbed doses may be used with confidence as an estimate for organs for which no experimental data are available.

#### Trends of Absorbed Dose in Organs as Function of Age

For selected radiological exposures, the absorbed dose in various organs as a function of age are shown in Figures 41 to 44. Absorbed dose for these selected exposure situations of children have been compared with those for the adult. The adult data were obtained from the work of Rosenstein (1976). In Figures 43 and 44 the data for lateral exposures follow closely that of the AP exposures. Therefore, the lateral data were not plotted to simplify the figures. No data for the thymus were available in the adult.

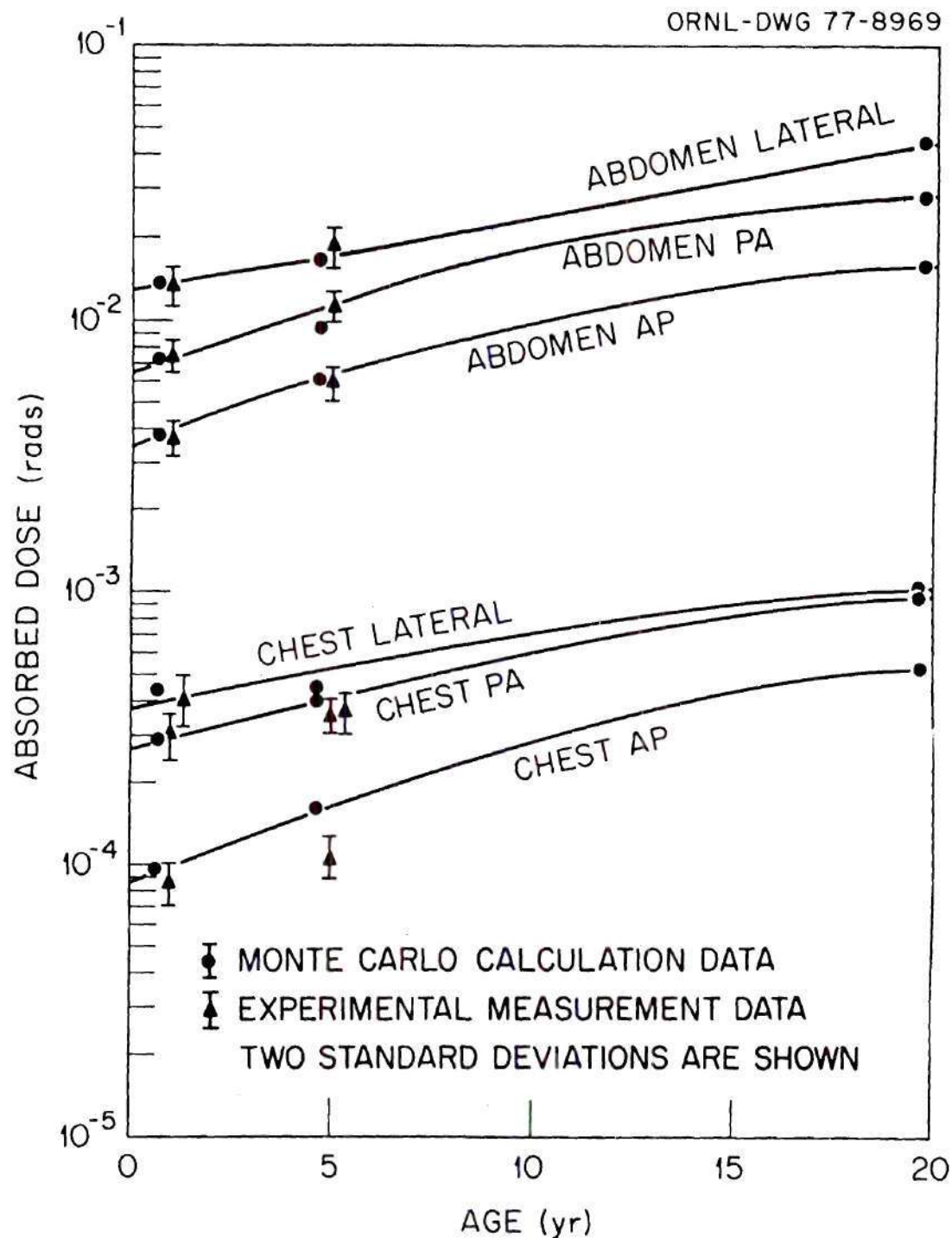


Figure 41. The Mean Active Bone Marrow Dose as Function of Age for Selected Radiological Exposures.

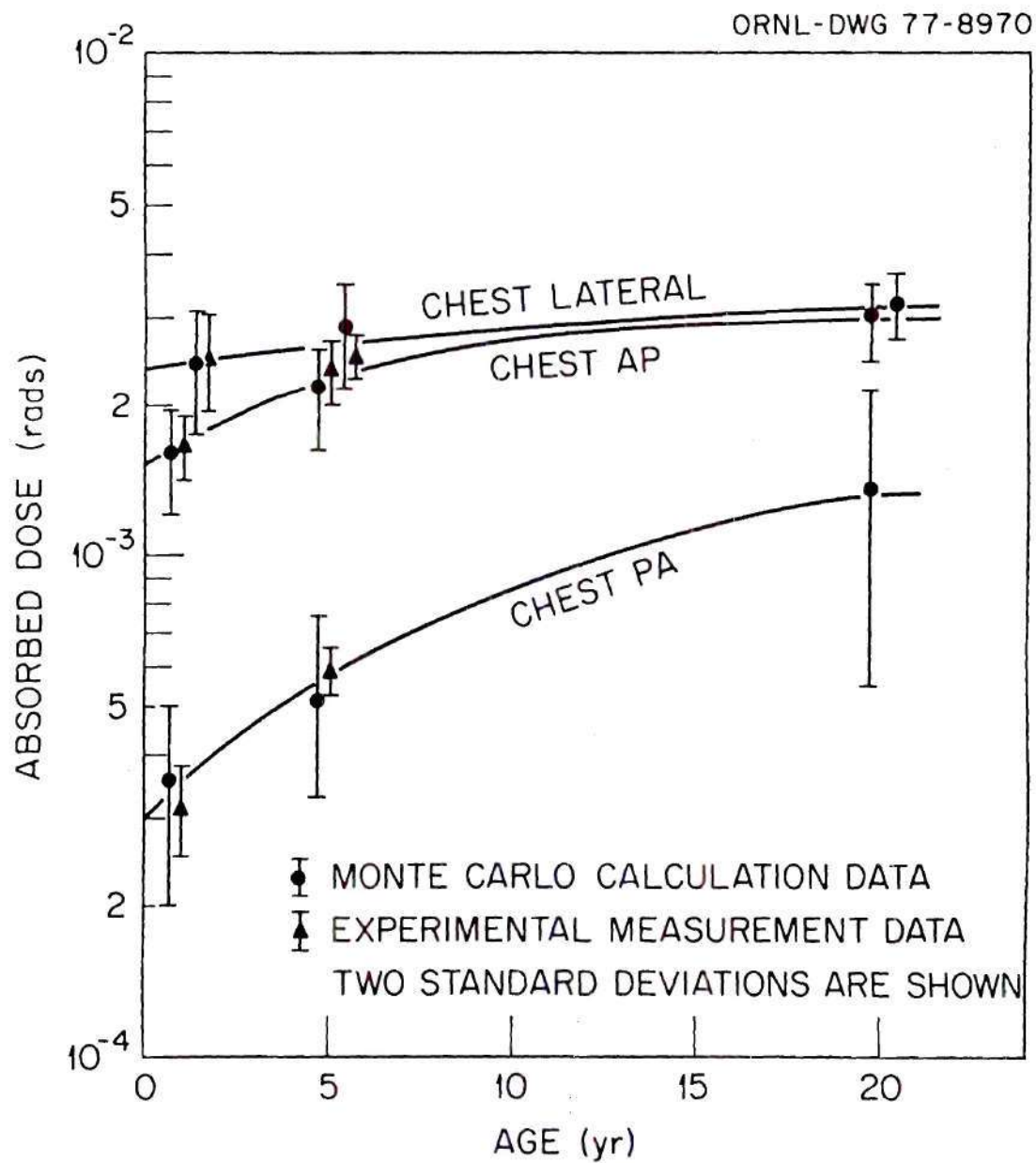


Figure 42. The Absorbed Dose of the Thyroid as Function of Age for Selected Radiological Exposures.

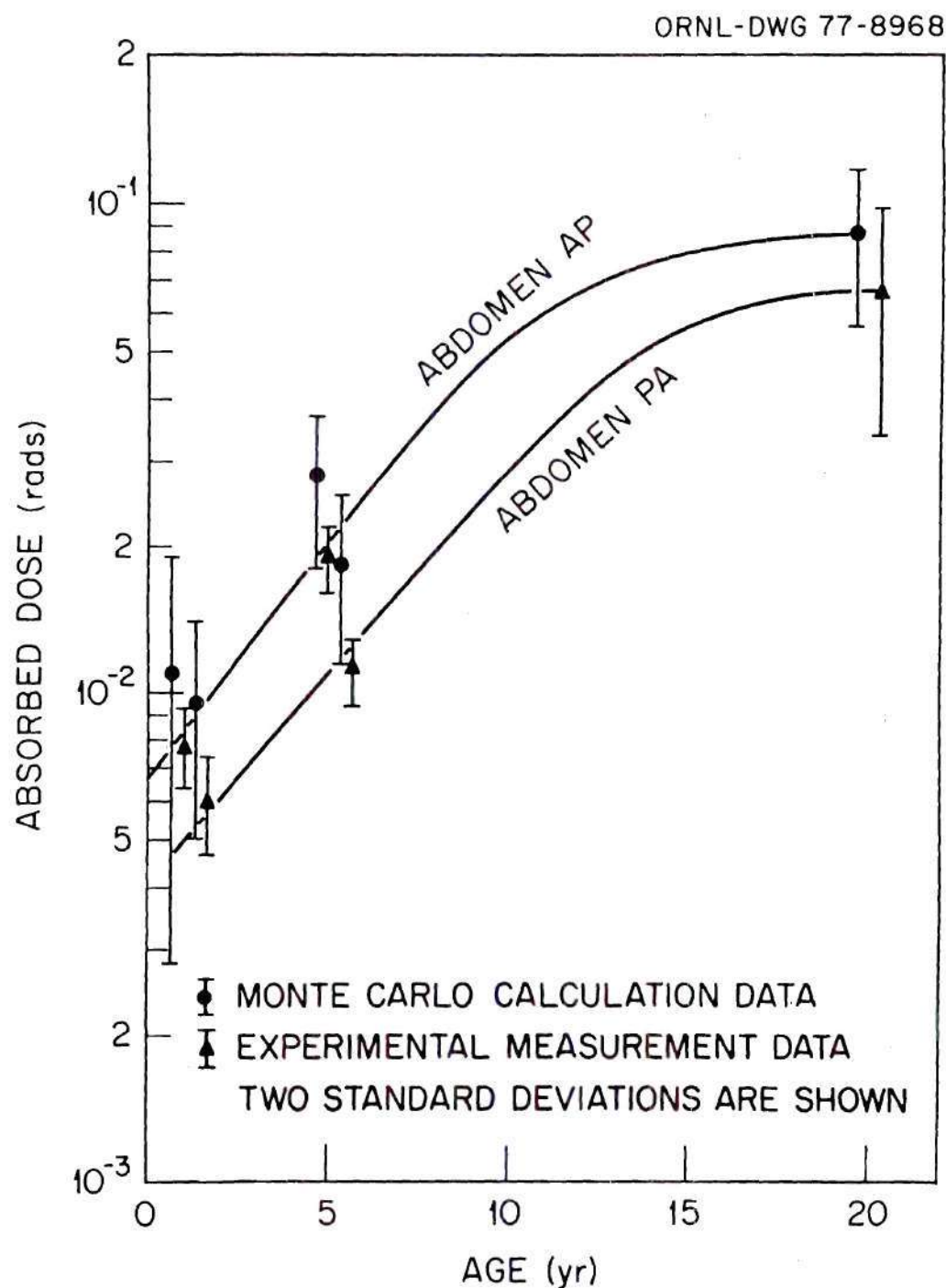


Figure 43. The Absorbed Dose of the Ovaries as Function of Age for Selected Radiological Exposures.



ORNL-DWG 77-8967

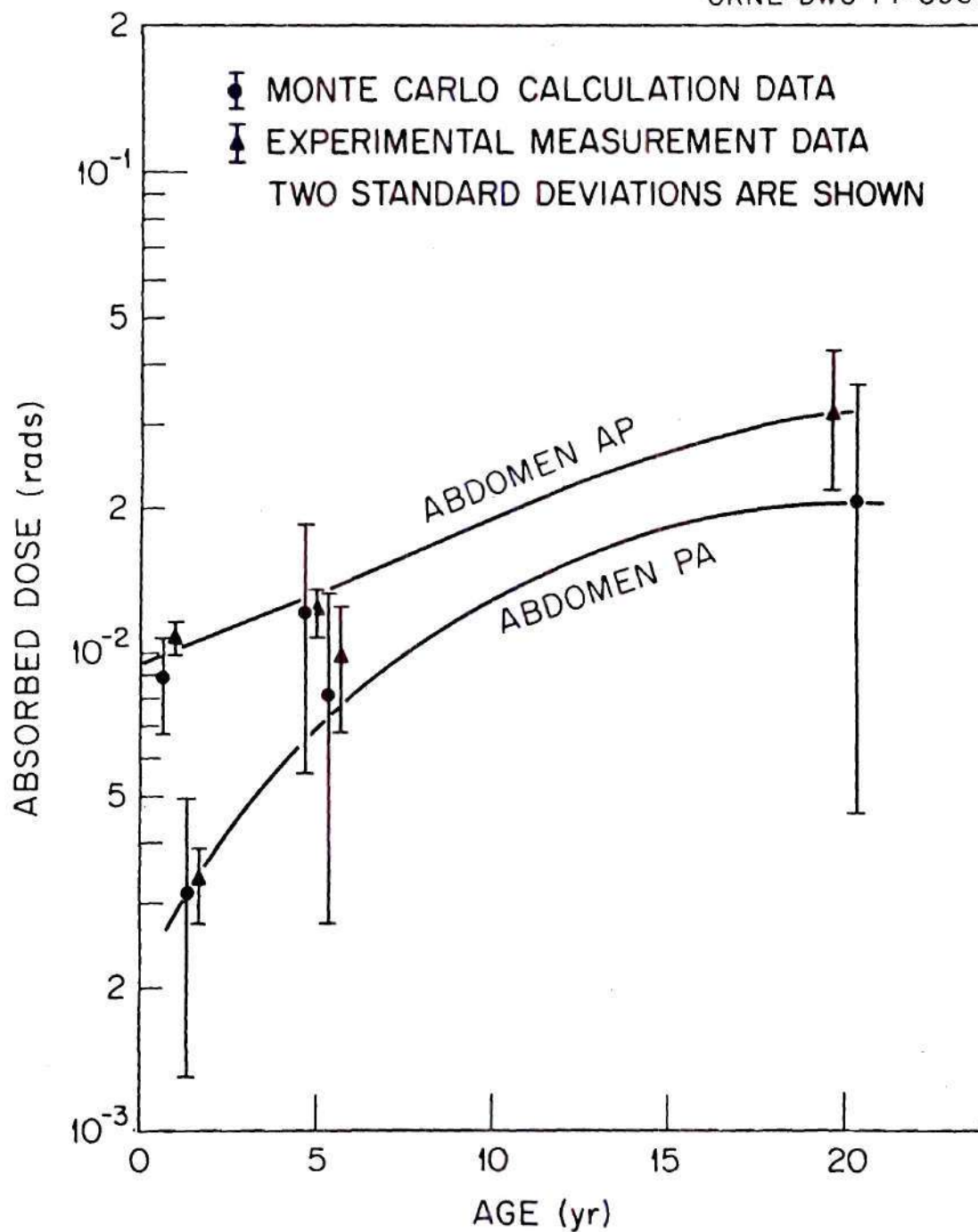


Figure 44. The Absorbed Dose of the Testes as Function of Age for Selected Radiological Exposures.

As might be expected the absorbed doses in the adult are higher than the absorbed dose in children when appropriate adjustments of tube current, exposure time and voltage are made in terms of the physical dimensions of the patient. This reduction in the absorbed dose in children can be linked to the technical factors used in the examinations as well as to the differences in physical size between the children and adult.

The body of children is not as thick as an adult and therefore lower generating potentials can be used while still obtaining the same detail on the film. In addition, beam size can be reduced due to the smaller area to be irradiated in children than in adults. For example, more than one third of the total red bone marrow is contained in the lower spine and pelvis. For an exposure in which these two regions were in the direct x-ray beam the dose to the red bone marrow will be significantly higher than the dose due to other exposures. An examination of Figure 41 makes this clear. For an abdominal examination (lower spine and pelvis in the beam) the absorbed dose is more than a factor of ten higher than for a typical chest examination.

A similar argument can be made for small organs and their location relative to the incident beam. That is, the closer the organ is to the direct radiation beam the higher the absorbed dose in the organ. For example, compare the data in Figures 43 and 44 for the dose to the ovaries and testes for AP and PA incidence. These figures indicate that the absorbed dose in the same type examination may be

different by a factor of 1.5 to more than 5 if the proper technical factors are employed in the examinations. Thus, these figures present a strong argument for close attention to proper procedures in pediatric (as well as adult) radiological examinations.

#### Risk Factor Estimation

From the earlier concept of keeping radiation doses as low as practical to recent use of the linear nonthreshold hypothesis for estimation of radiation risks, the need for justifying the benefits of radiation has become increasingly important. Morgan (1974) indicated "Medical diagnostic exposure in the U.S. is two to ten times that in most advanced countries of the world and in many respects our medical benefits per dollar spent on medical care are not better or worse than these other countries." Effective standards or legislation are urgently required to provide adequate radiation protection of the medical patient (ELASH, 1974). In this study, both the theoretical and experimental estimation of the absorbed dose in selected organs of interest has been investigated for some diagnostic types of pediatric radiology. The results provide some useful data in pediatric diagnostic processes and a quantitative basis for benefit-risk estimation.

The BEIR (1972) report suggests two ways of expressing risk: absolute risk or relative (comparative) risk. The absolute risk is the excess of risk due to irradiation. In practice, this is the difference between the risk in the irradiated population and the risk in the nonirradiated population. The absolute risk may be expressed

as the number of excess (radiation-related) cases of cancer per unit of time in an exposed population of given size per unit dose (e.g., 1 case/ $10^6$  exposed persons-year-rad).

The relative risk is the ratio between the risk in the irradiated population and the risk in the nonirradiated population. It is stated usually as a multiple of natural risk (e.g., the doubling dose).

Absolute risk estimates are generally more useful for purposes of radiation protection than are relative risk estimates because they specify directly the number of persons affected (UNSCEAR, 1964).

The absolute risk value of 3.0 cases/yr/ $10^6$  person-rem for radiation-induced leukemia in children to age 10 (BEIR, 1972) was used in calculating the risk factor for various radiographic examinations presented in this study.

The risk of radiation-induced thyroid cancer appearing in adolescence after irradiation in childhood has been investigated by many authors. It is estimated to be of the order of 1.6 to 9.3 cases per year per million children exposed per rem (Beach, 1962; Hempelmann, 1967, 1968; Jablon et al., 1971). The absolute risk value of 2.5 (BEIR, 1972) was used in calculating the risk factor for various radiographic examinations presented in this study. For the genetic risk factor it was assumed that if 1 rad was received by a parental population of one million persons  $1.9 \times 10^3$  genetic deaths would occur over the first ten generations, and  $8.5 \times 10^3$  to infinity (ICRP, 1966). The value of  $1.9 \times 10^3$  was used as the absolute risk factor in calculating the risk for various roentgenographic examinations presented in this study.



The results of risk factor for representative radiological exposures were estimated and are listed in Tables 20 and 21 for the one-year- and five-year-old children, respectively. These risk values may supply the physician a valuable reference in evaluating the cost-benefit analysis between medical benefits and radiation risk.

#### Error Evaluation

Experimental errors are introduced from many sources. These sources include the precision of the Radocon III ionization measurement system, the statistical uncertainty in the TLD readings, the uncertainty in the effective energy determinations and errors associated with positioning of the TLDs inside the phantom and aligning the x-ray field on the surface of the phantom.

The uncertainty of Radocon III is claimed to be  $\pm 2\%$  in the energy range of 15 keV to 1025 keV. The standard deviation of the TLD reading was estimated to be less than  $\pm 5\%$  in most of the TL measurements.

In the TLD energy response calibration, all TLDs were exposed in air. The energy response curves have been shown in Figures 30 and 31, pages 108-109. The x-ray spectra inside the phantom should be different than those measured in air. Two effects are responsible for a change in the x-ray spectra inside the phantom from that in air: (1) a contribution of scattered radiation from the surrounding phantom material which will tend to soften the x-ray spectra, i.e., decrease the effective energy; (2) a filtration of the incident beam with depth

Table 20. The Absorbed Dose and Risk Factors for Representative Radiological Exposures—One-Year-Old Phantom

Exam- ination	Risk Type		Leukemia	Thyroid Cancer	Genetic Death	
	Tissue		Bone Marrow	Thyroid	Testes	Ovaries
Head (PA) <sup>a</sup>	A.D. <sup>b</sup>		$1.01 \times 10^{-3}$	$3.95 \times 10^{-3}$	---	---
	R.F. <sup>c</sup>		$7.58 \times 10^{-2}$	$2.96 \times 10^{-1}$	---	---
Head (Lat) <sup>a</sup>	A.D. <sup>b</sup>		$2.70 \times 10^{-4}$	$4.30 \times 10^{-3}$	---	---
	R.F. <sup>c</sup>		$2.03 \times 10^{-2}$	$3.23 \times 10^{-1}$	---	---
Chest (AP) <sup>a</sup>	A.D. <sup>b</sup>		$8.47 \times 10^{-5}$	$1.64 \times 10^{-3}$	---	---
	R.F. <sup>c</sup>		$6.35 \times 10^{-3}$	$1.23 \times 10^{-1}$	---	---
Chest (PA) <sup>a</sup>	A.D. <sup>b</sup>		$2.98 \times 10^{-4}$	$3.13 \times 10^{-4}$	---	---
	R.F. <sup>c</sup>		$2.24 \times 10^{-2}$	$2.35 \times 10^{-2}$	---	---
Chest (Lat) <sup>a</sup>	A.D. <sup>b</sup>		$4.00 \times 10^{-4}$	$2.48 \times 10^{-3}$	---	---
	R.F. <sup>c</sup>		$3.00 \times 10^{-2}$	$1.86 \times 10^{-1}$	---	---
Abdomen (AP) <sup>a</sup>	A.D. <sup>b</sup>		$3.71 \times 10^{-3}$	---	$6.60 \times 10^{-3}$	$7.73 \times 10^{-3}$
	R.F. <sup>c</sup>		$2.78 \times 10^{-1}$	---	12.54	14.69
Abdomen (PA) <sup>a</sup>	A.D. <sup>b</sup>		$7.52 \times 10^{-3}$	---	$3.32 \times 10^{-3}$	$5.95 \times 10^{-3}$
	R.F. <sup>c</sup>		$5.64 \times 10^{-1}$	---	6.31	11.31
Abdomen (Lat) <sup>a</sup>	A.D. <sup>b</sup>		$1.33 \times 10^{-2}$	---	$9.16 \times 10^{-3}$	$9.71 \times 10^{-3}$
	R.F. <sup>c</sup>		$9.98 \times 10^{-1}$	---	18.26	18.45

<sup>a</sup>For the technical factors see Table T.<sup>b</sup>Absorbed dose in rad or rem.<sup>c</sup>Risk factor (R.F.) is the total risk, assuming a total risk period of 25 years for leukemia and 30 years for thyroid cancer. Units are cases/10<sup>6</sup> person-rem.

Table 21. The Absorbed Dose and Risk Factors for Representative Radiological Exposures—Five-Year-Old Phantom

Examination	Risk Type	Tissue	Leukemia	Thyroid Cancer	Genetic Death	
			Bone Marrow	Thyroid	Testes	Ovaries
Head (PA) <sup>a</sup>	A.D. <sup>b</sup>		$2.12 \times 10^{-3}$	$8.31 \times 10^{-3}$	---	---
	R.F. <sup>c</sup>		$1.59 \times 10^{-1}$	$6.23 \times 10^{-1}$	---	---
Head (Lat) <sup>a</sup>	A.D. <sup>b</sup>		$6.16 \times 10^{-4}$	$1.42 \times 10^{-2}$	---	---
	R.F. <sup>c</sup>		$4.62 \times 10^{-2}$	$1.07 \times 10^{-2}$	---	---
Chest (AP) <sup>a</sup>	A.D. <sup>b</sup>		$1.07 \times 10^{-4}$	$2.36 \times 10^{-3}$	---	---
	R.F. <sup>c</sup>		$8.03 \times 10^{-3}$	$1.77 \times 10^{-1}$	---	---
Chest (PA) <sup>a</sup>	A.D. <sup>b</sup>		$3.55 \times 10^{-6}$	$5.89 \times 10^{-4}$	---	---
	R.F. <sup>c</sup>		$2.66 \times 10^{-2}$	$4.42 \times 10^{-2}$	---	---
Chest (Lat) <sup>a</sup>	A.D. <sup>b</sup>		$3.59 \times 10^{-4}$	$2.52 \times 10^{-3}$	---	---
	R.F. <sup>c</sup>		$2.69 \times 10^{-2}$	$1.89 \times 10^{-1}$	---	---
Abdomen (AP) <sup>a</sup>	A.D. <sup>b</sup>		$5.88 \times 10^{-3}$	---	$1.22 \times 10^{-2}$	$1.88 \times 10^{-2}$
	R.F. <sup>c</sup>		$4.41 \times 10^{-1}$	---	23.18	35.72
Abdomen (PA) <sup>a</sup>	A.D. <sup>b</sup>		$1.13 \times 10^{-2}$	---	$9.75 \times 10^{-3}$	$1.12 \times 10^{-2}$
	R.F. <sup>c</sup>		$8.48 \times 10^{-1}$	---	18.53	21.28
Abdomen (Lat) <sup>a</sup>	A.D. <sup>b</sup>		$1.87 \times 10^{-2}$	---	$2.04 \times 10^{-2}$	$3.85 \times 10^{-2}$
	R.F. <sup>c</sup>		$1.40 \times 10^{-2}$	---	38.76	73.15

<sup>a</sup>For the technical factors see Table T.<sup>b</sup>Absorbed dose in rad or rem.<sup>c</sup>Risk factor (R.F.) is the total risk, assuming a total risk period of 25 years for leukemia and 30 years for thyroid cancer. Units are cases/10<sup>6</sup> person-rem.

in the phantom which will remove the low energy photons and will tend to harden the x-ray spectra, i.e., increase of the effective energy. In the effective energy range 30 to 40 keV, soft tissue changes the effective energy of the spectrum only slightly from that measured in air (Maillie et al., 1968; Koren, 1974). Therefore, calibration curves obtained in air can still be used satisfactorily for exposures in the phantom. In bone, the hardening effect dominates. However, the rad/R conversion factor decreases from 4.4 to 4.0 for a change in the effective energy from 30 keV to 40 keV (Koren, 1974; Stansbury, 1977). If an average rad/R conversion factor of 4.2 is chosen in the effective energy range 30 keV to 40 keV, the error introduced will be less than  $\pm 5\%$ . For practical applications, the effective energy is not usually determined in medical diagnostic radiology.

In this study, the LiF:Mn and CaF:Mn tandem method was used to determine the effective x-ray energy in the phantom. The error associated with the use of this method was assumed to be less than  $\pm 3\%$  in the effective energy range 30 keV to 40 keV. This is the average energy range which is found in most diagnostic x-ray spectra.

The angular response of the TLDs, measured during calibration, was found to be  $\pm 2\%$  except for the CaF:Mn rods which were  $\pm 5\%$ . This difference was for a change in angle of from  $0^\circ$  (normal incidence) to  $90^\circ$  (incidence on end of rod). This is shown clearly in Figure 26, page 100. Therefore, by considering the expected angle of incidence and paying close attention to the proper orientation, it was assumed that the error introduced by angular dependence for all the TLDs was less than  $\pm 2\%$ .



A meter stick, a plumb-bob, and a laser beam generator were used to determine the position of TLD holders inside the phantom and the x-ray beam center and field size on the phantom. It was estimated that overall positioning accuracy was 3mm. It was assumed that the positioning uncertainty was less than  $\pm 1\%$ .

By using a square-root of the sum of squares method to calculate the error propagation, the total experimental uncertainty from all these sources was estimated to be  $\pm 7\%$  (16.5%) in this study.

To provide an indication of the statistical uncertainty associated with the Monte Carlo calculations a standard statistical technique is employed. The procedure used to calculate the standard deviation is described in the following discussion.

Let  $E_{ni}$  be the energy deposited in the region under consideration on the  $n^{\text{th}}$  interaction of the  $i^{\text{th}}$  source photon. This energy may be zero, as it will be in the frequently occurring case when the  $n^{\text{th}}$  interaction does not occur within the region. The total energy deposited by the  $i^{\text{th}}$  photon, or by the  $i^{\text{th}}$  history, in the region will be

$$E_i^* = \sum_{n=1}^{M_i} E_{ni}^*$$

in which  $M_i$  is the number of interactions occurring in the  $i^{\text{th}}$  history before termination. An estimate of the average energy deposited per photon in the region is then

$$\bar{E} = \frac{1}{M} \sum_{i=1}^M E_i^*$$

in which M source photons were followed.

For the standard deviation,  $\sigma$ , of the estimate  $\bar{E}$ , one has

$$\sigma^2 = \frac{1}{M(M-1)} \sum_{i=1}^M (E_i^* - \bar{E})^2 .$$

The computer printout usually gives both the standard deviation and the coefficient of variation (C.V.) for each estimate of absorbed dose. Here C.V. =  $100 \frac{\sigma}{\bar{E}}$  in percent.

When the distribution of  $\bar{E}$  is known to be approximately normal, one can determine a confidence interval by using the standard deviation. However, there are several indications that  $\bar{E}$  is not normally distributed in cases where the coefficient of variation is greater than 50%. This generally occurs when there are fewer than 100 interactions contributing to the calculated absorbed dose. Under these circumstances  $\sigma$  cannot be used to estimate confidence intervals as is customary when the sample is normally distributed. A small number of interactions may occur in a region that has a small volume or that is many mean free paths from the source. Sometimes both conditions may apply. The computer records the number of photons that have an interaction in each region, and this has been examined also to estimate subjectively the accuracy of the estimate.

Examination of results in cases where the coefficient of variation exceeds 50%, compared with results of independent recalculation of such estimates, indicate that the dose estimates may be in error by a factor of 2 to 5. Thus, dose estimates with coefficients of variation greater than 50% are not used when comparing experimental and calculational results. In some cases, a coefficient of variation of less than 25% is chosen as the upper limit of acceptability of these calculated dose estimates (Poston, 1975).

## CHAPTER V

### CONCLUSION

#### Discussion

The data obtained in this study are not applied easily to the estimate of absorbed dose in pediatric radiology published previously. Hashizume et al. (1972b) have published estimates of the mean bone marrow dose per examination in Japanese child phantoms 0-2, 3-7, 8-14, and 15 years and older. Their values for chest examinations for 0-2 and 3-7 years are 4 mrad and 5 mrad, respectively. In this study, the estimates of the mean bone marrow dose are in the range 0.1 to 0.5 mrad for both the one-year- and five-year-old phantoms (see Figure 41, page 143), and these results agree reasonably well with the estimates obtained from the Monte Carlo calculations.

There are many factors which influence the comparison of these results; for example, difference in body size and unknown technical factors involving the x-ray examination. The most important seems to be the small number of dosimeters used to obtain their estimates. Hashizume and his colleagues made their estimates by exposing only five dosimeters in any particular examination. In this research, approximately 13-14 dosimeters were used (see Figures 33 and 34, pages 115 and 116). In the opinion of this author, the data obtained in this study give a more realistic value for the mean bone marrow dose



when radiographic procedures are representative of those used in the better pediatric radiological facilities in the U.S.

For an abdominal examination, Hashizume and his colleagues report values of the mean bone marrow dose per examination of 9 mrad for 0-2 year and 15 mrad for 3-7 year old children. The experimental measurements in this study range from 4-13 mrad for one-year-old and 6-20 mrad for five-year-old.

The absorbed dose estimates obtained in this study, for the testes and ovaries were compared to other work reported by Hashizume et al. (1972a). For children in the 0-2 year range, they estimated the gonad dose for an abdominal examination to be 20 mrad/examination for a male and 28 mrad/examination for a female. The results of this research gave 3-10 mrad/examination for males and 5-15 mrad/examination for females. For children in the range 3-7 years, Hashizume and his colleagues report 31 mrad/examination for the female. Again the data obtained in this research gave 7-14 mrad/examination in the male (see Figure 44, page 146) and 12-30 mrad examination in the female (see Figure 43, page 145).

In summary, the data of Hashizume et al. are generally higher than those obtained in the study presented here. Because of the number of parameters which influence the results, the temptation to draw concrete conclusions from this comparison must be resisted. However, if the results presented here are valid, then the absorbed dose (and thus the risk) from the better pediatric diagnostic procedures used in the U.S. is not as high as that estimated by using the data of Hashizume et al.

The purpose of this study was to obtain estimates of absorbed dose in selected organs and regions of phantoms representing children one year and five years of age when the better radiographic procedures (e.g., Table 16, page 113) are used. The estimates were to be compared to Monte Carlo results which simulated the experimental exposure situation as closely as possible. In addition, these absorbed dose estimates were to be inserted into existing risk estimates in order to quantify the risk estimates for some of these procedures.

These tasks were completed during this study. The estimates obtained in the physical phantom agreed with the calculated results. The risk estimates indicated that in general when the proper exposure parameters are used the risk per examination is quite low. Thus, with proper technique, the benefit of obtaining the diagnostic information should far outweigh the risk due to exposure to ionizing radiation. This of course assumes the x-ray diagnosis is needed and many publications have shown that this assumption is not justified in many cases (Morgan, 1974).

However, several points should be discussed. These items are enumerated below:

1. It appears that thermoluminescent dosimetry systems can be used to measure absorbed doses in the diagnostic energy range. However, for large organs or for distributed organs (red bone marrow) a large number of measuring sites is necessary to obtain reliable results. It is very difficult to use "point" detectors to obtain the volume averaged dose over a large organ.

2. For small organs position becomes a problem. Because the organ is small, it is easy to assume that a point measurement represents the dose to that organ. However, if the point detector is not located properly, an erroneous measurement will occur.

3. In children the measurement of the absorbed dose to the bone marrow present in the ribs is very difficult. Such measurements would increase the reliability of the results. However, in this study no measurements were made in the ribs or in the skull because of the small size of the bone cavities.

4. The tandem technique of dosimetry, using  $\text{LiF:Mn}$  and  $\text{CaF}_2\text{:Mn}$ , does not seem applicable in the diagnostic energy range (see Figure 31, page 109). There are two factors in action here. First, there is little variation of the effective energy of the x-ray spectrum over the usual generating potentials employed in pediatric radiology. Secondly, a TLD material with significantly different characteristics must be found so that the ratio of responses for the various detectors will be single-valued at all energies. A dosimeter containing high-Z material such as barium (e.g.,  $\text{BaF}_2$ ) may be quite useful in the tandem application in the diagnostic energy range.

5. The Monte Carlo results presented in this study represent a compromise between accuracy and cost. The accuracy of the calculated results could be improved by increasing significantly the number of photon histories traced in each calculation.



## Recommendations

Medical diagnostic radiology accounts for at least 90% of the total man-made radiation dose to which the U.S. population is exposed. In order to limit patient exposure as low as practicable without losing its benefits, the following recommendations are made for applications during pediatric diagnostic radiography:

1. Due to the small body size and volume of young children, a large portion of their total body is exposed to radiation beams that would cover only a small area in the adult. Therefore, confining the x-ray beams to the smallest area commensurate with adequate illumination of the field of interest not only improves detailed discrimination of radiographic images, but can reduce patient dosage and decreases the scattered radiation dose to attending personnel and technicians.

2. Whenever possible gonadal shielding is always recommended for most diagnostic procedures. It can reduce the gonadal dose in some procedures by a factor of 30. Usually lead of 0.16 cm thickness or equivalent lead rubber will satisfy the requirement. Using a lead glass to shield out-of-beam parts of the patient's body can reduce the radiation which is scattered from the collimator.

Radiography depends on the fact that a small portion of the radiation energy impinging on the patient emerges on the other side of the body and then selectively blackens the x-ray film. The difference in energy between the entry and exit radiation, constituting the greater part of the total radiation, is either absorbed by the



skin and deep tissue structures or scattered to surrounding areas. The input radiation may be dramatically reduced without loss of the necessary exit radiation required to produce the film image in the following ways:

3. Increased filtration at the x-ray tube head amounting to 0.3 to 0.6 cm of aluminum should be used. Since low energy photons generally cannot pass through the patient's body, they contribute little to producing an image on the x-ray film. The filter will absorb selectively these lower energy photons. Thus, the added filtration reduces the entry dose to the patient without sacrificing detail of the film image.

4. Increasing the energy (kilovoltage) of primary beam in conjunction with a grid (or Bucky diaphragm) technique can greatly reduce the scattered radiation and reduce the patient dose without loss of much detail of the film image.

5. The use of high-speed intensifying screens and high speed film can also reduce the patient dose without loss of the quality of image on the x-ray film.

6. The judicious use of clinical x-ray examination of pediatric patients, avoiding as far as possible, unnecessary repetitive diagnostic radiography, and technically nondiagnostic radiography is most desirable. Technically unsatisfactory roentgenograms are a waste of time, effort, and money. Moreover, every nondiagnostic film requires a retake and thus a doubling of patient exposure and associated radiation risks.

## Appendix A

The Sectional Plots of the One-Year-  
and Five-Year-Old Phantoms

CRM-L-DWG 75-5827

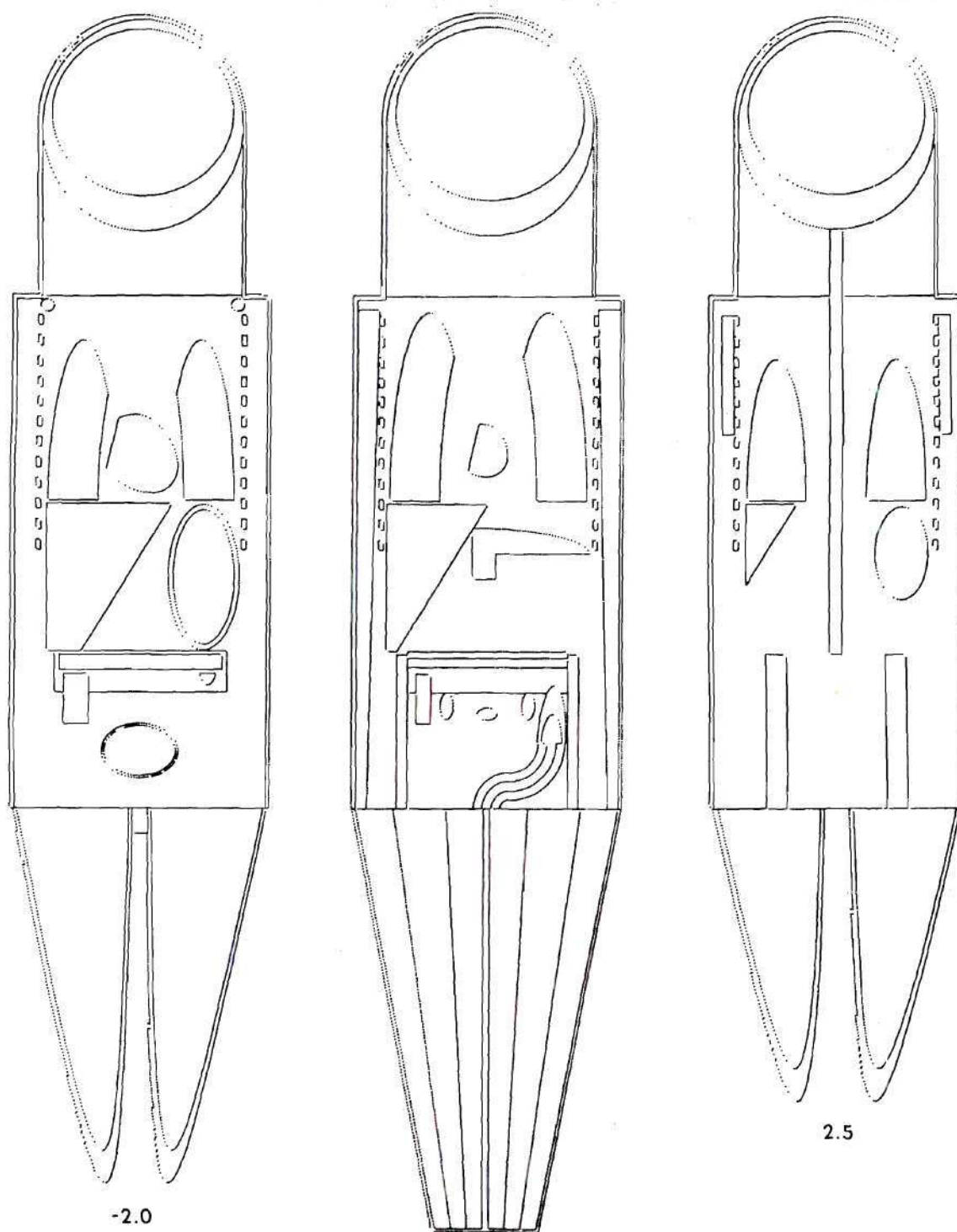


Figure A-1. X-Z Sectional Plots of the One-Year-Old Phantom.

ORNL-DWG 75-6298

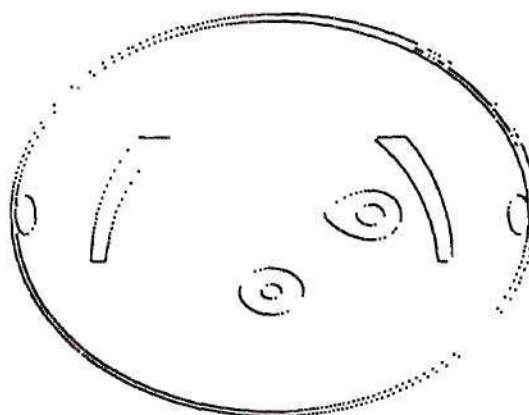
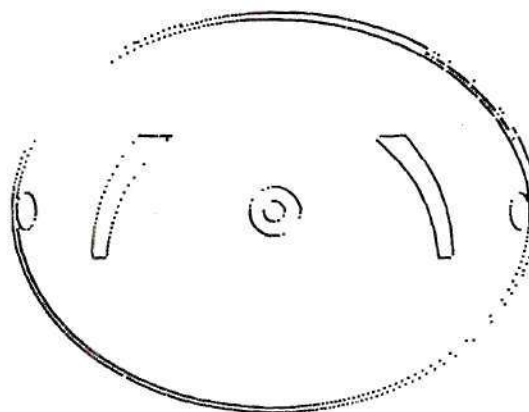
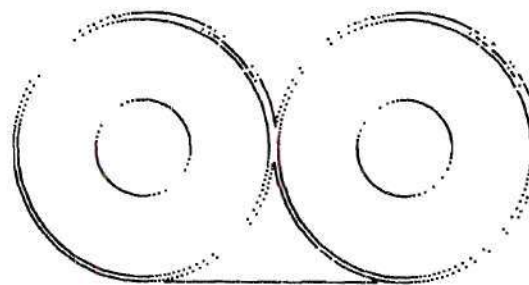
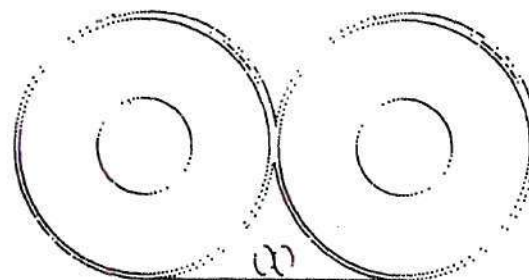
 $Z = 2.80$  $Z = 0.50$  $Z = 0.0$  $Z = -0.50$ 

Figure A-2. X-Y Sectional Plots of the One-Year-Old Phantom Showing the Upper Leg and Hip Regions.

ORNL-DWG 75-6305

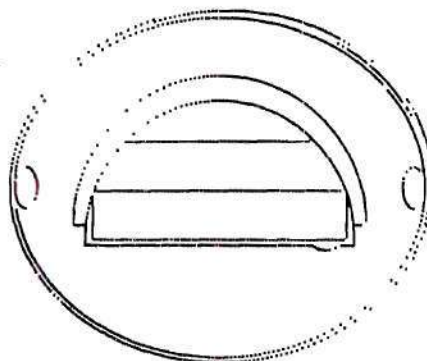
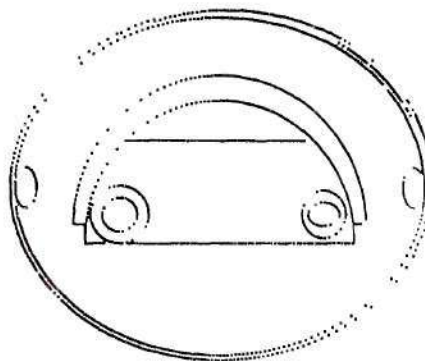
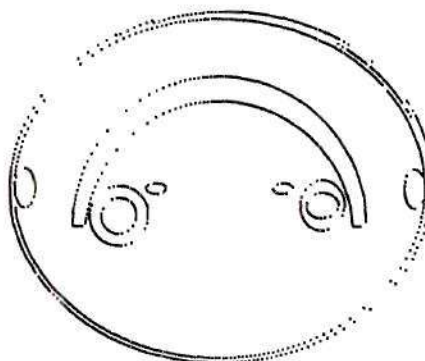
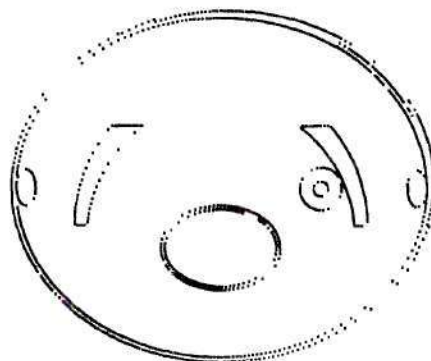
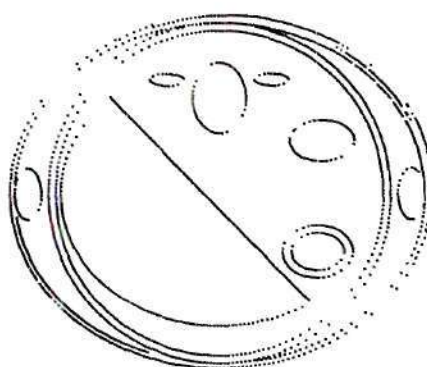
 $Z = 9.50$  $Z = 8.00$  $Z = 6.50$  $Z = 4.00$ 

Figure A-3. X-Y Sectional Plots of the One-Year-Old Phantom Showing the Lower Abdomen.

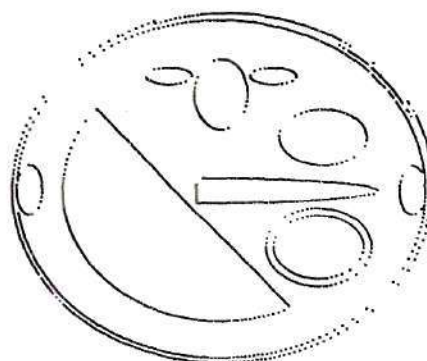


ORNL-DWG 75-6304

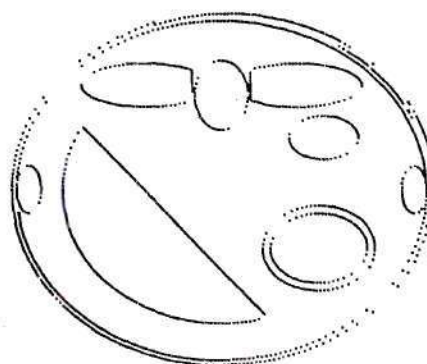
Z = 18.00



Z = 16.00



Z = 14.00



Z = 12.00

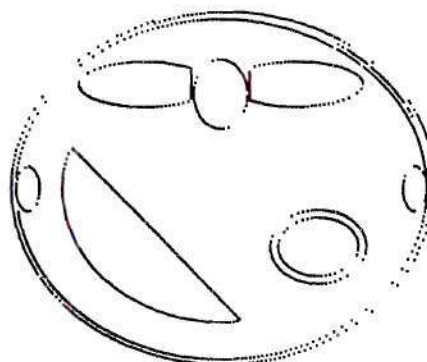
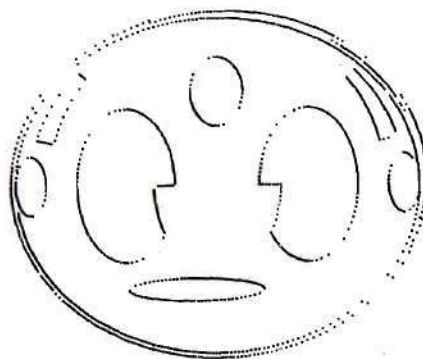


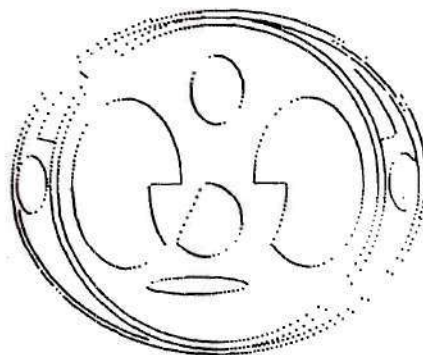
Figure A-4. X-Y Sectional Plots of the One-Year-Old Phantom Showing the Upper Abdomen.

ORNL-DWG 75-5826

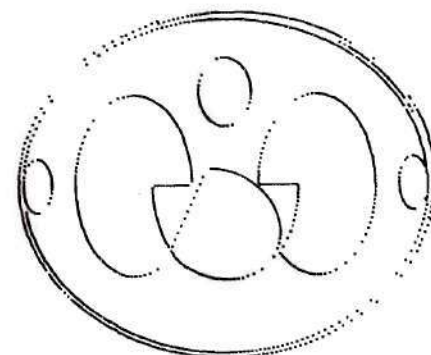
Z = 26.00



Z = 24.00



Z = 22.00



Z = 20.00

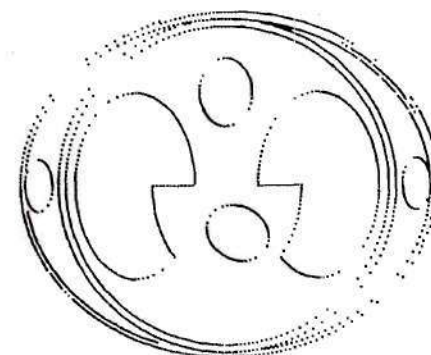
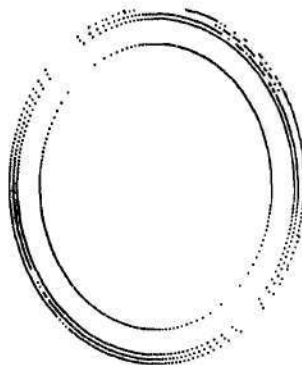


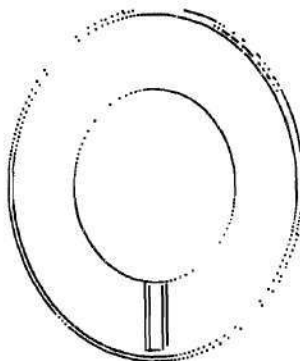
Figure A-5. X-Y Sectional Plots of the One-Year-Old Phantom Showing the Chest Region.

ORNL-DWG 75-6299

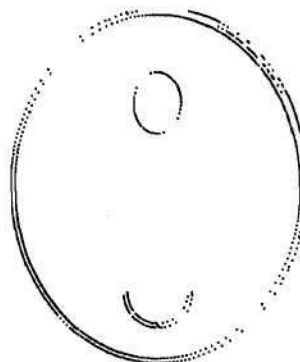
Z = 41.00



Z = 37.00



Z = 33.00



Z = 31.00

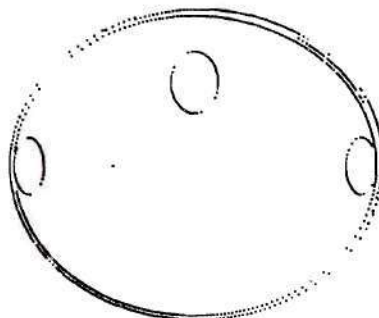


Figure A-6. X-Y Sectional Plots of the One-Year-Old Phantom Showing the Shoulder and Head Regions.

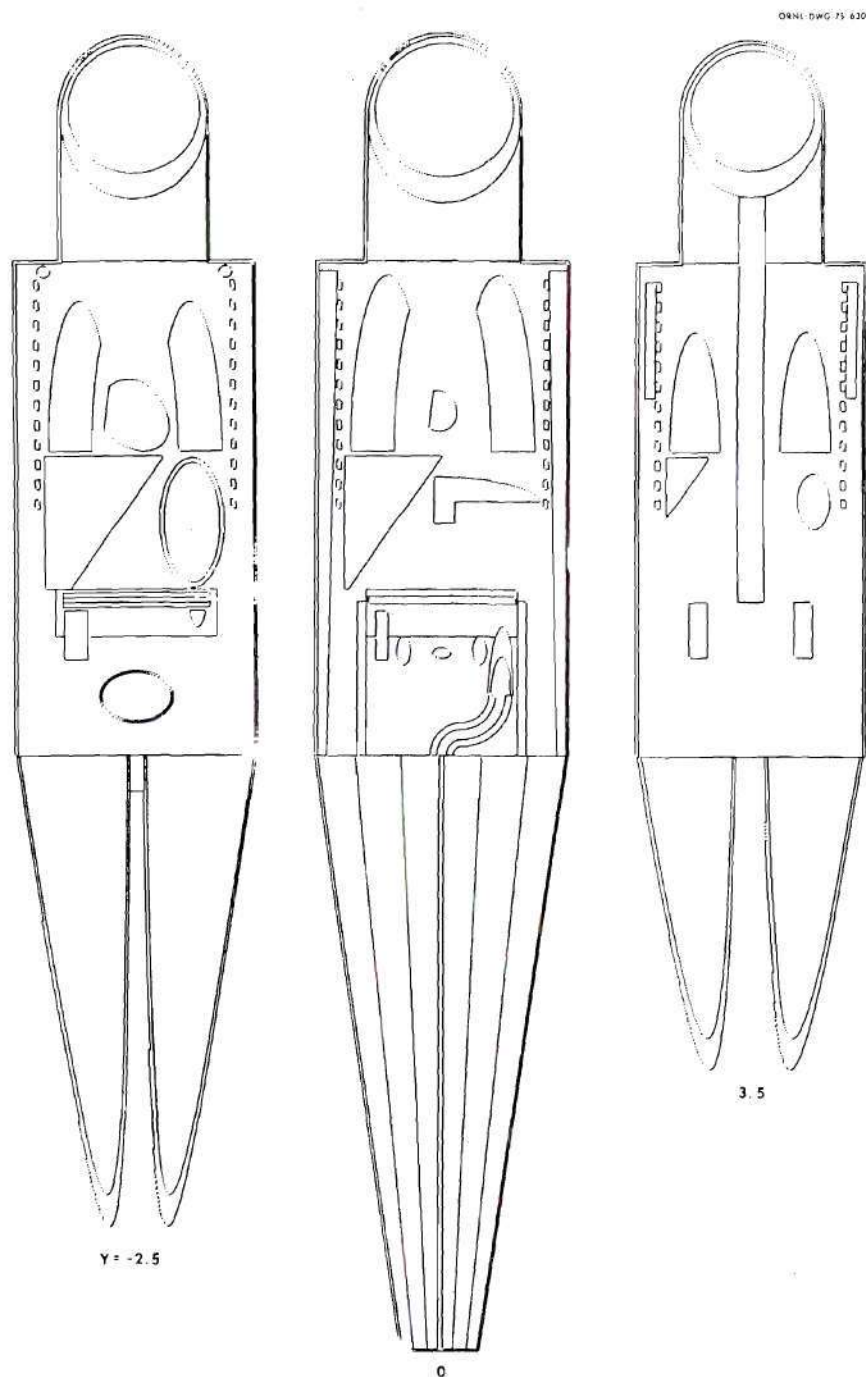


Figure A-7. X-Z Sectional Plots of the Five-Year-Old Phantom.



ORNL-DWG 75-6301

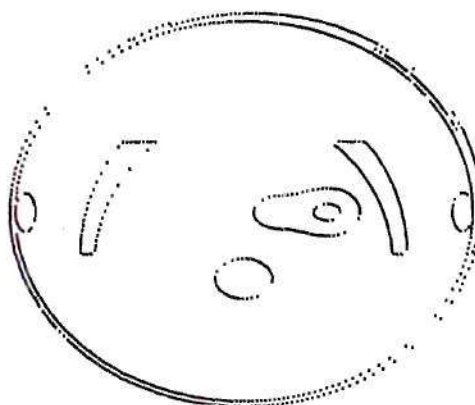
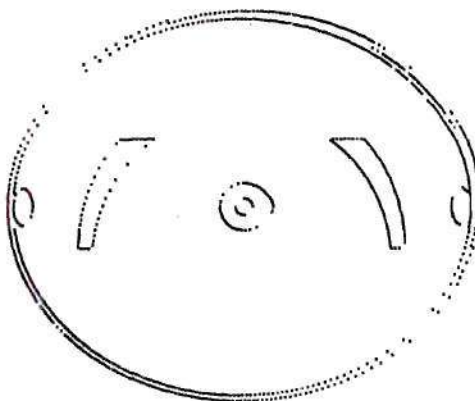
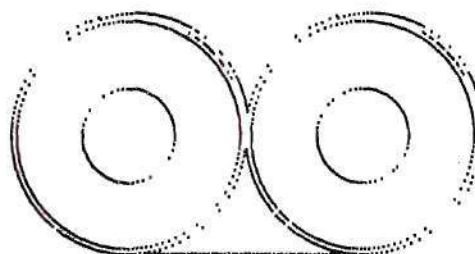
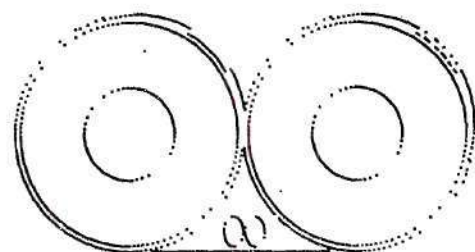
 $Z = 2.00$  $Z = 0.50$  $Z = 0.0$  $Z = -1.00$ 

Figure A-8. X-Y Sectional Plots of the Five-Year-Old Phantom Showing the Upper Leg and Hip Regions.

ORNL-DWG 75-6302

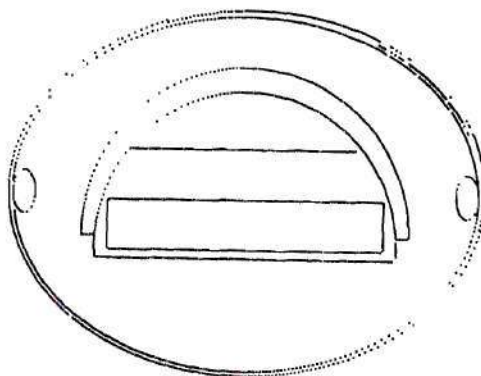
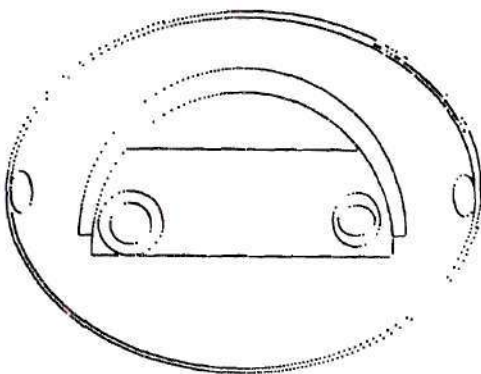
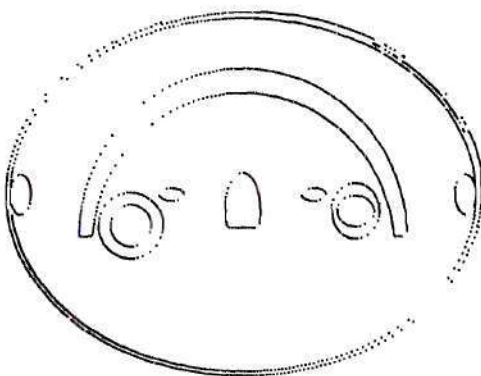
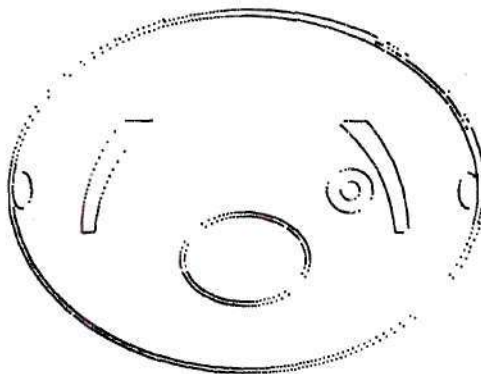
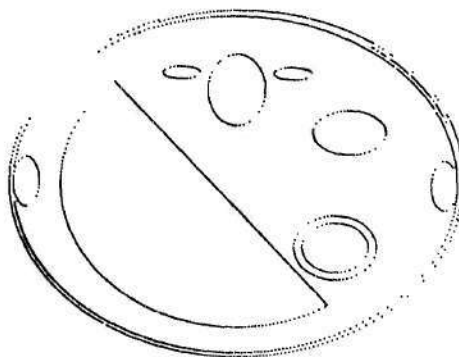
 $Z = 12.50$  $Z = 10.50$  $Z = 8.50$  $Z = 4.00$ 

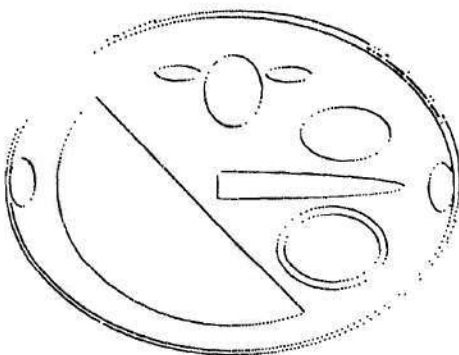
Figure A-9. X-Y Sectional Plots of the Five-Year-Old Phantom Showing the Lower Abdomen.

ORNL-DWG 75-5825

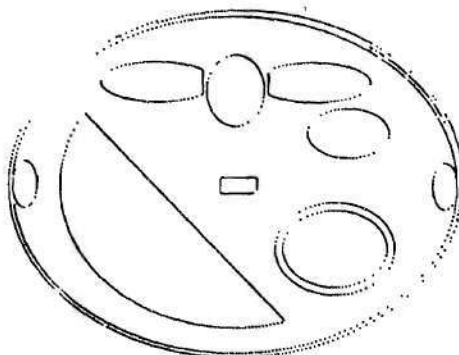
Z = 24.00



Z = 22.00



Z = 20.00



Z = 18.00

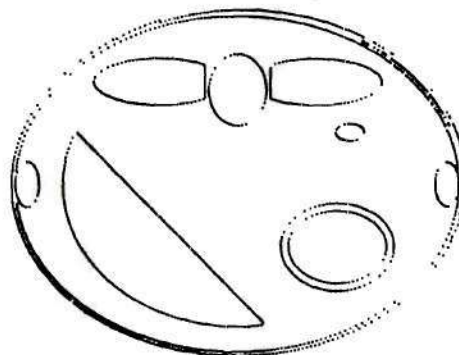
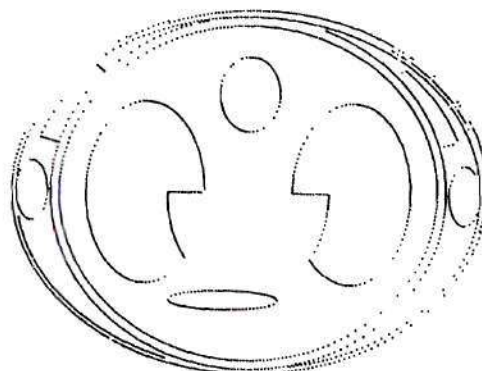


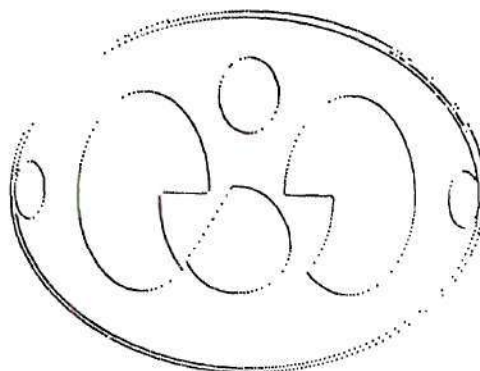
Figure A-10. X-Y Sectional Plots of the Five-Year-Old Phantom Showing the Upper Abdomen.

ORNL-DWG 75-6303

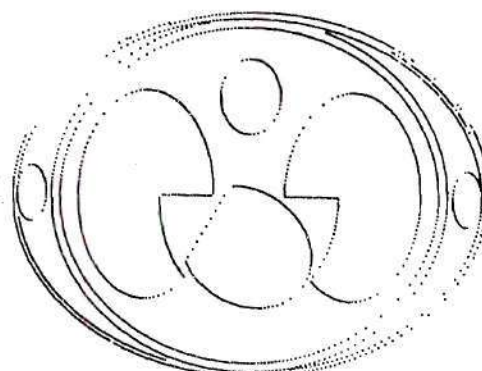
Z = 33.50



Z = 30.50



Z = 28.50



Z = 26.50

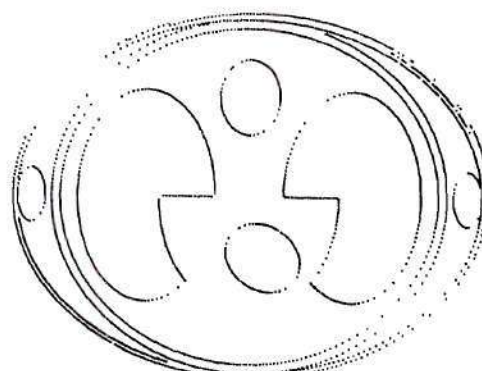
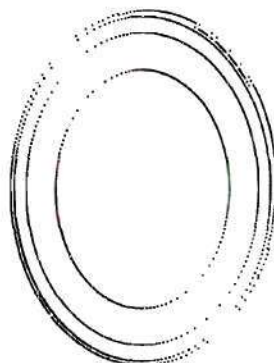


Figure A-11. X-Y Sectional Plots of the Five-Year-Old Phantom Showing the Chest Region.

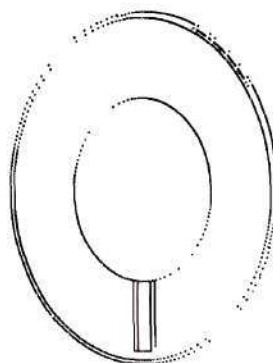


ORNL-DWG 75-6306

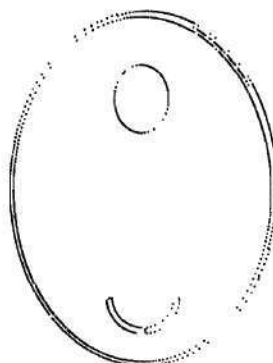
Z = 51.00



Z = 48.00



Z = 43.50



Z = 41.30

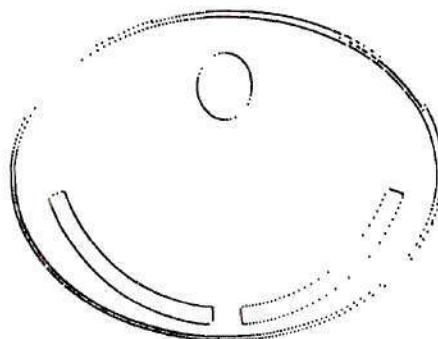


Figure A-12. X-Y Sectional Plots of the Five-Year-Old Phantom Showing the Shoulder and Head Regions.

## Appendix B

## Summary of Some Phantom Material

Table B-1. Composition of Soft Tissue Equivalent Material  
(Weight Percentage)

Reference	This Study (1977)	Tipton et al. (1966)	Lea (1946)	ICRU 10 <sup>b</sup> (1964)	Young (1974)
Material	Soft Tissue <sup>a</sup>	Soft Tissue <sup>b</sup>	Wet Tissue	Muscle (Striated)	Muscle
Element					
H	11.3	10.5	10.00	10.20	10.3
C	7.5	23.0	12.00	12.30	9.9
N		2.3	4.00	3.50	3.2
O	81.0	63.2	73.00	72.90	75.7
Na	0.1	0.1	0.10	0.08	0.1
Mg		0.1	0.04	0.02	
P		0.2	0.20	0.20	0.2
S		0.2	0.20	0.50	0.3
Cl	0.1	0.1	0.10		0.1
K		0.2	0.35	0.30	0.3
Ca			0.01	0.01	
Fe		0.1			
Density g-cm <sup>-3</sup>	1	1	1	1	1
Eff. Atomic Number $\bar{Z}$	7.31	7.30	7.48	7.46	7.48
Ele. Density $\text{Ne} \times 10^{-23}\text{g}^{-1}$	3.35	3.32	3.42	3.31	3.32

<sup>a</sup>The liquid soft tissue substitute, composed of 80% water, 18.0% methanol, 1.8% sucrose, and 0.2% sodium chloride by weight percentage (Stansbury, 1977).

<sup>b</sup>This is the composition of soft tissue in "Reference Man" which was used in the Monte Carlo dose calculations.

Table B-1 (continued)

Reference					Weast (1962)	Weast (1962)	Weast (1962)			
Material	Air		Water		Bakelite H <sub>6</sub> C <sub>8</sub> O	Polystyrene H <sub>8</sub> C <sub>8</sub>	Perspex. H <sub>6</sub> C <sub>4</sub> O <sub>2</sub>			
Chemical composition in parts by weight	N	75.5	H	11.19	H	5.7	H	7.03		
	O	23.2	O	88.81	C	77.5	C	92.26	C	55.81
	A	1.3			O	16.8			O	37.17
Density ρ gm-cm <sup>-3</sup>	0.001293		1.0		1.31 ~ 1.32		1.04 ~ 1.08		1.18 - 1.20	
Eff. Atomic Number $\bar{Z}$	7.64		7.42		6.10		5.69		8.61	
Ne × 10 <sup>-23</sup> gm <sup>-1</sup>	3.01		3.34		3.18		3.24		3.22	

Reference	Mayneord (1937)	Jones and Raine (1949)	Lindsay and Stern (1953)	Spiers (1946)	Hashizume et al. (1972)
Material	Tissue	Mix-D	Bolus	Excised muscle tissue specimen	M3 Phantom
Chemical composition in parts by weight	H <sub>2</sub> O 80.0	Paraffin 60.8	Sugar	Skin, bicep	Paraffin 76.9 MgO 22.4 CaCO <sub>3</sub> 0.7
	Protein 18.9	Poly- 30.4	MgCO <sub>3</sub>		
	NaCl 1.0	ethylene	Mg(OH) <sub>3</sub>		
	KCl 0.05	MgO 6.4	H <sub>2</sub> O 11.0		
	CaCl <sub>2</sub> 0.03	TiO <sub>2</sub> 2.4			
	NaHCO <sub>3</sub> 0.02				
Density $\rho$ $g\text{-}cm^{-3}$	1.0	0.99	1.0	1.0	1.0
Eff. Atomic Number $\bar{Z}$	7.33	7.47	7.33	7.31	
$Ne \times 10^{-23}$ $g^{-1}$	3.34	3.395	3.32	3.36	

Table B-1 (continued)

Reference	NBS Handbook 47 (1950)	Solomen (1952)	Marinelli (1953)	Lea (1955)	NBS Handbook 63 (1957)
Material Element	Tissue $C_{21}H_{140}O_{57}N_3$	Tissue $C_{22}H_{170}O_{68}N_3$	Tissue $C_5H_{40}O_{18}N$	Tissue $C_7H_{20}O_{32}N_2$	Tissue $C_{42}H_{277}O_{109}N_6CaP$
C	18.72	16.90	14.95	12.1	18.82
H	10.45	10.97	10.02	10.1	10.40
O	67.70	69.50	71.50	73.8	65.10
N	3.13	2.63	3.53	4.0	3.14
Ca					1.40
P					1.14
Eff. Atomic Number $\bar{Z}$	7.1	7.12	7.208	7.36	7.85
Ele. Density $Ne\ g^{-1} \times 10^{-23}$	3.279	3.2812	3.307	3.8925	3.3169

Reference	Rossi (1953)	Rossi (1953)	Rossi and Failla (1956)	Weast (1962)	Weast (1962)
Material Element	T. E. gel $H_2O_2CN_2$	T. E. elastic $H_2O_2CN$	T. E. elastic Markite HCN	Teflon CF	Polyethylene CH
C	15.8	82.7	86.4	24	85.5
H	9.7	10.1	10.1		14.5
N	3.5	3.7	3.5		
O	71.0	3.5			
F				76	
Density $\rho$ $g\text{-cm}^{-3}$	---	---	---	2.36	0.93
Eff. atomic Number $\bar{Z}$	7.3	5.77	5.65	8.45	5.047
$Ne \times 10^{-23}$ $g^{-1}$	3.2607	3.26	3.304	3.0	3.763



Table B-1 (continued)

Reference	Shonka et al. (1958)		Stacy et al. (1961)	Weast (1962)	Weast (1962)	Weast (1962)
Material Element	T. E. muscle		Temex fluid rubber	Lucite $H_8C_5O_2$	Lexan $H_{14}C_{16}O_3$	Nylon $H_{22}N_2O_2C_{12}$
	a	b				
H	10.90		H 9.60	8.06	5.55	9.80
C	75.60	57.4	C 87.00	59.98	75.57	63.68
N	3.50		N 0.06			12.38
O	5.10		O 0.47	31.96	18.88	14.14
F	1.08	42.6	S 1.53			
Si	1.04		Ti 0.33			
Ca	2.00		Zn 0.45			
Density $\rho$ $g\text{-cm}^{-3}$	1.07	1.4	1.01	1.2	1.2	1.13 - 1.15
Eff. Atomic Number $\bar{Z}$	7.3	7.5	7.05	6.47	6.26	6.12
$Ne \times 10^{-23}$ $g^{-1}$	3.285	2.932	3.273	3.25	3.17	3.30

<sup>a</sup>Photon and neutron sensitive.<sup>b</sup>Insensitive to neutron.

Table B-2. Composition of Some Dosimetry Materials and Their Important Dosimetric Constants

Reference	Miller (1975)		Weast (1962)		Weast (1962)		Weast (1962)		Weast (1962)	
Material	Fricke dosimeter solution		LiF:Mn		CaF <sub>2</sub> :Mn		CaSO <sub>4</sub> :Dy		Li <sub>2</sub> B <sub>4</sub> O <sub>7</sub> :Mn	
Chemical composition in parts by weight	H	10.84	Li	27	F	48.67	O	47.03	Li	8.4
	O	87.91	F	73	Ca	51.33	S	23.52	B	24.1
	S	1.25					Ca	29.45	O	67.5
Density $\rho$ gm-cm <sup>-3</sup>	1.0		2.63		3.18		2.96		2.36	
Eff. Atomic Number $\bar{Z}$	7.66		8.19		16.53		15.22		7.23	
Ne $\times 10^{-23}$ gm <sup>-1</sup>	3.33		2.79		2.93		3.01		2.92	

Table B-3. Composition of Bone Equivalent Material

Reference	This Study (1977)	Tipton et al. (1966)	ICRU 10b (1964)	Shonka et al. (1958)	Spiers (1946)
Material Element	Skeleton <sup>a</sup>	Skeleton <sup>b</sup>	Bone femur	T.E. Bone	Bone femur
H	6.5	7.0	6.4	6.36	3.4
C	19.1	22.7	27.8	53.60	15.5
N	3.9	3.9	2.7	2.69	4.0
O	53.0	48.6	41.0	3.05	44.1
Na	0.2	0.3			0.2
Mg	0.2	0.1	0.2		
P	6.8	7.0	7.0		10.2
S		0.2	0.2		0.3
Ca	10.3	9.9	14.7	17.60	22.2
Cl		0.1			
K		0.2			
F				16.70	
Density $\rho$ g-cm <sup>-3</sup>	1.49	1.50	1.87	1.37	
Eff. Atomic Number $\bar{Z}$	9.75	10.76	11.6	11.6	13.8
Electron density $N_e \times 10^{-23}$	3.24	3.21	3.19	3.15	3.23

<sup>a</sup>The homogeneous bone substitute composed of 27.0% water, 19.5% bone flour, 39.5% sucrose, 8.0% ammonium phosphate, 6.0% ammonium nitrate by weight percentage (Stansbury, 1977).

<sup>b</sup>This is the composition of the skeleton in "Reference Man" which is used in the Monte Carlo dose calculations.

## Appendix C

## Tissue-Air Ratio Comparison

Table C-1. Tissue-Air Ratio Comparison,  
One-Year-Old Phantom Head Examination  
(Posterior/Anterior View, 75 kVcp, 287 mAs, FSD = 101.6 cm)

ORGAN		T.A.R. <sup>a</sup> (rad/R)	C.V. <sup>b</sup> (%)	T.A.R. + 2 C.V. up limit (rad/R)	T.A.R. - 2 C.V. low limit (rad/R)
Brain	Calculation	0.3493	0.08	0.3562	0.3425
	Measurement	0.3097	4.10	0.3356	0.2837
Thyroid	Calculation	0.0845	26.05	0.1285	0.0405
	Measurement	0.0945	6.38	0.1065	0.0824
Thymus	Calculation	0.0116	21.80	0.0167	0.0065
	Measurement	0.0101	7.50	0.0116	0.0086
Ovaries	Calculation	----	----	----	----
	Measurement	----	----	----	----
Testes	Calculation	----	----	----	----
	Measurement	----	----	----	----
Red Marrow of L. Arm	Calculation	0.0144	15.57	0.0189	0.0099
	Measurement	0.0143	6.93	0.0163	0.0123
Red Marrow of R. Arm	Calculation	0.0123	15.42	0.0162	0.0085
	Measurement	0.0145	6.81	0.0165	0.0125
Red Marrow of Spine (up)	Calculation	0.4937	7.53	0.5680	0.4193
	Measurement	0.4460	8.31	0.5201	0.3719
Red Marrow of Spine (med)	Calculation	0.0211	6.27	0.0238	0.0185
	Measurement	0.0167	25.87	0.0254	0.0081
Red Marrow of Spine (low)	Calculation	----	----	----	----
	Measurement	----	----	----	----
Red Marrow of Pelvis	Calculation	----	----	----	----
	Measurement	----	----	----	----
Red Marrow of L. Leg	Calculation	----	----	----	----
	Measurement	----	----	----	----
Red Marrow of R. Leg	Calculation	----	----	----	----
	Measurement	----	----	----	----
Red Marrow Total Body	Calculation	0.0259	1.08	0.0265	0.0253
	Measurement	0.0242	12.40	0.0302	0.0182

<sup>a</sup>Tissue-Air Ratio (T.A.R.) is the average absorbed dose to the organ of interest (rad) per unit exposure (R, free-in-air) in the center of beam at the surface of body. For a C.V. greater than 50% or a T.A.R. less than  $10^{-4}$  (rad/R) no comparison is given.

<sup>b</sup>Coefficient of variation (C.V.) =  $\frac{\text{standard error}}{\text{average energy deposited}} \times 100$ .



Table C-2. Tissue-Air Ratio Comparison,  
One-Year-Old Phantom Head Examination  
(Left Lateral View, 60 kVcp 685 mAs, FSD = 101.6 cm)

ORGAN		T.A.R. <sup>a</sup> (rad/R)	C.V. <sup>b</sup> (%)	T.A.R. + 2 C.V. up limit (rad/R)	T.A.R. - 2 C.V. low limit (rad/R)
Brain	Calculation	0.2809	1.13	0.0273	0.2746
	Measurement	0.2396	5.11	0.2640	0.2151
Thyroid	Calculation	0.2045	18.57	0.3360	0.1540
	Measurement	0.2453	7.31	0.2811	0.2094
Thymus	Calculation	0.0159	20.99	0.0226	0.0092
	Measurement	0.0128	14.78	0.0166	0.0090
Ovaries	Calculation	----	----	----	----
	Measurement	----	----	----	----
Testes	Calculation	----	----	----	----
	Measurement	----	----	----	----
Red Marrow of L. Arm	Calculation	0.0155	15.12	0.0202	0.0108
	Measurement	0.0228	7.68	0.0268	0.0193
Red Marrow of R. Arm	Calculation	0.0060	24.89	0.0090	0.0030
	Measurement	0.0036	6.11	0.0041	0.0002
Red Marrow of Spine (upper)	Calculation	0.2124	4.29	0.2306	0.1942
	Measurement	0.2795	28.27	0.4775	0.1215
Red Marrow of Spine (middle)	Calculation	0.0153	7.25	0.0175	0.0130
	Measurement	0.0101	19.24	0.0140	0.0062
Red Marrow of Spine (lower)	Calculation	----	----	----	----
	Measurement	----	----	----	----
Red Marrow of Pelvis	Calculation	----	----	----	----
	Measurement	----	----	----	----
Red Marrow of L. Leg	Calculation	----	----	----	----
	Measurement	----	----	----	----
Red Marrow of R. Leg	Calculation	----	----	----	----
	Measurement	----	----	----	----
Red Marrow Total Body	Calculation	0.0197	1.03	0.2011	0.1929
	Measurement	0.0152	13.27	0.1923	0.1117

<sup>a</sup>Tissue-Air Ratio (T.A.R.) is the average absorbed dose to the organ of interest (rad) per unit exposure (R, free-in-air) in the center of beam at the surface of body. For a C.V. greater than 50% or a T.A.R. less than  $10^{-4}$  (rad/R) no comparison is given.

<sup>b</sup>Coefficient of variation (C.V.) =  $\frac{\text{standard error}}{\text{average energy deposited}} \times 100$ .

Table C-3. Tissue-Air Ratio Comparison,  
One-Year-Old Phantom Chest Examination  
(Anterior/Posterior View, 60 kVcp, 990 mAs, FSD = 121.9 cm)

ORGAN		T.A.R. <sup>a</sup> (rad/R)	C.V. <sup>b</sup> (%)	T.A.R. + 2 C.V. up limit (rad/R)	T.A.R. - 2 C.V. low limit (rad/R)
Brain	Calculation	0.0047	8.02	0.0055	0.0040
	Measurement	0.0033	10.24	0.0040	0.0027
Thyroid	Calculation	0.4693	11.51	0.5773	0.3613
	Measurement	0.4910	7.31	0.5628	0.4193
Thymus	Calculation	0.6834	3.21	0.7273	0.6395
	Measurement	0.6940	6.49	0.7841	0.6039
Ovaries	Calculation	----	----	----	----
	Measurement	----	----	----	----
Testes	Calculation	----	----	----	----
	Measurement	----	----	----	----
Red Marrow of L. Arm	Calculation	0.2075	3.90	0.2222	0.1913
	Measurement	0.1618	6.24	0.1820	0.1416
Red Marrow of R. Arm	Calculation	0.2106	3.89	0.2270	0.1942
	Measurement	0.1811	5.49	0.2010	0.1612
Red Marrow of Spine (up)	Calculation	0.0570	7.70	0.0658	0.0482
	Measurement	0.0564	9.86	0.0675	0.0453
Red Marrow of Spine (med)	Calculation	0.0761	3.25	0.0810	0.0711
	Measurement	0.0818	11.55	0.1010	0.0629
Red Marrow of Spine (low)	Calculation	0.0090	12.34	0.0112	0.0068
	Measurement	0.0118	10.52	0.0143	0.0095
Red Marrow of Pelvis	Calculation	0.0013	19.44	0.0018	0.0008
	Measurement	0.0015	10.43	0.0018	0.0012
Red Marrow of L. Leg	Calculation	----	----	----	----
	Measurement	----	----	----	----
Red Marrow of R. Leg	Calculation	----	----	----	----
	Measurement	----	----	----	----
Red Marrow Total Body	Calculation	0.0286	0.85	0.0291	0.0281
	Measurement	0.0254	8.94	0.0299	0.0209

<sup>a</sup>Tissue-Air Ratio (T.A.R.) is the average absorbed dose to the organ of interest (rad) per unit exposure (R, free-in-air) in the center of beam at the surface of body. For a C.V. greater than 50% or a T.A.R. less than  $10^{-4}$  (rad/R) no comparison is given.

<sup>b</sup>Coefficient of variation (C.V.) =  $\frac{\text{standard error}}{\text{average energy deposited}} \times 100$ .

Table C-4. Tissue-Air Ratio Comparison,  
One-Year-Old Phantom Chest Examination  
(Posterior/Anterior View, 60 kVcp 990 mAs, FSD = 121.9 cm)

ORGAN		T.A.R. <sup>a</sup> (rad/R)	C.V. <sup>b</sup> (%)	T.A.R. + 2 C.V. up limit (rad/R)	T.A.R. - 2 C.V. low limit (rad/R)
Brain	Calculation	0.0041	8.01	0.0047	0.0034
	Measurement	0.0034	9.40	0.0040	0.0028
Thyroid	Calculation	0.1044	21.40	0.1491	0.0597
	Measurement	0.0939	10.12	0.1130	0.0748
Thymus	Calculation	0.1377	7.21	0.1576	0.1178
	Measurement	0.1402	6.50	0.1585	0.1221
Ovaries	Calculation	----	----	----	----
	Measurement	0.0021	10.15	0.0025	0.0017
Testes	Calculation	----	----	----	----
	Measurement	0.0013	24.95	0.0020	0.0007
Red Marrow of L. Arm	Calculation	0.1845	4.25	0.2009	0.1688
	Measurement	0.1927	3.37	0.2057	0.1797
Red Marrow of R. Arm	Calculation	0.1914	4.17	0.2074	0.1755
	Measurement	0.1983	3.97	0.2141	0.1826
Red Marrow of Spine (up)	Calculation	0.2144	3.84	0.2308	0.1979
	Measurement	0.1705	24.12	0.2528	0.0883
Red Marrow of Spine (med)	Calculation	0.3350	1.50	0.3451	0.3249
	Measurement	0.3610	12.67	0.4524	0.2695
Red Marrow of Spine (low)	Calculation	0.0145	10.97	0.0176	0.0113
	Measurement	0.0178	13.20	0.2243	0.1306
Red Marrow of Pelvis	Calculation	0.0012	19.32	0.0017	0.0007
	Measurement	0.0014	10.34	0.0017	0.0011
Red Marrow of L. Leg	Calculation	----	----	----	----
	Measurement	----	----	----	----
Red Marrow of R. Leg	Calculation	----	----	----	----
	Measurement	----	----	----	----
Red Marrow Total Body	Calculation	0.0860	0.7	0.0872	0.0848
	Measurement	0.0893	9.58	0.1064	0.0722

<sup>a</sup>Tissue-Air Ratio (T.A.R.) is the average absorbed dose to the organ of interest (rad) per unit exposure (R, free-in-air) in the center of beam at the surface of body. For a C.V. greater than 50% or a T.A.R. less than  $10^{-4}$  (rad/R) no comparison is given.

<sup>b</sup>Coefficient of variation (C.V.) =  $\frac{\text{standard error}}{\text{average energy deposited}} \times 100$ .



Table C-5. Tissue-Air Ratio Comparison,  
One-Year-Old Phantom Chest Examination  
(Left Lateral View, 75 kVcp, 417 mAs, FSD = 121.9 cm)

ORGAN		T.A.R. <sup>a</sup> (rad/R)	C.V. <sup>b</sup> (%)	T.A.R. + 2 C.V. up limit (rad/R)	T.A.R. - 2 C.V. low limit (rad/R)
Brain	Calculation	0.0076	6.48	0.0086	0.0066
	Measurement	0.0071	8.97	0.0084	0.0058
Thyroid	Calculation	0.3032	13.97	0.3879	0.2185
	Measurement	0.3130	11.32	0.3838	0.2421
Thymus	Calculation	0.3146	5.09	0.3466	0.2826
	Measurement	0.3616	2.19	0.4188	0.3044
Ovaries	Calculation	----	----	----	----
	Measurement	0.0056	5.67	0.0062	0.0050
Testes	Calculation	----	----	----	----
	Measurement	----	----	----	----
Red Marrow of L. Arm	Calculation	----	----	----	----
	Measurement	----	----	----	----
Red Marrow of R. Arm	Calculation	0.0845	6.65	0.0957	0.0732
	Measurement	0.1102	6.97	0.1256	0.0949
Red Marrow of Spine (up)	Calculation	0.1719	4.63	0.1903	0.1581
	Measurement	0.1431	7.28	0.1639	0.1222
Red Marrow of Spine (med)	Calculation	0.2075	2.08	0.2162	0.1989
	Measurement	0.1859	5.90	0.2078	0.1640
Red Marrow of Spine (low)	Calculation	0.0177	10.78	0.0215	0.0139
	Measurement	0.0193	12.49	0.0241	0.0145
Red Marrow of Pelvis	Calculation	0.0027	15.85	0.0036	0.0019
	Measurement	0.0035	3.35	0.0037	0.0033
Red Marrow of L. Leg	Calculation	----	----	----	----
	Measurement	----	----	----	----
Red Marrow of R. Leg	Calculation	----	----	----	----
	Measurement	----	----	----	----
Red Marrow Total Body	Calculation	0.0541	0.81	0.0549	0.0532
	Measurement	0.0506	10.46	0.0612	0.0400

<sup>a</sup>Tissue-Air Ratio (T.A.R.) is the average absorbed dose to the organ of interest (rad) per unit exposure (R, free-in-air) in the center of beam at the surface of body. For a C.V. greater than 50% or a T.A.R. less than  $10^{-4}$  (rad/R) no comparison is given.

<sup>b</sup>Coefficient of variation (C.V.) =  $\frac{\text{standard error}}{\text{average energy deposited}} \times 100$ .



Table C-6. Tissue-Air Ratio Comparison,  
One-Year-Old Phantom Abdomen Examination  
(Anterior/Posterior View, 75 kVcp, 287 mAs, FSD - 101.6 cm)

ORGAN		T.A.R. <sup>a</sup> (rad/R)	C.V. <sup>b</sup> (%)	T.A.R. + 2 C.V. up limit (rad/R)	T.A.R. - 2 C.V. low limit (rad/R)
Brain	Calculation	----	----	----	----
	Measurement	----	----	----	----
Thyroid	Calculation	----	----	----	----
	Measurement	----	----	----	----
Thymus	Calculation	0.0261	20.90	0.0370	0.0152
	Measurement	0.0211	9.38	0.0251	0.0171
Ovaries	Calculation	0.4740	37.20	0.8267	0.1213
	Measurement	0.3414	9.24	0.4045	0.2783
Testes	Calculation	0.2102	21.53	0.3007	0.1197
	Measurement	0.2912	6.40	0.3285	0.2539
Red Marrow of L. Arm	Calculation	0.0051	26.14	0.0078	0.0025
	Measurement	0.0071	10.12	0.0085	0.0057
Red Marrow of R. Arm	Calculation	0.0065	26.08	0.0099	0.0031
	Measurement	0.0081	14.30	0.0105	0.0058
Red Marrow of Spine (up)	Calculation	0.0014	44.58	0.0026	0.0002
	Measurement	0.0022	12.34	0.0027	0.0017
Red Marrow of Spine (med)	Calculation	0.0342	5.97	0.0383	0.0301
	Measurement	0.0369	6.14	0.0414	0.0324
Red Marrow of Spine (low)	Calculation	0.1430	4.64	0.1562	0.1297
	Measurement	0.1576	5.65	0.1754	0.1398
Red Marrow of Pelvis	Calculation	0.2325	2.00	0.2418	0.2232
	Measurement	0.2532	9.00	0.2988	0.2076
Red Marrow of L. Leg	Calculation	0.0512	5.48	0.0572	0.0459
	Measurement	0.0477	7.34	0.0547	0.0407
Red Marrow of R. Leg	Calculation	0.0650	5.44	0.0636	0.0511
	Measurement	0.0540	9.22	0.0640	0.0440
Red Marrow Total Body	Calculation	0.1651	1.42	0.1698	0.1604
	Measurement	0.1637	7.37	0.0878	0.1396

<sup>a</sup>Tissue-Air Ratio (T.A.R.) is the average absorbed dose to the organ of interest (rad) per unit exposure (R, free-in-air) in the center of beam at the surface of body. For a C.V. greater than 50% or a T.A.R. less than  $10^{-4}$  (rad/R) comparison is given.

<sup>b</sup>Coefficient of variation (C.V.) =  $\frac{\text{standard error}}{\text{average energy deposited}} \times 100$ .

Table C-7. Tissue-Air Ratio Comparison,  
One-Year-Old Phantom Abdomen Examination  
(Posterior/Anterior View, 75 kVcp, 287 mAs, FSD = 101.6 cm)

ORGAN		T.A.R. <sup>a</sup> (rad/R)	C.V. <sup>b</sup> (%)	T.A.R. + 2 C.V. up limit (rad/R)	T.A.R. - 2 C.V. low limit (rad/R)
		----	----	----	----
Brain	Calculation	----	----	----	----
	Measurement	----	----	----	----
Thyroid	Calculation	----	----	----	----
	Measurement	----	----	----	----
Thymus	Calculation	0.0136	22.75	0.0198	0.0074
	Measurement	0.0140	9.41	0.0666	0.0114
Ovaries	Calculation	0.4181	24.02	0.6190	0.2172
	Measurement	0.2626	11.17	0.3213	0.2039
Testes	Calculation	0.1356	78.95	0.2141	0.0571
	Measurement	0.1465	9.26	0.1736	0.1194
Red Marrow of L. Arm	Calculation	0.0079	21.28	0.0113	0.0046
	Measurement	0.0081	7.95	0.0093	0.0068
Red Marrow of R. Arm	Calculation	0.0075	20.83	0.0106	0.0044
	Measurement	0.0060	10.28	0.0073	0.0048
Red Marrow of Spine (up)	Calculation	0.0017	49.20	0.0033	0.0003
	Measurement	0.0016	8.53	0.0019	0.0013
Red Marrow of Spine (med)	Calculation	0.0991	3.37	0.1057	0.0924
	Measurement	0.1062	6.33	0.1196	0.0928
Red Marrow of Spine (low)	Calculation	0.5181	2.38	0.5426	0.4912
	Measurement	0.5208	3.46	0.5568	0.4848
Red Marrow of Pelvis	Calculation	0.4174	1.45	0.4295	0.4053
	Measurement	0.4466	4.39	0.4858	0.4074
Red Marrow of L. Leg	Calculation	0.0480	5.75	0.0535	0.0425
	Measurement	0.0372	7.93	0.0431	0.0313
Red Marrow of R. Leg	Calculation	0.0467	5.81	0.0521	0.0415
	Measurement	0.0352	10.77	0.0428	0.0277
Red Marrow Total Body	Calculation	0.3167	1.03	0.3232	0.3102
	Measurement	0.3321	6.75	0.3769	0.2873

<sup>a</sup>Tissue-Air Ratio (T.A.R.) is the average absorbed dose to the organ of interest (rad) per unit exposure (R, free-in-air) in the center of beam at the surface of body. For a C.V. greater than 50% or a T.A.R. less than  $10^{-4}$  (rad/R) no comparison is given.

<sup>b</sup>Coefficient of variation (C.V.) =  $\frac{\text{standard error}}{\text{average energy deposited}} \times 100$ .

Table C-8. Tissue-Air Ratio Comparison,  
One-Year-Old Phantom Abdomen Examination  
(Left Lateral View, 90 kVcp, 191 mAs, FSD = 101.6 cm)

ORGAN		T.A.R. <sup>a</sup> (rad/R)	C.V. <sup>b</sup> (%)	T.A.R. + 2 C.V. up limit (rad/R)	T.A.R. - 2 C.V. low limit (rad/R)
Brain	Calculation	----	----	----	----
	Measurement	----	----	----	----
Thyroid	Calculation	----	----	----	----
	Measurement	----	----	----	----
Thymus	Calculation	0.0200	19.07	0.0276	0.0124
	Measurement	0.0208	8.23	0.0243	0.0174
Ovaries	Calculation	0.2036	47.78	0.4021	0.0091
	Measurement	0.1854	7.69	0.2139	0.1569
Testes	Calculation	0.2202	27.39	0.3408	0.0996
	Measurement	0.1750	8.42	0.2045	0.1455
Red Marrow of L. Arm	Calculation	----	----	----	----
	Measurement	----	----	----	----
Red Marrow of R. Arm	Calculation	0.0100	20.90	0.0141	0.0056
	Measurement	0.0092	9.02	0.0109	0.0075
Red Marrow of Spine (up)	Calculation	0.0029	36.40	0.0050	0.0008
	Measurement	0.0035	5.49	0.0039	0.0031
Red Marrow of Spine (med)	Calculation	0.0757	4.12	0.0820	0.0695
	Measurement	0.0746	9.55	0.0889	0.0604
Red Marrow of Spine (low)	Calculation	0.3093	3.24	0.3310	0.2875
	Measurement	0.2721	6.50	0.3075	0.2367
Red Marrow of Pelvis	Calculation	0.3734	1.53	0.3977	0.3741
	Measurement	0.3733	5.90	0.4174	0.3293
Red Marrow of L. Leg	Calculation	0.0667	5.06	0.0734	0.0599
	Measurement	0.0631	11.08	0.0771	0.0491
Red Marrow of R. Leg	Calculation	0.0352	7.43	0.0405	0.0300
	Measurement	0.0336	9.48	0.0400	0.0273
Red Marrow Total Body	Calculation	0.2590	1.17	0.2651	0.2529
	Measurement	0.2540	7.32	0.2912	0.2168

<sup>a</sup>Tissue-Air Ratio (T.A.R.) is the average absorbed dose to the organ of interest (rad) per unit exposure (R, free-in-air) in the center of beam at the surface of body. For a C.V. greater than 50% or a T.A.R. less than  $10^{-4}$  (rad/R) no comparison is given.

<sup>b</sup>Coefficient of variation (C.V.) =  $\frac{\text{standard error}}{\text{average energy deposited}} \times 100$ .



Table C-9. Tissue-Air Ratio Comparison,  
Five-Year-Old Phantom Head Examination  
(Posterior/Anterior View, 80 kVcp, 240 mAs, FSD - 101.6 cm)

ORGAN		T.A.R. <sup>a</sup> (rad/R)	C.V. <sup>b</sup> (%)	T.A.R. + 2 C.V. up limit (rad/R)	T.A.R. - 2 C.V. low limit (rad/R)
Brain	Calculation	0.3169	1.05	0.3235	0.3103
	Measurement	0.3484	10.08	0.4187	0.2782
Thyroid	Calculation	0.0836	19.34	0.0998	0.0674
	Measurement	0.0907	9.21	0.1074	0.0740
Thymus	Calculation	0.0179	16.64	0.0239	0.0119
	Measurement	0.0177	7.96	0.0205	0.0149
Ovaries	Calculation	----	----	----	----
	Measurement	----	----	----	----
Testes	Calculation	----	----	----	----
	Measurement	----	----	----	----
Red Marrow of L. Arm	Calculation	0.0075	17.57	0.0101	0.0048
	Measurement	0.0064	9.42	0.0076	0.0052
Red Marrow of R. Arm	Calculation	0.0088	14.84	0.0115	0.0062
	Measurement	0.0083	8.35	0.0097	0.0069
Red Marrow of Spine (up)	Calculation	0.4028	2.30	0.4214	0.3843
	Measurement	0.4577	6.07	0.5133	0.4021
Red Marrow of Spine (med)	Calculation	0.0191	5.28	0.0211	0.0171
	Measurement	0.0192	15.94	0.0253	0.0131
Red Marrow of Spine (low)	Calculation	----	----	----	----
	Measurement	----	----	----	----
Red Marrow of Pelvis	Calculation	----	----	----	----
	Measurement	----	----	----	----
Red Marrow of L. Leg	Calculation	----	----	----	----
	Measurement	----	----	----	----
Red Marrow of R. Leg	Calculation	----	----	----	----
	Measurement	----	----	----	----
Red Marrow Total Body	Calculation	0.0224	0.87	0.0228	0.0220
	Measurement	0.0238	11.36	0.0292	0.0184

<sup>a</sup>Tissue-Air Ratio (T.A.R.) is the average absorbed dose to the organ of interest (rad) per unit exposure (R, free-in-air) in the center of beam at the surface of body. For a C.V. greater than 50% or a T.A.R. less than  $10^{-4}$  (rad/R) no comparison is given.

<sup>b</sup>Coefficient of variation (C.V.) =  $\frac{\text{standard error}}{\text{average energy deposited}} \times 100$ .



Table C-10. Tissue-Air Ratio Comparison,  
Five-Year-Old Phantom Head Examination  
(Left Lateral View, 70 kVcp, 439 mAs, FSD = 101.6 cm)

ORGAN		T.A.R. <sup>a</sup> (rad/R)	C.V. <sup>b</sup> (%)	T.A.R. + 2 C.V. up limit (rad/R)	T.A.R. - 2 C.V. low limit (rad/R)
Brain	Calculation	0.3741	1.07	0.3821	0.3661
	Measurement	0.3674	5.86	0.4104	0.3243
Thyroid	Calculation	0.3623	11.11	0.4428	0.2818
	Measurement	0.2832	6.65	0.3209	0.2455
Thymus	Calculation	0.0207	17.65	0.0280	0.0134
	Measurement	0.0212	14.69	0.0275	0.0150
Ovaries	Calculation	----	----	----	----
	Measurement	----	----	----	----
Testes	Calculation	----	----	----	----
	Measurement	----	----	----	----
Red Marrow of L. Arm	Calculation	0.0119	15.11	0.0145	0.0078
	Measurement	0.0183	8.45	0.0214	0.0152
Red Marrow of R. Arm	Calculation	0.0045	26.97	0.0069	0.0021
	Measurement	0.0042	9.62	0.0051	0.0034
Red Marrow of Spine (up)	Calculation	0.2359	3.36	0.2518	0.2201
	Measurement	0.2182	6.70	0.2474	0.1890
Red Marrow of Spine (med)	Calculation	0.0163	6.48	0.0184	0.0142
	Measurement	0.0138	11.23	0.0169	0.0107
Red Marrow of Spine (low)	Calculation	----	----	----	----
	Measurement	----	----	----	----
Red Marrow of Pelvis	Calculation	----	----	----	----
	Measurement	----	----	----	----
Red Marrow of L. Leg	Calculation	----	----	----	----
	Measurement	----	----	----	----
Red Marrow of R. Leg	Calculation	----	----	----	----
	Measurement	----	----	----	----
Red Marrow Total Body	Calculation	0.0191	0.87	0.0194	0.0188
	Measurement	0.0123	12.83	0.0154	0.0091

<sup>a</sup>Tissue-Air Ratio (T.A.R.) is the average absorbed dose to the organ of interest (rad) per unit exposure (R, free-in-air) in the center of beam at the surface of body. For a C.V. greater than 50% or a T.A.R. less than  $10^{-4}$  (rad/R) no comparison is given.

$$^b\text{Coefficient of variation (C.V.)} = \frac{\text{standard error}}{\text{average energy deposited}} \times 100.$$

Table C-11. Tissue-Air Ratio Comparison,  
Five-Year-Old Phantom Chest Examination  
(Anterior/Posterior View, 80 kVcp, 827 mAs, FSD = 182.9 cm)

ORGAN		T.A.R. <sup>a</sup> (rad/R)	C.V. <sup>b</sup> (%)	T.A.R. + 2 C.V. up limit (rad/R)	T.A.R. - 2 C.V. low limit (rad/R)
Brain	Calculation	0.0143	5.89	0.0159	0.0129
	Measurement	0.0150	16.71	0.2001	0.0100
Thyroid	Calculation	0.5405	10.03	0.6489	0.4321
	Measurement	0.5905	7.19	0.6754	0.5056
Thymus	Calculation	0.8851	3.46	0.9463	0.8239
	Measurement	0.8649	5.55	0.9609	0.7690
Ovaries	Calculation	----	----	----	----
	Measurement	----	----	----	----
Testes	Calculation	----	----	----	----
	Measurement	----	----	----	----
Red Marrow of L. Arm	Calculation	0.0878	6.16	0.0986	0.0770
	Measurement	0.0785	7.32	0.0900	0.0670
Red Marrow of R. Arm	Calculation	0.0899	6.22	0.1011	0.0788
	Measurement	0.0449	7.13	0.0973	0.0725
Red Marrow of Spine (up)	Calculation	0.0812	6.59	0.0919	0.0705
	Measurement	0.1141	5.40	0.1153	0.0929
Red Marrow of Spine (med)	Calculation	0.0991	3.12	0.1053	0.0929
	Measurement	0.1027	6.09	0.1152	0.0902
Red Marrow of Spine (low)	Calculation	0.0083	14.92	0.0107	0.0058
	Measurement	0.0068	8.54	0.0079	0.0056
Red Marrow of Pelvis	Calculation	0.0012	22.44	0.0017	0.0007
	Measurement	0.0015	10.63	0.0019	0.0012
Red Marrow of L. Leg	Calculation	----	----	----	----
	Measurement	----	----	----	----
Red Marrow of R. Leg	Calculation	----	----	----	----
	Measurement	----	----	----	----
Red Marrow Total Body	Calculation	0.0390	0.87	0.0406	0.0393
	Measurement	0.0269	8.49	0.0315	0.0223

<sup>a</sup>Tissue-Air Ratio (T.A.R.) is the average absorbed dose to the organ of interest (rad) per unit exposure (R, free-in-air) in the center of beam at the surface of body. For a C.V. greater than 50% or a T.A.R. less than  $10^{-4}$  (rad/R) no comparison is given.

$$^b\text{Coefficient of variation (C.V.)} = \frac{\text{standard error}}{\text{average energy deposited}} \times 100.$$

Table C-12. Tissue-Air Ratio Comparison,  
Five-Year-Old Phantom Chest Examination  
(Posterior/Anterior View, 80 kVcp, 827 mAs, FSD = 182.9 cm)

ORGAN		T.A.R. <sup>a</sup> (rad/R)	C.V. <sup>b</sup> (%)	T.A.R. + 2 C.V. up limit (rad/R)	T.A.R. - 2 C.V. low limit (rad/R)
Brain	Calculation	0.0142	5.92	0.0159	0.0125
	Measurement	0.0144	11.64	0.0175	0.0105
Thyroid	Calculation	0.1356	19.75	0.1892	0.0820
	Measurement	0.1475	5.44	0.1636	0.1315
Thymus	Calculation	0.1822	7.99	0.2113	0.1531
	Measurement	0.1989	8.03	0.2309	0.1670
Ovaries	Calculation	----	----	----	----
	Measurement	----	----	----	----
Testes	Calculation	----	----	----	----
	Measurement	----	----	----	----
Red Marrow of L. Arm	Calculation	0.0794	6.78	0.0901	0.0686
	Measurement	0.0831	7.29	0.0952	0.0710
Red Marrow of R. Arm	Calculation	0.0896	6.51	0.1013	0.0779
	Measurement	0.0852	7.61	0.0983	0.0721
Red Marrow of Spine (up)	Calculation	0.4295	2.83	0.4538	0.4052
	Measurement	0.4615	12.31	0.5751	0.3479
Red Marrow of Spine (med)	Calculation	0.3889	1.53	0.4008	0.2770
	Measurement	0.3995	8.12	0.4644	0.3346
Red Marrow of Spine (low)	Calculation	0.0109	13.78	0.0131	0.0079
	Measurement	0.0151	8.07	0.0175	0.0126
Red Marrow of Pelvis	Calculation	0.0009	21.49	0.0013	0.0005
	Measurement	0.0010	13.59	0.0013	0.0007
Red Marrow of L. Leg	Calculation	----	----	----	----
	Measurement	----	----	----	----
Red Marrow of R. Leg	Calculation	----	----	----	----
	Measurement	----	----	----	----
Red Marrow Total Body	Calculation	0.0994	0.72	0.1008	0.0980
	Measurement	0.0889	7.12	0.1016	0.0762

<sup>a</sup>Tissue-Air Ratio (T.A.R.) is the average absorbed dose to the organ of interest (rad) per unit exposure (R, free-in-air) in the center of beam at the surface of body. For a C.V. greater than 50% or a T.A.R. less than  $10^{-4}$  (rad/R) no comparison is given.

<sup>b</sup>Coefficient of variation (C.V.) =  $\frac{\text{standard error}}{\text{average energy deposited}} \times 100$ .



Table C-13. Tissue-Air Ratio Comparison,  
Five-Year Old Phantom Chest Examination  
(Left Lateral View, 100 kVcp, 521 mAs, FSD - 182.9 cm)

ORGAN		T.A.R. <sup>a</sup> (rad/R)	C.V. <sup>b</sup> (%)	T.A.R. + 2 C.V. up limit (rad/R)	T.A.R. - 2 C.V. low limit (rad/R)
Brain	Calculation	0.0221	4.89	0.0243	0.0200
	Measurement	0.0193	7.36	0.0222	0.0165
Thyroid	Calculation	0.4472	11.63	0.5512	0.3432
	Measurement	0.3979	4.75	0.4358	0.3601
Thymus	Calculation	0.3414	5.76	0.3807	0.3021
	Measurement	0.3868	3.86	0.4167	0.3569
Ovaries	Calculation	----	----	----	----
	Measurement	----	----	----	----
Testes	Calculation	----	----	----	----
	Measurement	----	----	----	----
Red Marrow of L. Arm	Calculation	----	----	----	----
	Measurement	----	----	----	----
Red Marrow of R. Arm	Calculation	0.0810	7.61	0.0933	0.0686
	Measurement	0.0450	7.49	0.0517	0.0383
Red Marrow of Spine (up)	Calculation	0.3098	3.41	0.3309	0.2886
	Measurement	0.3468	4.06	0.3750	0.3186
Red Marrow of Spine (med)	Calculation	0.2033	2.21	0.2123	0.1943
	Measurement	0.2151	4.76	0.2356	0.1946
Red Marrow of Spine (low)	Calculation	0.0010	13.67	0.0013	0.0007
	Measurement	0.0010	10.28	0.0012	0.0008
Red Marrow of Pelvis	Calculation	0.0015	20.00	0.0021	0.0009
	Measurement	0.0013	4.59	0.0065	0.0011
Red Marrow of L. Leg	Calculation	----	----	----	----
	Measurement	----	----	----	----
Red Marrow of R. Leg	Calculation	----	----	----	----
	Measurement	----	----	----	----
Red Marrow Total Body	Calculation	0.0691	0.84	0.0703	0.0679
	Measurement	0.0567	8.31	0.0661	0.0473

<sup>a</sup>Tissue-Air Ratio (T.A.R.) is the average absorbed dose to the organ of interest (rad) per unit exposure (R, free-in-air) in the center of beam at the surface of body. For a C.V. greater than 50% or a T.A.R. less than  $10^{-4}$  (rad/R) no comparison is given.

<sup>b</sup>Coefficient of variation (C.V.) =  $\frac{\text{standard error}}{\text{average energy deposited}} \times 100$ .



Table C-14. Tissue-Air Ratio Comparison,  
Five-Year-Old Phantom Abdomen Examination  
(Anterior/Posterior View, 80 kVcp, 240 mAs, FSD = 101.6 cm)

ORGAN		T.A.R. <sup>a</sup> (rad/R)	C.V. <sup>b</sup> (%)	T.A.R. + 2 C.V. up limit (rad/R)	T.A.R. - 2 C.V. low limit (rad/R)
Brain	Calculation	0.0001	44.91	0.0003	0.0000
	Measurement	----	----	----	----
Thyroid	Calculation	----	----	----	----
	Measurement	----	----	----	----
Thymus	Calculation	0.0212	25.58	0.0320	0.0103
	Measurement	0.0242	6.32	0.0272	0.0211
Ovaries	Calculation	0.6570	17.12	0.8820	0.0432
	Measurement	0.4520	7.89	0.5233	0.3807
Testes	Calculation	0.2883	26.51	0.4412	0.1354
	Measurement	0.2938	5.50	0.3261	0.2615
Red Marrow of L. Arm	Calculation	0.0062	29.78	0.0098	0.0025
	Measurement	0.0073	7.33	0.0084	0.0062
Red Marrow of R. Arm	Calculation	0.0047	24.76	0.0070	0.0024
	Measurement	0.0070	6.59	0.0079	0.0061
Red Marrow of Spine (up)	Calculation	0.0018	49.60	0.0036	0.0000
	Measurement	0.0026	7.09	0.0030	0.0023
Red Marrow of Spine (med)	Calculation	0.0339	5.74	0.0378	0.0300
	Measurement	0.0405	7.92	0.0464	0.0346
Red Marrow of Spine (low)	Calculation	0.1143	5.00	0.1257	0.1028
	Measurement	0.1358	4.07	0.1468	0.1247
Red Marrow of Pelvis	Calculation	0.2168	2.00	0.2255	0.2082
	Measurement	0.2451	3.81	0.2638	0.2264
Red Marrow of L. Leg	Calculation	0.0319	5.95	0.0357	0.0281
	Measurement	0.0287	8.96	0.0338	0.0236
Red Marrow of R. Leg	Calculation	0.0306	6.01	0.0342	0.0269
	Measurement	0.0291	11.28	0.0356	0.0225
Red Marrow Total Body	Calculation	0.1460	1.44	0.1502	0.1418
	Measurement	0.1410	6.47	0.1593	0.1228

<sup>a</sup>Tissue-Air Ratio (T.A.R.) is the average absorbed dose to the organ of interest (rad) per unit exposure (R, free-in-air) in the center of beam at the surface of body. For a C.V. greater than 50% or a T.A.R. less than  $10^{-4}$  (rad/R) no comparison is given.

<sup>b</sup>Coefficient of variation (C.V.) =  $\frac{\text{standard error}}{\text{average energy deposited}} \times 100$ .

Table C-15. Tissue-Air Ratio Comparison,  
Five-Year-Old Phantom Abdomen Examination  
(Posterior/Anterior View, 80 kVcp, 240 mAs, FSD = 101.6 cm)

ORGAN		T.A.R. <sup>a</sup> (rad/R)	C.V. <sup>b</sup> (%)	T.A.R. + 2 C.V. up limit (rad/R)	T.A.R. - 2 C.V. low limit (rad/R)
Brain	Calculation	----	----	----	----
	Measurement	----	----	----	----
Thyroid	Calculation	----	----	----	----
	Measurement	----	----	----	----
Thymus	Calculation	0.0089	30.55	0.0144	0.0038
	Measurement	0.0084	9.67	0.0100	0.0068
Ovaries	Calculation	0.4366	19.05	0.6029	0.2703
	Measurement	0.2681	7.95	0.3107	0.2255
Testes	Calculation	0.1939	33.19	0.3226	0.0652
	Measurement	0.2341	14.63	0.3026	0.1656
Red Marrow of L. Arm	Calculation	0.0034	36.24	0.0058	0.0009
	Measurement	0.0029	13.26	0.0036	0.0021
Red Marrow of R. Arm	Calculation	0.0039	25.17	0.0060	0.0020
	Measurement	0.0043	14.18	0.0056	0.0030
Red Marrow of Spine (up)	Calculation	----	----	----	----
	Measurement	0.0012	49.03	0.0024	0.0000
Red Marrow of Spine (med)	Calculation	0.1210	2.98	0.1283	0.1138
	Measurement	0.1239	7.61	0.1428	0.1050
Red Marrow of Spine (low)	Calculation	0.4739	2.34	0.4961	0.4518
	Measurement	0.4244	3.75	0.4562	0.3926
Red Marrow of Pelvis	Calculation	0.3975	1.42	0.4088	0.3862
	Measurement	0.4025	4.41	0.4380	0.3670
Red Marrow of L. Leg	Calculation	0.0325	5.75	0.0362	0.0288
	Measurement	0.0353	12.26	0.0440	0.0266
Red Marrow of R. Leg	Calculation	0.0323	5.93	0.0381	0.0302
	Measurement	0.0367	6.42	0.0414	0.0319
Red Marrow Total Body	Calculation	0.2205	1.00	0.2249	0.2161
	Measurement	0.2720	5.87	0.3039	0.2401

<sup>a</sup>Tissue-Air Ratio (T.A.R.) is the average absorbed dose to the organ of interest (rad) per unit exposure (R, free-in-air) in the center of beam at the surface of body. For a C.V. greater than 50% or a T.A.R. less than  $10^{-4}$  (rad/R) no comparison is given.

$$^b \text{Coefficient of variation (C.V.)} = \frac{\text{standard error}}{\text{average energy deposited}} \times 100.$$

Table C-16. Tissue-Air Ratio Comparison,  
Five-Year-Old Phantom Abdomen Examination  
(Left Lateral View, 100 kVcp, 152 mAs, FSD = 101.6 cm)

ORGAN		T.A.R. <sup>a</sup> (rad/R)	C.V. <sup>b</sup> (%)	T.A.R. + 2 C.V. up limit (rad/R)	T.A.R. - 2 C.V. low limit (rad/R)
Brain	Calculation	----	----	----	----
	Measurement	----	----	----	----
Thyroid	Calculation	----	----	----	----
	Measurement	0.0023	7.82	0.0027	0.0020
Thymus	Calculation	0.0143	27.93	0.0227	0.0063
	Measurement	0.0121	7.00	0.0139	0.0105
Ovaries	Calculation	0.5473	19.18	0.7572	0.3374
	Measurement	0.3897	7.67	0.4495	0.3299
Testes	Calculation	0.1757	31.09	0.2850	0.0665
	Measurement	0.2065	4.73	0.2245	0.1884
Red Marrow of L. Arm	Calculation	0.0064	23.02	0.0093	0.0035
	Measurement	0.0056	5.30	0.0062	0.0050
Red Marrow of R. Arm	Calculation	0.0084	26.57	0.0128	0.0039
	Measurement	0.0013	6.60	0.0147	0.0013
Red Marrow of Spine (up)	Calculation	0.0014	47.86	0.0027	0.0000
	Measurement	0.0010	15.61	0.0014	0.0007
Red Marrow of Spine (med)	Calculation	0.0711	4.10	0.0769	0.0652
	Measurement	0.0809	9.54	0.9634	0.0655
Red Marrow of Spine (low)	Calculation	0.2304	3.61	0.2471	0.2138
	Measurement	0.2389	4.37	0.2598	0.2180
Red Marrow of Pelvis	Calculation	0.3415	15.50	0.4474	0.2356
	Measurement	0.3011	3.53	0.3224	0.2798
Red Marrow of L. Leg	Calculation	0.0481	4.84	0.0528	0.0435
	Measurement	0.0471	11.55	0.0580	0.0362
Red Marrow of R. Leg	Calculation	0.0156	8.83	0.0183	0.0128
	Measurement	0.0225	15.13	0.0293	0.0157
Red Marrow Total Body	Calculation	0.1654	1.19	0.1693	0.1615
	Measurement	0.1898	8.32	0.2214	0.1582

<sup>a</sup>Tissue-Air Ratio (T.A.R.) is the average absorbed dose to the organ of interest (rad) per unit exposure (R, free-in-air) in the center of beam at the surface of body. For a C.V. greater than 50% or a T.A.R. less than  $10^{-4}$  (rad/R) no comparison is given.

<sup>b</sup>Coefficient of variation (C.V.) =  $\frac{\text{standard error}}{\text{average energy deposited}} \times 100$ .



## BIBLIOGRAPHY

- Adrian Committee, Radiological Hazard to Patients, First Report of the Committee, H.M.S.O. London (1956).
- Adrian Committee, Radiological Hazard to Patients, Second Report of the Committee, H.M.S.O. London (1960).
- Adrian Committee, Radiological Hazard to Patients, Final Report of the Committee, H.M.S.O. London (1966).
- Albert, E. R., and A. R. Omran, "Follow-up Study of Patients Treated by X-Ray Epilation for Tinea Capitis," Arch. Environ. Health 17 (1968).
- Almond, R. P., and A. McCray, "The Energy Response of LiF, CaF<sub>2</sub>, and Li<sub>2</sub>B<sub>4</sub>O<sub>7</sub>:Mn to High Energy Radiations," Phys. Med. Biol. 15, 335 (1970).
- Anas, M. El-Mahdi, M. Richard, W. N. Thornton, and C. C. Williams, "Sequelae of Pelvic Irradiation in Infancy," Radiology 110, 665 (1974).
- Antoku, S., W. J. Russell, R. C. Milton, H. Nashinaga, K. Takeshita, and S. Sawada, "Dose to Patients from Roentgenography," Health Phys. 23, 291 (1972).
- Baruch, M., B. Dikla, M. Hannah, S. Ruth, and G. L. Sheldon, "Radiation-Induced Head and Neck Tumors," Lancet, 277 (February 1974).
- Beach, S. A., and W. G. Dolphin, "A Study of the Relationship of X-Ray Dose Delivered to the Thyroids of Children and Subsequent Development of Malignant Tumors," Phys. Med. Biol. 6, 583 (1962).
- Beebe, G. W., H. Kato, and C. E. Land, "Studies of the Mortality of A-Bomb Survivors, 4. Mortality and Radiation Dose, 1950-1966," Radiat. Res. 48, 613 (1971).
- BEIR, The Effects on Population of Exposure to Low Levels of Ionizing Radiation, National Academy of Science - National Research Council Advisory Committee on the Biological Effects of Ionizing Radiation (Washington, DC, 1972).
- Billings, M. S., A. Norman, and M. A. Greenfield, "Gonadal Dose during Routine Roentgenography," Radiology 69, 37 (1957).



- Binder, W., and J. R. Cameron, "Dosimetric Properties of  $\text{CaF}_2:\text{Dy}$ ," Health Phys. 17, 613 (1969).
- Bjarngard, B. E., and D. Jones, "Thermoluminescent Dosimeters of LiF and  $\text{CaF}_2:\text{Mn}$  Incorporated in Teflon," Solid State and Chemical Radiation Dosimetry in Medicine and Biology, Proc. Symp., Vienna IAEA (1966).
- Blair, H. A., editor, Biological Effects of External Radiation, p. 508 (McGraw-Hill Book Co., Inc., New York, 1954).
- Bross, I. D. J., and N. Natarajan, "Leukemia from Low-Level Radiation Identification of Susceptible Children," New Eng. J. Med. 287, 107 (1972).
- Brown, R. F., J. Heslep, and W. Eads, "Number and Distribution of Roentgenologic Examinations for 100,000 People," Radiology 74, 353 (1960).
- Burch, M. W., "Two Level Isothermal Readout for High Precision Thermoluminescence Dosimetry with LiF," Phys. Med. Biol. 13, 627 (1968).
- Bushong, S. C., P. M. Gray, N. Prasad, and S. A. Glaze, "Measurement of X-Ray Quality Using TLD," Health Phys. 26, 358 (1974).
- Cameron, J. R., and G. Kenney, "A New Technique for Determining Quality of X-Ray Beams," Radiat. Res. 19, 199 (1963).
- Cameron, J. R., D. Zimmerman, G. Kenney, R. Buch, R. Bland, and R. Grant, "Thermoluminescent Dosimetry Utilizing LiF," Health Phys. 10, 25 (1964).
- Cameron, J. R., N. Suntharalingam, and G. N. Kenney, Thermoluminescent Dosimetry, p. 168 (The University of Wisconsin Press, Madison, Wis., 1968).
- Carlsson, A. C., B. A. Bengt, and G. A. Carlsson, "High Precision Dosimetry Using Thermoluminescent LiF," Proceedings of Second International Conference on Luminescence Dosimetry, CONF-680920 USAEC (1968).
- Carlsson, A. C., "Thermoluminescence of LiF: Dependence of Thermal History," Phys. Med. Biol. 14, 107 (1969).
- Cashwell, E. D., and C. J. Everett, Monte Carlo Method for Random Walk Problem, p. 27 (Pergamon Press, 1959).
- Clark, S. D., "Where Are the Cases of Radium Poisoning?" J. Am. Med. Assoc., 168, 761 (1958).

- Conrad, R. A., R. M. Dobyns, and W. W. Sutow, "Thyroid Neoplasia as Late Effect of Exposure to Radioactive Iodine in Fallout," J. Am. Med. Assoc., 214, 316 (1971).
- Court-Brown, W. M., and R. Doll, Leukemia and Aplastic Anemia in Patients Irradiated for Ankylosing Spondylitis, (London, Her Majesty's Stationary Office, 1957).
- Court-Brown, W. M., and R. Doll, "Mortality from Cancer and Other Causes after Radiotherapy for Ankylosing Spondylitis," Brit. Med. J. 5474, 1327 (1965).
- Dawson, W. D., "Growth Impairment Following Radiotherapy in Childhood," Clin. Radiol. 19, 241 (1962).
- Debakan, A. S., "Abnormalities in Children Exposed to X-Radiation during Various Stages of Gestation: Tentative Timetable of Irradiation Injury to Human Fetus," J. Nucl. Med. 9, 471 (1968).
- Dhar, H., L. H. Dewerd, and T. G. Stobe, "Effects of Annealing and Cooling Processes on Thermoluminescence of LiF (TLD 100)," Health Phys. 25, 427 (1973).
- Dixon, R. L., "The Use of BaF<sub>2</sub> Thermoluminescence in Determining Radiation Quality," Phys. Med. Biol. 17, 81 (1972).
- Dolphin, G. W., "The Risk of Thyroid Cancer Following Irradiation," Health Phys. 15, 219 (1968).
- ELASH, "Medical Radiographic Exposure Limits," Illinois Department of Public Health, Springfield, Illinois (1974).
- Ellett, W. H., G. L. Bronell, and A. R. Reddy, "An Assessment of Monte Carlo Calculations to Determine Gamma Ray Dose from Internal Emitters," Phys. Med. Biol. 13, 219 (1968).
- Epp, E. R., H. Weiss, and J. S. Laughlin, "Measurement of Bone Marrow and Gonadal Dose from the Chest X-Ray Examination as a Function of Field Size, Field Alignment, Tube Kilovoltage, and Added Filtration," Brit. J. Radiol. 34, 85 (1961).
- Epp, E. R., H. Weiss, J. S. Laughlin, and R. S. Sherman, "Measurement of Bone Marrow and Gonadal Dose from X-Ray Examination of the Pelvis, Hip, and Spine as a Function of Field Size, Tube Kilovoltage and Added Filtration," Brit. J. Radiol. 36, 247 (1963).
- Facey, R. A., "Dose and Photon-Energy Measurement for Bone Marrow in a Human Phantom by Thermoluminescence," Health Phys. 14, 557 (1968).



- Fisher, H. L., Jr., and W. S. Snyder, Annual Progress Report for Period Ending July 31, 1966, Health Physics Division, Oak Ridge National Laboratory Report ORNL-4007 (1966).
- Fisher, H. L., Jr., and W. S. Snyder, Annual Progress Report for Period Ending July 31, 1967, Health Physics Division, Oak Ridge National Laboratory Report ORNL-4168 (1967).
- Federal Radiation Council, Background Material for the Development of Radiation Protection Standards, Report No. 1, Federal Radiation Council, Washington, DC (1960).
- Federal Radiation Council, Background Material for the Development of Radiation Protection Standards, Report No. 2 of the Federal Radiation Council, Washington, DC (1961).
- Gibson, R., S. Graham, A. Libenfeld, L. Schuman, J. E. Dowd, and M. Levin, "Irradiation in the Epidemiology of Leukemia among Adults," J. Natl. Cancer Inst. 48, 301 (1972).
- Gibson, J. A. B., G. M. Ardran, L. H. J. Peale, M. Marshall, H. E. Crooks, and R. Birch, "Standardization of the Output from Diagnostic X-Ray Generators," in Biomedical Dosimetry, Symp. Proc. on Advances in Biomedical Dosimetry held in Vienna, ISBN 92-0-01050575-0, p. 509 (1975).
- Ginther, R. J., and R. D. Kirk, Thermoluminescence of  $\text{CaF}_2:\text{Mn}$  and Its Application to Dosimetry, Progr. Rept., NRL (1956).
- Ginther, R. J., and R. D. Kirk, "The Thermoluminescence of  $\text{CaF}_2:\text{Mn}$ ," J. Electrochem. Soc. 104, 365 (1957).
- Gitlin, J. N., "Preliminary Dose Estimates from the U.S. Public Health Service, 1970 X-Ray Exposure Study," Paper presented at the 49th Annual Meeting of the American College of Radiology, Miami Beach, Florida (1972).
- Glasser, O., E. H. Quimby, L. S. Taylor, J. L. Weatherwax, and R. H. Morgan, Physical Foundation of Radiology, Chapter 1 (Hoeber, New York, 1961).
- Goldman, K. P., "Mortality of Coal Miners from Carcinoma of the Lung," Brit. J. Indust. Med. 22, 72 (1965).
- Gooden, S. D., and T. J. Brickner, "The Routine Use of Thermoluminescence Dosimetry for Radiation Therapy," Radiology 102, 685 (1972).
- Gorbics, S. G., H. F. Attix, and J. A. Pfaff, "Temperature Stability of  $\text{CaF}_2:\text{Mn}$  and  $\text{LiF(TLD-100)}$  Thermoluminescent Dosimeters," Int. J. Appl. Radiat. 18, 625 (1967).

- Gorbics, G. S., and F. H. Attix, "LiF and CaF<sub>2</sub>:Mn Thermoluminescent Dosimeters in Tandem," Int. J. Appl. Radiat. 19, 81 (1968).
- Graham, D., and K. F. Hamilton, "Genetic Variation in the Acute Lethal Response of Four Inbred Mouse Strains to Whole-Body X-Irradiation," Genetics 42, 189 (1957).
- Graham, S., M. L. Levin, A. M. Lilienfeld, L. M. Shuman, R. Gibson, J. E. Dowd, and L. Hemplemann, "Preconception, Intrauterine, and Postnatal Irradiation as Related to Leukemia," Natl. Cancer Inst. Monogr. 19, 347 (1966).
- Greenhouse, A. N., Jr., H. D. Maillie, and H. Mermagen, "A Thermoluminescent Microdosimetry System for the Measurement of Photon Quality," Radiat. Res. 32, 641 (1967).
- Hald, A., Statistical Theory with Engineering Application, p. 99 (John Wiley & Sons, Inc., 1952).
- Hammer-Jacobsen, E., "Genetically Significant Radiation Dose in Diagnostic Radiology, Acta Radiol. Suppl. 222 (1963).
- Harley, H. N., R. E. Albert, R. E. Shore, and B. S. Pasternack, "Follow-up Study of Patients Treated by X-Ray Epilation for Tinea Capitis. Estimation of Dose to the Thyroid and Pituitary Glands and Other Structures of the Head and Neck," Phys. Med. Biol. 21, 631 (1976).
- Harris, M. A., and J. H. Jackson, "On the Low Temperature Annealing of TLD-LiF," Health Phys. 18, 162 (1970).
- Hashizume, T., Y. Kato, T. Maruyama, Y. Kumamoto, A. Shiragai, and A. Nishimura, "Genetically Significant Dose from Diagnostic Medical X-Ray Examinations in Japan, 1969," Health Phys. 23, 827 (1972a).
- Hashizume, T., Y. Kato, T. Maruyama, A. Shiragai, and A. Nishimura, "Population Mean Marrow Dose and Leukemia Significant Dose from Diagnostic Medical X-Ray Examinations in Japan, 1969," Health Phys. 23, 845 (1972b).
- Hemplemann, L. H., J. W. Pifer, G. J. Burke, R. Terry, and W. R. Ames, "Neoplasms in Persons Treated with X-Rays in Infancy for Thymic Enlargement, A Report of Third Follow-up Survey," J. Natl. Cancer Inst. 38, 317 (1967).
- Hemplemann, L. H., "Risk of Thyroid Neoplasms after Irradiation in Childhood," Science 160, 163 (1968).
- Hemplemann, L. H., and D. Grossman, "The Association of Illnesses with Abnormal Immunologic Features with Irradiation of the Thymic Gland in Infancy," Radiat. Res. 58, 122 (1974).



- Hemplemann, L. H., W. J. Hall, M. Philips, R. A. Cooper, and W. R. Ames, "Neoplasms in Persons Treated with X-Rays in Infancy: Fourth Survey in 20 Years," J. Natl. Cancer Inst. 55, 519 (1975).
- Hall, T. E., and A. R. Dobell, "Random Number Generators," S.I.A.M. Rev. 4, 230 (1962).
- Hursh, J. B., and G. Casarette, The Lethal Effect of Acute X-Irradiation on Rats as a Function of Age, USAEC University of Rochester Report UR-403 (1955).
- Hwang, M. L., J. W. Poston, R. L. Shoup, and G. G. Warner, Mathematical Descriptions of a One- and Five-Year-Old Child for Use in Dosimetric Calculations, ORNL-TM-5293 (1976).
- International Commission on Radiological Protection, Recommendations of the International Commission on Radiological Protection, ICRP Publication No. 1, p. 15 (Pergamon Press, New York, 1958).
- International Commission on Radiological Protection, Committee 1, "The Evaluation of Risk from Radiation," Health Phys. 12, 239 (1966).
- International Commission on Radiological Protection, Radiosensitivity and Spatial Distribution of Dose, ICRP Publication 14, p. 8 (Pergamon Press, New York, 1970a).
- International Commission on Radiological Protection, Protection of the Patient in X-Ray Diagnosis, ICRP Publication 16, p. 8 (Pergamon Press, New York, 1970b).
- International Commission on Radiological Units and Measurements, Physical Aspects of Radiation, ICRU Report 106 (U.S. Government Printing Office, Washington, DC, 1964).
- Indiana State Board of Health and Indiana University Medical Center, Department of Radiology, Pediatric Low Dosage Medical Radiography, Indianapolis (1969).
- Ishimaru, T., T. Hashino, M. Ichimaru, H. Okada, T. Tomiyasu, T. Tsuchimoto, and T. Yamamoto, "Leukemia in Atomic Bomb Survivors, Hiroshima and Nagasaki, 1 October 1950 - 30 September 1966," Radiat. Rev. 45, 216 (1971).
- Jablon, S., and J. L. Belsky, "Radiation Induced Cancer in Atomic Bomb Survivors," Paper presented to the 10th International Cancer Congress in Houston (1970).
- Jablon, S., K. Tachikawa, J. Belsky, and A. Steer, "Cancer in Japanese Exposed as Children to Atomic Bombs," Lancet 1, 927 (1971).

- Jacobson, A., T. Banks, and M. Ackerman, "Evaluation of Personnel Dosimetry Method for Diagnostic X-Ray Special Procedure Work," Health Phys. 25, 76 (1973).
- James, A. E., (editor), Radiation Nuclear Medicine, p. 34 (1974).
- Jansson, B., Random Number Generators, p. 16 (Victor Petersons Bekindustri Aktiebolag Stockholm, 1966).
- Jayachandran, C. A., "The Response of Thermoluminescent Dosimetric Lithium Borates Equivalent to Air, Water and Soft Tissue and of LiF TLD-100 to Low Energy X-Rays," Phys. Med. Biol. 15, 325 (1970).
- Johns, H. E., and J. R. Cunningham, The Physics of Radiology, p. 135 (Thomas, Springfield, Ill., 1974).
- Jones, D. E. A., and H. C. Raine, "Correspondence," Brit. J. Radiol. 22, 549 (1949).
- Kendall, M. G., and G. G. Smith, Table of Random Sampling Numbers (Cambridge University Press, 1939).
- Kereiakes, J. G., R. A. Seltzer, B. Blackburn, and E. L. Saenger, "Radionuclide Doses to Infants and Children: A Plea for a Standard Child," Health Phys. 11, 999 (1965).
- Koblinger, L., and P. Zarand, "Dose and Image Quantity Calculation for Chest X-Ray Examination," presented to the Third International Conference on Medical Physics, Goetenborg, Sweden (August 1972).
- Koren, K., "Absorbed Dose/Exposure Conversion Factors for Mineral Bone," Brit. J. Radiol. 47, 790 (1974).
- Larsson, L. E., "Radiation Dose to the Gonads of Patients in Swedish Roentgen Diagnostic," Acta Radiol. Suppl. 157, 7 (1958).
- Laue, M., V. W. Friedrich, and P. Knipping, "Interferenzerscheinungen bei Roentgenstrahlen," Ann. Phys. 41, 971 (1913).
- Laughlin, J. S., and I. Pullman, Gonad Dose Produced by the Medical Use of X-Rays (National Academy of Sciences, National Research Council, Washington, DC, 1957).
- Laughlin, J. S., "Ionization Chamber for Diagnostic X-Ray Exposure Studies," Technological Needs for Reduction of Patient Dosage from Diagnostic Radiology, M. L. Janower (editor) (Thomas, Springfield, Ill., 1963).
- Law, J., "The Dosimetry of Low Energy X-Rays Using LiF," Phys. Med. Biol. 18, 38 (1973).



- Lea, D. E. A., Actions of Radiation on Living Cells (Cambridge University Press, 1st Edition, 1946).
- Lea, D. E. A., Actions of Radiation on Living Cells (Cambridge University Press, 2nd Edition, 1955).
- Lehmer, D. H., "Mathematical Methods in Large-Scale Computing Units," Harvard University Computing Annals 26, 141 (1951).
- Lindsay, D. D., and B. E. Stern, "A New Tissue-Like Material for Use Bolus," Radiology 60, 355 (1953).
- Long, C., Biochemists' Handbook, p. 639 (D. Van Nostrand Co., Princeton, NJ, 1961).
- McClure, P. L., A Handbook of Pediatric Radiographic Technology, Department of Radiology Henrietta Ogleston Hospital for Children, Atlanta, Georgia (1976).
- MacMahon, B., "Prenatal X-Ray Exposure and Childhood Cancer," J. Natl. Cancer Inst. 28, 1173 (1962).
- MacMahon, B., "X-Ray Exposure and Malignancy," J. Am. Med. Assoc. 193, 721 (1963).
- Maillie, D. H., A. M. Dutton, and H. Mermagen, "The Relationship between Effective-Energy and rad/R Conversion Factors in Heterogeneous Photon-Energy Fields," Health Phys. 14, 522 (1968).
- Marinelli, W. V., "Radiation Dosimetry and Protection," Ann. Rev. Nucl. Sci. 3, 257 (1953).
- Martin, J. H., "Radiation Dose to the Gonad in Diagnostic Radiology and Their Relation to the Long-Term Genetic Hazard," Med. J. Australia 2, 806 (1955).
- Martin, J. H., "The Contribution to the Gene Material of the Population from the Medical Use of Ionizing Radiation," Med. J. Australia 5, 79 (1958).
- Mayneord, W. V., "The Significance of the Roentgen," Acta Int. Union against Cancer 2, 271 (1937).
- Miller, H. R., "Experimental X-Ray Attenuation Coefficient at Low Photon Energies for Substance of Medical Importance," Phys. Med. Biol. 20, 974 (1975).
- Miller, R. W., "Some Potential Hazards of the Use of Roentgen Ray in Pediatrics," Pediatrics 11, 294 (1953).

- Miller, R. W., "Safeguarding Children from Radiation Risks," Children 3, 203 (1956).
- Miller, R. W., "Radiation-Induced Cancer," J. Natl. Cancer Inst. 49, 1221 (1972).
- Miller, R. H., "Experimental X-Ray Attenuation Coefficients at Low Photon Energies for Substances of Medical Importance," Phys. Med. Biol. 20, 974 (1975).
- Modal, B., D. Baidatz, H. Mart, R. Steinitz, S. G. Levin, "Radiation-Induced Head and Neck Tumors," Lancet 1, 227 (1974).
- Morgan, K. Z., "Type of Data Needs for the Establishment of Adequate Standards of Protection from Radionuclides that Become Deposited inside the Body," presented at the International Congress of Biophysics, Stockholm, Sweden (1961).
- Morgan, K. Z., and J. E. Turner, Principles of Radiation Protection, Chapter 1 (John Wiley & Sons, Inc., New York, 1967).
- Morgan, K. Z., "Reducing Medical Exposure to Ionizing Radiation," Landauer Memorial Lecture given at Stanford University, September 27, 1974.
- Nader, C., "The Dispute Over Safe Uses of X-Rays in Medical Practice," Health Phys. 29, 1 (1975).
- NBS Handbook 47, Recommendation of International Commission on Radiological Protection of the International Commission Radiological Unit, Protection against Neutron Radiation up to 300 Million Electron Volts, 1950.
- NBS Handbook 63, Recommendation of International Commission on Radiological Protection of the International Commission Radiological Unit, Protection against Neutron Radiation up to 300 Million Electron Volts, 1957.
- Neufeld, J., L. C. Emerson, F. J. Davis, and J. E. Turner, Principles of Radiation Protection, K. Z. Morgan and J. E. Turner (editors), p. 96 (John Wiley & Sons, Inc., New York, 1967).
- Neuhauser, E. B. D., M. H. Wittenborg, C. Z. Berman, and J. Cohen, "Irradiation Effects of Roentgen Therapy on the Growing Spine," Radiology 59, 637 (1952).
- Norris, P. W., T. W. Speckman, and P. E. Gutafson, "Studies of the Metabolism of Radium in Man," Am. J. Roentgenol Radium Ther. Nucl. Med. 73, 705 (1955).



- Norwood, W. D., H. W. Healy, E. E. Donaldson, W. C. Roesch, and C. W. Kirklin, "The Gonad Radiation Dose Received by the People of Small American Cities Due to the Diagnostic Use of Roentgen Rays," Am. J. Roentgenol Radium Ther. Nucl. Med. 82, 1081 (1959).
- Pasternack, B. S., and M. B. Heller, "Genetically Significant Dose to the Population of New York City from Diagnostic Medical Radiology," Radiology 90, 217 (1968).
- Pifer, J. W., E. T. Toyooka, R. W. Murray, W. R. Ames, and L. H. Hempelmann, "Neoplasms and Mortality," J. Natl. Cancer Inst. 31, 1333 (1963).
- Poston, J. W., G. G. Warner, and P. S. Stansbury, Medical X-Ray Dose Estimation Program Progress Report for Period Ending August 31, 1974, Oak Ridge National Laboratory Report ORNL-TM-4722 (1974).
- Poston, J. W., personal communication (1975).
- Puite, K. J., and D. L. J. M. Grebolder, "Energy Dependence of the Thermoluminescent Dosimeters for X-Ray Dose and Dose Distribution Measurements in a Mouse Phantom," Phys. Med. Biol. 19, 341 (1974).
- Puite, K. J., "A Thermoluminescence System for the Intercomparison of Absorbed Dose and Radiation Quality of X-Rays with a HVL of 0.1 to 3.0 mmCu," Phys. Med. Biol. 21, 216 (1976).
- RAND Corporation, A Million Random Digits with 100,000 Normal Deviates, (The Free Press, New York, 1965).
- Randall, J. T., and M. H. F. Wilkins, "Phosphorescence and Electron Traps," Proc. R. Soc. (A) 184, 366 (1945).
- Reissland, A. J., P. Kay, and G. W. Dolphin, "The Observation and Analysis of Cancer Deaths among Classified Radiation Workers," Phys. Med. Biol. 21, 903 (1976).
- Robinow, M., and F. M. Silverman, "Radiation Hazards in the Field of Pediatrics," Pediatrics 20, 5 (1957).
- Rosenstein, M., Organ Doses in Diagnostic Radiology, U.S. Department of Health, Education, and Welfare. HEW Publication (FDA)76-8030 (1976).
- Rossi, H. H., "The n Unit and Energy Absorption in Tissue," Radiology 61, 93 (1953).
- Rossi, H. H., and G. Failla, "Tissue-Equivalent Ionization Chambers," Nucleonics 14, No. 2, 32 (1956).

- Rossiter, M. J., "The Use of Precision Thermoluminescence Dosimetry for Intercomparison of Absorbed Dose," Phys. Med. Biol. 20, 735 (1975).
- Rubin, P., B. R. Duthie, and W. L. Young, "The Significance of Scoliosis in Postirradiated Wilms' Tumor and Neuroblastoma," Radiology 79, 539 (1962).
- Rugh, R., and W. Leach, "X-Ray Effects on the Embryo and Fetus: A Review of Experimental Finding," Paper presented at the International Radiation Protection Association, Third International Congress, Washington, DC (1973).
- Saengerte, E. L., R. A. Seltzer, T. D. Sterling, and J. G. Kereiakes, "Carcinogenic Effects of I-131 Compared with X-Irradiation," Health Phys. 9, 1371 (1964).
- Schayes, R., C. Brooke, I. Kizlowitz, and M. Lheureux, "New Developments in Thermoluminescent Dosimetry," Health Phys. 14, 251 (1968).
- Scherzer, V. O., "Über die Ausstrahlung bei der Bremsung von Protonen und Schnellen Electronen," Ann. Phys. 13, 137 (1932).
- Schmid, W. F., and R. W. Mooney, "Thermoluminescence of  $\text{CaF}_2:\text{Mn}$ ," Electrochem. Soc. 110, 340 (1963).
- Schulman, J. H., R. J. Ginther, R. D. Kirk, and H. S. Goulart, "Thermoluminescent Dosimeter Has Storage Stability, Linearity," Nucleonics 18, 92 (1960).
- Seltzer, R., and P. E. Sartwell, "The Influence of Occupational Exposure to Radiation on Mortality of American Radiologists and Other Medical Specialists," Am. J. Epidemiol. 81, 2 (1965).
- Shiragai, A., "Annealing of a LiF Thermoluminescence Dosimetry," Health Phys. 13, 1040 (1967).
- Shleien, B., A Review of Determinations of Radiation Dose to the Active Bone Marrow from Diagnostic X-Ray Examinations, DHEW Publication (FDA)74-8007 (1973).
- Shonka, F. R., J. E. Rose, and G. Failla, "Conducting Plastic Equivalent to Tissue, Air and Polystyrene," Geneva Conference paper P/753 (1958).
- Silverman, C., and D. A. Hoffman, "Tumor Risk from Radiation during Childhood," Proceedings of the Eighth Midyear Topical Symposium of the Health Physics Society, p. 121 (1974).



- Snyder, W. S., M. R. Ford, G. G. Warner, and H. L. Fisher, Jr., MIRD Pamphlet No. 5, J. Nucl. Med., Suppl. No. 3 (1969).
- Snyder, W. S., M. J. Cook, E. S. Nasset, L. Karhausen, G. P. Howells, and I. H. Tipton, Report of the Task Group on Reference Man, ICRP Publication 23 (1975).
- Solomen, A. K., Symposium in Radiology, J. J. Nickson (editor) (John Wiley & Sons, Inc., New York, 1952).
- Spector, S. W., Handbook of Biological Data, p. 50 (W. B. Saunder Co., Philadelphia, 1956).
- Spiers, F. W., "Effective Atomic Number and Energy Absorption in Tissue," Brit. J. Radiol. 19, 53 (1946).
- Spiers, F. W., Radioisotopes in the Human Body (Academic Press, New York, 1968).
- Spurny, Z., C. Milu, and N. Racovenanu, "Comparison of X-Ray Beams Using Thermoluminescent Dosimeters," Phys. Med. Biol. 18, 276 (1973).
- Stacy, A. J., A. R. Bevan, and C. W. Dickens, "A New Phantom Employing Depolymerised Natural Rubber," Brit. J. Radiol. 34, 512 (1961).
- Stanford, R. W., and J. Vance, "The Quantity of Radiation Received by the Reproductive Organs of Patients during Routine Diagnostic X-Ray Examinations," Brit. J. Radiol. 28, 266 (1955).
- Stansbury, P. S., TECALC — A Program to Calculate Compton, Coherent, and Photoelectric Mass Attenuation Coefficients for Photons with Energy Less than 1 MeV and to Assist in the Evaluation and Formulation of Photon-Equivalent Materials, Oak Ridge National Laboratory Report ORNL-TM-4451 (1974).
- Stansbury, P. S., In-Phantom Spectrometry of Medical Diagnostic X-Rays, Ph.D. thesis, p. 36 (1977).
- Stewart, A., J. Webb, and D. Hewitt, "A Survey of Child Malignancies," Brit. Med. J. 1, 1495 (1958).
- Stewart, A., and G. W. Kneale, "Radiation Dose Effects in Relation to Obstetric X-Rays and Childhood Cancers," Lancet 1, 1185 (1970).
- Suntharalingam, N., J. R. Cameron, E. Shuttleworth, M. West, and J. F. Fowler, "Fading Characteristic of Thermoluminescent Lithium Fluoride," Phys. Med. Biol. 13, 97 (1968).

- Takeshita, K., S. Antoku, and S. Sawada, "Exposure Pattern, Surface, Bone Marrow, Integral and Gonadal Dose from Fluoroscopy," Brit. J. Radiol. 45, 53 (1972).
- Tanner, M. J., R. H. Whitehouse, and M. Takeshi, "Standard from Birth to Maturity for Height, Weight, Height Velocity, and Weight Velocity: British Children, 1965," Arch. Dis. Childhood 41, 454 (1966).
- Taylor, L. S., Radiation Protection Standard, (CRC Press, Cleveland, Ohio, 1971).
- Thomas, V. W., H. D. Maillie, and M. Mermagen, "The Whole- and Partial- Body Dosimetry of the Rat Exposed to 250 kVp X-Irradiation," Health Phys. 14, 365 (1967).
- Tipton, I. H., W. S. Snyder, and M. J. Cook, Elemental Composition of Standard Man, Oak Ridge National Laboratory Report ORNL 4007, 241 (1966).
- Townsend, P. D., C. D. Clark, and P. W. Levy, "Thermoluminescence in Lithium Fluoride," Phys. Rev. 155, 908 (1967).
- Toyooka, E. T., J. W. Pifer, S. L. Crump, A. M. Dutton, and L. H. Hemplemann, "Neoplasms in Children Treated with X-Rays for Thymic Enlargement. II. Tumor Incidence as a Function of Radiation Factors," J. Natl. Cancer Inst. 31, 1357 (1963a).
- Toyooka, E. T., J. W. Pifer, and L. H. Hemplemann, "Neoplasms in Children Treated with X-Rays for Thymic Enlargement. III. Clinical Description of Case," J. Natl. Cancer Inst. 31, 1379 (1963b).
- United Nations Scientific Committee on the Effect of Atomic Radiation, General Assembly Official Records, 17th Session, Suppl. No. 16, (A/5216) (1962).
- United Nations Scientific Committee on the Effects of Atomic Radiation, Report, General Assembly, 19th Session, Suppl. No. 14 (A/5814), p. 85 (1964).
- United Nations Scientific Committee on the Effects of Atomic Radiation, Vols. I & II, General Assembly Report, 27th Session, Suppl. No. 25 (A/8725) (1972).
- U.S. Public Health Service, Population Dose from X-Rays, U.S., 1964, PHS Publication No. 2001, Washington, DC (1969).
- U.S. Public Health Service, Population Exposure to X-Rays, U.S., 1970, DHEW Publication (FDA)73-8047 (1973).



- Walter, B., "Forschr. a.d. Geb. der Roentg.," 35, 929 (1929).
- Warner, G. G., and A. M. Craig, Jr., ALGAM, A Computer Program for Estimating Internal Dose from Gamma-Ray Sources in a Man Phantom, Oak Ridge National Laboratory Report ORNL-TM-2250 (1968).
- Warren, S., "The Basis for the Limit on Whole-Body Exposure -- Experience of Radiologists," Health Phys. 12, 737 (1966).
- Weast, C. Robert, Handbook of Chemistry and Physics (The Chemical Rubber Co., 49th Edition, Cleveland, Ohio, 1962).
- Webster, E. W., and O. E. Merrill, "Radiation Hazards. II. Measurements of Gonadal Dose in Radiographic Examination," New Engl. J. Med. 257, 811 (1957).
- Young, S. K., "Human Tissue: Chemical Composition and Photon Dosimetry Data," Radiat. Res. 57, 38 (1974).
- Zimmerman, D. W., C. R. Rhyner, and J. R. Cameron, "Thermal Annealing Effects on the Thermoluminescence of LiF," Health Phys. 12, 525 (1966).

## VITA

Wei-Li Chen was born in Si-An, China, on December 23, 1941. He entered Taipei Cheng-Kung Middle High School in 1956 and was graduated in 1962. The following October he entered Chung-Cheng Institute of Technology, and in February 1967, he received a Bachelor of Science degree in Physics. He has been employed by the Chinese Atomic Energy Council since February 1967.

In the fall of 1969, he accepted the Chinese Atomic Energy Council Special Training Program in Health Physics and was trained in the Health Physics Division of the Oak Ridge National Laboratory.

He entered Graduate School at the University of Tennessee in January 1970 and received a Master of Science degree with a major in Physics in June 1971.

He enrolled in Graduate School at the Georgia Institute of Technology in 1973. He performed his dissertation research in the Medical Physics and Internal Dosimetry Section of the Health Physics Division of the Oak Ridge National Laboratory. He received his Ph.D. degree in Nuclear Engineering with a major in Health Physics through the School of Nuclear Engineering of Georgia Institute of Technology in June 1977.

He is married to the former Wang San of Chiang-Su. They have a son.